NASA CONTRACTOR REPORT

NASA CR-112

NASA CR-112

EVALUATION OF TIROS III RADIATION DATA

by Fritz Möller and Ehrhard Raschke

Prepared under Grant No. NsG-305 *by*
UNIVERSITY OF MUNICH
Munich, Germany
for

NATIONAL AERONAUTICS AND SPACE ADMINISTRATION • WASHINGTON, D. C. • NOVEMBER 1964

NASA CR-112

EVALUATION OF TIROS III RADIATION DATA

By Fritz Möller and Ehrhard Raschke

Prepared under Grant No. NsG-305 by
UNIVERSITY OF MUNICH
Munich, Germany

for

NATIONAL AERONAUTICS AND SPACE ADMINISTRATION

For sale by the Office of Technical Services, Department of Commerce,
Washington, D.C. 20230 -- Price $3.50

Abstract : 11864

A method (MÖLLER, 1962; MÖLLER & RASCHKE, 1963*) for the determination of the mean relative humidity of the troposphere and of the surface temperature of clouds or of the ground from radiation data of the TIROS III meteorological satellite is discussed. The errors arising from the assumption of model conditions for the atmosphere have been estimated.

This method has been tested with radiation data measured during orbit 61 above the Atlantic Ocean. The results are represented in maps. Surface temperatures determined from measured values above cloudless regions are 8° - 9°C lower than the actual surface temperatures. From the geographical distribution of the relative humidity of the troposphere, the large scale circulation patterns of the atmosphere (ascending air in the inner tropical convergence zone and descending air in the subtropical belts) can be recovered.

By statistical investigations the correlation between the radiation data of all 5 channels has been investigated. The results however are strongly influenced by the meteorological conditions being present during the time of measurements. Thus some correlations are only apparent ones. author

*Interim Report No. 1 - "Evaluation of Tiros III Radiation Data", appears as Appendix III, p. 85 of this report.

CONTENTS

List of Figures.....
List of Tables.....
1. Introduction..... 1
2. Calculation of radiation diagrams..... 4
2.1 Measured radiation flux..... 5
2.2 Determination of the outgoing radiation flux..... 5
3. Radiation flux studies for atmospheric models 10
3.1 Synthetic atmospheres..... 10
3.2 Studies of the radiation intensities..... 13
3.21 channel 1 (5.8μ - 6.8μ)..... 14
3.22 channel 2 (8μ - 13μ) and channel 4 (7.5μ - 32.0μ)..... 18
3.3 Nadir angle dependence of measured data.. 24
3.4 Method of determination of surface temperatures and mean relative humidities... 28
3.41 Evaluation diagrams..... 28
3.42 Discussion of errors due to deviations of the actual atmosphere from model conditions..... 33
3.42.1 Accuracy of measurements..... 33
3.42.2 Deviations from model conditions..... 34
3.42.2.a Ideal inversion..... 36
3.42.2.b Tropospheric layers with different relative humidity..... 37
3.42.2.c Changes of the height and of the temperature of the tropopause..... 40
3.42.2.d Scattered clouds..... 41
3.42.2.e Nonblackness of emitting surfaces... 42
4. Evaluation of TIROS III radiation data..... 43
4.1 Geographical distribution of emerging radiation measured from TIROS III..... 43
4.11 Radiation data of channels 1, 2, and 4.. 44
4.12 Albedo..... 48
4.2 Surface temperatures and relative humidities determined fron channels 1 and 2.. 49

4.3 Correlations between simultaneous radiation data.. 57
4.31 Comparison of radiation data from distinct points..... 57
4.32 Correlations between single measured values..... 59
5. Concluding remarks..... 64
Appendix I..... 66
Appendix II..... 73
References..... 81
Appendix III 85

LIST OF FIGURES

Fig.1.1 : Spectral sensitivity of the channels 1, 2, and 4 (TIROS III) and a schematic graph of the absorption bands of water vapor, carbon dioxide, and ozone.....2

Fig.1.2 : Spectral sensitivity of the channels 3 and 5 (TIROS III) and the solar spectral irradiance (after JOHNSON, 1954).....3

Fig.2.1 : Radiation diagram (after YAMAMOTO, 1952).....8

Fig.2.2 : Auxiliary diagram (after YAMAMOTO, 1952).....8

Fig.3.1 : Vertical profiles of the temperature and dew (and frost) points of model atmospheres.....15

Fig.3.2 : Ozone stratification after PAETZOLD.....16

Fig.3.3 : Curves of $\frac{\partial \bar{\tau}}{\partial h}$ vs. the height h for the outgoing radiation flux which we defined in Equ.3.4 (channels 1 and 2).....17

Fig.3.4 : Curves of $\frac{\partial \bar{\tau}}{\partial h}$ vs. the height h for the outgoing radiation flux which we defined in Equ.3.4 (Channel 4 and 'difference channel 4 - 2').....19

Fig.3.5 : Radiation diagrams for the 3 infrared channels of the satellite TIROS III.....20

Fig.3.6 : Nadir angle dependence of the equivalent temperatures of the upward outgoing radiation flux in the spectral regions of the channels 1 and 2 calculated for model atmosphere 1.....26

Fig.3.7 : .....calculated for model atmosphere 3.....26

Fig.3.8 : Evaluation diagrams for the model atmosphere 1 and 3 and for the nadir angle $N = 0^{\circ}$.....29

Fig.3.9 : .....for the nadir angle $N = 40^{\circ}$.....30

Fig.3.10 : .....for the nadir angle $N = 50^{\circ}$.....31

Fig.3.11 : Calibration curves of channels 1 and 2.....35

Fig.3.12 : Decrease and increase of the equivalent temperature of the outgoing radiation flux in the sensitivity region of channel 2 arising from decrease and increase of the ground temperature (atmospheres 1 and 3; $N = 0^{\circ}$).....38

Fig.3.13 : Mean relative humidities of the upper troposphere determined for the model atmosphere 1 from radiation flux intensities which would

emerge from such an atmosphere if a 1.54 km saturated or very dry (10 %) layer with varying height is embedded
a) above a cloud surface
b) in a clear atmosphere.....39
Fig.4.1 : orbit 61 ; equivalent temperatures of channel 1.....45
Fig.4.2 : orbit 61 ; equivalent temperatures of channel 2.....46
Fig.4.3 : orbit 61 ; equivalent temperatures of channel 4.....47
Fig.4.4 : orbit 61 ; albedo - channel 3.....50
Fig.4.5 : orbit 61 ; averaged nadir angle.....51
Fig.4.6 : orbit 61 ; mean relative humidity of the upper troposphere.....53
Fig.4.7 : orbit 61 ; surface temperatures.....54
Fig.4.8 : orbit 61 ; schematic weather map.....55
Fig.4.9 : orbit 61 ; comparison of radiation data from 12 different points measured with constant nadir angle (30^{o} - 40^{o}).....58
Fig.4.10: orbit 61 ; frequency counting of the equivalent temperatures measured with nadir angles 30^{o} by
a) channels 1 and 2
b) channels 2 and 4.....62

LIST OF TABLES

Table 1.1 : Spectral regions of the 5 channels of the satellite TIROS III (1961 1).....1

Table 2.1 : Exponents k for the pressure correction of the quantity of absorbing gases according to the Equ.

$$w^* = w \left(\frac{p}{p_o}\right)^k \quad \text{.....10}$$

Table 3.1 : Characteristics of the vertical temperature profiles of the model atmospheres 1 and 3 which are shown in Fig.3.1.....10

Table 3.2 : Equivalent temperatures (^oK) of radiation flux intensities calculated for model conditions in order to demonstrate the influence of H_2O, O_3, and CO_2 on the upward outgoing radiation flux - channel 2 (8μ - 13μ) - ...22

Table 3.3 : .....channel 4 (7.5μ - 32.0μ).....22

Table 3.4 : Values of K_1, the relative path length, for different heights and nadir angles.....25

Table 3.5 : Equivalent temperatures of emerging radiation intensities determined for ideal inversions and cloud levels in heights (normal case) corresponding to the assumed ground temperature.....36

Table 3.6 : Atmosphere 1 : Variations of the intensity of the outgoing radiation flux at variations of the temperature and the height of the tropopause.....41

Table 4.1 : Geographical coordinates of 12 points. Radiation data measured above them are compared in Fig.4.9.....57

Table 4.2 : Linear correlation coefficients calculated for radiation data of channels 1, 2, and 4, the albedo values of channels 3 and 5 and the cosine of the zenith distance of the sun ($\cos Z_\odot$). These correlation coefficients have been calculated for data from orbits 42, 61, and 114.....60

Table 4.3 : Linear partial correlation coefficients
for equivalent temperatures of
col.1 : channels 2 and 4 keeping constant
those of channel 1
col.2 : Channels 1 and 4 keeping constant
those of channel 2.....63

1. INTRODUCTION : Subject of the Investigations

Since the first launch of a weather satellite many authors developed ideas for the use and evaluation of their measurements and television photographs and to bring them into a correlation with the synoptic situation on the earth.
The research reported here (see also MÖLLER & RASCHKE; 1963)* is concerned with evaluations of TIROS III radiation data especially to infer from them ground and cloud surface temperatures and a mean relative humidity of the troposphere using radiation data measured in two different spectral regions (MÖLLER; 1962).
The TIROS III satellite (1961 ϙ 1) was launched at July 15th 1961. It was equipped with a five channel radiometer, which measures radiation emerging from the earth and its atmosphere in five different spectral regions in the visible and infrared, and with two television cameras for photographs of the earth's surface. Table 1.1 gives a review of the spectral regions and of the emitters which are effective in those particular spectral intervals.

	channel	sensitivity region	bands and / or emitting surfaces
terrestrial radiation	1	5.8μ- 6.8μ	center of the 6.3μ- band of water vapor
	2	8.0μ- 13.0μ	thermal radiation of the ground or cloud surfaces; CO_2 - 15μ- band; O_3 - 9.6μ- band; weak lines and continuum in the water vapor window
	4	7.5μ- 32.5μ	like channel 2 but additionally rotational band of H_2O (> 18μ)
solar radiation	3	0.2μ- 6.0μ	solar radiation reflected and scattered by ground, clouds and the air in the entire spectral region
	5	0.5μ- 0.75μ	the same in the visible region

Table 1.1 : Spectral regions of the 5 radiometers of TIROS III (1961 ϙ 1)

The curves of spectral sensitivity of all five channels are shown in the Figs.1.1 and 1.2. Because all analog records of TIROS III radiation data were digitized and the data located into geographic coordinates with the help of an IBM 7090 computer (TIROS III, User's

* See Appendix III, p. 85 of this report.

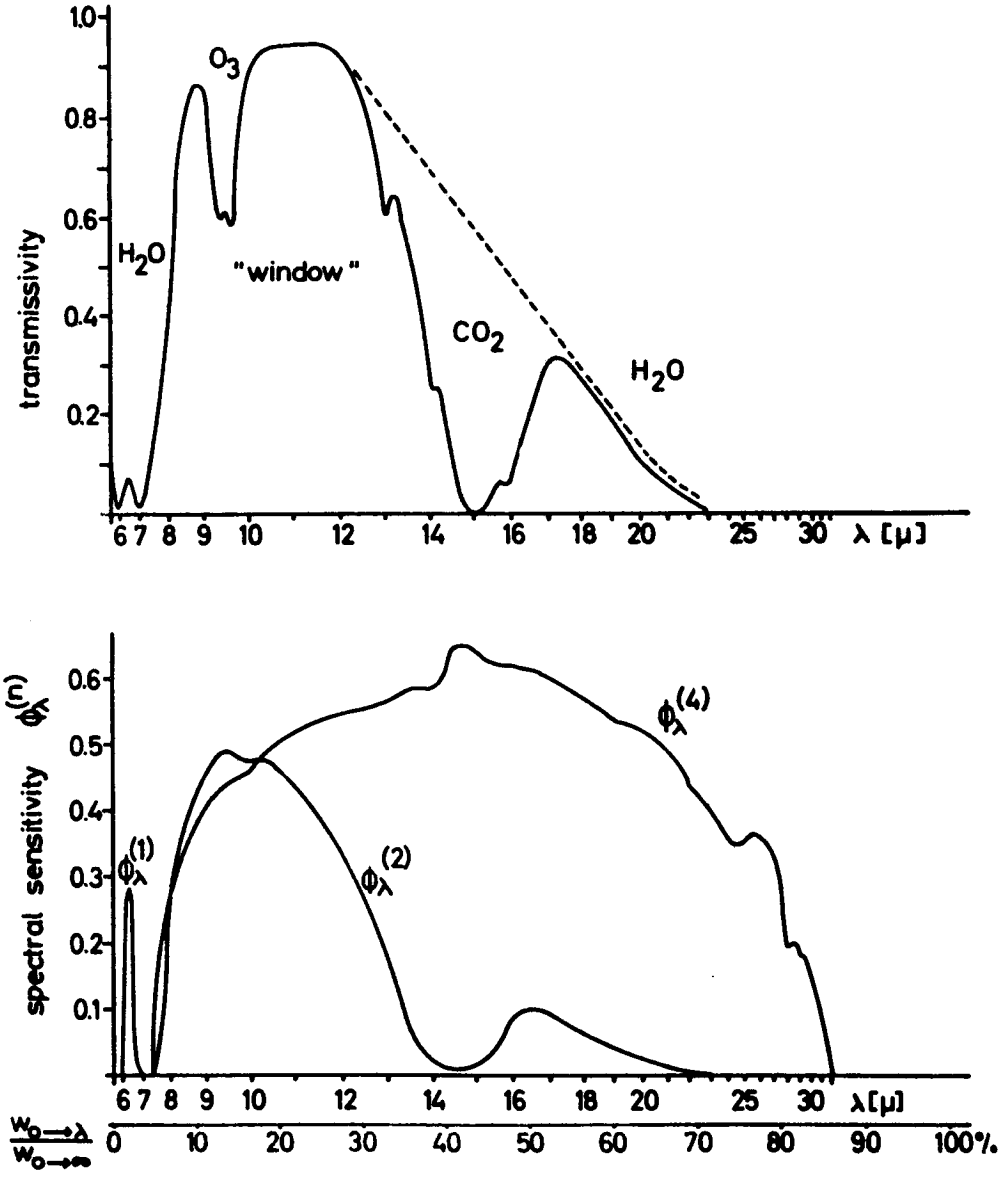

Fig. 1.1 : TIROS III, spectral sensitivity of channels 1 ($\phi^{(1)}$), 2 ($\phi^{(2)}$) and 4 ($\phi^{(4)}$)

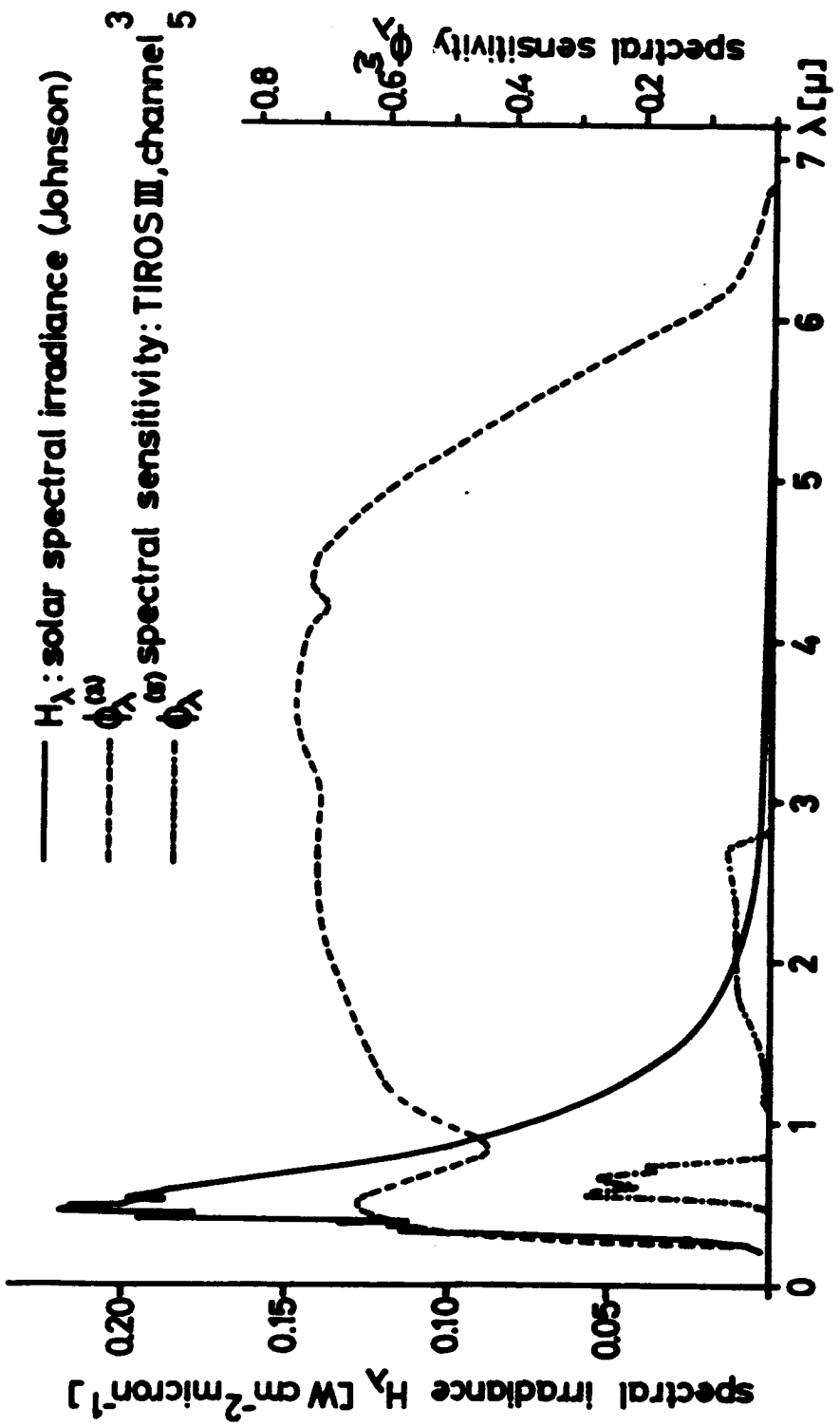

Fig. 1.2 : Spectral sensitivity of the channels 3 and 5 (TIROS III) and the solar spectral irradiance (JOHNSON, 1954)

Manual) the users of such radiation data are now able to construct geographic maps of the measured radiation for all 5 spectral regions. MÖLLER (1962) suggested a method to infer from simultaneous data of channel 1 and channel 2 the mean relative humidity of the upper troposphere and the temperature of cloud surfaces or the ground for the conditions of a model atmosphere. Since there are only two measured values many assumptions have to put into the model. These assumptions and the influence of deviations from them on the outgoing upward radiation flux will be discussed in chapter 3.
For the infrared radiation flux calculations radiation diagrams were constructed for the sensitivity regions of the 3 infrared channels, using the diagram model of YAMAMOTO (1952). These diagrams and the transmission functions which were used for the calculations are shortly reported in chapter 2. A detailed discussion was given in our 1. INTERIM REPORT (MÖLLER, RASCHKE; 1963)*. Drawings of the diagrams and tables of the transmission functions are attached in two appendices of this report.
In chapter 4 results of evaluations (temperatures and humidities) will be discussed in detail and also correlations between simultaneous radiation data (in the visible: albedo) measured during orbit 60 (16.7.1961) over the Atlantic Ocean. The correlations will show the existence of fundamental connections between the measured data which are due to the same emitter or other circumstances. For the determination of temperatures and humidities and of the linear correlation coefficients special computer programs have been developed.

2. Calculation of Radiation Diagrams

For the determination of the outgoing radiation flux we used radiation diagrams which were constructed according to the pattern of YAMAMOTO (1952). Calculations with a high-speed computer might be more accurate but they would require a much longer time to complete the computer program.
Here we will give only a short review of the problems which had to be solved in order to calculate the radiation diagrams. All details are reported in our previous report. Additionally, tables and figures of the transmission functions used for the calculations of the radiation diagrams and also figures of the diagrams are attached as appendices to this report.

* See Appendix III, p. 85 of this report.

2.1 : Measured Radiation Flux

The radiation flux measured by each receiver n can be determined by the equation

$$\bar{W}^{(n)} = \int_0^\infty B_\nu (T_{equ})\, \phi_\nu^{(n)}\, d\nu \qquad (2.1)$$

where ν means the wave number (cm^{-1}) and $\phi_\nu^{(n)}$ the spectral sensitivity of each receiver (Figures 1.1 and 1.2). $B_\nu (T_{equ})$ is the spectral irradiance incident from a black hemisphere with the temperature T_{equ} on the receiver's aperture. Although all 5 radiometers had an aperture angle of about 5 degrees (details see FUJITA; 1963) all 5 instruments were calibrated in units of incident hemispherical radiation (TIROS III, User's Manual). According to equation 2.1 NASA published all infrared radiation data of TIROS III in units of that equivalent temperature T_{equ} .

2.2 : Determination of the Outgoing Radiation Flux

With the assumption of local thermodynamical equilibrium in the atmosphere and no scatter of infrared radiation by the molecules of the air the upward outgoing radiation flux measured with receivers with the spectral sensitivity $\phi_\nu^{(n)}$ can be determined from

$$\bar{W}^{(n)} = \int_0^\infty \phi_\nu^{(n)}\, B_\nu (T_s)\, d\nu + \int_0^\infty \int_{\tau_s}^{\tau_o} \frac{d\, B_\nu (T)}{dT}\, \phi_\nu^{(n)}\, \tau_\nu (w)\, dT\, d\nu \qquad (2.2)$$

T_s and T_o are the temperatures at the receiver's aperture and on the emitter (cloud or ground). $\tau_\nu(w)$ is the spectral transmittance of an absorber with the mass w (measured in units of cm NTP (CO_2 and O_3) or g cm^{-2} for water vapor). The atmospheric gases water vapor, carbon dioxide and ozone mainly influence the infrared radiation flux of the atmo -

sphere by absorption and thermal emission within their absorption bands. The influence of minor constituents will be neglected here. On principle we will assume that clouds and the ground emit like black bodies through the entire spectral region considered here. A short discussion of this problem will be given in chapter 3.42.2.
If we assume only one absorber in the atmosphere a transformation of equation 2.2 gives :

$$(2.3) \qquad \bar{W}^{(n)} = S(T_s) + \int_{S(T_s)}^{S(T_0)} \frac{}{\tau(w(T))}\, dS(T)$$

where

$$(2.3\,a) \qquad S(T) = \int_0^T \frac{dS(T)}{dT}\, dT = \int_0^T \int_0^\infty \phi_\nu^{(n)} \frac{dB_\nu(T)}{dT}\, d\nu\, dT$$

is the radiation of a black body measured by the receiver n with the spectral sensitivity $\phi_\nu^{(n)}$, $\overline{\tau(w(T))}$ is the transmissivity averaged over all wavelengths according to

$$(2.3\,b) \qquad \overline{\tau(w(T))} = \frac{1}{\int_0^\infty \phi_\nu^{(n)} \frac{dB_\nu(T)}{dT}\, d\nu} \times \int_0^\infty \phi_\nu^{(n)} \frac{dB_\nu(T)}{dT}\, \tau_\nu(w(T))\, d\nu .$$

w (T) gives the absorber quantity between the receiver and the level with the temperature T as it is given in an atmosphere profile. Equation 2.3 permits the construction of diagrams with $\overline{\tau(w)}$ as ordinate and S (T) as abscissa which contain lines of constant w (= absorber quantity) and T (= temperature) (Fig.2.1). Such a diagram will be constructed for the main absorber in the considered interval, what is here water vapor.
Now we will consider spectral regions where the absorption bands of two or more absorbers overlap each other. As it is

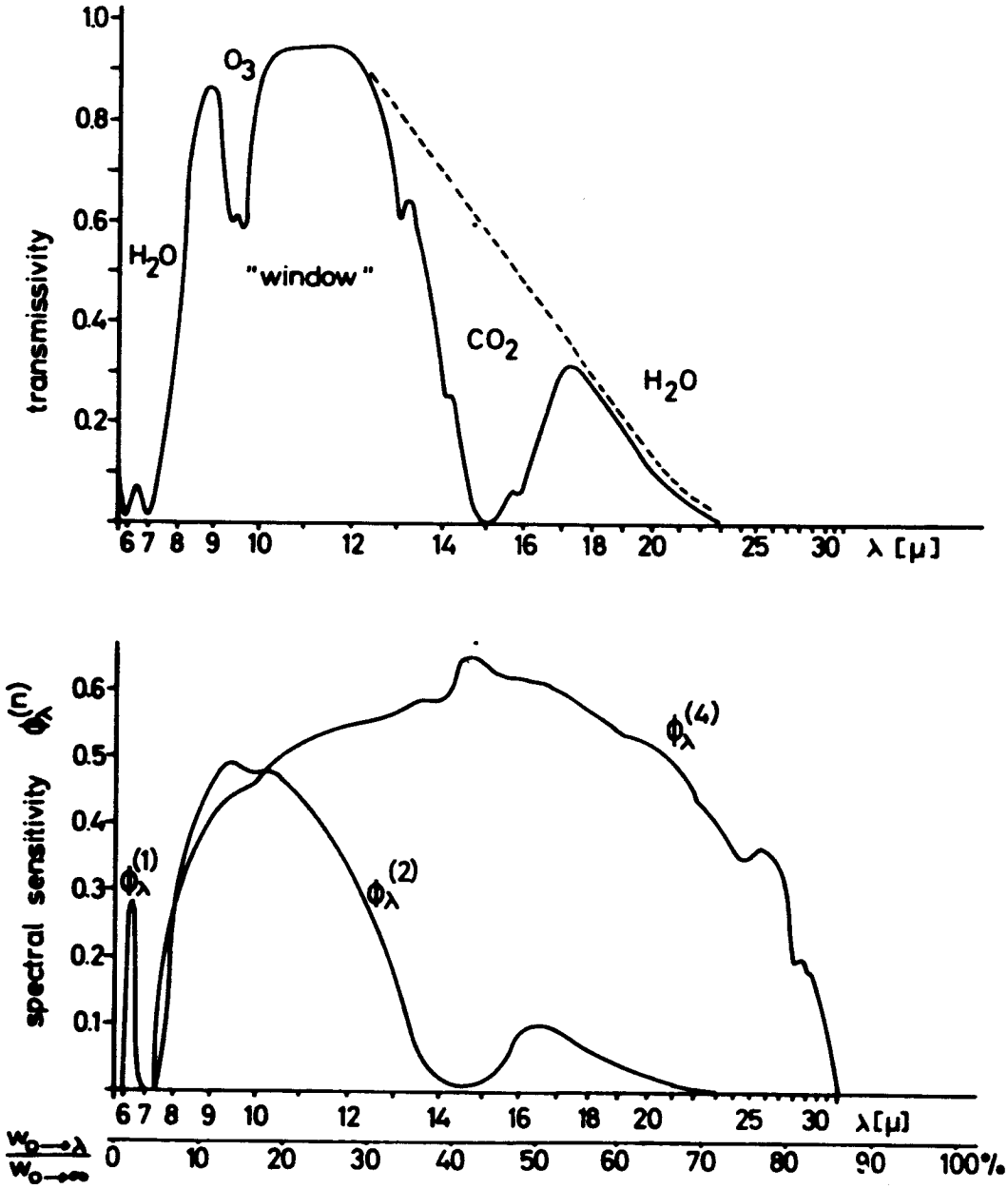

Fig. 2.3 : TIROS III, spectral sensitivity of channels 1, 2 and 4

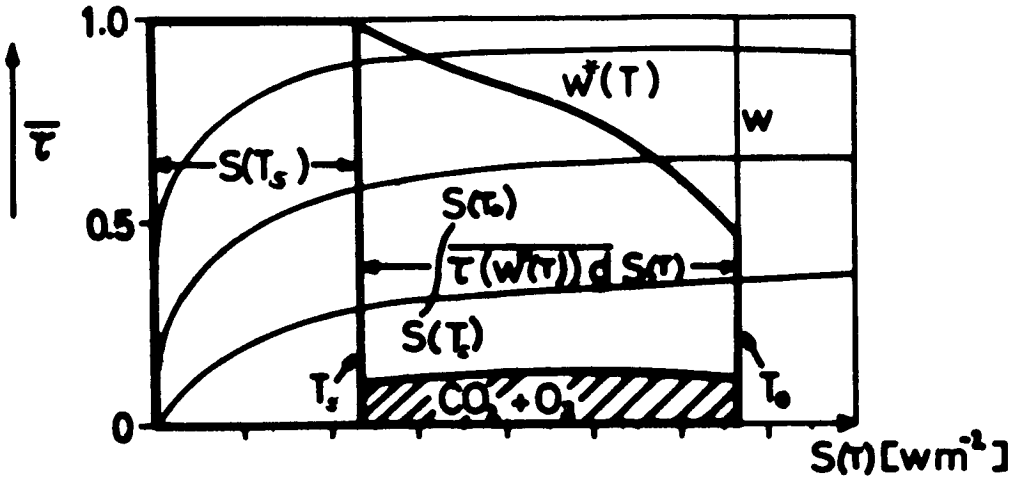

Fig. 2.1 : Radiation diagram

(YAMAMOTO, 1952)

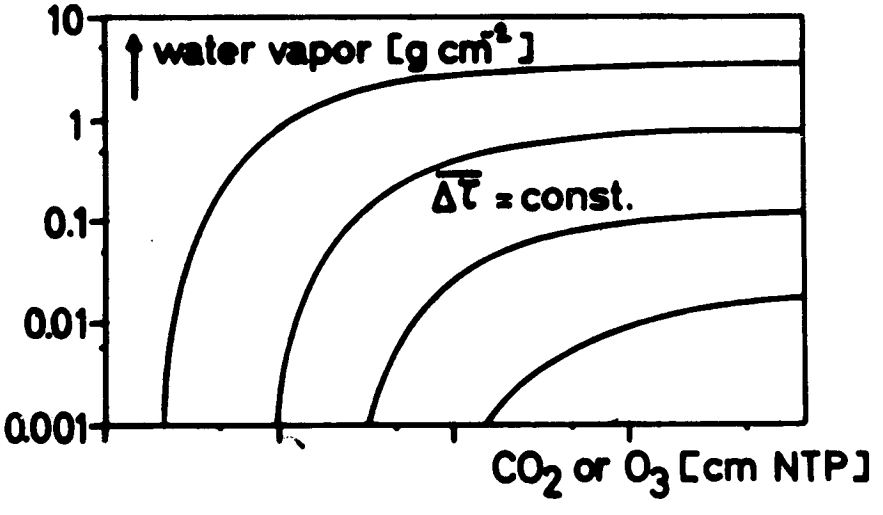

Fig. 2.2 : Auxiliary diagram

(YAMAMOTO, 1952)

the pressure dependence of the absorption had to be taken into consideration in another way. According to ELSASSER (1942) a 'pressure corrected' absorber quantity (or optical path length) was computed by the integral

$$(2.6) \qquad w^* = \int_0^w \left(\frac{p(w)}{p_0}\right)^k dw$$

This pressure correction is a simplification of the complicated pressure dependence of the absorption of a band. Since the temperature can be used as coordinate in atmospheric profiles the absorber quantity w should be given as w (T), which means the absorber quantity between the receiver and the layer with the temperature T (Fig.2.1).
For the construction of the radiation diagrams and the auxiliary diagrams transmission functions with the convenient form (ELSASSER; 1942) :

$$(2.7) \qquad \tau_\nu = \tau \ (l_\nu \cdot w^*)$$

were derived from laboratory spectral data (Table 2.1).
Here is l_ν the 'generalized absorption coefficient' which describes the wave number and also the temperature dependence of the absorption of a band. It is a very smoothed function since it was determined for wide spectral intervals (10 cm^{-1}) which contain many spectral lines. This form of transmission functions contains also the assumption of a connection between the transmissivity and the absorber quantity over all spectral regions of an absorbing band.
These above mentioned simplifications of all the complicated connections between the absorption, pressure, temperature and the absorber quantity introduce some systematic errors into the calculations of the radiation flux. But comparisons between measured spectra (and also computed spectra by WYATT et.al.; 1963) and spectra calculated after Equ.2.7 showed good agreement (MÖLLER, RASCHKE; 1963)* which leads to the assumption that these errors are not too large.

* See Appendix III, p. 85 of this report.

In the Table 2.1 the values of the exponent k for pressure correction are given :

absorbing gas	band	exponent k	references
H_2O	6.3 window region 30	0.72 •	HOWARD et. al. (1955); ROACH, GOODY;(1958); BOLLE et al. (1963); PALMER (1960);
CO_2	17	0.65	BURCH et al. (1960);
O_3	9.6	0.41 for p 150 mb 0 for p 150 mb	WALSHAW (1957); (integrated absorption of the entire 9.6μ-band)

Table 2.1 : Exponents for the pressure correction of the quantity of absorbing gases.

This exponent was derived by HOWARD et al. (1955) from their own measurements for strong absorption by the 6.3μ-band.

3. Radiation Flux Studies for Atmsopheric Models

The intensity of infrared radiation emerging from the earth and its atmosphere depends on the temperature of the ground and of cloud surfaces, on the temperature profile and on the distribution and the amount of all gases in the atmosphere which absorb and emit infrared radiation . This dependence will be investigated here particularly for the sensitivity regions of the channels 1, 2 and 4. In doing so typical temperature profiles and distributions of the main important absorbers H_2O, CO_2 and O_3 are used which are based on measurements under different conditions.

3.1 : Synthetic Atmospheres

The investigations will be continued only with 2 model atmospheres, which correspond with our models 1 and 3 (MÖLLER, RASCHKE; 1963)*. These models can be considered to be representative for typical weather situations in tropical and

* See Appendix III, p. 85 of this report.

midlatitude regions. Arctic conditions are not considered here since TIROS III orbital paths covered only the earth's surface between ±60 degrees latitude.
The vertical temperature profiles and the profiles of the frost point and dew point respectively are shown in Fig.3.1. The characteristics of the temperature profiles are summarized additionally in Table 3.1.

atmosphere	1	3
ground temperature	+ 15° C	35° C
temperature gradient in the troposphere	- 6.5°/km	- 6.5°/km
tropopause temperature and height	- 56.5° C 11.0 km	- 75.0° C 16.9 km

Table 3.1 : Characteristics of the vertical temperature profiles which are shown in Fig.3.1

For both models a vertical temperature distribution in the stratosphere according to that of the ARDC (1959) atmosphere has been assumed. For the tropical model the stratospheric temperature profile has been extrapolated downward until the isotherm level of - 75° C, in doing so a constant temperature gradient of - 3°/km has been assumed. From that a temperature profile of the tropical model results which deviates somewhat from a typical model proposed by STROUD and NORDBERG (1961) as determined by sounding rocket measurements. In stratospheric regions these deviations might not be important because of the small concentration of the absorbing gases (chapter 3.2). In the troposphere the temperature gradient (about 7.3°/km) and the ground temperature (+42° C) of that model are somewhat higher than in our model.
To characterize the water vapor content a constant relative humidity in the troposphere and a constant frost point gradient through the tropopause have been assumed as it is shown in Fig.3.1. The vertical water vapor distribution in the stratosphere was supposed to be the same in both models according to the midlatitude model given by GUTNICK (1962). The mixing ratio im heights above 30 km has been assumed to be constant (= 0.1 g/kg). In the case of the tropical model that mixing ratio might be somewhat too high as it results from measurements of MASTENBROCK (1962) over Hyderabad (India).

Dividing the atmosphere into m layers the effective amount of precipitable water can be determined after

$$(3.1) \qquad u^* = 0.438 \cdot 10^{-2} \sum_{i=1}^{m} \frac{\overline{\varepsilon_i}}{\overline{p_i}\ 0{,}24} \Delta p_i \ (\text{g cm}^{-2} \text{ or cm ppt})$$

where $\overline{\varepsilon_i}$ is the mean vapor pressure corresponding to the assumed relative humidity over ice (for $T < -20^{\circ}C$) or over water (for $T > -20^{\circ}C$) in the i-th layer and $\overline{p_i}$ is the mean pressure in the i-th layer with the 'thickness' Δp_i .
The effective mass of carbon dioxide can be determined after

$$(3.2) \qquad c^* = 0.1595 \cdot 10^{-2} \sum_{i=1}^{m} (p_i^{\,1.65} - p_{i-1}^{\,1.65}) \ (\text{cm})$$

which corresponds to an assumed constant mixing ratio through the atmsophere of 0.03% per volume. p_i and p_{i-1} are the pressures at the upper and lower boundary of the i-th layer. From Equ.3.2 results an effective carbon dioxide amount of 145 cm.
The profiles of the vertical ozone distribution were derived from Fig.3.2 (FAETZCLD) for model 1 from 45° latitude (autumn) and for the model 3 from 30° latitude (autumn) respectively. According to the pressure correction (chapter 2) the amount of ozone determined from Fig.3.2 for each layer above the 150 mb level has to be multiplied by $(\frac{p_i}{p_o})^{0.41}$
Since fluctuations of the ozone distribution do not influence the radiation flux intensity in the sensitivity regions of the channels 2 and 4 in a decisive degree (MÖLLER & RASCHKE; 1963)* no further investigations of that problem were carried out here. In all cases the summation over all layers has to begin at the surface of the receiver, which is here the satellite outside the atmosphere.

* See Appendix III, p. 85 of this report

3.. : Studies of the Radiation Intensities

For investigations of the radiation intensities sensed by the radiometers of the TIROS III viewing the system earth - atmosphere, we will use another equation, which results from equation (2.3) by a slight transformation.
The upwelling radiation flux intensity $\bar{W}^{(n)}$ measured in the channel n may be determined from

$$(3.3) \qquad \bar{W}^{(n)} = S(T_o') \cdot \overline{\tau(w(T_o))} + \int_{T_o}^{T_s} S(T) \frac{\partial \overline{\tau(w(T))}}{\partial T} dT$$

Here we assume in a more general way that the temperature T_o' of the ground or of cloud surfaces is not identical with that (T_o) of the air adjacent to it. T_s is the temperature of the ambient medium at the satellite. If we use the height h as the vertical variable instead of T according to the relation $T = T(h)$, equation (3.3) may be written in the form

$$(3.4) \qquad \bar{W}^{(n)} = S'(h_o) \cdot \overline{\tau(w(h_o))} + \int_{h_o}^{h_s} S(h) \frac{\partial \overline{\tau(w(h))}}{\partial h} dh$$

where h_s and h_o are the height of the satellite and the height of the cloud surface or ground ($h_o = 0$) respectively. Here is according to the assumption made above

$$S'(h_o) \neq S(h_o)$$

In equation 3.4 the upward radiation flux intensity measured in the sensitivity region of the channels n = 1, 2 and 4 is determined by the radiation $S'(h_o)$ emitted from a surface (first term) and that emitted from the atmosphere (second term). Thus, this form of the radiation flux equation gives a good possibility to estimate the influence of the different radiation layers or surfaces on the total flux intensity.
The contribution of the surface to the entire flux is given by the transmissivity $\overline{\tau(w(h_o))}$ of the whole atmosphere in the spectral region considered here. The contribution

of the atmosphere itself depends on the values of $\frac{\partial \overline{\tau(w\ (h))}}{h}$ for each layer where S (h) might be considered as a weighting factor. Curves of $\frac{\partial \overline{\tau}}{\partial h}$ therefore will be useful for an estimation of the share of the atmospheric layers in the radiation flux intensity within the spectral region n.

3.21 : channel 1 (5.8μ - 6.8μ)

Since the sensitivity region of channel 1 is located in the center of the 6.3μ - band of H_2O, the measured radiation flux intensities will depend only on the water vapor distribution and the temperature profile. The curves of $\frac{\partial \overline{\tau}}{\partial h}$ in Fig.3.3 give the shape of that 'influencing function' for very low tropospheric humidities and saturation as well as for the model atmospheres 1 and 3 (Fig.3.1). They show that the radiation emitted from the ground and from layers of the lower troposphere will not penetrate the whole atmosphere. Mainly those layers will contribute to the measured radiation flux intensity for which the curves show typical maximum values. In the saturation case, these layers are located in the upper troposphere near the same temperature levels in both models since the total water vapor content is then determined by the temperature profile only. In the case of low relative humidity the maximum value is located in the middle of the troposphere but in both model atmospheres at nearly the same temperature level of about -15°C. A mean relative humidity which would be determined from channel 1 radiation data, therefore will be representative for these layers of the upper troposphere. If a height of a fictitious level corresponding to the equivalent temperature of the measured radiation intensity will be sought, that height will be located within the mentioned layers or better temperatures.
Changes of the water vapor content in the lower stratosphere can produce variations of the upward radiation flux. As it was shown in our previous report a comparison of results calculated for a relative humidity of 5 % in the troposphere with a water-vapor-less stratosphere and with a stratosphere saturated in its lower part showed a difference of equivalent temperature of 8° (atmosphere 1). This result shows that changes of the water vapor content in the lower stratosphere will

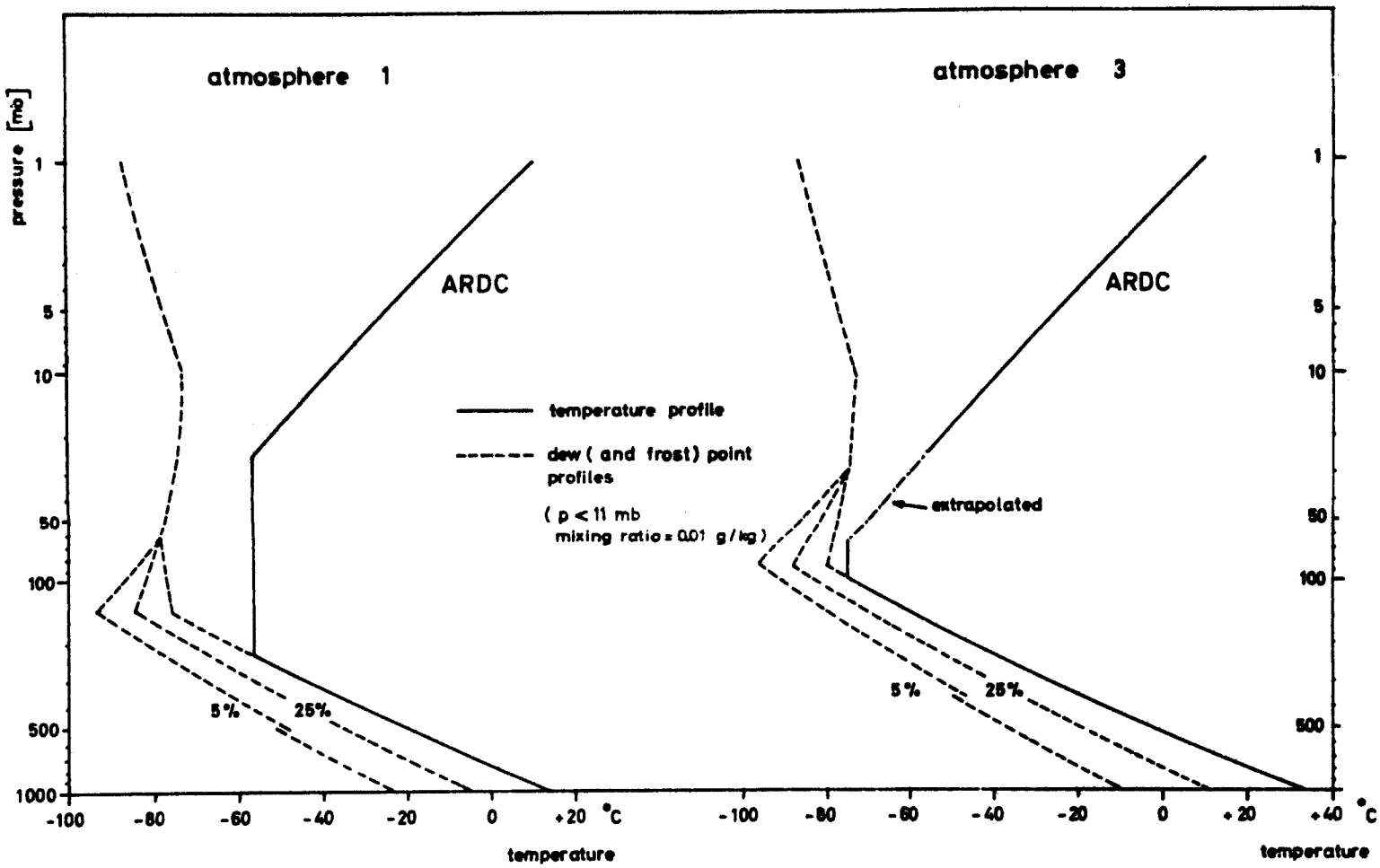

Fig. 3.1 : Vertical profiles of temperature and dew (and frost) points of model atmospheres

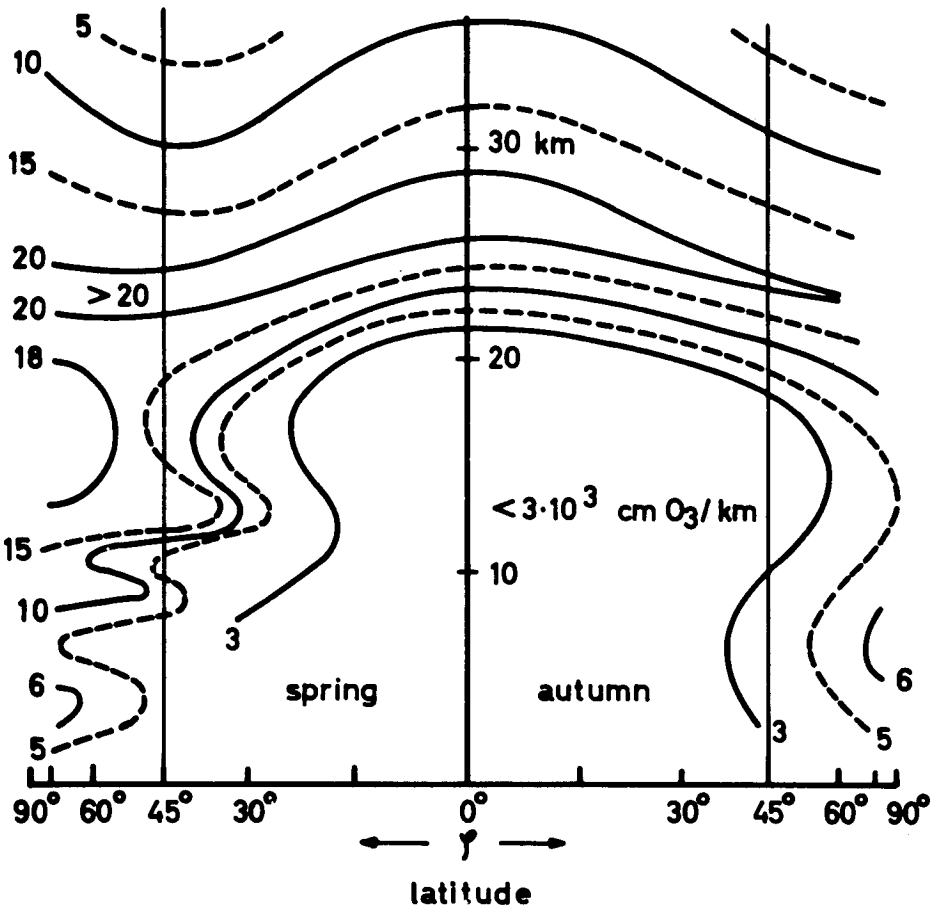

Fig. 3.2 : Ozone stratification after PAETZOLD

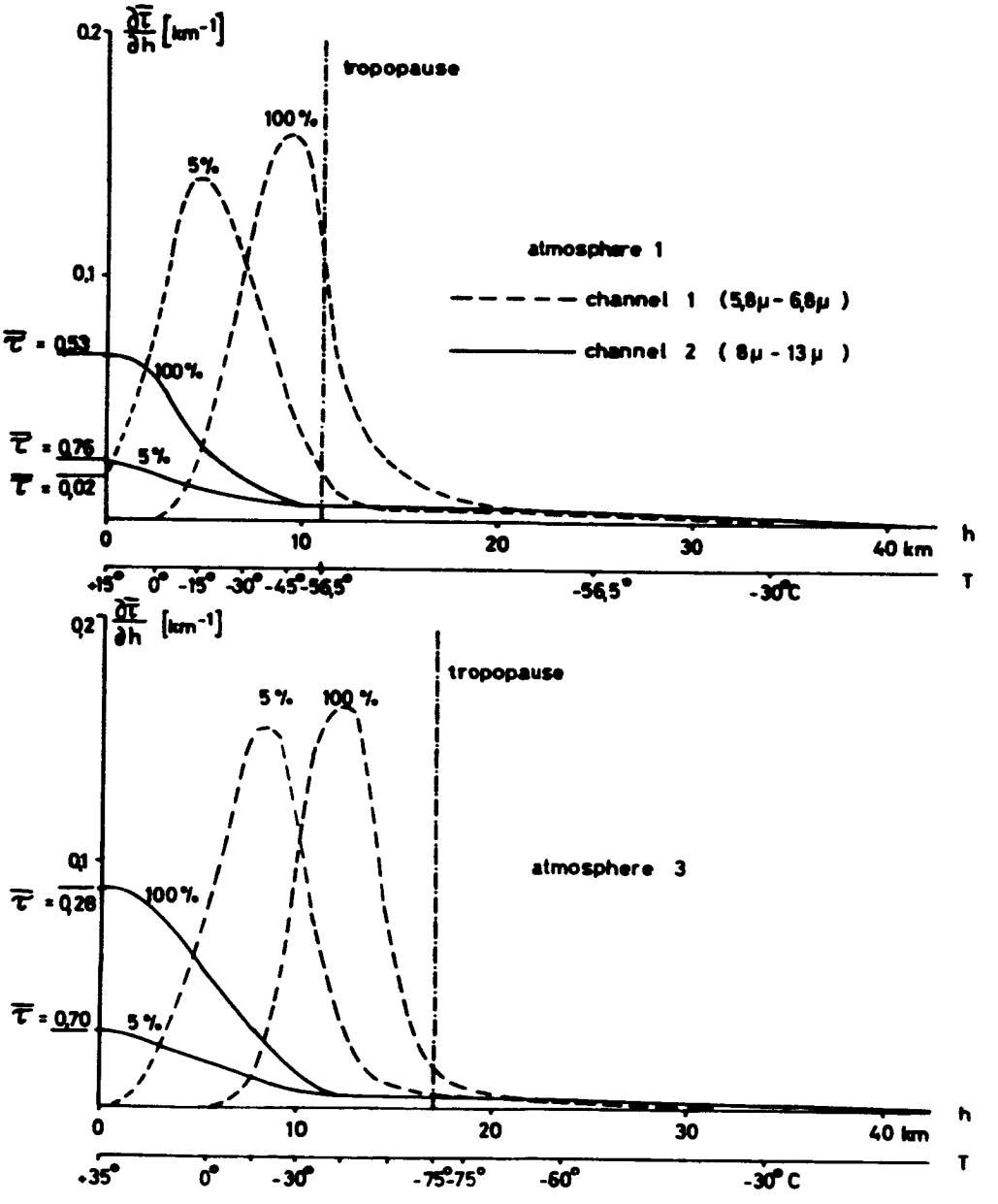

Fig. 3.3 : Curves of $\frac{\partial\bar{\tau}}{\partial h}$ vs. the height h for the outgoing radiation flux which are defined in Equ. 3.4

effect essential variations of the radiation intensity. If mean relative humidities shall be determined from evaluations of radiation data the results may be disturbed in that way.

3.22 : channel 2 (8μ - 13μ) and channel 4 (7.5μ - 32.0μ)

The sensitivity regions of the channels 2 and 4 overlap each other (Fig. 2.1). Channel 4 may be considered to cover 80% of the whole spectrum of the infrared radiation emitted from the system earth - atmosphere into space (WARK, YAMAMOTO, LIENESCH; 1963).
Particularly in the region of the 15μ - band of CO_2 and in the rotational band of the water vapor channel 4 receives radiation where the sensitivity of channel 2 is zero. The sensitivity region of channel 2 , however, covers only the region of the water vapor window between 8μ and 13μ.
A comparison of the curves $\frac{\partial \bar{\tau}}{\partial h}$ in Fig. 3.3 and Fig. 3.4 and of the values of the remaining transmissivities $\bar{\tau}$ of the whole atmosphere (at the left side of the ordinate) shows that in channel 2 a great portion of the radiation received is emitted from the ground. In the case of clouds the portion is yet higher.

The radiation emitted from the atmosphere in that spectral region is comparatively small but can not be neglected in radiation flux calculations as it will be shown later. The curves of $\frac{\partial \bar{\tau}}{\partial h}$ for channel 4 show a typical maximum in heights of 4 and 6 km respectively which is due to the rotational band of water vapor. It is much lower than the maximum for channel 1 because of the weaker absorption compared to the 6.3μ - band. As it might be seen from the curves $\frac{\partial \bar{\tau}}{\partial h}$ and also from the radiation diagrams in Fig. 3.5, only the layers of the lower troposphere have a perceivable influence on the radiation flux in both channels. Variations of $\frac{\partial \bar{\tau}}{\partial h}$ are mainly due to the water vapor.
Analogously to channels 1 , it should be expected to get from channel 4 radiation data some information on the water vapor content in the lower troposphere as channel 1 is responding to the water vapor in the hi gh troposphere. The radiation emitted in the region of the water vapor window will however

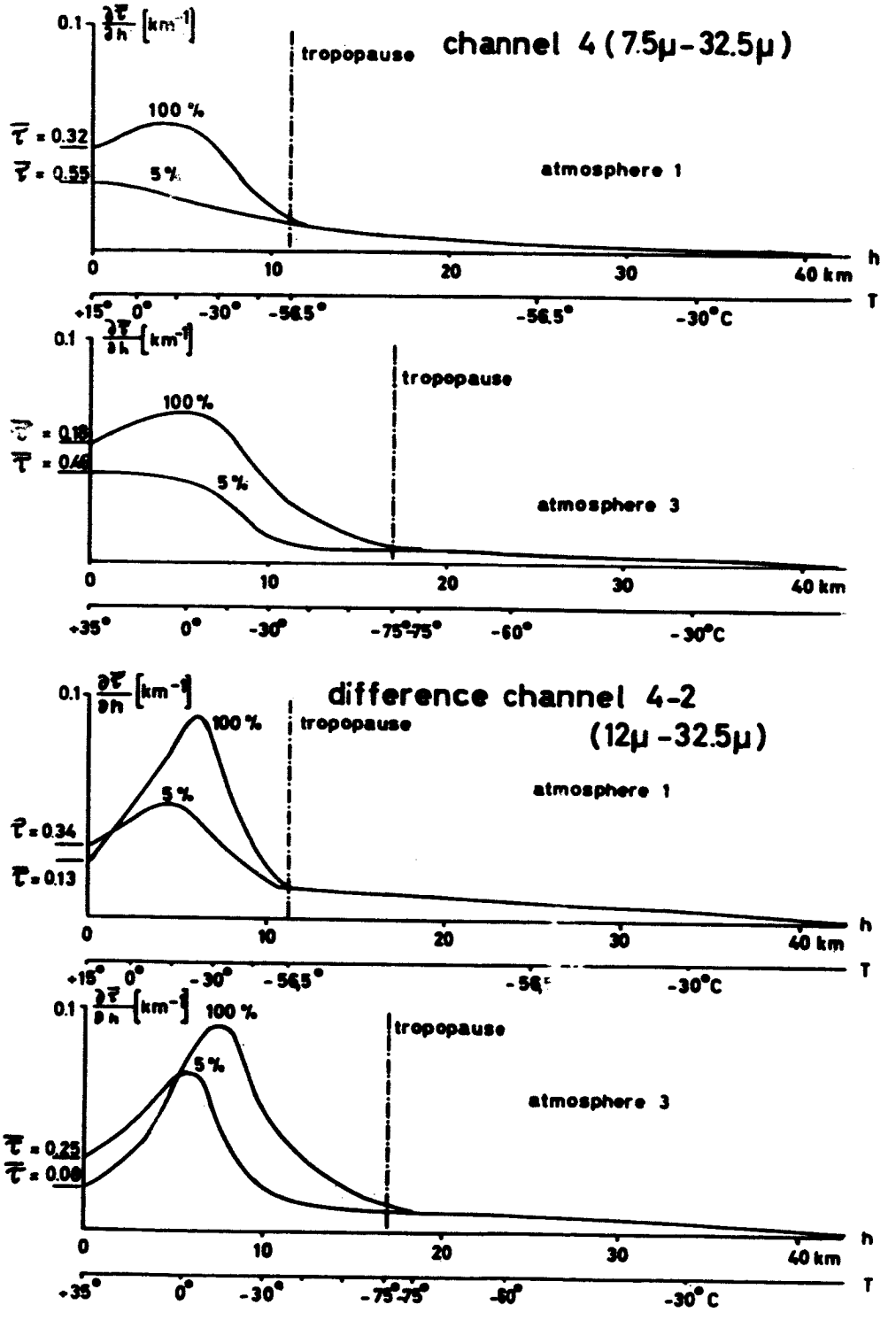

Fig. 3.4 : Curves of $\frac{\partial \bar{\tau}}{\partial h}$ vs. the height h for the outgoing radiation flux which are defined in Equ. 3.4

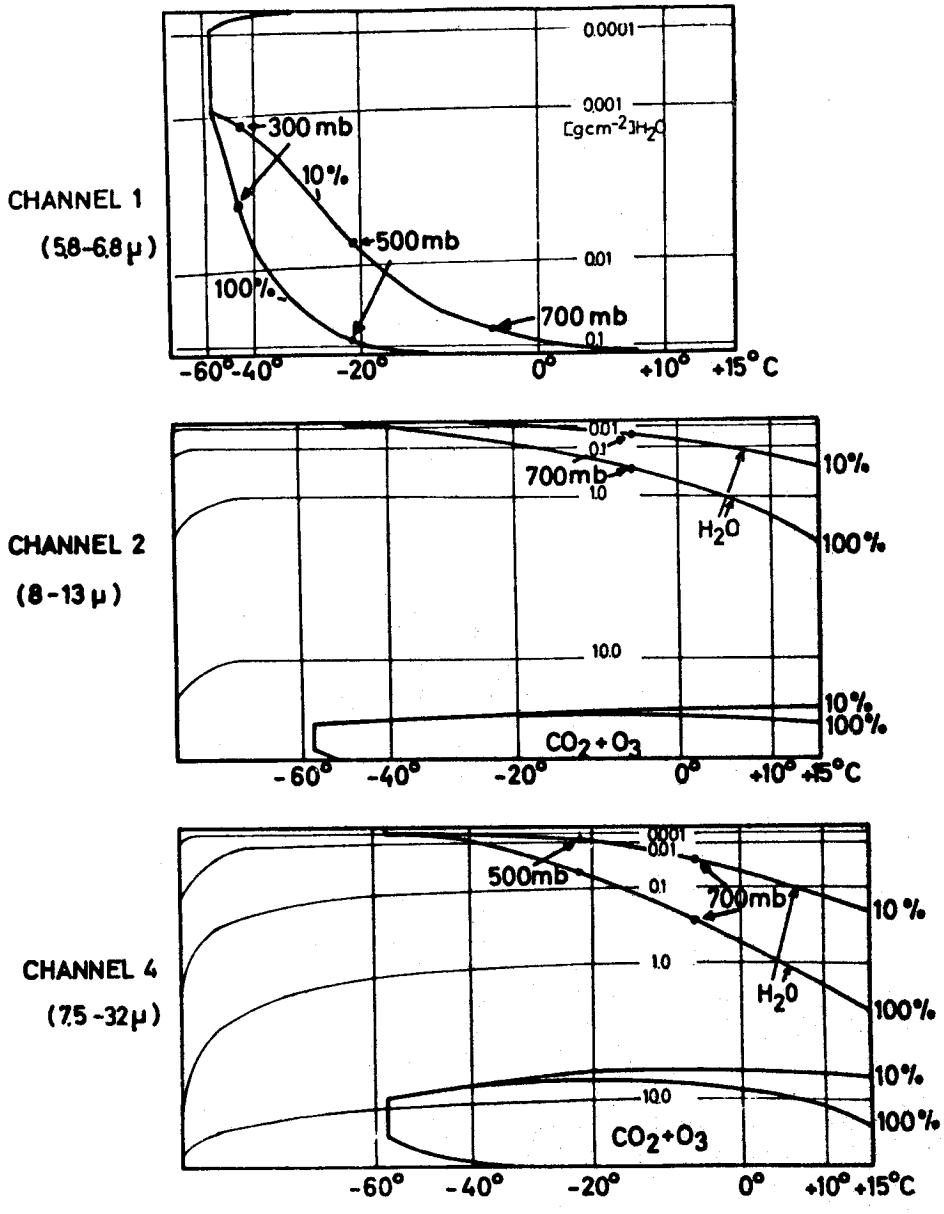

Fig. 3.5 : Radiation diagrams for the 3 infrared channels of TIROS III

strongly influence the whole intensity measured in channel 4. Therefore it was tried to diminish that influence by the definition of a new synthetic channel (MÖLLER & RASCHKE, 1963)* with a sensitivity region defined by the difference ($\phi_\nu^{(4)} - \phi_\nu^{(2)}$) of the sensitivities of the channels 4 and 2. The radiation flux intensity sensed in such a synthetic channel would then be equal to the difference $\overline{W}_4 - \overline{W}_2$ of the intensities measured in the channels 4 and 2 simultaneously.

In order to estimate the contribution of surface radiation and of the atmosphere curves of $\frac{\partial \overline{F}}{\partial h}$ are given in Fig.3.4 below for that synthetic channel. The results show lower transmissivity of the whole atmosphere for radiation emitted from the ground than for channel 4. The influence of the radiation in the water vapor window has been diminished on that way. Further the shape of the curves $\frac{\partial \overline{F}}{\partial h}$ shows typical maxima in higher layers.

These maxima are situated at levels between those of channel 1 and 4 and the intensities of the maxima also are between the others, thus indicating that a determination of the relative hunidity in a layer below that of channel 1 ought to be possible.

But as it has been shown in our previous report, a determination of a second relative humidity from these radiation data differences would require a much higher accuracy of measurements. A short estimation of errors leads to the statement that the difference ($\overline{W}^{(4)} - \overline{W}^{(2)}$) of radiation data of TIROS III can not be used because of too large errors of measurements.

In order to show the influence of atmospheric water vapor, carbon dioxide, and ozone on the radiation flux intensities which are sensed by the channels 4 and 2 at our model conditions some results are given in Tables 3.2 and 3.3. The calculations have been carried out taking into account different relative humidities (100 %, 25 %, 5 %) of the troposphere, different cloud heights, and variations of the CO_2 and O_3 content. These different cases are :

case 1 : without regard of CO_2 and O_3
case 2 : with regard of H_2O and O_3
case 3 : with regard of H_2O and CO_2
case 4 : with regard of H_2O and CO_2 and O_3

* See Appendix III, p. 85 of this report

The results are given in form of equivalent temperatures T_{equ} (^{o}K).

atmosphere 1					
height and temperature of cloud surfaces	rel. hum. (%)	1	2	3	4
tropopause (11 km, 216.5°K)	100 25 5	216.5	218.5	217.0	220.0
5.4 km 253.0°K	100 25 5	253.0	251.0	252.0	250.0
2.3 km 273.0°K	100 25 5	270.5 271.5 272.5	267.5 268.5 269.0	269.5 271.0 271.5	266.5 267.2 268.0
ground (288°K)	100 25 5	282.0 285.0 287.0	277.0 280.5 282.5	280.5 283.5 285.0	275.8 279.3 280.7
atmosphere 3					
tropopause (16.9 km, 198°K)	100 25 5	198.0	199.5	198.5	201.7
5.4 km 273.0°K	100 25 5	271.5 272.5 273.0	268.0 269.0 270.0	270.0 271.0 271.5	266.9 268.3 268.7
2.3 km 293.0°K	100 25 5	286.5 290.0 292.0	282.0 285.5 287.5	285.5 288.5 290.0	280.6 284.0 286.0
ground (308°K)	100 25 5	294.0 301.5 305.0	289.0 296.0 299.5	294.0 299.5 303.5	287.3 294.0 297.7

Table 3.2 : channel 2 (8μ- 13μ)

Equivalent temperatures (^{o}K) of radiation flux intensities calculated for model conditions in order to demonstrate the influence of H_2O, CO_2, and O_3 on the upward outgoing radiation flux. For definition of cases 1 to 4 see p. 21.

atmosphere 1					
height amd temperature of cloud surfaces	rel. hum. (%)	1	2	3	4
tropopause (11km, 216.5°K)	100 25 5	216.5	217.0	220.0	220.5
5.4 km 253.0°K	100 25 5	251.0 252.0 252.5	250.0 251.0 251.5	247.5 248.5 249.0	246.5 247.4 248.2
2.3 km 273.0°K	100 25 5	266.5 269.5 271.0	264.5 267.5 270.0	259.5 262.5 264.5	257.5 260.5 263.0
ground (288.0°K)	100 25 5	275.5 281.5 284.5	273.5 278.5 282.5	267.0 271.0 274.5	265.5 267.7 271.5
atmosphere 3					
tropopause (16.9 km, 198.0°K)	100 25 5	198.0	199.5	202.0	203.0
5.4 km 273.0°K	100 25 5	267.5 269.5 271.5	266.0 268.5 270.5	260.0 262.5 263.0	259.0 261.5 262.0
2.3 km 293.0°K	100 25 5	279.5 285.0 291.0	277.5 283.5 287.5	271.0 274.5 278.0	268.2 273.0 275.0
ground (308.0°K)	100 25 5	285.0 295.0 301.0	283.0 291.5 298.0	275.0 282.0 288.0	273.0 278.0 284.5

Table 3.3 : channel 4 (7.5μ- 32.0μ)

These computed values of equivalent temperature T_{equ} allow a good estimation of the errors which would result if one of the main important absorbers will be neglected in the radiation flux determinations. The first line of any table in which a cloud has been assumed at the tropopause shows the influence of absorbers within the stratosphere. In the sensitivity regions of both channels the water vapor of the stratospheric layers does not contribute any amount to the whole radiation flux intensity (see also Fig.3.5).

The contributions of the atratospheric carbon dioxide and ozone is demonstrated in cases 2 and 3. Here the equivalent temperatures of the radiation flux intensities are a few degrees higher than those of the cloud surfaces.

3.3 : Nadir Angle Dependence of Measured Data

When the satellite TIROS III progresses along its path it spins around its axis which points in the same direction in space at least for the time of one orbit. As a result of this spinning the radiometers will receive radiation emerging from the system earth - atmosphere under different nadir angles. This is the angle between the earth's radius vector through the satellite and the optical axis of the radiometers. Since the TIROS III radiometers have a relatively small aperture angle of about 5 degrees the measured radiation may be considered to be radiation of a beam, although we always determine radiation flux intensities because of the calibration of the radiometers in units of the radiation flux. Therefore the outgoing radiation flux has been calculated for several nadir angles in order to determine the anisotropy of the outgoing radiation. The results have to be included into an evaluation method of the TIROS III radiation data. These calculations contain only the region of nadir angles where the earth's surface is fully viewed by the radiometer (FUJITA, 1963). They are not contemplated to determine the earth's infrared horizon (HANEL et al.; 1963; ANTHONY, SMILEY; 1962; KONDRAT'YEV and YAGUSHEVSKAJA; 1962). Assuming spherical symmetry of the absorber distribution in each layer within the atmosphere the path length w_i in the i-th layer may be determined after

$$w_i^* = K_i \cdot w_{v,i}^*$$

where $w_{v,i}^*$ is the vertical absolute path length. K_i, the relative path length, can be determined after

(3.5) $$K_i = \frac{1}{\sqrt{1 - \frac{(R + H)^2 \cdot \sin^2 N}{(R + \bar{h}_i)^2}}}$$

N = nadir angle
R = 6370 km (radius of the earth)
H = 780 km (averaged height of the satellite above the ground)
$\bar{h}_i$ = mean height of the i-th layer

Values of K_i are given for several heights and nadir angles in Table 3.4.

$\bar{h}_i$ (km)	nadir angle N					
	20°	30°	40°	50°	55°	60°
50	1.081	1.203	1.432	1.913	2.435	3.785
40			1.434	1.924	2.462	3.866
30			1.436	1.933	2.481	3.953
20			1.438	1.941	2.501	4.047
15			1.439	1.945	2.512	4.096
10			1.441	1.949	2.522	4.148
8				1.951	2.526	4.170
6			1.442	1.953	2.531	4.191
4				1.954	2.535	4.214
2				1.956	2.540	4.236
0	1.083	1.208	1.444	1.958	2.544	4.259

Table 3.4 : values of K_i

Results of calculations in form of curves $\Delta T = T_{equ}(N) - T_{equ}(N=0)$, where $T_{equ}(N)$ designates the equivalent temperature of radiation flux at nadir angle N, confirm that the outgoing upward radiation intensity is anisotropic and decreases with increasing nadir angle. Only if clouds are located at the tropopause the measured flux increases with increasing nadir angle since the layers above the tropopause are warmer than the cloud levels and contribute an increasing part to the measured radiation flux (Fig.3.6).
LARSEN et al. (1963) empirically derived the nadir angle dependence of radiation data of channels 2, 3, and 4 from

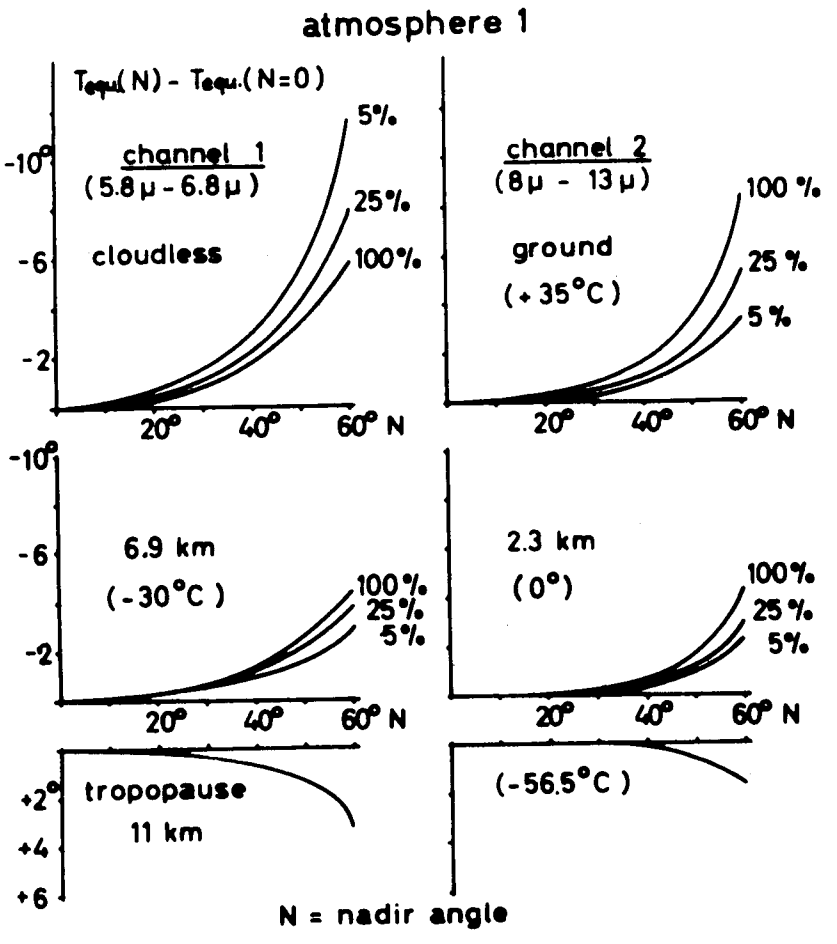
atmosphere 1
$T_{equ.}(N) - T_{equ.}(N=0)$
channel 1
(5.8 μ - 6.8 μ)
cloudless
5%
25%
100%
channel 2
(8 μ - 13 μ)
ground
(+35°C)
100 %
25 %
5 %
6.9 km
(-30°C)
2.3 km
(0°)
tropopause
11 km
(-56.5°C)
-10°
-6
-2
+2°
+4
+6
20°
40°
60° N
N = nadir angle

Fig. 3.6

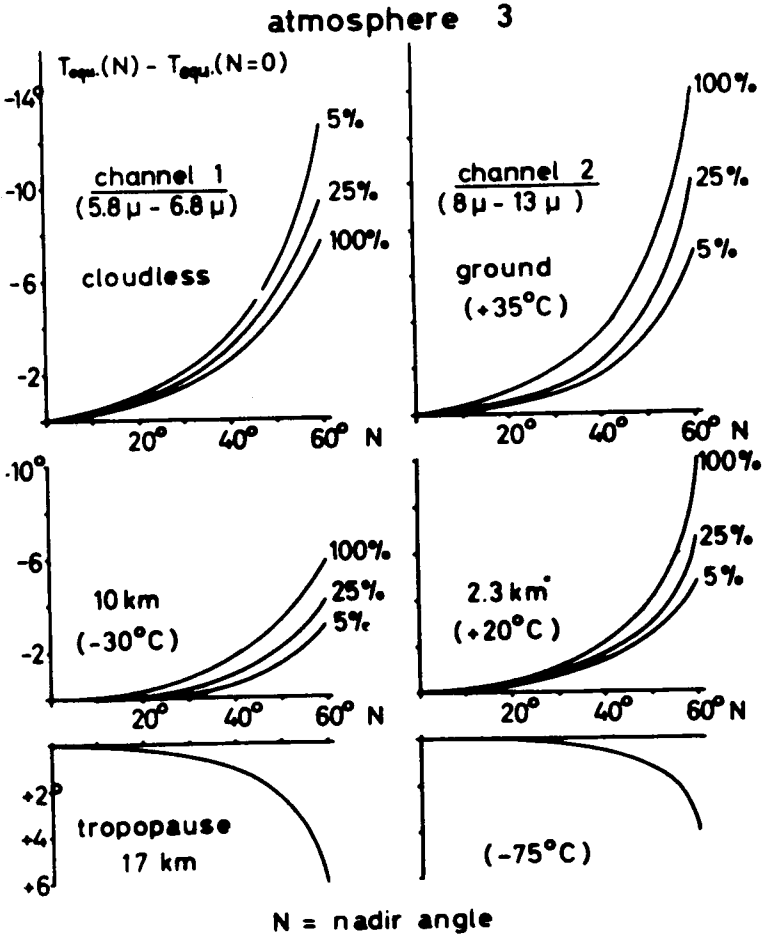
atmosphere 3
$T_{equ.}(N) - T_{equ.}(N=0)$
channel 1
(5.8 μ - 6.8 μ)
cloudless
5%
25%
100%
channel 2
(8 μ - 13 μ)
ground
(+35°C)
10 km
(-30°C)
2.3 km
(+20°C)
tropopause
17 km
(-75°C)
-14°
-10
-6
-2
+2°
+4
+6
20°
40°
60° N
N = nadir angle

Fig. 3.7

measurements, made at different nadir angles (and different scans) over the same point. They found a decrease of the equivalent temperature of channel 2 by approximately 5^{o} over the cloudless Sahara desert if the nadir angle increases to about 55^{o}. These results correspond to our calculations for a relative humidity of 5 % for atmosphere 3 (Fig.3.7). The radiation flux intensity in the spectral region of channel 1 shows at cloudless sky a larger nadir angle dependence for a dry troposphere than for a moist troposphere. With increasing cloud height this effect overturns (Figs.3.6 and 3.7). It might be seen directly from Fig.3.5 (radiation diagram for channel 1) that in case of cloudless sky an increase of the path lengthin each layer will have a larger effect in the outgoing radiation for a dry troposphere (here 10 %) than for a saturated troposphere. In the latter case, the curve has such a steep slope that an increase of the path length will have a very weak effect only while it will have a strong effect in the case of the 10 % troposphere. Correspondingly the overturn of the nadir angle effect may be explained for very high clouds.

For the channel 2 radiation data the nadir angle dependence increases with increasing relative humidity of the troposphere. This also may be explained with the help of the radiation diagrams in Fig.3.5. The vertical distance between the lines $w \approx 0.1$ and 1.0 in the diagram is much smaller than the distance between 1.0 and 10.0. An increase of the path length of an oblique beam will therefore effect a much stronger variation of the upper limiting line of the area in the diagrams for the case 100 % than for 10 %.

3.4 : Method of determination of surface temperatures and mean relative humidities

It has been shown, that the intensity of emerging radiation is mainly influenced by the temperature of the lower surface of the atmosphere (clouds and/or ground) and by the relative humidity of the atmosphere particularly of the middle and high layers of the troposphere. This holds for the spectral region of channel 1 as well as channel 2. Thus, diagrams can be constructed, which deliver the surface temperature and relative humidity as determined by the intensities or equivalent temperatures of both these channels. Basic assumptions of such diagrams are the vertical structure of the atmosphere (lapse rate and humidity gradient) and the viewing nadir angle.

3.41 : Evaluation diagrams

From radiation flux calculations for the intensity regions of the channels 1 and 2 at the model conditions of the atmospheres 1 and 3 evaluation diagrams were designed with relative humidity and surface temperature as ordinate and abscissa respectively and isolines of the equivalent temperatures as parameters. Figs. 3.8 - 3.10 show such diagrams for the nadir angles N = 0^{o}, 40^{o}, and 50^{o}. The slight curvature of the isolines for channel 2 again confirms that water vapor does hardly influence the intensity of radiation in the spectral region of channel 2. The isolines for channel 1 (dashed) however turn from the vertical into the horizontal direction. In the section with horizontal direction of those curves the cloud height and the water vapor content below the level of the indicated temperature may change without any influence on the radiation flux measured in channel 1. In the section with vertical direction of the curves the water vapor amount between the satellite and the cloud surface is extremely small and the only influence on the radiation flux intensity is effected by the (low) surface temperature of clouds. In that part of the diagram it may happen that the isolines of both measured equivalent temperatures do not intersect nor coincide. It is easy to be seen that even small errors of the measurements will lead to this consequence.

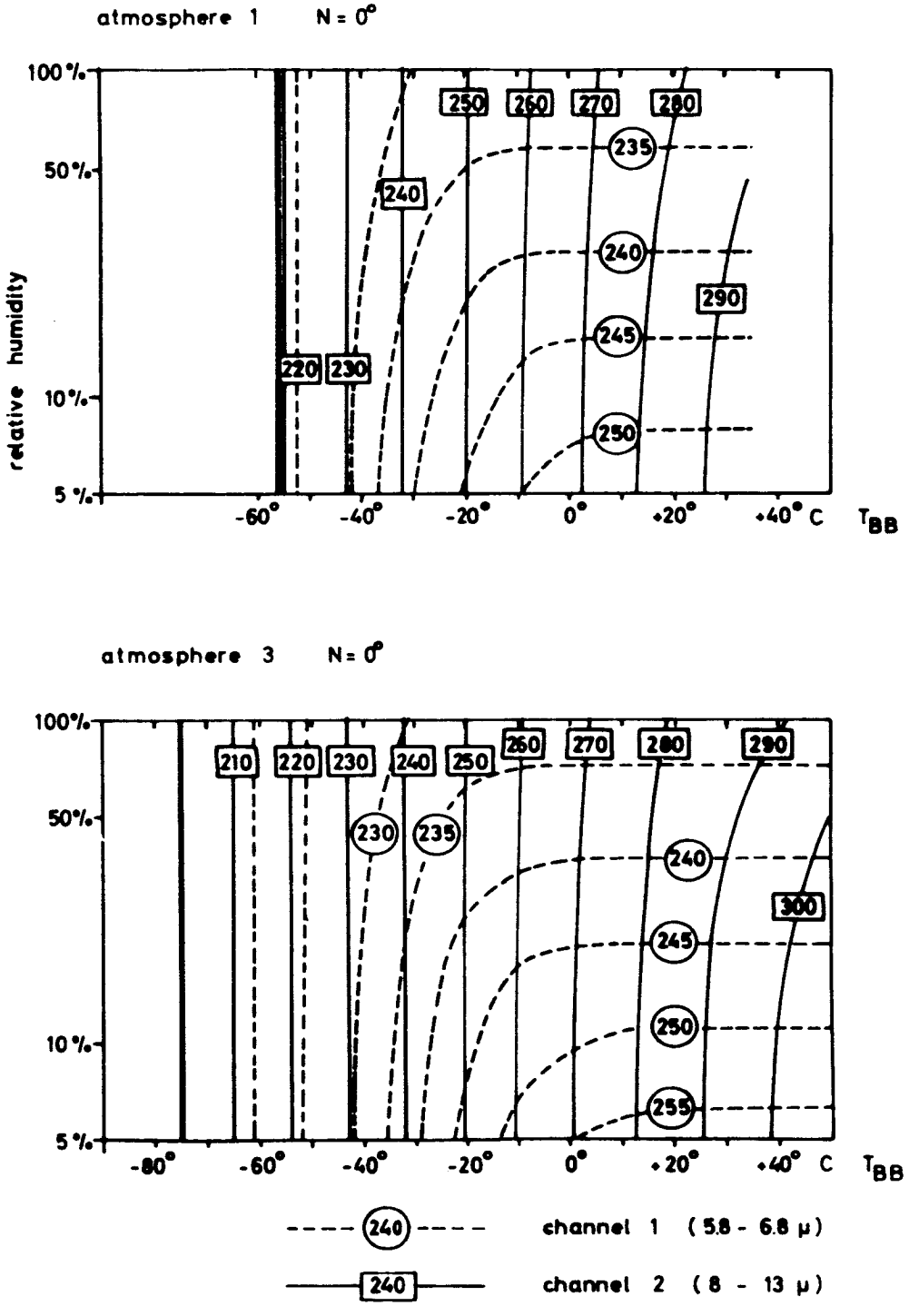

Fig. 3.8 : Evaluation diagrams for the nadirangle N = 0°

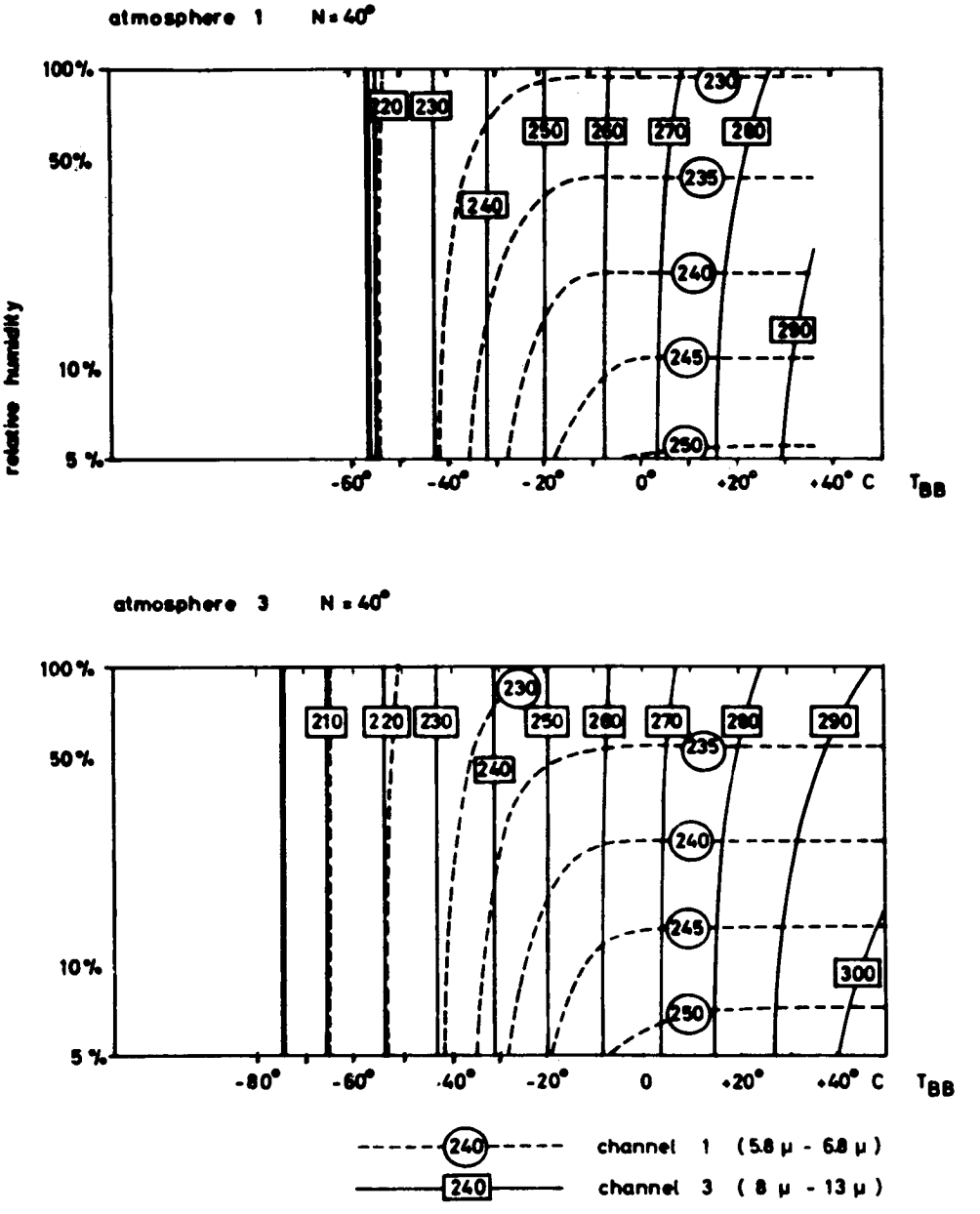

Fig. 3.9 : Evaluation diagrams for the nadir angle N = 40°

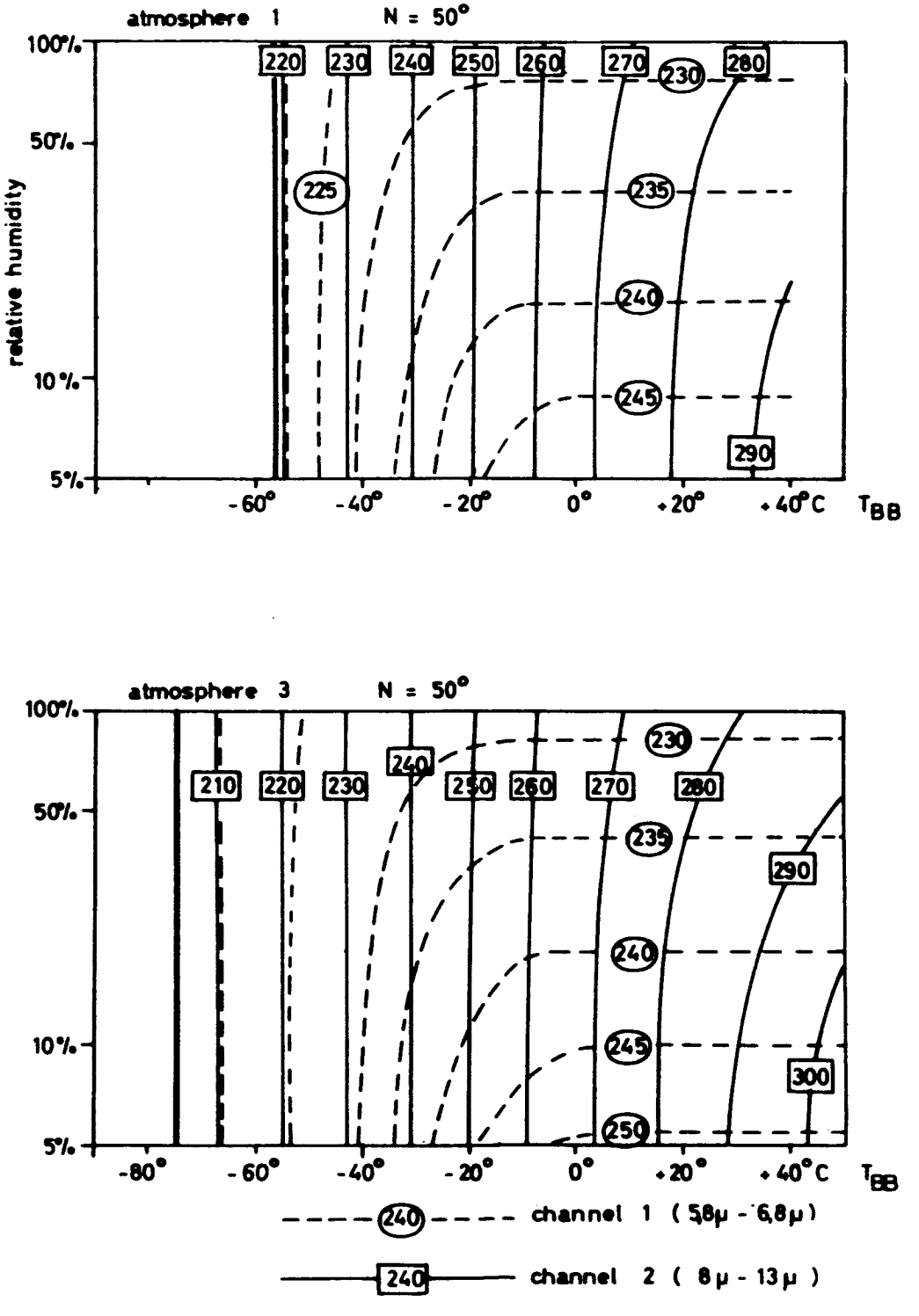

Fig. 3.1o : Evaluation diagrams for the nadir angle N = 5o°

Another source of errors may arise in the right upper part of the diagram where points of intersection may only be found for relative humidities higher than 100 %. Then a determination of the relative humidities has no sense for the evaluation of radiation data. In such cases the real water vapor amount in the upper troposphere and lower stratosphere may be higher than it is assumed in the models or the temperature of the stratosphere is lower than in our models. Additionally such errors may arise by the extremely high errors of measurements (chapter 3.42.1). In order to include cases into our evaluation method where the ground temperature is higher than that of the air adjacent to it the diagrams have been extrapolated to higher temperatures. In doing so the atmospheric profile remained unchanged. Then according to Equation 3.4 the increase of outgoing radiation flux is determined by the product of the increase of the radiation intensity emitted from the ground times the transmissivity of the whole atmosphere (first term of Equ.3.4). For practical use the evaluation procedure has been programmed for a computer (IBM 7090). The computer first separates the radiation data into 3 nadir angle groups (0° - 30°, 31° - 45°, $> 45^\circ$) and seeks for each simultaneous pair of equivalent temperatures of the channels 1 and 2 the values of the relative humidity and the surface temperature which are the coordinates of the points of intersection of the correspondend isolines. For such cases which are located outside the diagram regions (no intersection etc.) particular symbols will be given by the computer as evaluation results.
In order to estimate the errors resulting from the choise of different model atmospheres for the determination of surface temperatures and relative humidities from radiation data it has been assumed for instance that the channels 1 and 2 have measured simultaneously the following equivalent temperatures :

channel 1 : $237.5^\circ \pm 2.5^\circ$ K
channel 2 : $272.5^\circ \pm 2.5^\circ$ K

The evaluation procedure gives the following surface temperatures and relative humidities for the exact values of T_1 = 237.5°K and T_2 = 272.5° K :

nadir angle :	0^{o}	40^{o}	50^{o}
atmosphere 1	$+ 9^{o}$ 40 %	$+ 8^{o}$ 30 %	$+ 8^{o}$ 25 %
atmosphere 3	$+ 8^{o}$ 50 %	$+ 7^{o}$ 37 %	$+ 7^{o}$ 27 %

The differences between the results which are due to different model atmospheres are small compared with those of measurements. The surface temperatures determined for model atmosphere 3 are somewhat lower ($1 - 2^{o}$) than those for model 1 while the resulting relative humidities are higher. The former fact can be explained by the different ozone and carbon dioxide amount between the emitting surface and the satellite. In model 3 the emitting surface is at lower pressure than in model 1. From that results a lower carbon dioxide amount between emitter and satellite and consequently a lower temperature to produce the same intensity of the emerging radiation flux (channel 2). Similarly the effective water vapor amount will be smaller in the case of model 3 than in model 1 which is due to the pressure correction. Additionally the different tropopause temperatures influence the intensity of the outgoing radiation flux (see chapter 3.42.2.c). So a higher relative humidity than that of the model 1 is required to yield the same intensity of outgoing radiation flux. The assumed error of measurements of $\pm 2.5^{o}$ leads to errors of the surface temperatures of again $\pm 2.5^{o}$. The error of the relative humidity ranges between $\pm$ 10 % and $\pm$17 %. It increases with increasing relative humidity.

3.42 : Discussion of errors due to deviations of the actual atmosphere from model conditions

3.42.1 : Accuracy of measurements

The absolute accuracy of measurements was determined by the NASA laboratories and has been found to be $\pm 5^{o}$ for channel 1 and $\pm 4^{o}$ for the channels 2 and 4 for the mid-range of target

intensities. Assuming that mid-range of target intensities for channel 1 is 0.4 W/m^2 and for channel 2 75 W/m^2 (Fig.3.11) the absolute accuracy of measurements of intensities is then $\pm$ 0.08 W/m^2 and $\pm$ 6.5 W/m^2 respectively. As it may be seen with the help of the example drawn into Fig.3.9 the accuracy of radiation data given in form of equivalent temperatures will decrease with decreasing target intensity. For instance - from an intensity of 0.22 $\pm$ 0.08 W/m^2 measured in channel 1 an equivalent temperature may be determined ranging between 213.5°K and 231.0°K. From this point of view all measured radiation data with such low equivalent temperatures may be considered to be not useful for our interpretation.

BANDEEN, KUNDE, NORDBERG, and THOMPSON (1963) discussed in a very detailed study many errors which may adhere to TIROS III radiation data. These are

a) errors in the calibration, due to degradation of the response after launch. To take into consideration these errors they developed a correction method with the main assumption that the upward outgoing radiation flux emerging daily from the entire system earth - atmosphere does not change during the time of TIROS III measurements.

b) errors by system noise. These errors increase if the ratio response-noise decreases. Using measurements of the space noise level they developed also a correction method.

c) errors, which are due to inaccurate agreement of the field of view of the channels. The instantaneous response field of channel 1 may up to 0.15 parts of the area lie outside of the response field of channel 2 and vice versa.

Since these investigations became known to us only during the course of our own investigations they will be neglected here. The degradation effect was not considerable until orbit 114. The influence of the system noise will be diminished by the use of radiation data averaged over squares of 2 degrees geographical longitude and latitude.

3.42.2 : Deviations from model conditions

According to the evaluation method described above relative humidities and surface temperatures (clouds or ground) will be

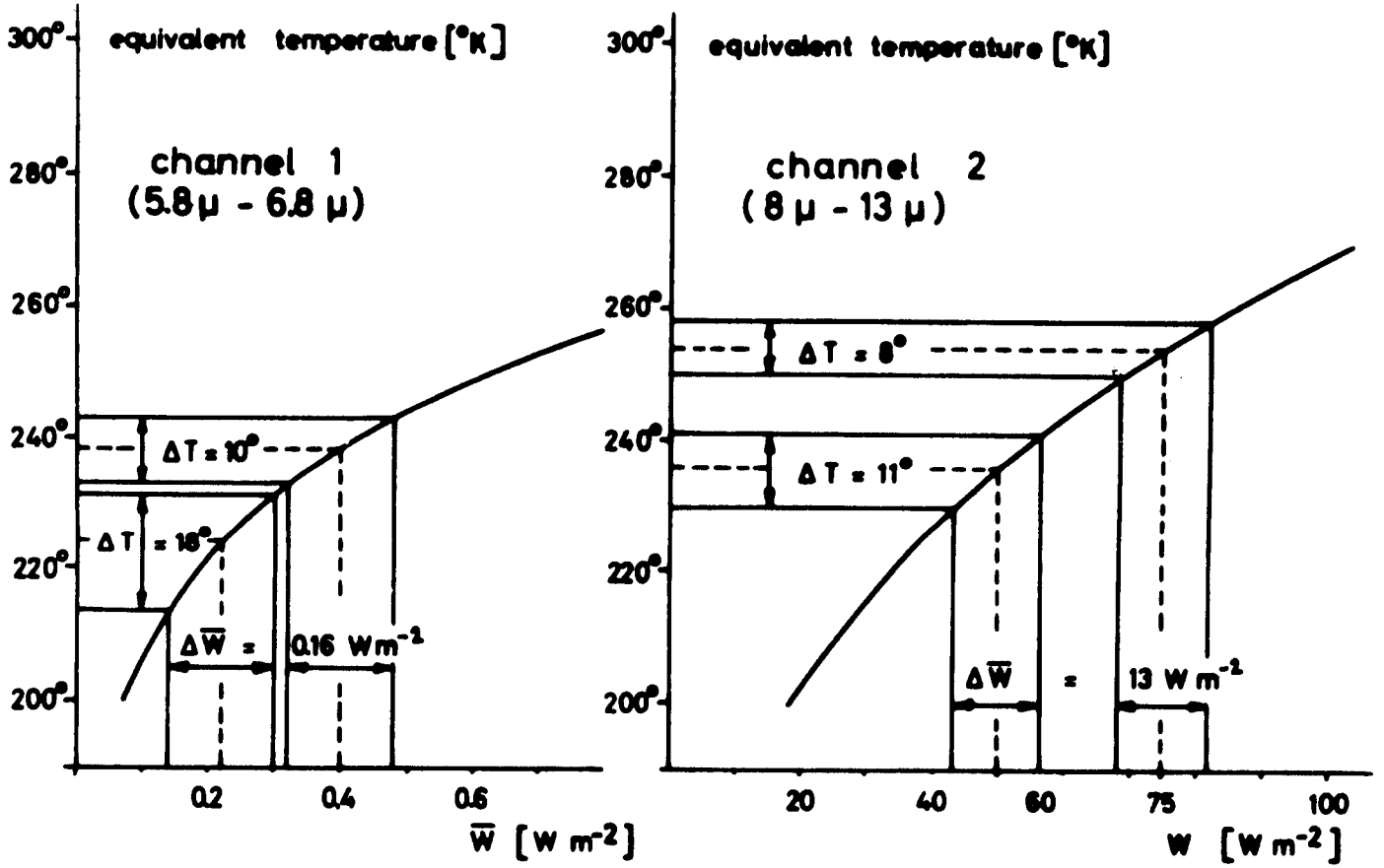

Fig. 3.11 : Calibration curves of channels 1 and 2

determined from the TIROS III radiation data. Hereby standardized atmospheric conditions with fixed tropopause heights, tropopause temperatures, and constant lapse rate and relative humidity are assumed to be given. Since in the most cases the actual atmospheric profiles of temperature and humidity will deviate from those models the influence of some specific deviations on the intensity of the upwelling radiation will be investigated here.

a) Ideal inversions. From temperature inversions above surfaces(like the ground inversions during cloudless nights) may arise errors in the determination of surface temperatures. For an estimation ideal inversions above the ground (cloudless sky) have been assumed what means a temperature difference between the ground and the air adjacent to it. No change of the temperature profile has been assumed but ground temperature differences up to a difference of - 20° C. In that case only the first term at the right hand side of Equ.3.4 will change its value. The equivalent temperatures which were determined for such an ideal ground inversion of - 10° and - 20° are compared with those computed for the same models but with cloud levels in the heights which correspond to the ground temperature in the original model.

Table 3.5 : Equivalent temperatures of emerging radiation intensities determined for ideal inversions and cloud levels in heights (normal case) corresponding to the assumed ground temperature.

difference between temperatures of air and ground	rel. hum. (%)	atmosphere 1		atmosphere 3	
		inversion	normal case	inversion	normal case
- 10°	100	269.9	269.5	284.0	283.2
	25	272.0	271.5	288.0	287.6
	5	272.5	272.0	290.0	289.8
- 20°	100	263.9	262.4	280.7	279.4
	25	264.2	263.0	282.0	280.1
	5	265.2	263.6	282.5	281.0

The equivalent temperatures of the radiation intensities calculated for the inversion case are somewhat

higher than those calculated for cloud surfaces in the correspondend heights, but the deviations are not higher than 2.0°. They even diminish if similar comparisons were carried out for inversions above cloud levels. Additionally radiation flux calculations were carried out assuming positive temperature differences close to the ground. They may occur with cloudless sky during day time due to strong isolation. In Fig.3.12 curves show the dependence of the equivalent temperatures of the emerging radiation flux on the difference between the temperatures of the ground and the air adjacent to it. For instance a temperature difference ground - air of - 20° may arise for model atmosphere 1 (100 %) a decrease of the intensity of the emerging radiation flux which corresponds a decrease of the equivalent temperature of - 12° C. In such a case the ground temperature determined from channel 2 radiation data will be 8 degrees higher than in reality.
The slope of that straight lines is determined by the transmissivity of the whole atmosphere for theradiation emitted from the ground (Equ.3.4).

b) Tropospheric layers with different relative humidity

Our model assumption of a constant relative humidity will not be realized in the most cases. Therefore some schematical variations of the model will be studies here. In the first case 1.55 km thick layers with another relative humidity than that of the remaining entire troposphere are assumed to be embedded in a troposphere with constant relative humidity (10 %, 25 %, 50 %). Results are given in Fig.3.13 in form of deviations of the apparent relative humidities determined under the assumption of constant humidity. The calculations were carried out here for model atmosphere 1. In Fig.3.13.a, saturated layers of 1.55 km thickness are assumed above cloud surfaces and above the saturated layers a constant relative humidity (10 % and 25 %). The points design the cloud surface height. In Fig.3.13.b the calculations are based on the assumption of a saturated (curves 1) or very dry (10 %, curves 2) layer (1.55 km thick), embedded in an

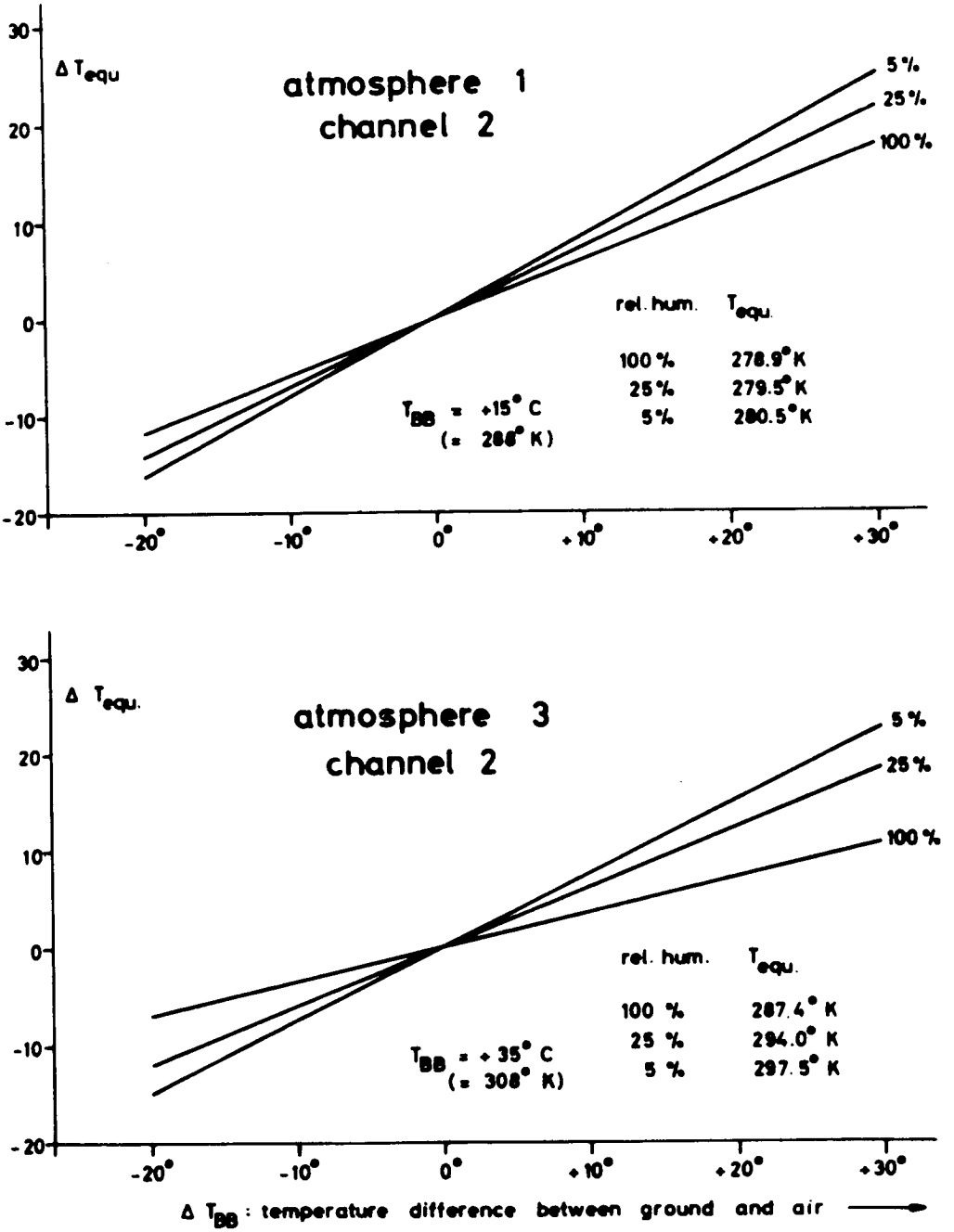

Fig. 3.12 : (see page 37)

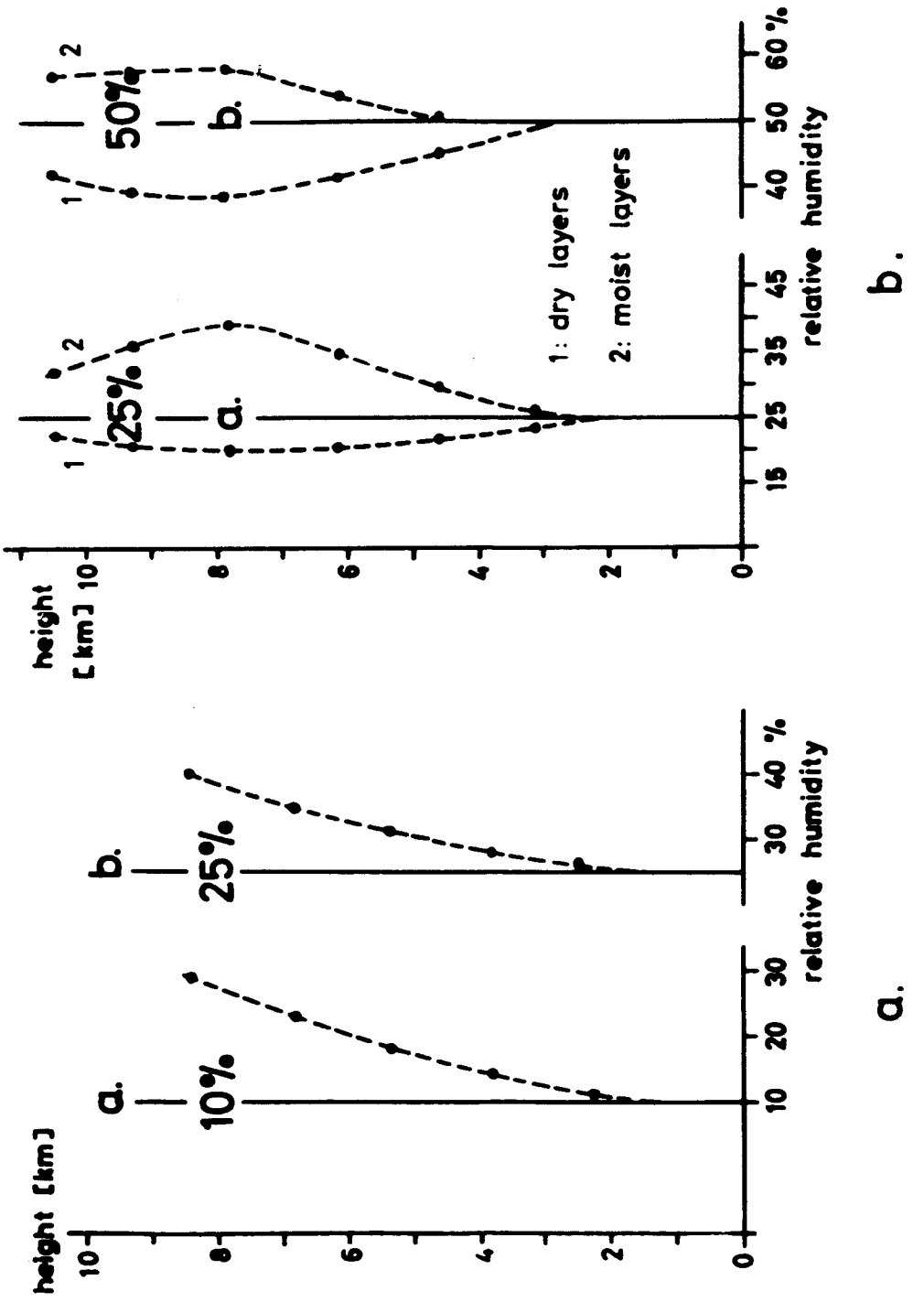
height [km]
10
8
6
4
2
0
a.
10%
b.
25%
10
20
30
relative humidity
30
40 %
a.
b.
25%
50%
1
2
15
25
35
45
relative humidity
40
50
60 %
1: dry layers
2: moist layers

Fig. 3.13

atmosphere with constant relative humidity (25 % and 50 %). The points give the height of the middle of the layer. The curves in Fig. 3.3 b show the largest deviations from the mean value at heights of about 8 km which correspond to the height where the variation of the transmission $\frac{\partial \bar{T}}{\partial h}$ has its maximum (see Fig.3.3). Both examples show that variations of the humidity and temperature in the lower troposphere below 2 km do not influence the radiation data of channel 1. If temperature inversions exist above very high clouds the interpretation of channel 1 data may lead to large errors of the determined relative humidities.

c) Changes of the height and of the temperature of the tropopause

Since actual atmospheric temperature profiles can deviate from our standard models radiation flux intensities have been calculated for the same models but with schematic changes of the height and temperature of the tropopause. In doing so changes of the height result in changes of the temperature of the tropopause and of the lower stratosphere according to the lapse rate in the troposphere (see Fig.5.5 in MÖLLER & RASCHKE, 1963)*. The isothermal part of the lower stratosphere has been limited in the upper side by the stratospheric profile with the lapse rate of + 3°/km. The model stratifications of the water vapor, carbon dioxide, and of ozone have not been changed. The calculations have been carried out only for the vertical direction. Results of radiation flux calculations for channels 2 and 4 for tropopause temperatures which are 10° higher or lower than those of the standard models (this corresponds changes of the height by ± 1.54 km) do not show perceivable changes of the radiation flux intensities. That confirms that atmospheric ozone and carbon dioxide of those layers do not influence essentially the intensity of radiation flux in those spectral regions. Correspondend results of calculations for the spectral region of channel 1, however, give results which noticably deviate from results for the standard models. In Table 3.6

* See Appendix III, p. 85 of this report.

the differences between the intensities and between the corresponding equivalent temperatures of the radiation fluxes are given. They are calculated for the standard model 1 with changed temperature of the tropopause (indicated in the first column). Particularly for warmer tropopauses the deviations will be remarkable. They might be even larger as it is shown here if changes of the tropopause temperature are correlated (positively) with changes of the water vapor content in the lower stratosphere. In such cases which show extreme deviations from our standard models, relative humidities determined by the evaluation of radiation data will not only represent the upper troposphere, they additionally reflect conditions of the lower stratosphere. The accuracy of such evaluation will be much higher if some additional knowledge about the atmospheric profile is available. Particularly simultaneous radiation data of a channel in the region of the center of the 15μ - band of CO_2 (like that in TIROS VII) would give informations about the mean temperature of the lower stratosphere and of the upper most troposphere. Unfortunately, in TIROS VII that CO_2 channel has replaced the H_2O channel so that simultaneous measurements are not available.

tropopause temperature and height	rel. hum. (%)	N = 0°		N = 50°	
		$\bar{W}$ (W/m^2)	T_{equ}	$\bar{W}$ (W/m^2)	T_{equ}
- 45° C (9.2 km)	100	+ 0.041	+ 3°	+ 0.050	+ 4.3°
	25	+ 0.024	+ 1.3°	+ 0.031	+ 2.0°
	5	+ 0.013	+ 0.7°	+ 0.015	+ 0.7°
- 65° C (13.1 km)	100	- 0.003	- 0.2°	- 0.011	- 0.9°
	25	- 0.003	- 0.2°	- 0.003	- 0.2°
	5	- 0.001	- 0.0°	- 0.003	- 0.2°

Table 3.6 : atmosphere 1

Variations of the intensity of the outgoing radiation flux at variations of temperature and height of the tropopause.

d) scattered clouds

If the radiometer of channel 2 views areas with scattered clouds the measured radiation intensity will be emitted

partly from the cloud surfaces and partly from the ground (or surfaces of deeper clouds). Temperatures which were derived from those data are therefore between both temperatures. If no other information of the cloudiness is available they have to be interpreted as surface temperatures of intermediate clouds.
Additionally the presence of very thin clouds which transmit infrared radiation emerging from deeper layers complicates strongly the interpretation of surface temperatures. SHAW and GATES (1960) tried to derive values of the transmissivity of thin clouds from measurements of the solar radiation through clouds and between the clouds. But their values can not easily be used because the thickness of clouds is unknown and very thin veils of clouds which are not visible for the eye may yet influence the transmission of infrared radiation. Such influences are known from measurements of the atmospheric down coming radiation.
Therefore the interpretation of channel 2 radiation data we used additional data available from TV - pictures on the cloudiness and albedo values which were determined for measurements of the channels 3 and 5.

e) nonblackness of emitting surfaces

Some authors would show that the ground as well as clouds may not emit completely like black bodies. LYON and BURNS (1962) e.g. measured for obsidian, granite and dunite a mean emissivity of 0.8 at 350° K in the spectral region of channel 2. BUETTNER derived from TIROS III radiation data of channel 2 above the cloudless Sahara and the Mediterranean Sea mean emissivities of 0.67 and 0.91. Both values are based on different assumptions on the temperature difference between the sand surface in the Sahara and the air adjacent to it. BELL (1962) and KISLOVSKIJ (1962) found from measurements and calculations a typical band structure of the spectral emissivity and reflectivity of water surface. In the spectral region of channel 2 the emissivity of a water surface might be 0.97 _ 0.98. DEIRMENDJAN (1960) found that clouds also are not completely black. Thick clouds, however, should

not transmit infrared radiation.
Surface temperatures, therefore, which were determined from radiation data of channel 2 at cloudless or completely overcast cases in the field of view of the radiometer have to be considered as 'radiation temperatures'. They are somewhat lower than the actual surface temperatures.

4: Evaluation of TIROS III Radiation Data

In the following investigations, listed radiation data from all 5 channels of TIROS III over the whole Atlantic Ocean during orbit 61 (July,16,1961; 15.14 - 15.51 GMT) were used. For a more convenient handling in the analysis, these data and the nadir angle and the geographic coordinates of each scan spot have been punched into punching charts. Computer programs have been set up first to compute albedo values for any single scan spot, then averages of all radiation and albedo data over quadrants of 2 · 2 degrees geographical longitude and latitude and finally correlation coefficients of these radiation data. All these calculations have been carried out on an IBM - 7090 computer.

4.1: Geographical Distribution of Emerging Radiation Measured from TIROS III

For the representation of the listed data in geographical maps all measured values within quadrants of 2 · 2 degrees longitude and latitude have been averaged arithmetically. In doing so some errors can enter into our evaluation procedure.

a) As it can be seen from television pictures such quadrants of 2 · 2 degrees longitude and latitude are not complete overcast nor cloudless in the very most cases. So measured values where the field of view of the radiometer was complete overcast or only partly cloudy, have been averaged with those measured above complete cloudless areas. The averages are weighted means of all measured values where the numbers of measurements above cloudless or cloudy regions are the weighting factors. The

amplitude of that error however may not be too large because of the wide aperture angle of the radiometers.

b) During the phase of alternating mode of the measurements some areas may be viewed by the radiometers at small and later at larger nadir angles or vice versa. The nadir angles are averaged for 2 · 2 degrees area in the same manner as the the radiation quantities. Then the reduction because of the averaged radiation values was performed with the averaged nadir angles. Therefore, the averages of such areas contain a small error because of the inhomogenity of the outgoing radiation flux and nadir angle (see chapter 3.3). Since the absolute accuracy of measurements is very low (chapter 3.42.1) these errors may not prevail upon those of the measurements.

4.11 : Radiation Data of Channels 1, 2, and 4

In Figs.4.1, 4.2, and 4.3 are plotted isolines of the equivalent temperatures of the emerging infrared radiation measured in the intensity regions of channels 1, 2, and 4.
Channel 1 viewed 'warm areas' especially at 20° latitude at both sides of the equator. These areas do not coincide exactly with warm areas viewed by the channels 2 and 4. Only areas with very low temperatures viewed by channels 2 and 4 coincide with those viewed by channel 1. This is due to the radiation of high clouds sensed also by channel 1 because of the small water vapor content on top of very high clouds. Additionally the relative humidity in the upper troposphere above high clouds may be higher than that above cloudless regions.
A comparison of the maps of channel 2 and channel 4 radiation data confirms the excellent correlation between the measured values of both channels. This is due to the overlapping of the sensitivity regions in the range of the water vapor window where the intensities are high. From the 'cold areas' at the Northern and Southern borders of the measured area on overcast cloud field with partly high and cold clouds may be inferred. The radiation emitted from the water surface under cloudless sky may cause the warm fields at the equator and at 20° - 30°

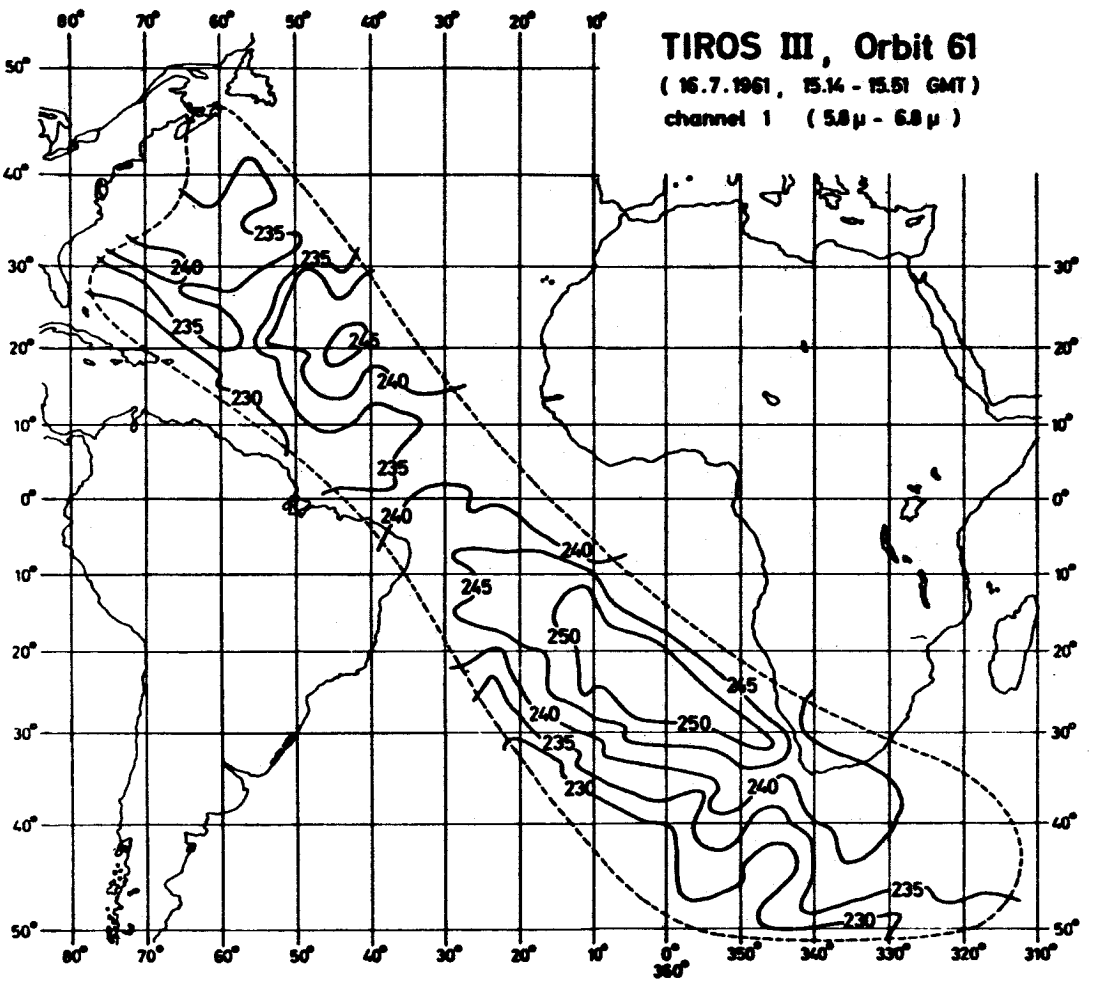
TIROS III, Orbit 61
(16.7.1961, 15.14 - 15.51 GMT)
channel 1 (5.8 μ - 6.8 μ)
80° 70° 60° 50° 40° 30° 20° 10°
50° 40° 30° 20° 10° 0° 10° 20° 30° 40° 50°
0° 350° 340° 330° 320° 310°
360°
235
240
235
235
240
230
235
240
240
245
250
245
240
250
235
230
240
235
230

Fig. 4.1

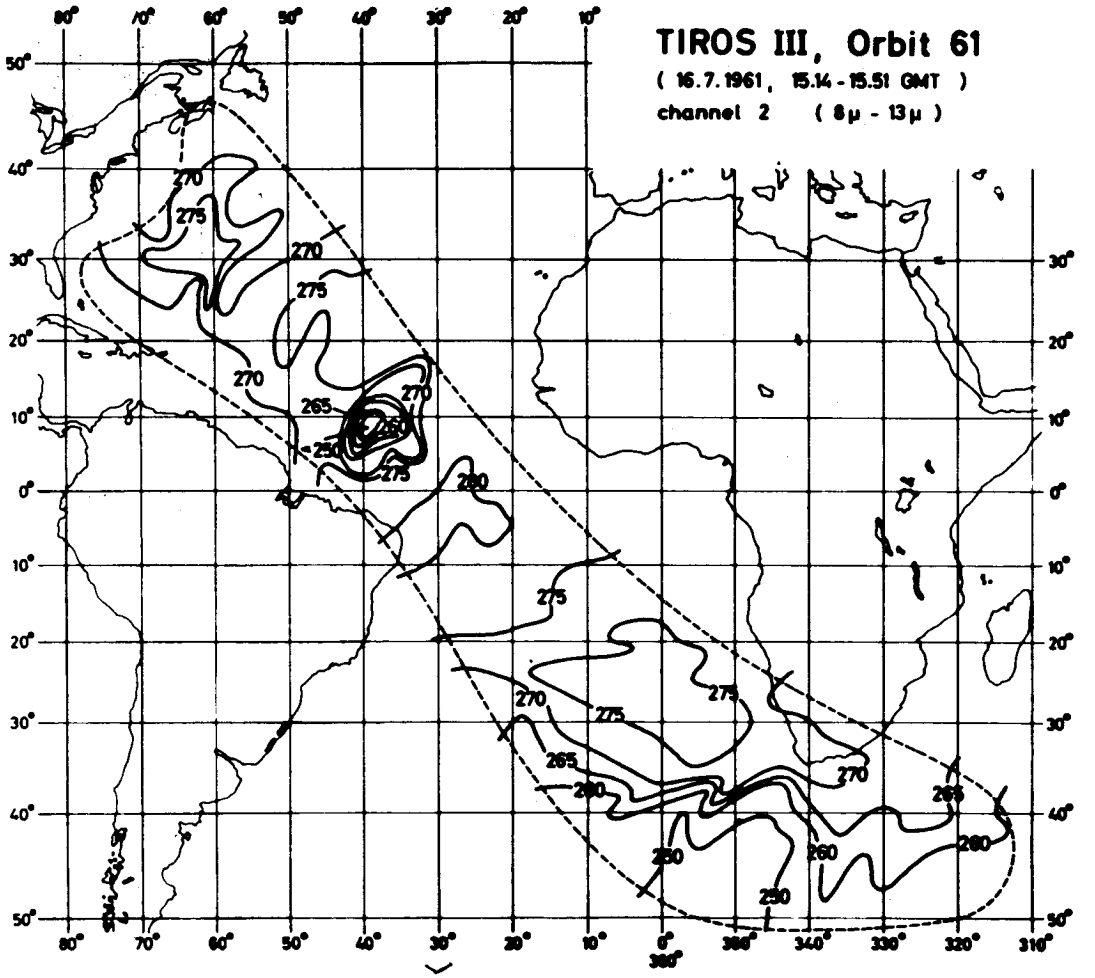

Fig. 4.2

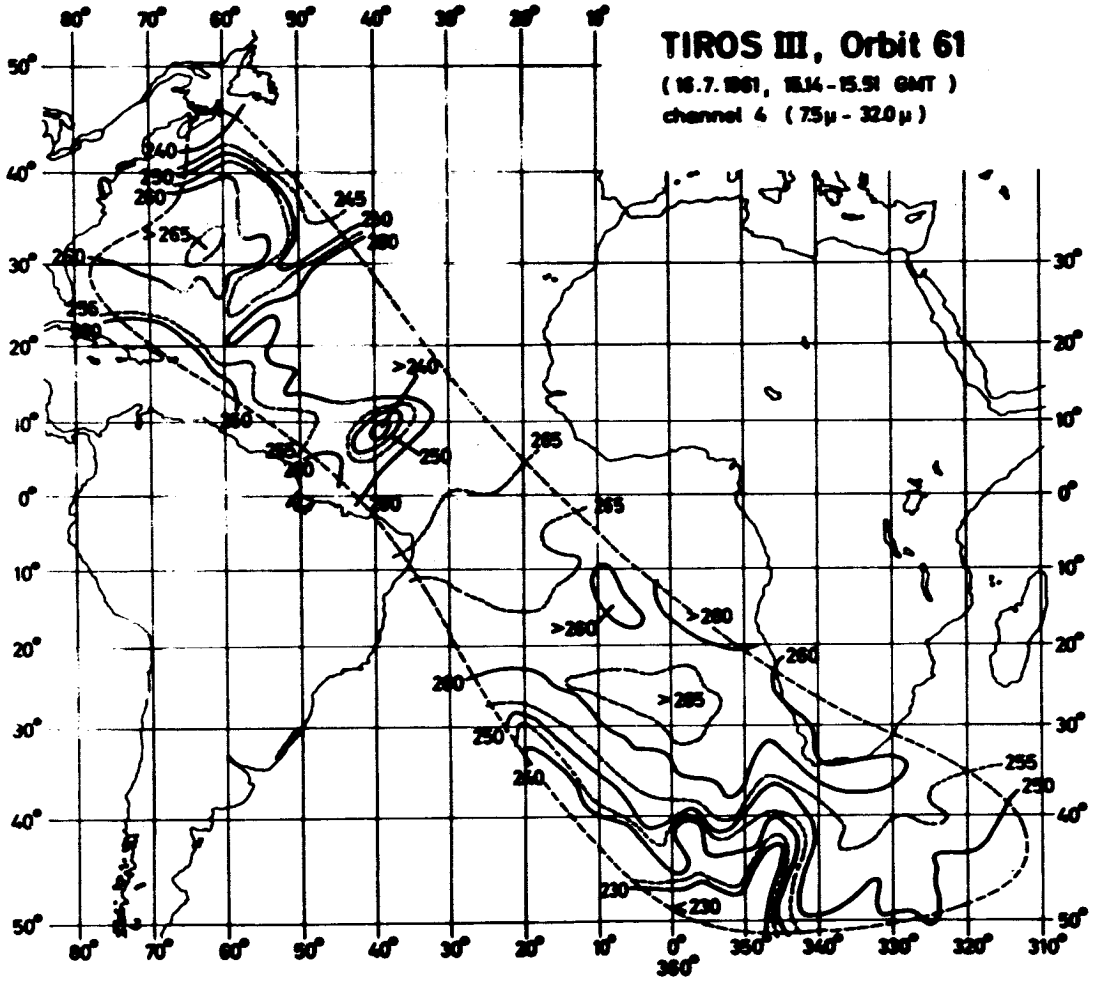

Fig. 4.3

Southern latitude. Because of the very high sensitivity of channel 4 in the region of the 15 - band of carbon dioxide the equivalent temperatures are lower than those of channel 2.

4.12 : Albedo

The sensitivity regions of the channels 3 and 5 cover the whole and a narrow part respectively of the solar spectrum reflected by clouds or the ground (Fig.2.2). Therefore albedo values calculated for those channels should allow to distinguish between cloudy (high albedo : 50 % - 70 %) and cloudless or partly cloudy regions (low albedo, dependent on the albedo of the ground and the cloud amount). Assuming that the spectral intensity of the solar radiation reflected and scattered from the system earth-atmosphere is equal to that of the incident solar radiation albedo values (values of a reflectivity of the system earth-atmosphere) can be determined according to Equ.4.1. The assumption is not absolutely correct because there is some extinction in the incident as well as in the reflected beam, effected by scattering and by absorption.

$$(4.1) \qquad A^{(3 \text{ or } 5)} = \frac{\overline{W}^{(3 \text{ or } 5)}}{\cos Z_{\odot} \cdot \overline{W}_{\odot}^{(3 \text{ or } 5)}}$$

$\overline{W}^{(3 \text{ or } 5)}$: radiation data of channel 3 or 5 respectively

$\cos Z_{\odot}$: cosine of the zenith distance of the sun at the place given by the coordinates of each scan spot.

$\overline{W}_{\odot}^{(3 \text{ or } 5)}$: incident solar radiation in the sensitivity regions of the channels 3 or 5 respectively. Using the spectral intensities derived by JOHNSON (1954) for the solar radiation incident onto the earth's atmosphere the values for $\overline{W}_{\odot}^{(3 \text{ or } 5)}$ are 765.5 W/m^2 and 101.6 W/m^2 respectively.

A computer program has been set up to calculate the albedo values according to Equ. 4.1 from the geographical coordinates of each scan spot, The declination of the sun, from the time of

the scan (assuming here a mean constant spin rate of the satellite) and from the measured radiation data. The results are given in form of isolines in Fig.4.4. Unfortunately due to a strong degradation of channels 3 and 5 the albedo values are very low. Particularly above the cloudless sea surface albedo values of at least 5 - 10 % should be expected instead of albedo = 0%. Above clouds the real albedo may be about three times higher than those derived from the given radiation data. Neglecting the extinction can not have such a strong effect. Since albedo values determined from the radiation data of channel 5 are yet somewhat lower than those from channel 3 only a map of albedo from channel 3 is given here.
The cloud systems which might be derived from the channel 2 radiation coincide with areas with relative high albedo. But conclusions from albedo values on the cloudiness (VIEZEE and DAVIS; 1963) are not possible because of the improbable data of channel 3 and channel 5.

4.2 : Surface Temperatures and Relative Humidities Determined from Channels 1 and 2

Using the evaluation diagrams, discribed in chapter 3, surface temperatures and relative humidities of the upper troposphere have been determined from the radiation data of the channels 1 and 2 which were averaged over squares of 2 · 2 degrees longitude and latitude. For that evaluation procedure a computer program has been set up in which these values were divided into two latitude groups and additionally in three nadir angle groups (0° - 29°, 30° - 45°, 46° - 60°). The first latitude group covers all radiation data from latitudes larger than 40 degrees North and South, and the second one all data between 40 degrees North and South. Assuming the model atmospheres 1 and 3 be representative for these latitude zones, surface temperatures, and relative humidities have been determined with the evaluation diagrams calculated for the nadir angles 0°, 40°, and 50° (chapter 3.41) for both model atmospheres. This part of the evaluation is also included in the evaluation program. On that way the nadir angle dependence of the radiation data has been taken into consideration. The isolines for the nadir angles of measurements in Fig.4.5

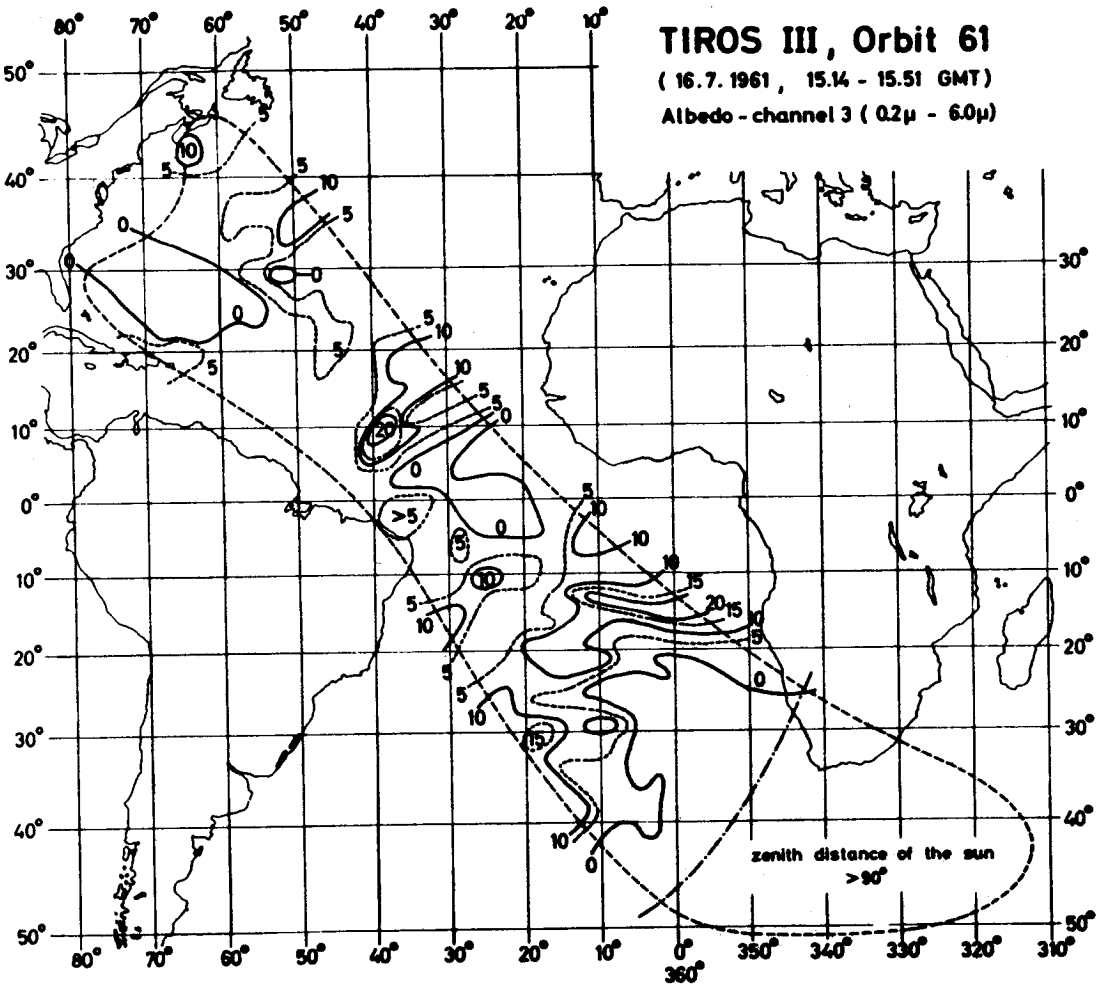
TIROS III, Orbit 61
(16.7. 1961, 15.14 - 15.51 GMT)
Albedo - channel 3 (0.2μ - 6.0μ)
zenith distance of the sun
>90°

Fig. 4.4

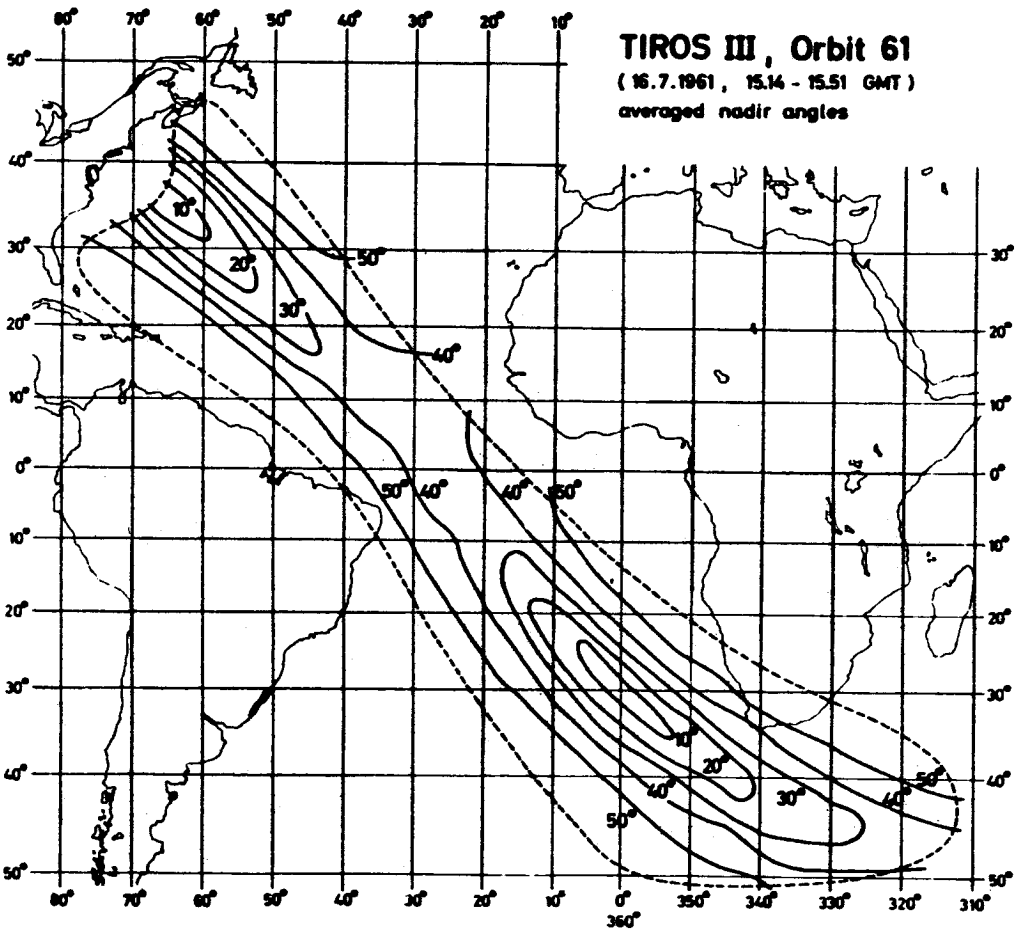
TIROS III, Orbit 61
(16.7.1961, 15.14 - 15.51 GMT)
averaged nadir angles

Fig. 4.5

show that most parts of the whole area were viewed by the satellite with nadir angles larger than 30°.

The surface temperatures and relative humidities of the upper troposphere again are presented in geographic maps (Figs.4.6 and 4.7). In order to compare the results of the evaluations with actual cloudiness, cloud fields which could be detected on television pictures of the orbits 59, 60, and 61 were plotted into a schematic weather map (Fig.4.8). Unfortunately TIROS III television pictures of the 16th of July cover only the Northern Atlantic Ocean (Catalogue of Meteorological Satellite Data - TIROS III TV-Cloud Photography; 1962). Therefore no direct informations on the cloudiness above the Southern part of the area were available. The overcast sky at the Northern boundary indicated by narrow straight lines is connected with a low pressure area. Turning in Southern direction the cloudiness decreases rapidly. But no areas were found which were completely cloudless within squares of 2 . 2 degrees longitude and latitude.

Additionally in Fig.4.8 isolines of the mean sea surface temperature for the month July are given (U.S.Navy, 1953).

A comparison between Figs.4.6 and 4.8 shows that dense cloud fields well coincide with fields of the derived surface temperatures lower than +5°C. The very low temperatures north of 40° N may be due to the apparent increase of cloudiness with increasing nadir angle since in that regions no cloud field has been found on the TV pictures. In the area between 15° and 20° North and 35° and 55° West the surface temperatures between +5° and +12°C are low as compared with the climatic ocean surface temperatures. This may be due to the influences of scattered and partly very deep clouds. The cloud field at 40° West and 10° North again can be detected on all maps as a field of low equivalent temperatures or of high albedo. Turning in South-Eastern direction relatively high temperatures have been found near the equator (+15° - +18°C) and at 25° South (+10° - +13°C). If the atmosphere was completely cloudless surface temperatures of about +26°C and 18° - 20°C respectively ought to be found from radiation data. But the surface temperatures derived from TIROS III data are about 9° lower than the actual surface temperatures. Similar results

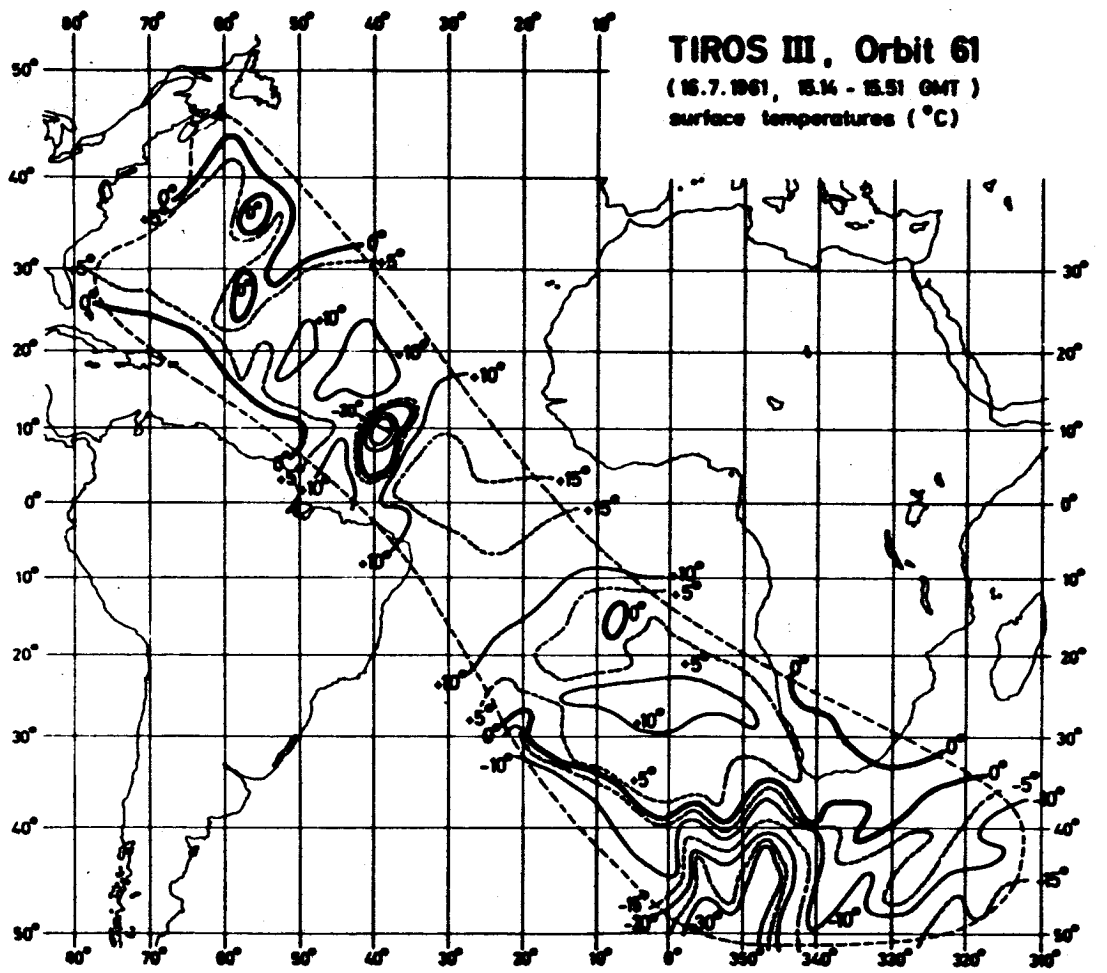
TIROS III, Orbit 61
(16.7.1961, 15.14 - 15.51 GMT)
surface temperatures (°C)

Fig. 4.6

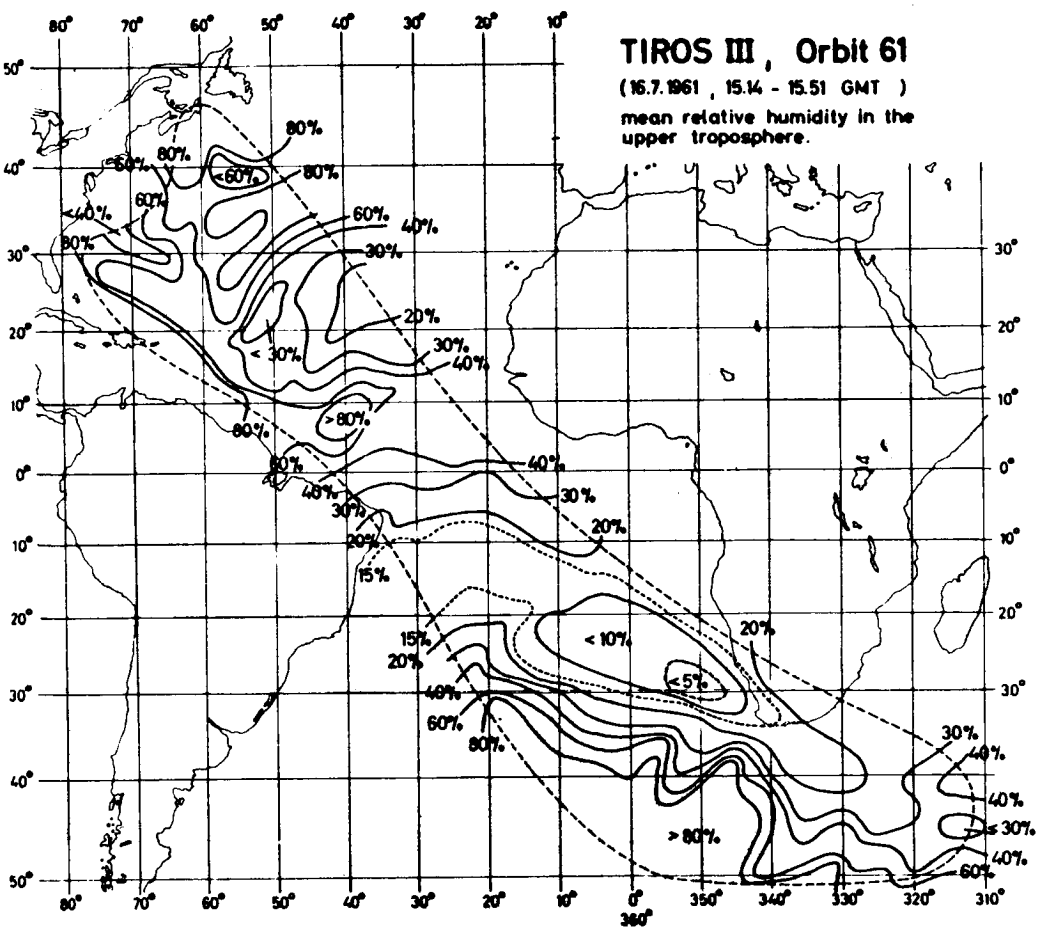
TIROS III, Orbit 61
(16.7.1961, 15.14 - 15.51 GMT)
mean relative humidity in the upper troposphere.

Fig. 4.7

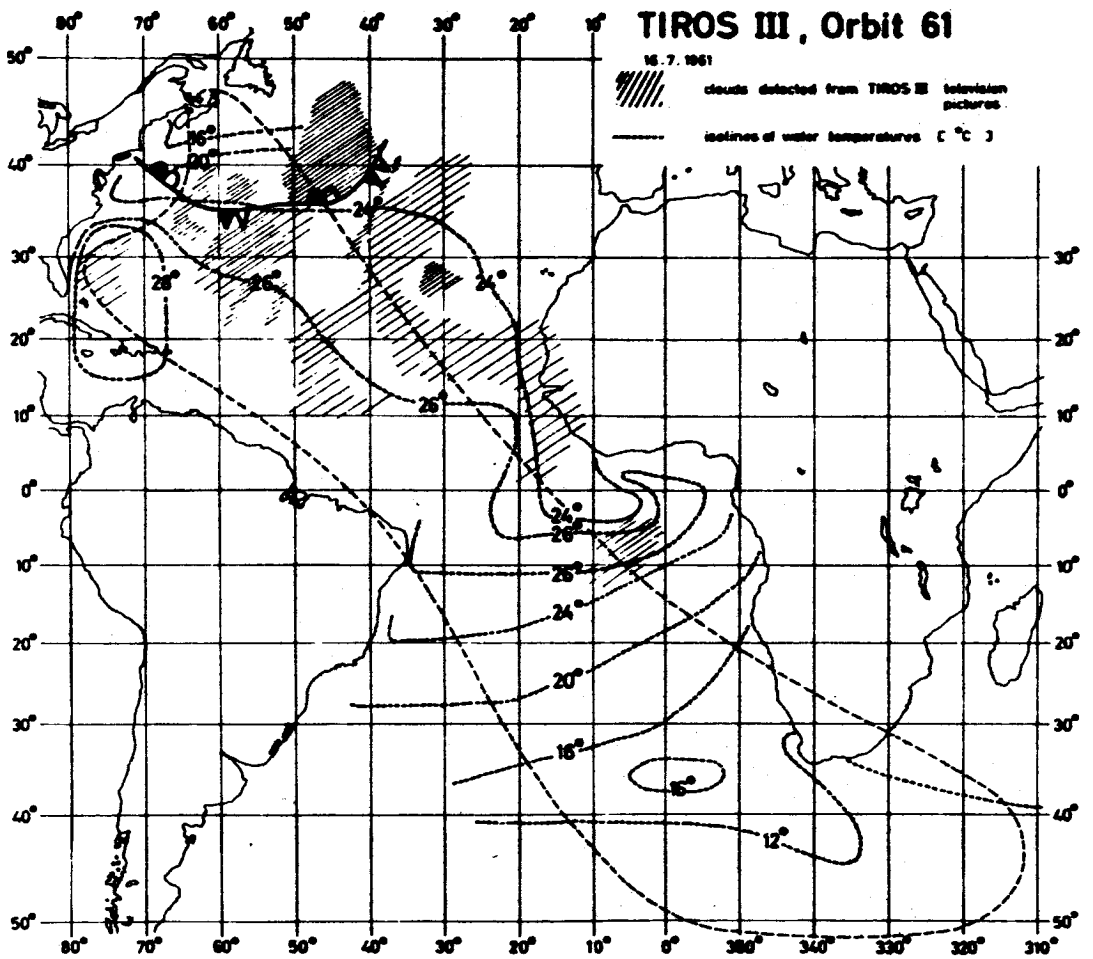
TIROS III, Orbit 61
16. 7. 1961
clouds detected from TIROS III television pictures
isolines of water temperatures (°C)
80° 70° 60° 50° 40° 30° 20° 10° 0° 350° 340° 330° 320° 310°
50° 40° 30° 20° 10° 0° 10° 20° 30° 40° 50°
28° 26° 24° 26° 24° 26° 24° 20° 16° 12°

Fig. 4.8

have been found by other authors for areas above sea and also above land which were completely cloudless. In order to verify these results similar evaluations have been carried out using the radiation measurements of channel 4. From that the same surface temperatures, mostly 1° higher, have been found. This difference can be explained with the following assumptions :

a) Thin and cold cirrus clouds or small but dense cumulus clouds or dust layers absorb partly the radiation emitted from the ground and deeper layers of the atmosphere. Such clouds can be present everywhere in the equatorial regions since they are seen on television pictures taken during orbit 59 approximately 5 degrees east of the area considered here. With other words, the sky may have been not completely cloudless, even when high thin cirrus clouds were not observed.

b) Owing to a degradation of the channels 2 and 4 the measured intensities might be somewhat lower than those incident on the aperture of the radiometer. For instance WEXLER (1964) could show that mean equivalent temperatures of both channels measured above a cloudless region of the midtropical Pacific Ocean decrease from orbits 1 - 5 to orbits 57 - 63 by about 8°.

These possibilities are not yet checked systematically.

On the map for the mean relative humidity of the upper troposphere a systematic humidity distribution at both sides of the equator can be seen which is due to the well known large scale circulation of the atmosphere. The ascending air of the troposphere in the equatorial zone (inner tropical convergence zone) is moist, while the subtropical belts (descending air) at about 25° North and South are very dry. This systematic distribution is disturbed by a high and cold cloud at 10° latitude North and 40° longitude West. There are no reports available to us of a hurricane in that place.

The areas with relative humidities larger than 80% coincide with areas of very low surface temperatures from which high clouds can be concluded. The water vapor mass between such high clouds and the satellite is too small to absorb completely the radiation emitted from the cloud surfaces. The humidity values of the layers above such high clouds however have some influence on the emerging radiation and can yet be derived from them. Errors of the relative humidities depend

mainly on

a) the errors of measurements (about ± 5°K)

b) the model assumptions on the water vapor distribution in the stratosphere. If the stratosphere is drier than the model atmosphere the derived mean relative humidities will be lower than an'actual mean relative humidity' and vice versa. The lower the relative humidity the lower will be these errors. As it can be seen in the evaluation diagrams there is an approximate logarithmic relation between the equivalent temperatures of channel 1 and the relative humidity of the troposphere.

c) the height and temperature of the tropopause.

In spite of all errors of the measurements the representations of radiation data and of the derived quantities give useful informations on the geographic location of cloud fields and of areas with a very dry or moist troposphere. But since only two measured radiation values can be used no informations on a moisture or temperature profile are available.

4.3 : Correlations between Simultaneous Radiation Data

4.31: Comparison of Radiation Data from Distinct Points

As it can be seen from the maps of equivalent temperatures and of the albedo values the data show a good correlation, which can be confirmed by a comparison of the data (again averaged over quadrants of 2 · 2 degrees longitude and latitude) from 12 points (Fig.4.9). In order to avoid influences of the nadir angle points are chosen that they all are viewed by the satellite under the same nadir angle of 30° - 40°. Their geographical coordinates are given in the Table.4.1.

Table 4.1 :

point	1	2	3	4	5	6	7	8	9	10	11	12
longitude	67°W	51°W	43°W	39°W	27°W	25°W	19°W	7°W	1°W	7°E	11°E	25°E
latitude	29°N	31°N	21°N	9°N	3°N	5°S	11°S	15°S	21°S	29°S	31°S	39°S

The profiles of the quantities shown in Fig.4.9 along the line given by the points of Table 4.1 show a quite similar behavior. The spatial variation of the equivalent temperatures of channels

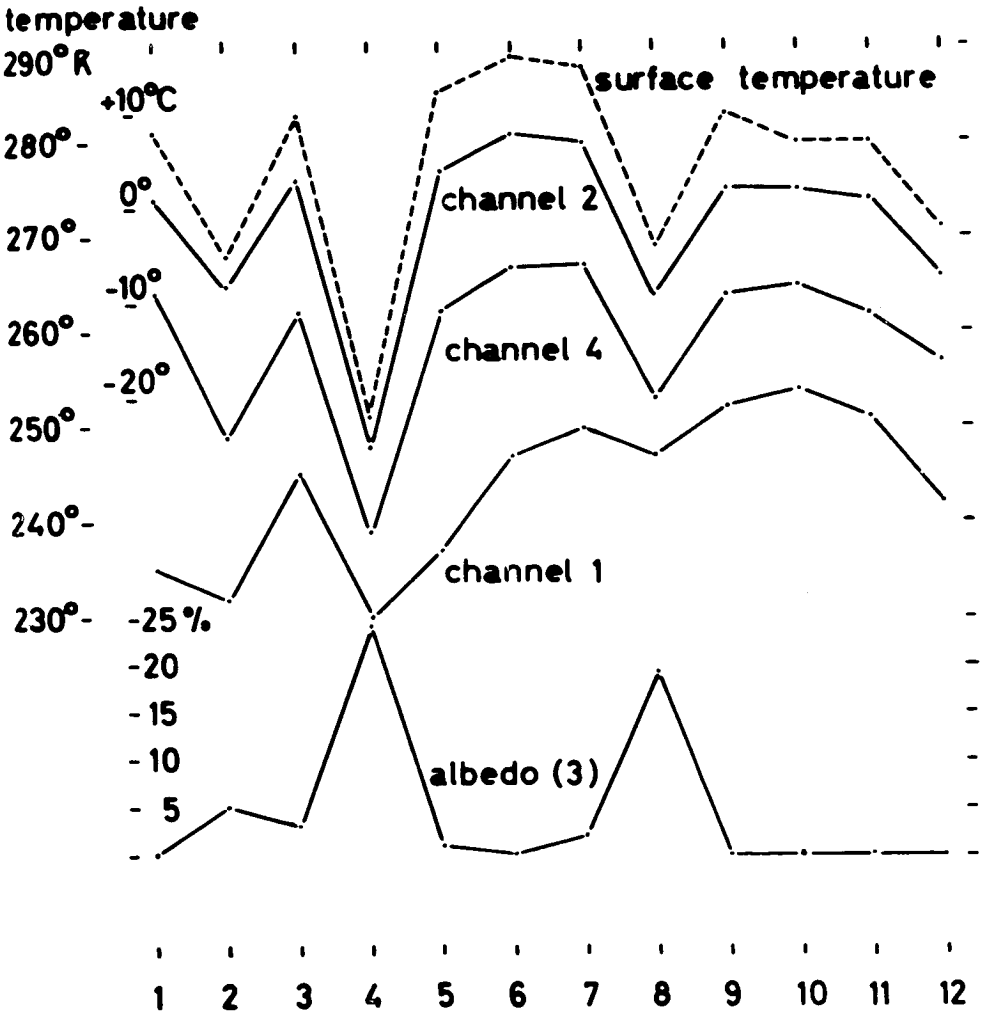

Fig. 4.9 : Comparison of radiation data from 12 points which were viewed with constant nadir angle (30^{o}-40^{o}) during orbit 61.

2 and 4 is nearly equal. The curve of the channel 1 values deviates somewhat from that of the other channels, particularly above cloudless regions or regions with very low clouds (points 5, 6, 9, 10). The spatial variation of the channel 3 albedo is nearly the mirror image of the variation of channel 2 effective temperatures. Above cloudy areas all infrared channels measured low equivalent temperatures while the channel 3 albedo is relatively high (points 2 and 4). But above cloudless regions, above which all infrared channels measure high effective temperatures, the albedo is nearly zero. This value is too low and due to the degradation of the channel 3.

4.32 : Correlations Between Single Measured Values

In the preceding chapter it has been shown that the radiation data of the channels 1, 2, and 4 show a good correlation. Similar results have been found with radiation data from the orbits 42 and 114 (MÖLLER & RASCHKE; 1963).* But that small number of samples may not be representative for statistical investigations of correlations.

Therefore linear correlation coefficients have been calculated from all data of the 3 orbits 61, 42, and 114 for the radiation data of the three infrared channels and the albedo values of channels 3 and 5 and the cosine of the zenith distance of the sun. In doing so the data have been divided into 4 nadir angle groups (0° - 30°, 30° - 40°, 40° - 50°, $>50^\circ$) and radiation data of a scan spot with equivalent temperatures lower than $200^\circ K$ have been omitted as not reliable. Additionally in all correlation coefficients of radiation data with albedo or cos $Z_\odot$ the data of the nightside (Fig.4.4) have been omitted as well. The correlation coefficients are given in Table 4.2.

A first glance on it shows that they confirm the results already found by comparisons of data from single points namely that the equivalent temperatures of channel 1 correlate with those of channel 2 and 4 narrower in orbits 42 and 114 than in orbit 61. This is a consequence of the synoptic distribution of clouds and cloudless areas. In orbits 42 and 114, there are large areas with high clouds and with cloudless sky over desert regions by which distribution the contrast bet-

* See Appendix III, p. 85 of this report.

	channel 1	channel 2		channel 4		albedo 3		albedo 5		cos $Z_\odot$	
		1	2	1	2	1	2	1	2	1	2
channel 1	XX	0.395 0.616 0.712 0.708	0.362 0.666 0.630 0.576	0.451 0.695 0.803 0.697	0.552 0.761 0.724 0.559	0.050 -0.358 -0.652 -0.373	-0.365 -0.245 -0.216 -0.212	0.135 -0.276 -0.553 -0.306	-0.409 -0.175 -0.124 -0.210	0.777 0.675 0.761 0.465	-0.420 0.550 0.496 0.336
channel 2	0.509 0.378 0.460 0.654	XX		0.968 0.979 0.971 0.945	0.860 0.898 0.895 0.907	-0.592 -0.818 -0.652 -0.373	0.198 -0.365 -0.348 -0.274	-0.551 -0.784 -0.673 -0.377	0.031 -0.328 -0.185 -0.164	0.385 0.475 0.603 0.245	0.231 0.662 0.657 0.143
channel 4	0.589 0.464 0.530 0.672	0.912 0.914 0.910 0.938		XX		-0.571 -0.808 -0.646 -0.265	0.005 -0.292 -0.342 -0.193	-0.546 -0.762 -0.649 -0.271	-0.130 -0.229 -0.178 -0.109	0.404 0.534 0.664 0.227	0.102 0.667 0.623 0.385
albedo 3	0.007 -0.096 -0.090 -0.044	-0.402 -0.619 -0.466 -0.140		-0.305 -0.506 -0.360 -0.053		XX		0.943 0.956 0.942 0.946	0.850 0.824 0.728 0.760	0.152 -0.317 -0.592 -0.736	0.583 -0.144 -0.104 -0.270
albedo 5	-0.079 -0.173 -0.128 0.058	-0.375 -0.586 -0.408 -0.050		-0.248 -0.512 -0.341 0.004		0.697 0.857 0.806 0.724		XX		0.295 -0.113 -0.465 -0.589	0.536 -0.363 0.118 0.057
cos $Z_\odot$	-0.380 -0.428 -0.311 -0.262	0.075 0.066 0.158 0.035		-0.061 -0.032 0.071 -0.046		0.240 0.125 0.053 0.025		0.130 0.022 -0.054 0.043		XX	

column 1 : orbit 42 (7.12 - 7.28 GMT)
column 2 : orbit 114 (7.20 - 8.14 GMT)
left side : orbit 61 (15.14 -15.41 GMT)

Table 4.2 : linear correlation coefficients

ween high and low surface temperature becomes parallel to the contrast betweeen moist and dry atmosphere. Orbit 61, however, does not show such strong differences in surface temperature and they are not accompanied by corresponding humidity differences.

From an independent consideration, it appears astonishing that there is at all a good correlation between channel 1 and 2 because they characterize humidity and surface temperature respectively. In order to show the details of the connexion, a counting diagram has been drawn which shows the frequency of channel 1 temperatures versus those of channel 2 (Fig.4.10). The numbers in the count diagram give the frequency of data in temperature intervalls of 5^{o} to 5^{o}. The curves in this Figure show the simultaneous change of the two equivalent temperatures when the surface (cloud) temperature changes. In the lower part of the diagram these curves are vertical indicating that there must be no correlation at all. When a good correlation between these temperatures is found it is caused by those situations where high clouds lower the temperatures of both channels simultaneously or by a good correlation between humidity and surface temperature (cloud height) depending on weather situations. But for such investigations radiation data of more orbits, perhaps divided into latitude groups according to climatic zones should be used. Such investigations will be continued in future.

According to our evaluation method, for those radiation data of channel 1 which lie on the left side of the 100 % - curve no relative humidities have been determined. Perhaps such low values particularly with high temperatures of channel 2 (260^{o} - 280^{o}K) might be caused by the large error and noise of measurements.

The correlation seems to increase with increasing nadir angle. The narrow correlation between the radiation data of the channels 2 and 4 as it has been show n earlier is due to the spectral sensitivity of both channels in the region of the water vapor window. But that correlation decreases slightly with increasing orbit number which could be due to a different dagradation of both channels. Again in a count diagram a large scattering can be shown of the measured values. The curves which give the dependence of T_{equ} (channel 2) from T_{equ} (chan-

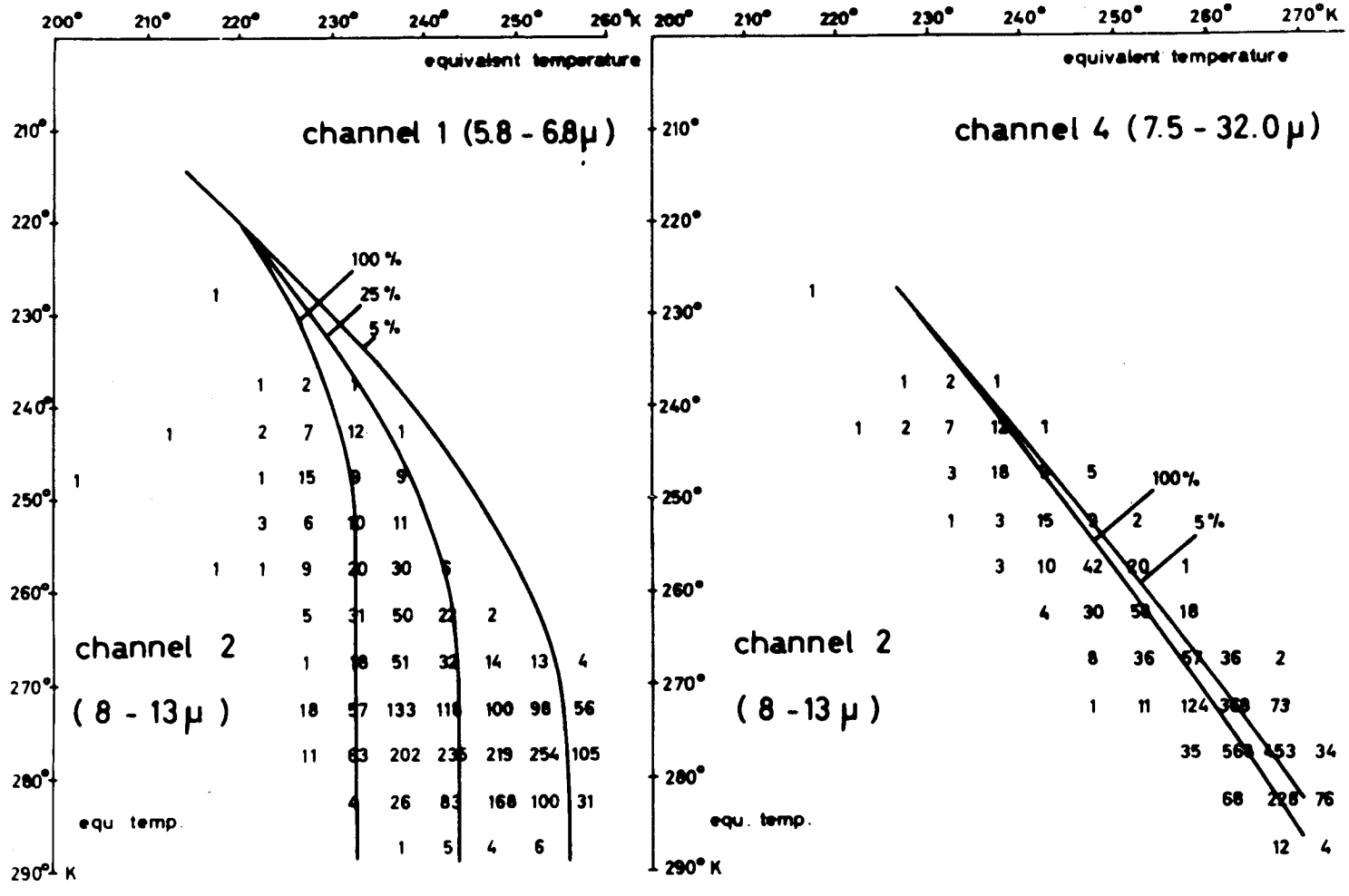

Fig. 4.1o : Frequency countings; N < 3o°

nel 4) for model atmosphere 3 (N = 0°; 100 % and 5 %) however show that particularly with low clouds or cloudless atmosphere (high temperatures) the correlation can not be linear since channel 4 is more sensitive in the regions of the 15 μ- carbon dioxide band and H_2O rotational band than channel 2.
In order to estimate the influence of water vapor on that correlation linear partial correlation coefficients have been calculated keeping constant those of channel 1 (assumed to be representative for relative humidity of the troposphere). But these coefficients (Table 4.3, column 1) are approximately equal to the general linear coefficients from which it can be inferred that the water vapor of the upper troposphere does not influence in a decisive degree the radiation fluxes. The same result will be found from partial correlation coefficients between the radiation data of channel1 and 4 keeping constant those of channel 2 (assumed to be representative for the surface temperature). These partial correlation coefficients (Table 4.3, column 2) are lower than the general linear coefficients which characterize all apparent correlations caused by meteorological conditions.

nadir angle group	orbit 42		61		114	
	1	2	1	2	1	2
1	0.950	0.291	0.881	0.354	0.788	0.506
2	0.980	0.570	0.902	0.317	0.805	0.515
3	0.958	0.603	0.885	0.305	0.826	0.461
4	0.892	0.150	0.890	0.230	0.862	0.110

Table 4.3 : linear partial correlation coefficients for equivalent temperatures of
col.1 : channels 2 and 4 keeping constant those of channel 1
col.2 : channels 1 and 4 keeping constant those of channel 2

The correlations between the infrared data and albedo values are mainly negative as it has already been shown by the comparison of radiation data from selected points. Above a uniform ground surface as it is given during orbit 61 above the Atlantic Ocean a negative correlation should be expected between channel 2 and the albedo values, which is narrower than above varying land surfaces. In the latter case not only clouds but also orographic conditions will influence the correlation

since cold clouds as well as warm desert surfaces have a high albedo. In the former case however the correlation is very low (orbit 61) which might be due to the high degradation of the channels 3 and 5. From albedo values of those channels cloudless regions (only albedo of the sea) could not be distinguished from regions with scattered clouds or vails (albedo of sea and clouds) because of the very low sensitivity of both channels.
Again the decreasing correlation between both albedo values with increasing orbit number seems to confirm a different degradation of both channels as it has been suggested also for the channels 2 and 4.
The relatively narrow correlation between infrared data and the cos $Z_{\odot}$ in orbits 42 and 114 seems to be caused by the coincidence of cloudless regions (with dry troposphere and high ground temperatures) with regions of low zenith distance of the sun during the time of measurements. In fact during orbits 42 and 114 TIROS III had passed Western Europe (cloudy sky) during sunrise but the cloudless regions (high surface temperatures) of Turkey and Arabia at local times near noon. These are typical examples of spurious correlations.

5 : Concluding Remarks

Former investigations of an evaluation method (MÖLLER & RASCHKE, 1963)*of TIROS III infrared radiation data for the determination of surface temperatures and mean relative humidities of the troposphere from the radiation data of the infrared channels 2 and 1 have been continued here. Herein it could be shown how much deviations of the atmospheric conditions from the used model atmosphere influence the radiation results. But errors resulting from those deviations do not exceed those arising from the large absolute errors of the measurements. The basic assumptions about the water vapor content in the stratosphere and the stratosphere height and temperature mainly influence the qualitative results of mean relative humidities. Therefore the evaluation method will be developed further to include also informations on the conditions in the lower stratosphere as they might be given in future by similar measurements in other spectral regions.

* See Appendix III, p. 85 of this report.

But evaluations of radiation data measured during orbit 61 over the entire Atlantic Ocean have revealed a typical distribution of the relative humidity of the upper troposphere arising from large scale vertical air circulation (Fig.4.7). Surface temperatures, however, determined from channel 2 above nearly cloudless regions are 9° - 10°C lower than the actual surface temperatures. This effect might be due to thin clouds or a slight degradation of the channel 2. Since the channels 3 and 5 show also a large loss of sensitivity our investigations will be continued with radiation data measured during earlier orbits of TIROS III. Some statistical investigations additionally confirm the conclusions already derived from sample studies and they again indicate the large scattering of measured values which is mainly due to the relatively large ratio noise-response.

In future work all these investigations will be continued with radiation data measured above the nightside of the earth.

A P P E N D I X I

Tables of the spectral transmittance τ ($_{10}\log$ ($l_\nu w^*$)) and of the decadic logarithms of the generalized absorption coefficients ($_{10}\log l_\nu$) for water vapor and carbon dioxide and a table for the integrated transmittance of the 9.6μ - band of ozone.

The "pressure corrected" absorbing gas quantity is defined by

$$w^* = w \left(\frac{p}{p_o} \right)^n ,$$

where p_o is the standard pressure.

absorbing gas	exponent n	w^*
H_2O	o.72	u^* [g·cm^{-2}]
CO_2	o.65	c^* [cm NTP]
O_3	o.41 for $p < 15o$ mb o for $p > 15o$ mb	m^* [cm NTP]

The curves of these tabulated data are given in MÖLLER & RASCHKE (1963).*

* See Appendix III, p. 85 of this report.

Table A : Decadic Logarithms of the Generalized Absorption Coefficients ($_{10}\log l_\nu$) for the 6.3μ - Band of Water Vapor

(4.7μ - 8.6μ ; 2120 cm^{-1} .. 1160 cm^{-1})

$\nu[cm^{-1}]$	300 °K	280 °K	260 °K	240 °K	220 °K	200 °K
1160	0.38 -1	0.30 -1	0.19 -1	0.04 -1	0.90 -2	0.72 -2
1200	0.80 -1	0.72 -1	0.60 -1	0.45 -1	0.32 -1	0.15 -1
1240	0.25	0.16	0.06	0.96 -1	0.80 -1	0.62 -1
1280	0.66	0.60	0.53	0.46	0.34	0.22
1320	0.10 +1	0.06 +1	0.02 +1	0.95	0.88	0.80
1360	0.58 +1	0.56 +1	0.52 +1	0.48 +1	0.44 +1	0.40 +1
1400	0.08 +2	0.08 +2	0.08 +2	0.08 +2	0.06 +2	0.00 +2
1440	0.50 +2	0.48 +2	0.46 +2	0.44 +2	0.40 +2	0.37 +2
1480	0.86 +2	0.84 +2	0.80 +2	0.80 +2	0.80 +2	0.80 +2
1520	0.76 +2	0.80 +2	0.80 +2	0.80 +2	0.80 +2	0.82 +2
1560	0.20 +2	0.22 +2	0.25 +2	0.30 +2	0.35 +2	0.40 +2
1580	0.08 +2	0.10 +2	0.15 +2	0.18 +2	0.22 +2	0.26 +2
1600	0.16 +2	0.25 +2	0.30 +2	0.36 +2	0.44 +2	0.50 +2
1640	0.70 +2	0.72 +2	0.74 +2	0.76 +2	0.78 +2	0.78 +2
1680	0.56 +2	0.56 +2	0.56 +2	0.56 +2	0.56 +2	0.56 +2
1720	0.20 +2	0.20 +2	0.20 +2	0.20 +2	0.20 +2	0.20 +2
1760	0.80 +1	0.76 +1	0.74 +1	0.72 +1	0.68 +1	0.66 +1
1800	0.45 +1	0.40 +1	0.35 +1	0.33 +1	0.30 +1	0.25 +1
1840	0.00 +1	0.98	0.96	0.94	0.90	0.85
1880	0.66	0.62	0.57	0.52	0.44	0.40
1920	0.36	0.30	0.24	0.15	0.04	0.90 -1
1960	0.06	0.00	0.90 -1	0.76 -1	0.64 -1	0.48 -1
2000	0.75 -1	0.62 -1	0.50 -1	0.37 -1	0.23 -1	0.03 -1
2040	0.31 -1	0.22 -1	0.10 -1	0.97 -2	0.82 -2	0.60 -2
2080	0.90 -2	0.80 -2	0.70 -2	0.55 -2	0.38 -2	0.15 -2
2120	0.46 -2	0.36 -2	0.25 -2	0.10 -2	0.95 -3	0.80 -3

Table B : Decadic Logarithms of the Generalized Absorption Coefficients ($_{10}\log l_\nu$) for the Rotation Band of Water Vapor

(12.5 μ - 50 μ ; 800 cm^{-1} - 200 cm^{-1})

ν [cm^{-1}]	300 °K	280 °K	260 °K	240 °K	220 °K
800	0.45 -1				
760	0.52 -1				
720	0.61 -1				
680	0.72 -1				
640	0.84 -1				
600	0.00				
560	0.28	0.27	0.26	0.25	0.24
520	0.72	0.68	0.65	0.61	0.57
480	0.17 +1	0.10 +1	0.02 +1	0.96	0.90
440	0.44 +1	0.36 +1	0.30 +1	0.22 +1	0.16 +1
400	0.63 +1	0.55 +1	0.50 +1	0.40 +1	0.34 +1
360	0.04 +2	0.96 +1	0.88 +1	0.80 +1	0.70 +1
320	0.30 +2	0.22 +2	0.14 +2	0.06 +2	0.98 +1
280	0.54 +2	0.48 +2	0.42 +2	0.37 +2	0.32 +2
240	0.78 +2	0.75 +2	0.72 +2	0.69 +2	0.66 +2
200	0.00 +3				

Table C : Spectral Transmittance τ ($_{10}\log$ ($l_\nu u^*$)) = τ($_{10}\log l_\nu$ + $_{10}\log u^*$) for the 6.3μ - Band and the Rotation Band of Water Vapor to be Used in Connection with Table A and B

$_{10}\log(l_\nu u^*)$	6.3μ	rotat.	$_{10}\log(l_\nu u^*)$	6.3μ	rotat.
0.8 -4	1.000	1.000	0.4 -1	0.737	0.737
0.9	1.000	0.998	0.5	0.700	0.708
0.0 -3	1.000	0.995	0.6	0.662	0.675
0.1	1.000	0.994	0.7	0.620	0.635
0.2	1.000	0.992	0.8	0.575	0.595
0.3	1.000	0.990	0.9	0.531	0.548
0.4	0.998	0.987	0.0 +0	0.485	0.500
0.5	0.995	0.985	0.1	0.438	0.450
0.6	0.993	0.983	0.2	0.393	0.398
0.7	0.990	0.978	0.3	0.350	0.345
0.8	0.987	0.975	0.4	0.307	0.298
0.9	0.984	0.970	0.5	0.262	0.244
0.0 -2	0.980	0.964	0.6	0.223	0.200
0.1	0.975	0.958	0.7	0.185	0.160
0.2	0.969	0.950	0.8	0.147	0.122
0.3	0.962	0.942	0.9	0.115	0.095
0.4	0.953	0.930	0.0 +1	0.087	0.067
0.5	0.944	0.918	0.1	0.065	0.047
0.6	0.932	0.905	0.2	0.047	0.028
0.7	0.917	0.890	0.3	0.033	0.015
0.8	0.900	0.875	0.4	0.022	0.005
0.9	0.880	0.855	0.5	0.014	0
0.0 -1	0.857	0.835	0.6	0.009	0
0.1	0.831	0.815	0.7	0.005	0
0.2	0.802	0.790	0.8	0	0
0.3	0.771	0.763	0.9	0	0

Table D : Absorption Coefficients η_ν and β_ν for the Water Vapor Window (8.3μ - 12.5μ ; 1200 cm^{-1} - 1800 cm^{-1})

$$\tau_\nu (u^*) = \exp - (\eta_\nu \sqrt{u^*} + \beta_\nu u^*)$$

ν	η_ν	β_ν	ν	η_ν	β_ν
$[cm^{-1}]$	$[cm\ g^{-0.5}]$	$[cm^2\ g^{-1}]$	$[cm^{-1}]$	$[cm\ g^{-0.5}]$	$[cm^2\ g^{-1}]$
800	0.160	0.135	1000	0.040	0.080
840	0.080	0.110	1040	0.045	0.080
880	0.050	0.095	1080	0.050	0.080
920	0.045	0.085	1120	0.065	0.085
960	0.040	0.080			

Table E : Integrated Transmittance τ ($_{10}\log m^*$) for the 9.6μ - Band of Ozone (8.8μ - 10.6μ ; 1140 cm^{-1} - 840 cm^{-1})

$_{10}\log m^*$	τ	$_{10}\log m^*$	τ	$_{10}\log m^*$	τ
0.3 -4	1.000	0.4 -3	0.967	0.5 -2	0.830
0.4	0.998	0.5	0.961	0.6	0.810
0.5	0.996	0.6	0.953	0.7	0.788
0.6	0.995	0.7	0.945	0.8	0.764
0.7	0.993	0.8	0.935	0.9	0.740
0.8	0.990	0.9	0.924	0.0 -1	0.717
0.9	0.988	0.0 -2	0.912	0.1	0.695
0.0 -3	0.985	0.1	0.898	0.2	0.675
0.1	0.981	0.2	0.883	0.3	0.655
0.2	0.977	0.3	0.867	0.4	0.635
0.3	0.973	0.4	0.850	0.5	0.616

Table F : Decadic Logarithms of the Generalized Absorption Coefficients ($_{10}\log l_\nu$) for the 15μ - Band of CO_2 (12.5μ - 19.2μ ; 800 cm^{-1} - 520 cm^{-1})

ν [cm^{-1}]	300 °K	260 °K	240 °K	220 °K
520	0.35 -5	0.25 -5	0.95 -6	0.80 -6
540	0.00 -4	0.65 -5	0.35 -5	0.15 -5
560	0.60 -4	0.30 -4	0.00 -4	0.75 -5
580	0.70 -3	0.30 -3	0.00 -3	0.75 -4
600	0.84 -2	0,45 -2	0.15 -2	0.90 -3
620	0.35 -1	0.10 -1	0.80 -2	0.53 -2
640	0.00	0.88 -1	0.72 -1	0.57 -1
660	0.65	0.70	0.75	0.80
670	0.80	0.82	0.84	0.86
680	0.60	0.62	0.65	0.70
700	0.95 -1	0.88 -1	0.70 -1	0.50 -1
720	0.27 -1	0.20 -1	0.05 -1	0.83 -2
740	0.55 -2	0.40 -2	0.20 -2	0.90 -3
760	0.65 -3	0.50 -3	0.25 -3	0.95 -4
780	0.65 -4	0.50 -4	0.20 -4	0.80 -5
800	0.40 -5	0.20 -5	0.00 -5	0.70 -6

Table G : Spectral Transmittance $\tau\,(\,{}_{10}\log\,(\,l_\nu\, c^*))\;=\;\tau\,(\,{}_{10}\log\, l_\nu\;+\;{}_{10}\log\, c^*\,)$ for the 15μ - Band of Carbon Dioxide to be Used in Connection with the Table F

${}_{10}\log(l_\nu\, c^*)$	τ	${}_{10}\log(l_\nu\, c^*)$	τ	${}_{10}\log(l_\nu\, c^*)$	τ
0.5 -4	1.000	0.5 -2	0.902	0.5 +0	0.325
0.6	0.997	0.6	0.891	0.6	0.287
0.7	0.995	0.7	0.878	0.7	0.250
0.8	0.993	0.8	0.865	0.8	0.213
0.9	0.990	0.9	0.850	0.9	0.180
0.0 -3	0.988,	0.0 -1	0.834	0.0 +1	0.150
0.1	0.985	0.1	0.817	0.1	0.125
0.2	0.983	0.2	0.796	0.2	0.100
0.3	0.981	0.3	0.772	0.3	0.080
0.4	0.979	0.4	0.747	0.4	0.063
0.5	0.976	0.5	0.717	0.5	0.048
0.6	0.972	0.6	0.687	0.6	0.035
0.7	0.968	0.7	0.652	0.7	0.025
0.8	0.963	0.8	0.617	0.8	0.018
0.9	0.957	0.9	0.580	0.9	0.010
0.0 -2	0.950	0.0 +0	0.535	0.0 +2	0.008
0.1	0.943	0.1	0.495	0.1	0.005
0.2	0.935	0.2	0.452	0.2	0.003
0.3	0.925	0.3	0.410	0.3	0
0.4	0.913	0.4	0.367	0.4	0

A P P E N D I X I I

Radiation diagrams for the channels 1, 2 and 4 of the meteorological satellite TIROS III and for a "difference channel (4-2)" which is defined by the difference between the spectral sensitivities of the channels 4 and 2, and auxiliary diagrams for the correction according to the absorption and emission by atmospheric ozone and carbon dioxide (see also chapter 3 in MÖLLER & RASCHKE, 1963)*

* See Appendix III, p. 85 of this report.

TIROS III : CHANNEL 1 (5.0 - 6.0 μ)
0°K
-80°
-60°
-40°
-20°
0°
+10°
+20°C
T_{BB}
$\bar{\tau}$
0.00001
0.0001
0.001
0.01
0.1
[g cm^{-2}] water vapour
2
3
4
6
1.0
.9
.8
.7
.6
.5
.4
.3
.2
.1
0
0
1/20
1/15
1/10
1/05
[Wm^{-2}]

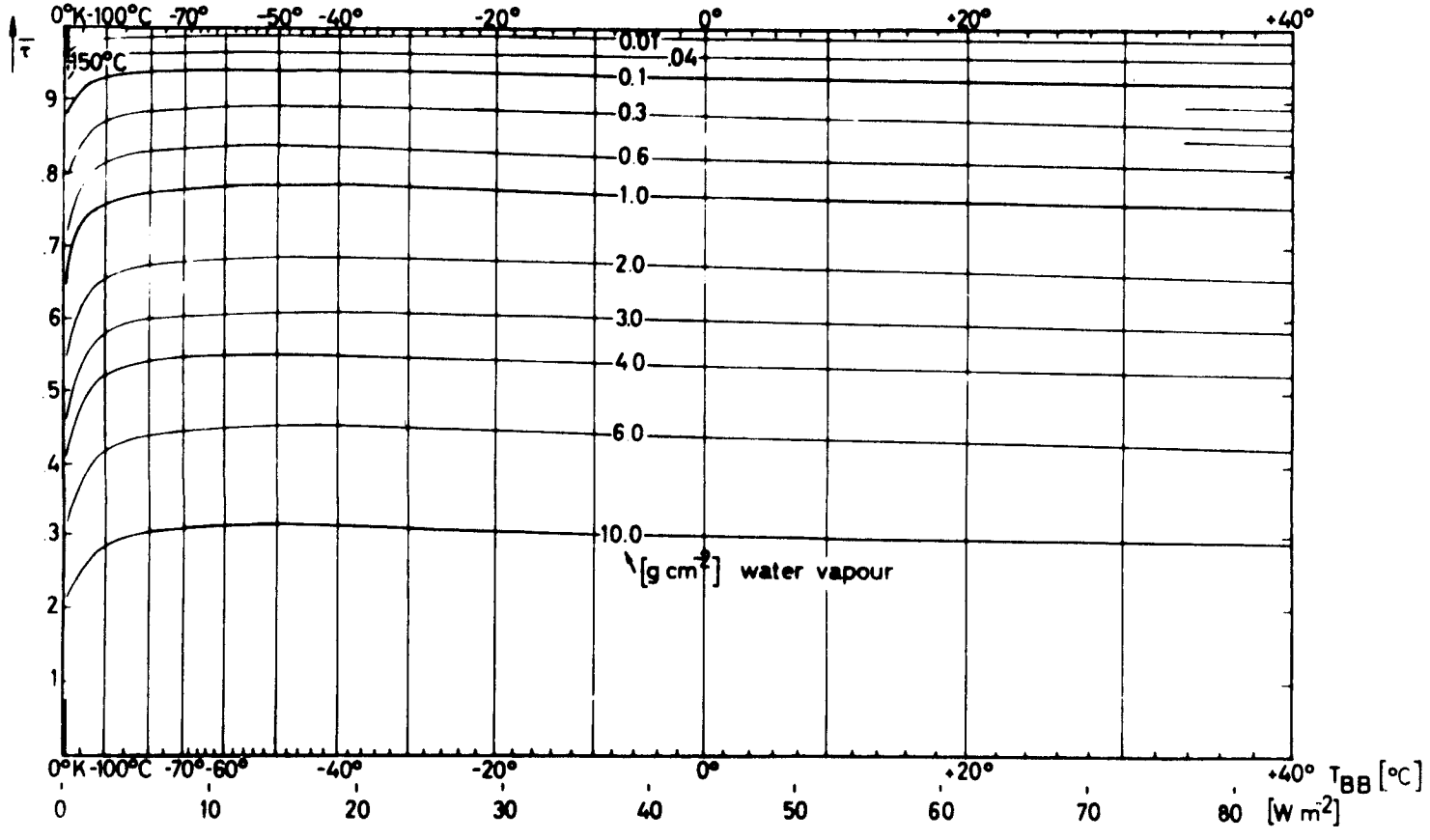

TIROS III : CHANNEL 2 (8 - 13 μ)

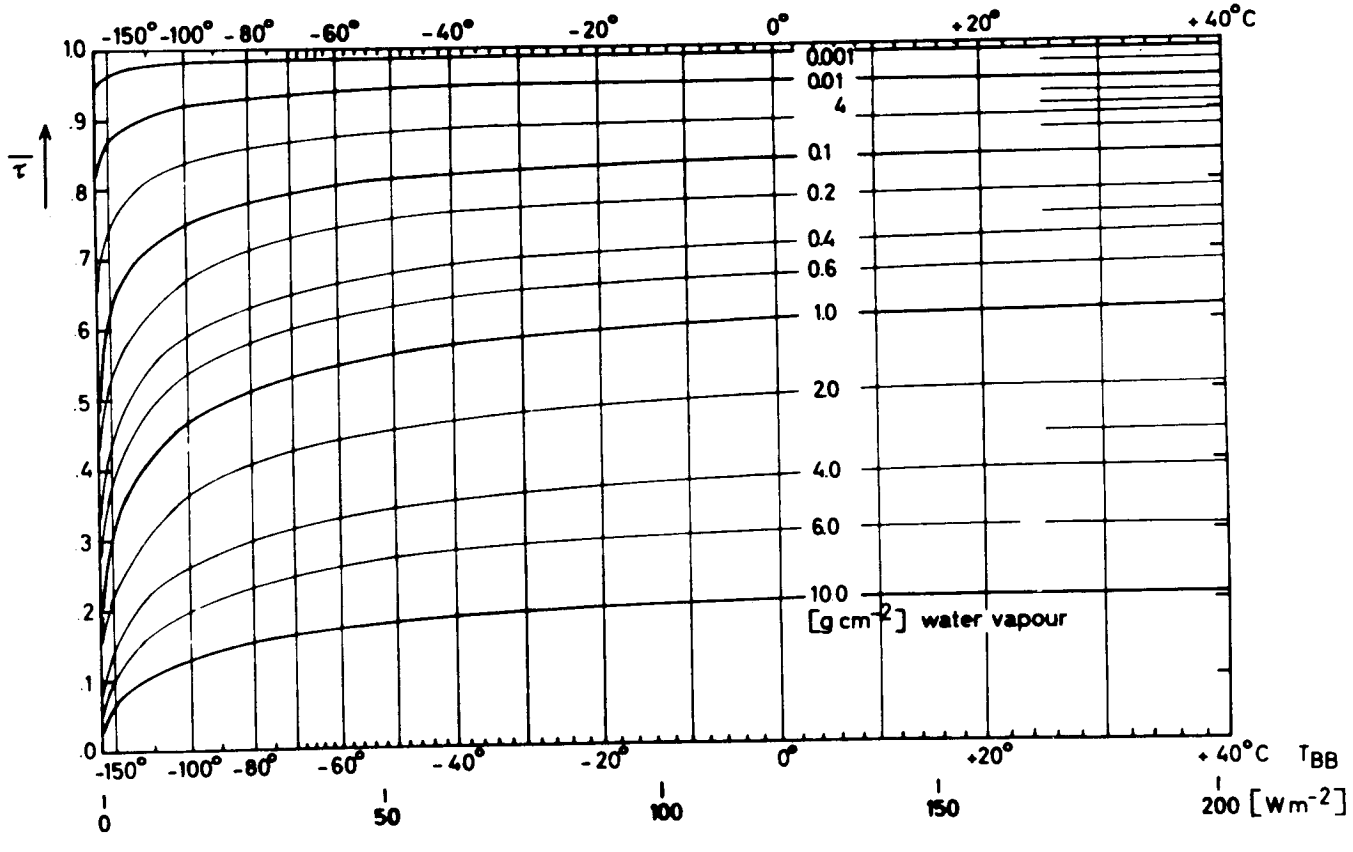

TIROS III : CHANNEL 4 (7.5 - 32.5 μ)

TIROS III : "difference channel (4-2)" (12-32.5 μ)

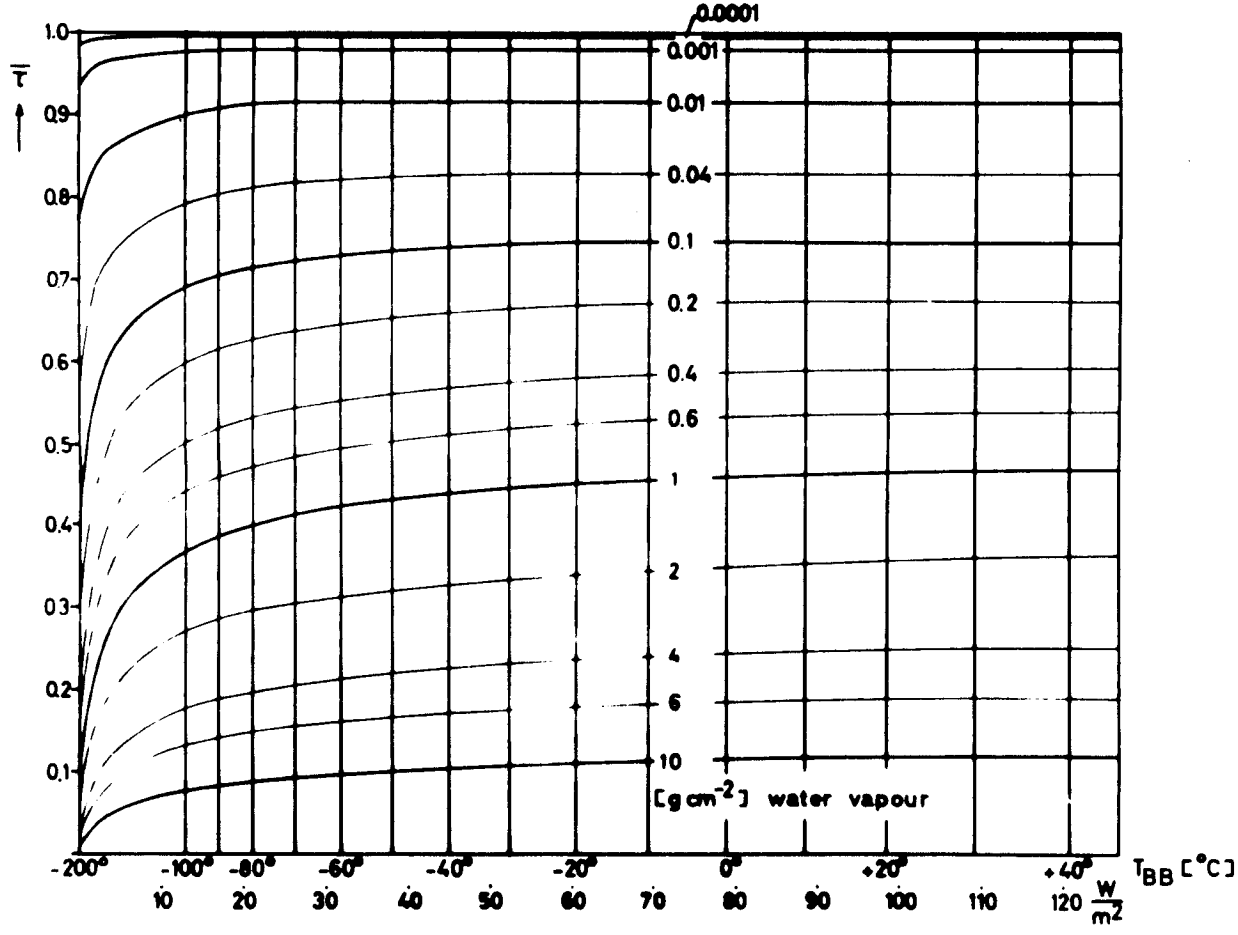

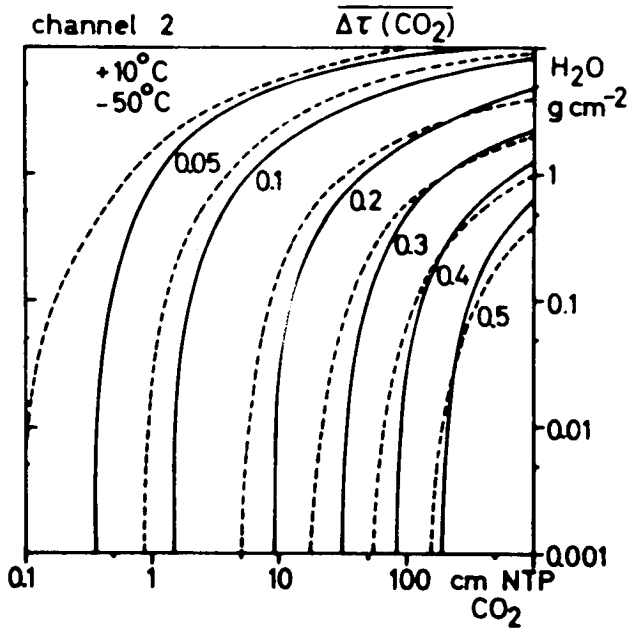
channel 2
$\overline{\Delta\tau\,(CO_2)}$
+10°C
-50°C
0.05
0.1
0.2
0.3
0.4
0.5
H_2O
g cm^{-2}
1
0.1
0.01
0.001
0.1
1
10
100 cm NTP
CO_2

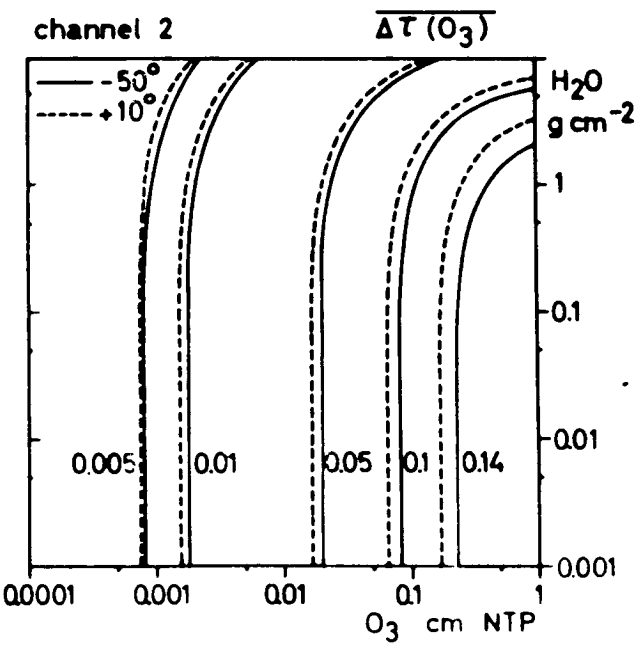
channel 2
$\overline{\Delta\tau\,(O_3)}$
-50°
+10°
0.005
0.01
0.05
0.1
0.14
H_2O
g cm^{-2}
1
0.1
0.01
0.001
0.0001
0.001
0.01
0.1
1
O_3 cm NTP

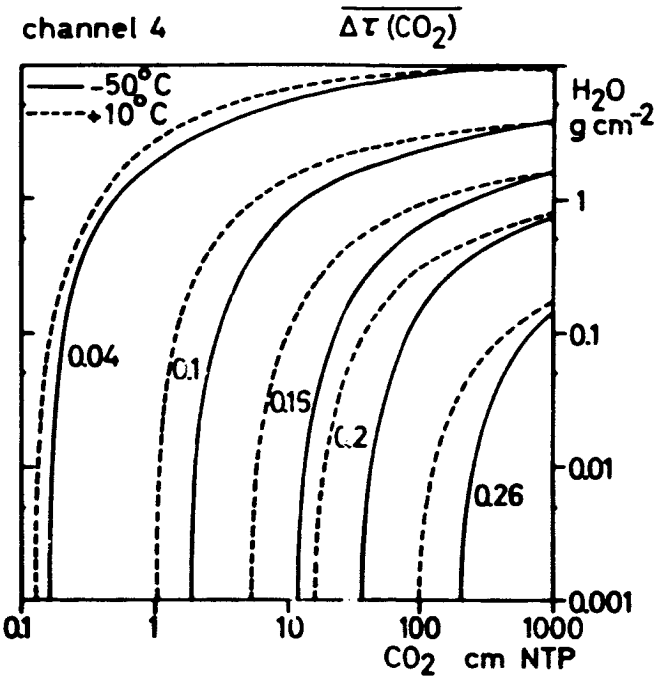
channel 4
$\overline{\Delta\tau(CO_2)}$
-50°C
+10°C
H_2O g cm^{-2}
1
0.1
0.01
0.001
0.04
0.1
0.15
0.2
0.26
0.1
1
10
100
1000
CO_2 cm NTP

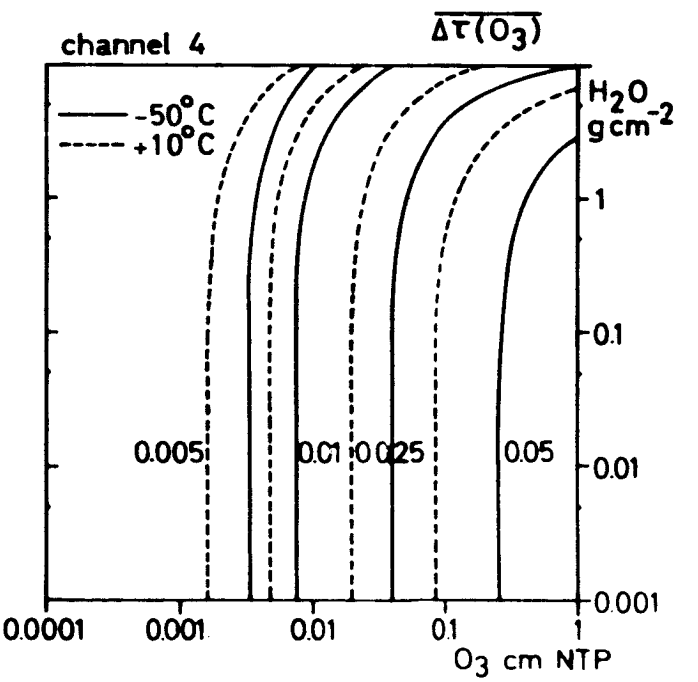
channel 4
$\overline{\Delta\tau(O_3)}$
-50°C
+10°C
H_2O g cm^{-2}
1
0.1
0.01
0.001
0.005
0.01
0.025
0.05
0.0001
0.001
0.01
0.1
1
O_3 cm NTP

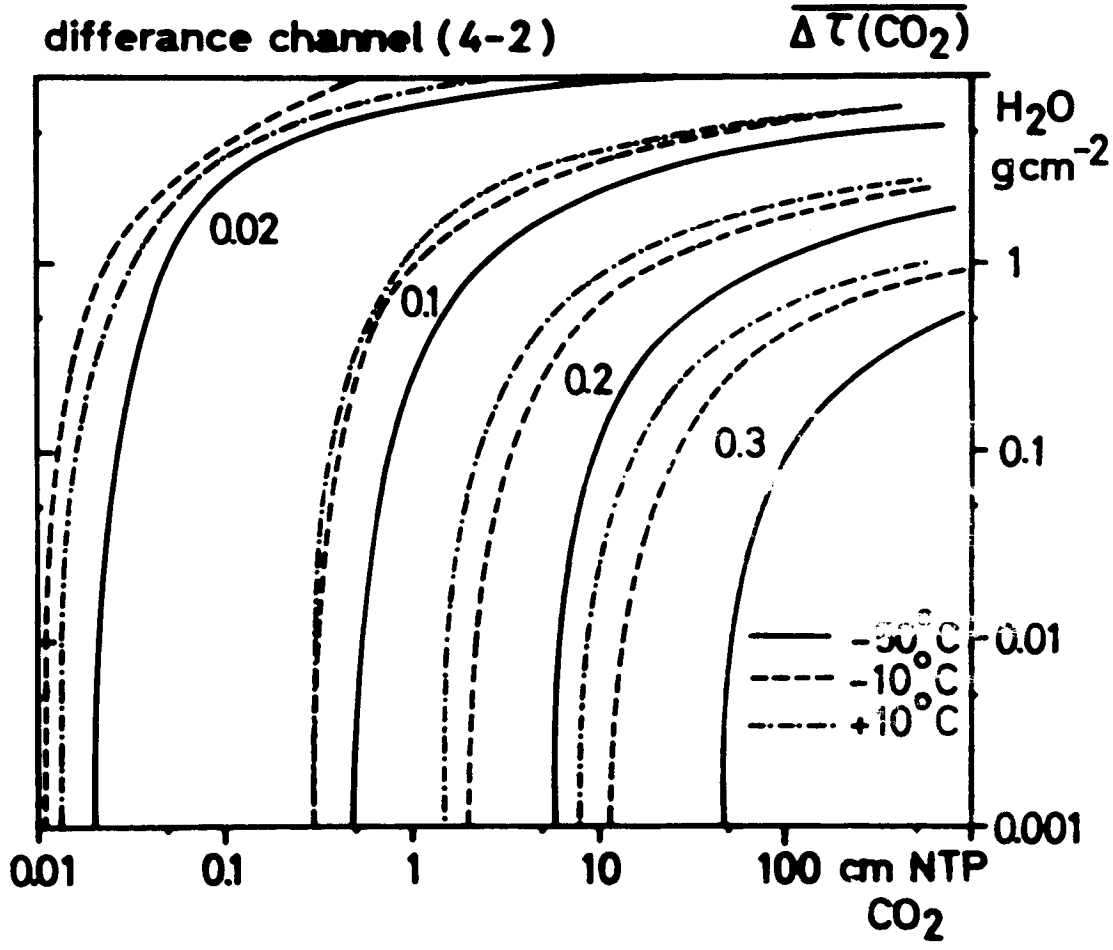
difference channel (4-2)
$\overline{\Delta\tau(CO_2)}$
H_2O gcm^{-2}
0.02
0.1
0.2
0.3
1
0.1
0.01
0.001
-50°C
-10°C
+10°C
0.01
0.1
1
10
100 cm NTP
CO_2

REFERENCES

Bandeen, W.R., W.Nordberg, V.Kunde, and H.P.Thompson (1963) : TIROS III Meteorological Radiation Observations of a Tropical Hurricane. NASA 1963

Bell, E.E. (1957) : An Atlas of Reflectivities of some Common Types of Materials. Report 659-6, Wright Air Division Center, Contract AF 33 (616) - 3313, AP 141795.

Bolle, H.-J., F.Möller, W.Zdunkowski (May 1963) : Investigation of the Infrared Emission Spectrum of the Atmosphere and Earth. Technical Report Nr.2, Meteorologisches Institut, München, Germany.

Burch, D.E., D.Gryvnak, and D.Williams (1960) : Infrared Absorption by Carbon Dioxide. The Ohio State University, Research Foundation, Columbus 12, Ohio. Science Report Nr.2, Contract No. AF 19 (604) - 2633.

Buettner, K.J.K. and C.D.Kern (1963) : Science , Vol.142, p.671.

Deirmendjan, D. (1960) : Atmospheric Extinction of Infrared Radiation. Quarterly Journal of Royal Meteorological Society, 86, 371-381.

Deirmendjan, D. (July 1962) : Scattering and Polarization of Polydispersed Suspensions with Partial Absorption. Memorandum RM - 3228 - PR. The RAND - Corp., Santa Monica, California.

Elsasser, W.M. (1942) : Heat Transfer by Infrared Radiation in the Atmosphere. Harvard Meteorological Studies Nr.6, Harvard University Milton, Mass.

Fritz, S. (1949) : The Albedo of the Planet Earth and of Clouds. J. of Met. 6, p.277.

Fujita, T. (Jan.1963) : A Technique for Precise Analysis for Satellite Data. Vol. I - Photogrammetry.

(Febr.1963) : Outline of a Theory and Examples for Precise Analysis of

Satellite Radiation Data. Research Paper Nr.15, Dept. of the Geoph.Sci., University of Chigago (NASA NsG.333; USWB Cwb WBG - 6).

Gates, D.M. and C.C.Shaw (1960) : Infrared Transmission of Clouds. J. of the Optical Society of America, Vol.50, Nr.9.

Gutnick, M. (July 1962) : Mean Annual Mid Latitude Moisture Profiles to 31 km. AFCRL - 62 - 681, Research Report.

Hanel, R.A., W.R.Bandeen, and B.Z.Conrath (1963) : The Infrared Horizon of the Earth. NASA Technical Note D - 1850.

Howard, J.N., D.E.Burch, and D.Williams (1956) : Infrared Transmission of Synthetic Atmospheres. J. Opt. Soc. Am. 46,186,237,242,334, 452.

Johnson, F.S. (1954) : The Solar Constant. J. of Met. 11,431.

Kislovskii, L.D. (1959) : Optical Characteristics of Water and Ice in the Infrared and Radiowave Regions of the Spectrum. Optics and Spectroscopy, Vol.VII, No.3, Sept. 1959.

Kondrat'yev, K.Y. and K.E.Jakuschevskaja (1962) : Angular Distribution of the Upward Heat Radiation in Different Spectral Ranges. Issk. sputniki semlji (Earth's Artificial Satellites) No.14.

Larsen, S.H.H., T.Fujita, and W.L.Fletcher (1963) : Evaluation of Limb Darkening from TIROS III Radiation Data. Res. Paper 18, Aug. 1963. Mesometeorological Project, Dep. of Geophys. Sciences, University of Chigago.

Lyon, R.J.P. and E.A.Burns (1962) : Infrared Spectral Analysis of the Lunar Surface from an Orbiting Spacecraft. NASA - 49 (04), N 63 - 14668, University of Michigan, Oct., 16,1962.

Mastenbrook, H.J. and J.E.Dinger (1961) : Distribution of Water Vapor in the Stratosphere. J. of Geophys. Res. 66, 1437 - 1444.

Mastenbrook, H.J. (Aug.1962) : The Vertical Distribution of Water Vapor over Hyderabad, India, and Comparison with Midlatitude Distribution. U.S. NRL - Report 5817, Washington 25, D.C.

Möller, F. (Jan.1962) : Some Preliminary Evaluations of TIROS II Radiation Measurements. Univ. München, Meteorolog. Institut, München 13, Amalienstr.52/III.

(1962) : Einige vorläufige Auswertungen der Strahlungsmessungen von TIROS II. Arch. f. Met., Geophys. und Biokl., Serie B, 12, 78 - 93.

Möller, F. and E.Raschke (1963)*: Evaluation of TIROS III Radiation Data. Interim Report No.1, NASA Research NsG - 305, Meteorolog. Institut der Universität München.

Paetzold, H.K. (1963) : Communication (unpublished).

Palmer, C.H. (1957) : Long Path Water Vapor Spectra with Pressure Broadening, I. 20 μ - 31.7 μ. J.O.S.A. 47, 1024.

(1960) : Experimental Transmission Function for the Pure Rotation Band of Water Vapor. J.O.S.A.50, 1232.

Roach, W.T. and R.M.Goody (1958) : Absorption and Emission in the Atmospheric Window from 770 to 1250 cm^{-1}. Quart.J.Roy.Met.Soc. 84, 319 - 333.

Stroud, W.G. and W.Nordberg (1961) : Seasonal, Latitudinal, and Diurnal Variations in the Upper Atmosphere. NASA - Technical Note D 703.

TIROS III (Aug.1962) : Radiation Data. User's Manual. NASA - Aeronomy and Meteorology Division, Goddard Space Flight Center, Greenbelt, Md.

U.S.Navy (1955,1958) : Marine Climatic Atlas of the World. Vol.1 : North Atlantic Ocean, NAVAER 50 - 1C - 528. Vol.4 : South Atlantic

* See Appendix III, p. 85 of this report.

Ocean, NAVAER 50 - 1C - 531, Sept.1958.

Viezee, W. and P.A.Davis : Preliminary Examination of Daytime Radiation Data from TIROS III over Cloudy Regions. SRI - Menlo Park, Calif., Contr. AF 19 (628) - 2777.

Walshaw, C.D. (1957) : Integrated Absorption by the 9.6 μ - Band of Ozone. Quart. J. Roy. Met. Soc. 83, 315 - 321.

Wark, D.Q., G.Yamamoto, and J.H.Lienesch (1962) : Methods of Estimating Infrared Flux and Surface Temperature from Meteorological Satellites. J. Atmos. Sci. 19, 369 - 384, Sept. 1962.

Wexler, R. (1964) : Infrared and Visual Radiation od Measurements from TIROS III. Applied Optics, 1964, Vol.3, No.2, p.215 - 219.

Wyatt, D.J., V.R.Stull, and G.N. Plass (Sept.1962) : Infrared Transmission Studies (Final Report). Vol.II: The Infrared Absorption of Water Vapor. SSD - TDR - 62 - 127. (Jan.63) : The Infrared Absorption of Carbon Dioxide. SSA - TDR - 62 - 127 - Vol.III. Aeronautic Division, Ford Motor Company, Newport Beach, California. Contract No. AF o4 (695) - 96, Project No.4479 - 730 F.

Yamamoto, G. (1952) : On a Radiation Chart. Sci. Rep. Tohoku Univ. Series 5, Geophysics 4, 9 - 23.

Anthony R., V. N. Smiley (1962): Infrared Horizon from Near-Orbiting Altitudes; Gen. Dyn. etc.; San Diego Calif.; AFCRL - 62 - 1oo1

APPENDIX III

EVALUATION OF TIROS III RADIATION DATA

Fritz Möller
Ehrhard Raschke

INTERIM REPORT NO. 1
under
NASA Research Grant
NsG-305

July 1963

ABSTRACT:

For the construction of radiation diagrams (according to YAMAMOTO's model, 1952) for the ranges of sensitivity of the 3 infrared channels of the satellite TIROS III transmission functions have been calculated from measured laboratory data published by several authors. The pressure dependence of absorption is discussed.

With these radiation diagrams the outgoing radiation flux is calculated for 3 model atmospheres with some modifications. A method (MÖLLER 1962) for the determination of a mean relative humidity of the troposphere and the surface temperature of clouds or ground from the measured radiation data is discussed and the results demonstrated as example in maps of the European part of orbit 42.

Preliminary statistical investigations show good correlations between the measured radiation data in different channels (demonstrated by averages over large areas). Single values, however, show a large scattering.

CONTENTS

	Page
List of figures	VII
1. Introduction	1
2. The Tiros experiment	2
2.1 The object of measurements	2
2.2 Data of the Five-Channel Medium Resolution Radiometer	2
3. Computation of radiation flux in the sensitivity regions of the infrared channels of satellite Tiros III.	9
3.1 Characteristics of measured radiation	9
3.2 Principle of the calculation of the radiation flux for arbitrary model atmospheres	10
3.21 Assumptions	10
3.22 Solution of the equation of radiation transfer.	10 a
3.23 Construction of a radiation diagram according to YAMAMOTO (1952)	11
3.23.1 Auxiliary diagrams for the correction relative to the absorption by other gases	14
4. Transmission functions τ_ν	15
4.1 Optical thickness and the transmission of an absorber	15
4.2 Investigation of pressure and temperature dependence of the absorption	17
4.21 Line absorption	17
4.22 Pressure and temperature dependence of the absorption	18
4.3 Derivation of transmission functions	24
4.31 Water vapor	27
4.32 Carbon dioxide	34
4.33 Ozone	36
4.34 Comparison between recalculated and measured spectra	41
4.4 Application of the pressure correction for the computation of radiation fluxes in the atmosphere.	45

Page

5. The radiation flux in the spectral regions of the 3 infrared channels 1, 2, and 4 of the satellite Tiros III..... 46
5.1 Radiation diagrams for the channels 1, 2, and 4 46
5.11 Channel 1 (5.8μ - 6.8μ) 49
5.12 Channels 2 (8μ - 13μ) and 4 (7.5μ - 32.5μ) 50
5.13 A difference channel "(4 - 2)" 50
5.2 Computations of the radiation flux for several model atmospheres 54
5.21 Model atmospheres 54
5.22 Results 56
5.22.1 Different water vapor quantities in the stratosphere 57
5.22.2 Different tropopause temperatures 59
5.22.3 The influence of absorption and emission of CO_2 and O_3 61
5.22.4 Nadir angle dependence 63
6. Preliminary results of the evaluation of radiation data .. 67
6.1 Determination of mean relative humidity and of a surface temperature (clouds or ground) 67
6.11 Evaluation diagrams 67
6.12 An example of evaluation 73
6.13 Albedo 82
6.2 Statistical investigations 84
6.21 Correlations between radiation data averaged over large areas 84
6.22 Correlations between single measured data 86
7. Conclusions 91
Appendix I 93
Appendix II 100
References 108

LIST OF FIGURES

Page

Fig. 2.1a : Components of a single channel 3

Fig. 2.1b : Geometry of the scanning motion of the radiometer 3

Fig. 2.2 : Spectral sensitivity of the channels 3 and 5 (TIROS III) and the solar spectral irradiance (after JOHNSON) 5

Fig. 2.3 : Spectral sensitivity of the channels 1, 2 and 4 (TIROS III) and a schematic graph of the absorption bands of water vapor, carbon dioxide and ozone 7

Fig. 3.1 : Radiation diagram (after YAMAMOTO) 13

Fig. 3.2 : Auxiliary diagram (after YAMAMOTO) 13

Fig. 4.1 : Pressure correction exponent versus the absorber quantity (6.3μ- band of water vapor) 21

Fig. 4.2 : Pressure correction exponent versus the absorber quantity (15μ - band of carbon dioxide) 22

Fig. 4.3 : Spectral absorptance of the 6.3μ- band and the rotation band of water vapor 28

Fig. 4.4 : Generalized absorption coefficients of the 6.3μ - band for several temperatures 29

Fig. 4.5 : Absorption coefficients for the water vapor window (8oo cm^{-1} - 12oo cm^{-1}) 33

Fig. 4.6 : Generalized absorption coefficients of the rotation band (8oo cm^{-1} - 2oo cm^{-1}) for several temperatures 35

Fig. 4.7 : Spectral absorptance of the 15μ - band of carbon dioxide 37

Page

Fig. 4.8 : Generalized absorption coefficients of the 15μ - band of CO_2 for several temperatures 38

Fig. 4.9 : Integrated absorptance of the 9.6μ - band of ozone 40

Fig. 4.1o : Comparison of measured with recalculated spectra (15μ - band of CO_2) 42

Fig. 4.11 : Comparison of measured with recalculated spectra (6.3μ - band of H_2O) 43

Fig. 5.1 : Radiation diagrams for the channels 1, 2 and 4. Curves are plotted on the ARDC Standard Atmosphere for constant relative humidity of the troposphere. 47

Fig. 5.2 : Ozone stratification after PAETZOLD

Fig. 5.3 : Radiation diagrams

a. : for the water vapor rotation band; sensitivity of channel 4 (16μ - 32.6μ)

b. : for the 15μ - band of CO_2 (14μ - 16μ) 52

Fig. 5.4 : Difference channel (4-2)

a. : Definition of the spectral sensitivity

b. : radiation diagram 53

Fig. 5.5 : Temperature profiles of the 3 model atmospheres and of the variations of the tropopause temperature 55

Fig. 5.6 : Calculated nadir angle dependence of the radiation flux which would be measured by a satellite flying over an ARDC Standard Atmosphere with constant relative humidity of the troposphere

Page

(Fig. 5.6) : a. : for cloudless sky
b. : for cloud surfaces in the -1o°C - level
c. : for cloud surfaces in the tropo-pause (-56.5°C) 65

Fig. 6.1 : Evaluation diagrams 68

Fig. 6.2 : Error estimation of the evaluation of radiation data with a given accuracy 70

Fig. 6.3 : TIROS III radiation data of channel 1 (orbit 42) 74

Fig. 6.4 : TIROS III radiation data of channel 2 (orbit 42) 75

Fig. 6.5 : TIROS III radiation data of channel 4 (orbit 42) 76

Fig. 6.6 : TIROS III radiation data of the difference channel (4-2) (orbit 42) 77

Fig. 6.7 : surface weather chart, 15.7.1961 , o.oo GMT 78

Fig. 6.8 : Mean relative humidities determined from TIROS III radiation data of the channels 1 and 2 (orbit 42) 80

Fig. 6.9 : Surface temperature determined from TIROS III radiation data of the channels 1 and 2 (orbit 42) 81

Fig. 6.1o : Albedo determined from TIROS III radiation data of channel 3 (orbit 42) 83

Fig. 6.11 : Large spatial averages of TIROS III radiation data and of surface temperatures
a. : Orbit 42
b. : orbit 114 85

Page

Fig. 6.12 : Frequency counting of the radiation data of the channels 2 and 4 (orbit 114) 87

Fig. 6.13 : Frequency counting of the radiation data of the channels 1 and 4 (orbit 114) 88

Fig. 6.14 : Frequency counting in dependence upon the nadir angle (orbit 114)
a. channel 1
b. channel 2 90

APPENDIX II : Radiation diagrams for the channels 1, 2, 4 and (4-2) and auxiliary diagrams to correct flux calculations according to the CO_2 and O_3 absorption and emission. 100

1. INTRODUCTION

In the last years the National Aeronautics and Space Administration (NASA) launched a series of meteorological satellites into orbits around the earth, which transmitted television pictures of the earth and cloud surfaces and also data of radiation measurements in several small spectral ranges of the long and short wave radiation.

The television pictures are nowadays an essential element of the wheather analysis and forecasting (nephanalysis maps).

Investigations of radiation data were carried out only to determine surface temperatures (NORDBERG et al., 1962; WARK et al, 1962), to determine cloud heights especially over hurricanes (FUJITA, 1962), and to show several correlations between synoptic situations and the outgoing radiation flux.

In the present report the possibility shall be discussed to derive a mean relative humidity of the troposphere and a surface temperature (clouds or ground) from radiation data (MÖLLER, 1962) in 2 different spectral ranges. For that the radiation transfer equations should be solved for the upward outgoing radiation flux in the sensitivity of the detectors used in the satellite. This solution was obtained by radiation diagrams which were constructed using transmission functions, which have been derived especially for this purpose.

In order to show the possible errors of the method and of the radiation data various statistical investigations of single radiation data and of averaged values were carried out.

2. THE TIROS EXPERIMENT.

First we will give a short introduction into the experiment as a basis for our study. More detailed informations can be found under references marked by (*).

2.1: The object of measurements.

The satellites of the TIROS series were especially designed for meteorological tasks what is also indicated by their name TIROS (Television and Infra-Red Observation Satellite). The instruments flown in the satellites include radiometers and television cameras. One of the radiometers is a five_channel medium resolution radiometer with an aperture angle of approximately 5 degrees. It measures:

a. in three spectral ranges the upward outgoing radiation flux emitted from the earth and its atmosphere
b. the solar radiation scattered and reflected by the earth and its atmosphere in two spectral ranges.

The TIROS satellite paths are nearly circular with a mean height of approximately 780 km above the earth's surface. The orbit inclination is about 48°. Thus, the coverage extends to about 50° latitude on each side of the equator. Measured data are stored during each orbit on an endless magnetic tape within the satellite and transmitted to the earth while the satellite is passing a Data Acquisition Station.

2.2:Data of the Five-Channel Medium Resolution Radiometer.

The principle of the radiometer is illustrated in Fig. 2.1a where the components of a single channel are pictured. The optical axis of each channel is bidirectional 180° apart. It inclines 45° to the satellite spin axis so that one optical system views the earth and the other the outer space. The measured radiation is the difference value between the radiation reaching both inputs of the radiometer. So the signal is determined by

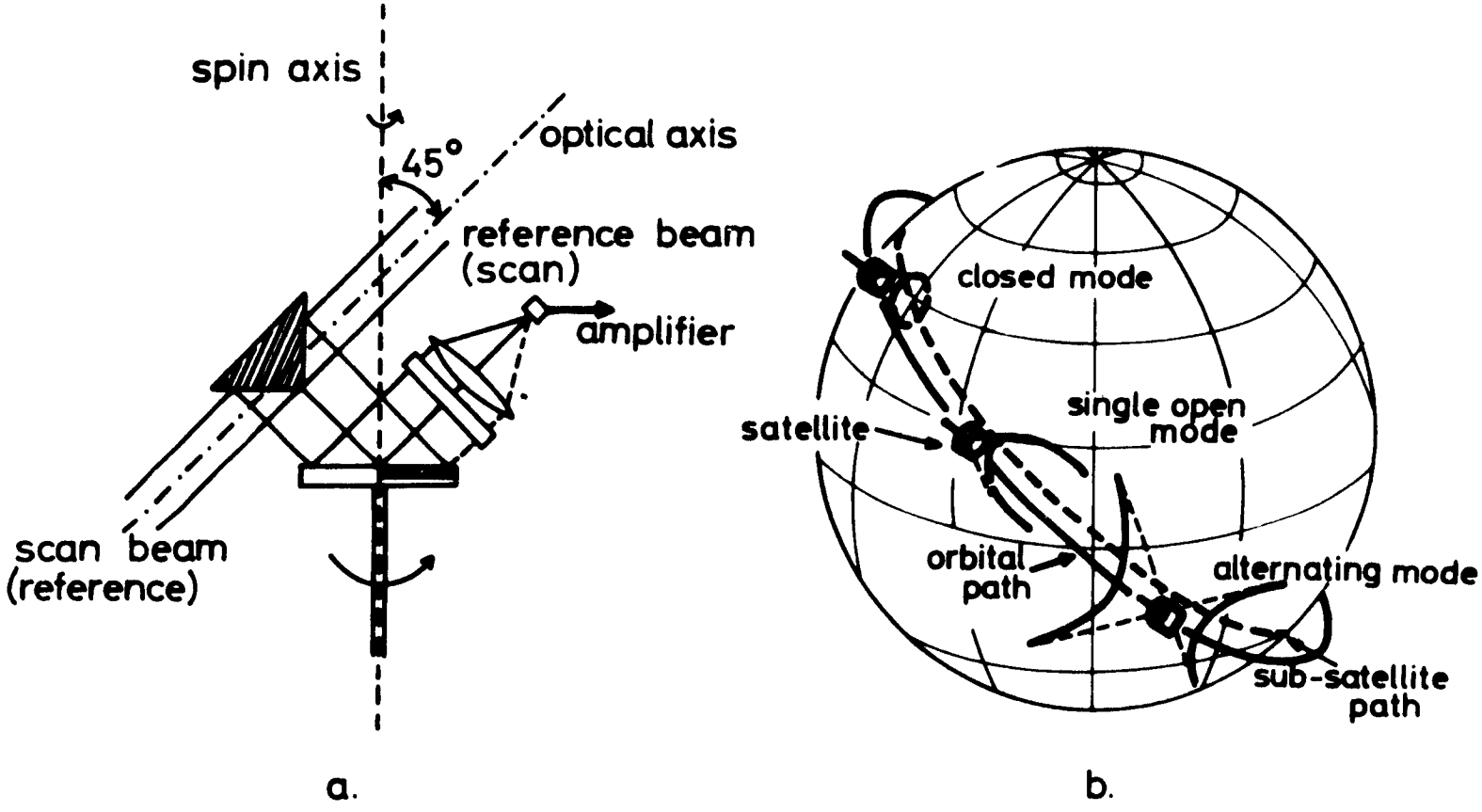

Fig. 2.1 : a.: Components of a single channel

b.: Geometry of the scanning motion

of the radiometer

$$(2.1) \qquad W = \int_0 (W_\nu^{wall} - W_\nu^{floor}) \Phi_\nu^{(n)} \, d\nu \left[W\ m^{-2}\right]$$

where "wall" and "floor" signify both inputs (Fig. 2.1a), $\Phi_\nu^{(n)}$ is the effective spectral sensitivity of the detector n (n = 1, 2, 3, 4, 5) at the wave number ν (HANEL, WARK 1961). Since theoretically the outer space level should be nearly zero, it can be used as a reference.

As the satellite rotates on its spin axis, the radiometer scan pattern on the earth's surface is defined by the intersection of a 45° half-angle cone and a sphere. The spin axis is nearly fixed in the space. The intersection curves are circles (spin vector parallel to the orbital radius vector), or single (spin vector inclined to the orbital radius vector), or double hyperbola-like branches (spin vector is perpendicular to the orbital radius vector), Fig. 2.1b. The spin rate amounts to about 6 sec. A permanent control of the position of the satellite, of its spinaxis vector, of the spin rate and also of the data acquisition time (end-of-tape-time) allows to determine for each moment of a measurement the nadir angle and azimuth angle and also the area viewed by the radiometer input.

Using an analog-to-digital-converter the analog data can be digitized suitable for an IBM 7090 computer. Radiation data and other data for orientation are available on a "Final Meteorological Radiation Tape".

FUJITA (1963) developed a procedure to directly evaluate analog data given on an analog record. As the aperture angle is about 5 degrees, the radiometer views an area on the earth's surface of a radius of about 35 km when the optical axis is parallel to the orbit radius vector. This area increases with increasing nadirangle (FUJITA, 1963).

The intensity of the infrared radiation reaching the detector surface depends on the temperature profile of the atmosphere, the content and distribution of emitting and absorbing gases, and the compactness and heights of clouds. Hence, three of the

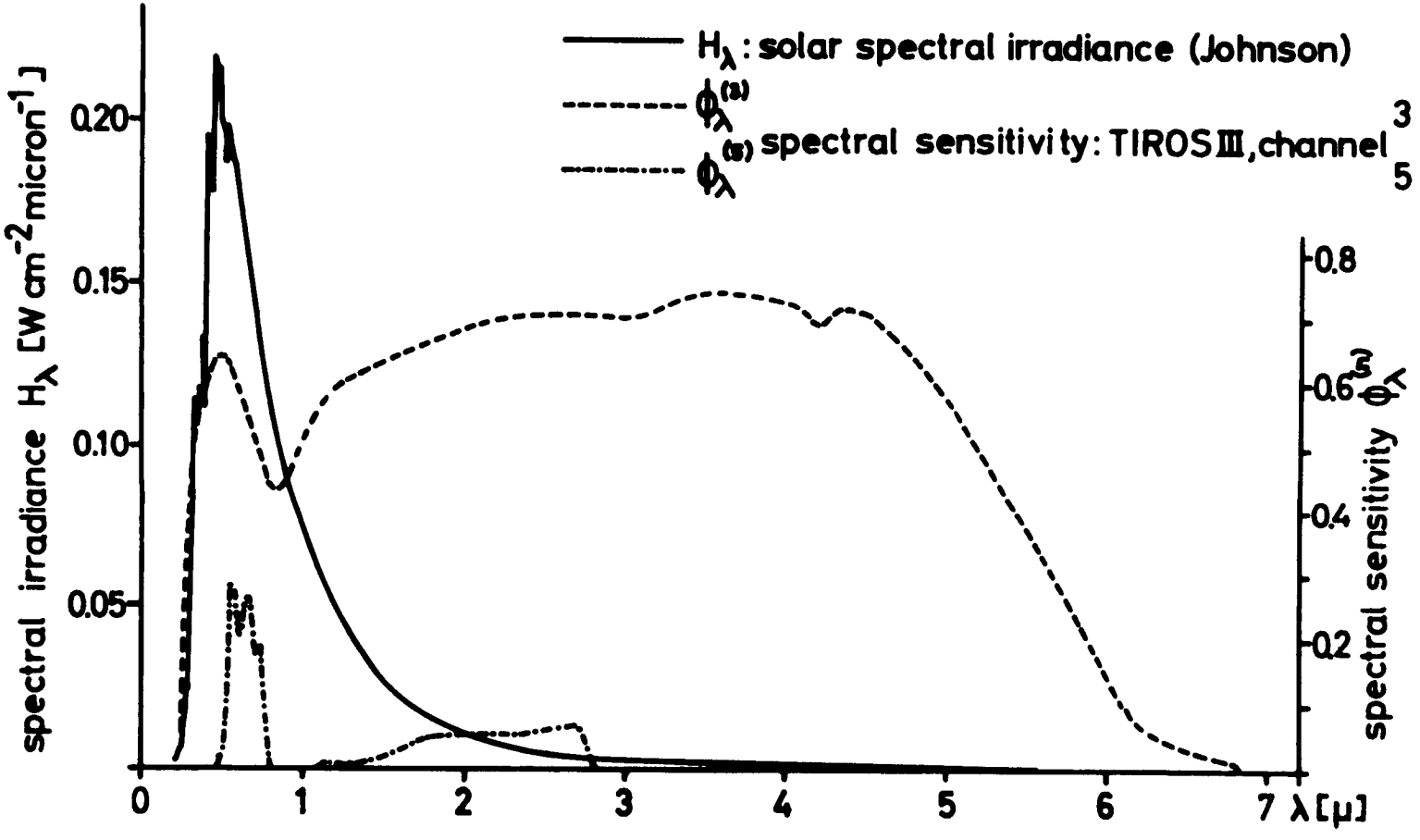
H_λ : solar spectral irradiance (Johnson)
$\phi_\lambda^{(3)}$
$\phi_\lambda^{(5)}$ spectral sensitivity: TIROS III, channel 3 5
spectral irradiance H_λ [W cm^{-2} micron^{-1}]
0.20
0.15
0.10
0.05
0.8
0.6
0.4
0.2
spectral sensitivity $\phi_\lambda^{(5)}$
0
1
2
3
4
5
6
7 λ [μ]

Fig. 2.2

five channels are equipped to measure the infrared radiation of the earth and its atmosphere in three different spectral ranges (table II,1). The other 2 radiometers measure solar radiation scattered and reflected from the atmosphere, the clouds, and the ground. (Fig. 2.2).

Table II.1: Ranges of sensitivity of the five-channel medium resolution radiometer.

	channel	range of sensitivity	bands of optic active gases
terrestrial radiation	1	5.8μ - 6.8μ	centre of the 6.3μ-band of water vapor
	2	8μ - 13μ	"water vapor window" around 10μ, 9.6μ-band of ozone and wing ranges of the 15μ-band of CO_2
	4	7.5μ-32.5μ	"water vapor window", water vapor rotation band ($\lambda > 18\mu$), 9.6μ-band of ozone and 15μ-band of CO_2
solar radiation	3	0.2μ - 6μ	reflected solar radiation in the entire spectral range of the incident solar radiation
	5	0.5μ-0.75μ	reflected solar radiation in the visible range

The infrared radiometer measure radiation, the propagation of which is influenced through the atmosphere by absorption and emission of one or more absorption bands of water vapor, carbon dioxide, and ozone (Fig. 2.4). These 3 gases have the main importance in the main importance in the infrared range considered here.

Channel 1: Its sensitivity range is located in the center of the strong absorbing rotation-vibration band of water vapor. So it should receive only radiation emitted by water vapor in higher layers (upper troposphere and lower stratosphere) with its characteristic temperature. If these layers are very dry, radiation of deep and warm layers of the troposphere should be received also. Consequently the measured intensity will be pro-

shown in Fig.1.1 this problem is important for radiation flux calculations for the spectral regions of the channels 2 and 4 where absorption bands of H_2O, CO_2 and O_3 are located.
The spectral transmissivity in such an overlapping region is determined by the product of the spectral transmissivities of the single constituents according to

$$\tau_\nu = \tau_{\nu,H_2O} \cdot \tau_{\nu,O_3} \cdot \tau_{\nu,CO_2} \qquad (2.4)$$

Fortunately the absorption bands of CO_2 (15μ-band) and O_3 (9.6μ-band) do not overlap each other in a first approximation. So we can strictly follow the correction method of YAMAMOTO (1952). If we define a correction transmission

$$\Delta\tau_\nu = \tau_{\nu,H_2O} - \tau_{\nu,\text{total}} \qquad (2.5)$$

for each spectral interval $d\nu$, an averaged 'correction transmission' can be calculated similar to the transmission in Equ. 2.3 b. In our considerations the integration over all wavenumbers was carried out for CO_2 ending at 900 cm^{-1} and beginning at 900 cm^{-1} for ozone. The summation of both integrals (or $\overline{\Delta\tau(u,c)} + \overline{\Delta\tau(u,m)}$, where u is the water vapor mass and c and m the mass of CO_2 and O_3 respectively) gives then the value of that transmissivity which is to substract from $\overline{\tau(u(T))}$ in the diagram (Fig.2.1).
$\overline{\Delta\tau(u,c)}$ or $\overline{\Delta\tau(u,m)}$ can be determined using auxiliary diagrams similar to that shown in Fig. 2.2. In Fig.2.1 the determination of the outgoing upward radiation flux according to Equ.2.3 is explained schematically. This flux is proportional to the area boundered by the ordinate , the abscissa until T_0, the curve w (T) and the upper boundary ($\overline{\tau} = 1$) of the diagram until $T = T_s$. Because of the presence of carbon dioxide and ozone the correction area is to substract from the area described above.
In radiation diagrams, the problems with varying pressure along the considered path have to be reduced to a problem where the conditions of a constant pressure p_0 can be considered. So

portional to an averaged relative humidity if a temperature profile is given (MÖLLER, 1961).

Channel 2: The main sensitivity is located in the range of the water vapor window where infrared radiation is absorbed only by the 9.6μ-band of ozone, a small continuum and weak lines of the water vapor (ROACH, GOODY, 1958). According to this absorption corrected data should be nearly equal to the radiation emitted by surfaces of clouds or the ground with its characteristic temperature.

Channel 4: The measured radiation intensity will be mostly influenced by the radiation reaching the receiver in the "window range" because of the maximum of the Planck-function for temperatures between 240°K and 280°K in this spectral range. Natural radiation of very high and cold layers will reach the detector in the spectral range of the very strong absorbing 15μ-band of CO_2. A small influence on the received radiation will be expected by variations of the water vapor content of the atmosphere because of the absorption in the rotation band of water vapor ($\lambda > 18\mu$). But it might be sufficient to determine a mean relative humidity in layers of the lower troposphere.

The radiation flux measured in channel 4 is about 80% of the whole upward heat radiation flux outgoing from the planet earth into outer space (WARK, 1962). To demonstrate this, in Fig. 2.3 the wavelength λ is given on the abscissa as a function of the ratio of the Planck-function integrated up to $\lambda(W_{0\rightarrow\lambda})$ to the whole black body radiation ($W_{0\rightarrow\infty}$) for the temperature T = 250°K. This temperature is called the "effective radiation temperature of the planet earth" (MÖLLER, 1957).

Radiation measurements were carried out only by the satellites TIROS II, III, and IV. But for our investigations we used only the radiation data of TIROS III since the radiometers of TIROS II were not calibrated accurately and TIROS IV did not contain the channel 4.

3. COMPUTATION OF RADIATION FLUX IN THE SENSITIVITY REGIONS OF THE INFRARED CHANNELS OF SATELLITE TIROS III.

The principle of the calculation of radiation fluxes by use of radiation diagrams will be explained.

3.1: Characteristics of measured radiation.

The reiceiver surface will be attained by radiation coming from a cone with an opening angle ($\Delta\omega$) of 5 degrees. The spectral irradiance shall be i_ν [W m^{-2} str^{-1}]. Because of the different spectral absorptivity of the filter, lenses, and prism, and the spectral reflectivity of the chopper the radiometer has an effective spectral sensitivity Φ_ν. The corresponding curves are shown in Fig. 2.2 and 2.3.

The measured irradiance [W m^{-2}] then can be calculated from

$$(3.1) \qquad \overline{W}'^{(n)} = \Delta\omega \int_0^\infty i_\nu \Phi_\nu^{(n)} d\nu \quad [W\ m^{-2}]$$

As it is usual in the literature, we will term the measured irradiance as a measured radiation flux, which designates all radiation coming through and from the atmosphere and incident on a receiver. But the calibration was carried through as for hemispheric symmetry, so we get

$$(3.2) \qquad \overline{W}^{(n)} = \frac{\pi}{\Delta\omega}\,\overline{W}'^{(n)} = \pi \int_0^\infty i_\nu \Phi_\nu^{(n)} d\nu = \int_0^\infty B_\nu \Phi_\nu^{(n)} d\nu \ .$$

That means the instruments are immediately calibrated in the corresponding black body radiation. The equivalent temperature for the measured radiation flux can then be calculated easily by the equation

$$(3.3) \qquad \overline{W}^{(n)} = \int_0^\infty B_\nu(T_{equ.}) \Phi_\nu^{(n)} d\nu \ .$$

The TIROS III radiation data of the infrared radiation are given in units of this equivalent temperature.

3.2: Principle of the calculation of the radiation flux for arbitrary model atmospheres.

3.21: Assumptions.

For the computation of radiation fluxes in the atmosphere several assumptions are necessary, which are satisfied in a first approximation and verified with measurements and calculations. They shall be mentioned for better understanding of the following considerations.

1. The infrared radiation will be not scattered by the molecules of the air (MÖLLER, 1957; HINZPETER, FOITZIK, 1958).
2. On each place in the atmosphere the local thermodynamical equilibrium is given. Then the Kirchhoff-law is valid (ELSASSER, 1960; etc.). CURTIS (1956) could show that this is correct up to a height of 50 km. The infrared radiation of layers higher than 50 km is almost without any significance because of the very small absorber quantities.
3. The surface of the earth and cloud surfaces emit infrared radiation like black bodies with an emissivity 1 (MÖLLER, 1957). Because thin cloud layers may have a small but measurable transmissivity, we will understand as cloud surface temperatures an effective radiation temperature, which can be the temperature of a level within the cloud but mostly close to its surface.

Further we will assume that we can use transmission functions for single rays, i.e. a bundle of rays with vanishing small aperture angle, although there is no direct but only diffuse infrared radiation in the atmosphere.

3.22: Solution of the equation of radiation transfer.

With the assumptions above mentioned the radiation transfer equation has the following solution for the spectral intensity W' of the upward radiation flux:

$$(3.4) \qquad W'_\nu = B_\nu(T_z) + \int_{T_z}^{T_o} \frac{dB_\nu(T)}{dT} \tau_\nu(w)\,dT$$

$B_\nu(T)$ is the spectral irradiance of a black body with the temperature T; T_z and T_o are the temperatures in the level z (satellite) and at the surface of a radiator (cloud or ground). The spectral transmissivity of an absorbing gas at the wave number ν is determined by $\tau_\nu(w)$, where w is the gas quantity between the places of the temperatures T_z and T. $\tau_\nu(w)$ and w will be discussed in the chapter 4.1. From equation 3.4 the amount of the radiation measured by a receiver n with the spectral sensitivity $\Phi_\nu^{(n)}$ can be determined by

$$(3.5) \quad W^{(n)} = \int_0^\infty \Phi_\nu^{(n)} W'_\nu d_\nu$$

$$= \int_0^\infty \Phi_\nu^{(n)} B_\nu(T_z)\,d\nu + \int_0^\infty \int_{T_z}^{T_o} \frac{dB_\nu(T)}{dT} \Phi_\nu^{(n)} \tau_\nu(w)\,dT\,d\nu \quad .$$

With a given temperature profile (and consequently $\frac{dB_\nu(T)}{dT}$) and a given absorber distribution w(T) in the atmosphere and their properties of transmission the equation (3.5) can be

integrated. Modern high speed computers can be used for a numerical integration (WARK et al., 1962); in doing this a program was written so that different temperature profiles, distributions of the absorber quantities and also different filter functions can be introduced.

A graphical integration is possible using radiation diagrams as were constructed by several authors (MÖLLER, 1932, 1944; ELSASSER, 1942, 1960; YAMAMOTO, 1952; KONDRATIEV, 1960). For our investigations we will use radiation diagrams designed for each channel according to YAMAMOTO's diagram.

3.23: Construction of a radiation diagram according to YAMAMOTO (1952).

The basic idea for the construction of any radiation diagram is to integrate over all wave lengths before the integration over all temperatures (or better layers) between T_z and T_o is carried out. Analogous to YAMAMOTO we introduce a weighted mean transmissivity $\overline{\tau(w(T))}$ of the entire sensitivity range for a constant temperature T and absorber quantity w(T):

$$(3.6)\quad \overline{\tau(w(T))} = \frac{1}{\int \Phi_\nu^{(n)} \frac{dB_\nu(T)}{dT} d\nu} \int_o^\infty \Phi_\nu^{(n)} \frac{dB_\nu(T)}{dT} \tau_\nu(w(T)) d\nu$$

w(T) is the absorber quantity given in an atmospheric profile as a function of the temperature T. The second term on the right side of equation (3.5) gets then the following form:

$$(3.7)\quad \int_o^\infty \int_{T_z}^{T_o} \frac{dB_\nu(T)}{dT} \Phi_\nu^{(n)} \cdot \tau_\nu(w(T)) dT d\nu = \int_{T_z}^{T_o} \left(\int_o^\infty \Phi_\nu^{(n)} \frac{dB_\nu(T)}{dT} d\nu \right) \overline{\tau(w(T))}\, dT.$$

Now we can set:

$$(3.8a)\qquad \frac{dS(T)}{dT} = \int_o^\infty \Phi_\nu^{(n)} \frac{dB_\nu(T)}{dT} d\nu$$

where S(T) is the radiation of a black body with the temperature T received by a receiver n with the effective spectral sensitivity $\Phi_\nu^{(n)}$:

$$S(T) = \int_0^T \frac{dS(T)}{dT}\, dT \quad . \tag{3.8b}$$

Substituting equation (3.8a) into equation (3.7) and changing the variable of integration gives now an equation for the upward radiation flux received by a receiver of the spectral sensitivity $\Phi_\nu^{(n)}$:

$$\overline{W}^{(n)} = S(T_z) + \int_{S(T_z)}^{S(T_o)} \overline{\tau(w(T))}\, dS(T) \quad . \tag{3.9}$$

Equation (3.9) now shows a way to construct a radiation diagramm with $\overline{\tau(w(T))}$ as ordinate and S(T) as abscissa. For practical purposes these functions are determined for several temperatures and absorber quantities. So the diagram contains lines of constant temperature (vertical straight lines, abscissae) and curves w(T) = constant (Fig. 3.1). For flux calculations the absorber quantities are determined according to an equation given in the next chapter.

The area limited by the curve w(T), T_o, the avscissa and the ordinate is then proportional to the radiation flux $\overline{W}^{(n)}$ (Eq. 3.9).

As is shown later, the transmissivity functions depend on pressure and temperature. The temperature dependence can be considered during the construction of the diagrams, but not the pressure dependence. Because the diagram should applicable to different arbitrary atmospheric profiles, it is constructed with transmission functions which are valied only for one reference pressure p_o and a "pressure correction" of the absorber quantity is introduced. Diagrams which are explained above were constructed for water vapor in all 3 sensitivity ranges but a

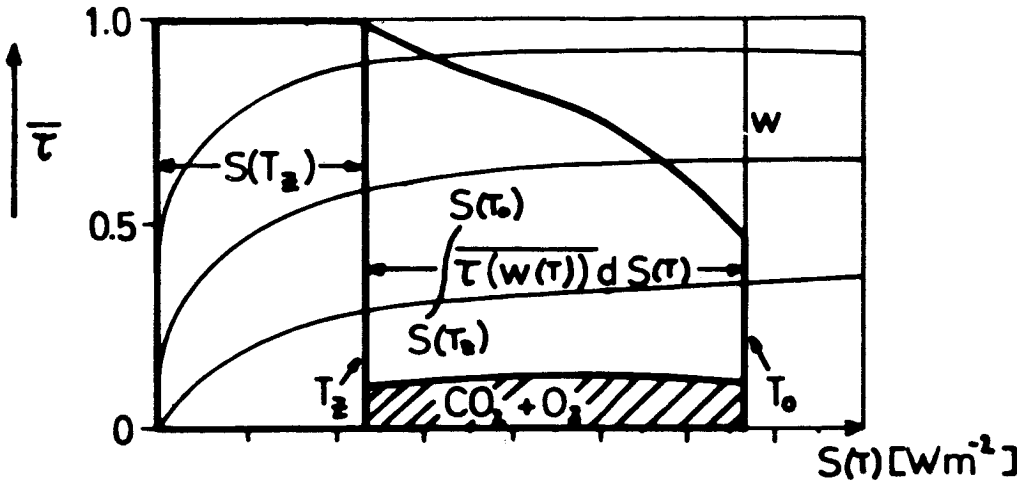

Fig. 3.1 : Radiation diagram
(YAMAMOTO, 1952)

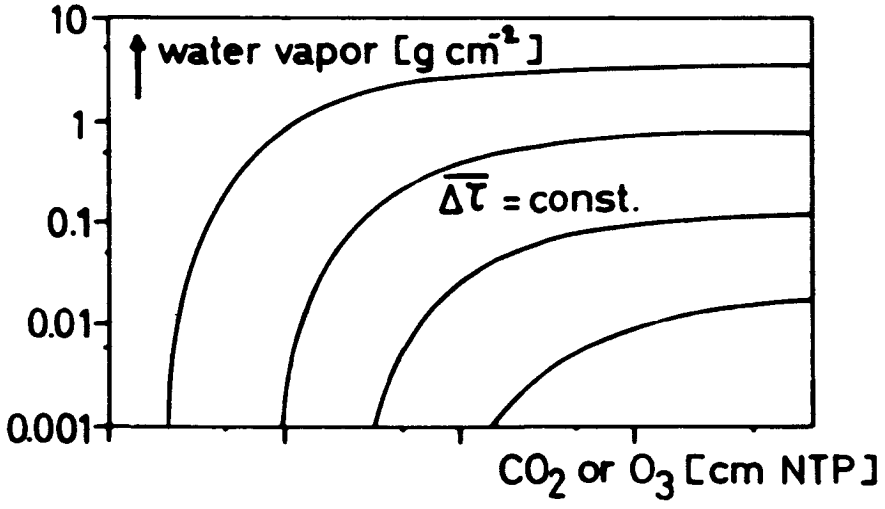

Fig. 3.2 : Auxiliary diagram
(YAMAMOTO, 1952)

correction according to the absorption by CO_2 and O_3 within the same ranges (channels 2 and 4) has to be applied.

3.23.1: Auxiliary diagrams for the correction relative to the absorption by other gases.

In spectral intervals dν where absorption bands of water vapor, carbon dioxide, and ozone overlap the transmissivity can be determined by the product of the transmissivities of the 3 gases:

$$\tau_\nu = \tau_{\nu,H_2O} \cdot \tau_{\nu,CO_2} \cdot \tau_{\nu,O_3} \quad . \tag{3.10}$$

Fortunately the 9.6μ-band of ozone and the 15μ-band of carbon dioxide do not overlap in a first approximation. So we can use the correction method developed also by YAMAMOTO.

According to equation (3.9) fundamental diagrams were constructed for the water vapor absorption. According to equation (3.10) the entire transmissivity is smaller than that of water vapor: $\tau_\nu < \tau_{\nu,H_2O}$. If we define

$$\Delta\tau_\nu = \tau_{\nu,H_2O} - \tau_\nu \quad , \tag{3.11}$$

we can calculate a correction transmissivity $\overline{\Delta\tau}$ for CO_2 and another one for O_3 (3.6) assuming that the transmissivity of the one gas in the absorption range of the other one is equal to 1. The entire correction is then to be determined by the summation

$$\overline{\Delta\tau(n,c,m)} = \overline{\Delta\tau(n,c)} + \overline{\Delta\tau(n,m)} =$$

$$\left[(H_2O + CO_2); (H_2O + O_3)\right]$$

$$= \frac{1}{\int_0^\infty \Phi_\nu(n)\,\frac{dB_\nu(T)}{dT}\,d\nu} \left[\int_0^{900\,cm^{-1}} \Phi_\nu(n)\,\frac{dB_\nu(T)}{dT}\,\tau_\nu(u)\left(1-\tau_\nu(c)\right)d\nu \right. \tag{3.12}$$

$$\left. + \int_{900\,cm^{-1}}^{\infty} \Phi_\nu(n)\,\frac{dB_\nu(T)}{dT}\,\tau_\nu(u)(1-\tau_\nu(m))\,d\nu \right]$$

u, c, and m signify the quantities of water vapor, carbon dioxide, and ozone. The quantity of water vapor is measured by [g cm^{-2}] or l.e. (liquid equivalent = heigth of water column over 1 cm^{-2} of the receiver's surface). CO_2 and O_3 quantities are measured by cm gas column over 1 cm^{-2} of the receiver's surface reduced to Normal Temperature and Pressure [cm NTP], where T = 0°C and P = 760 mm Hg.

For CO_2 and O_3 auxiliary diagrams were constructed which allow to find $\overline{\Delta\tau}$ for arbitrary quantities of water vapor and CO_2 or O_3. A schematic exhibition is shown in Fig. 3.2. Because an auxiliary diagram can be constructed only under the condition of a constant temperature it is advisable to use several auxiliary diagrams calculated for different temperatures. The way of the correction is shown in Fig. 3.1. For any level given by its temperature the absorber quantities u (H_2O) and c (CO_2) or m (O_3) are known and consequently also $\overline{\Delta\tau}$. For the whole temperature profile all $\overline{\Delta\tau}$ determine an area which is to subtract from the area under the water vapor curve.

4. TRANSMISSION FUNCTIONS τ_ν.

Transmission functions will be derived from measured absorption spectra published by several authors.

4.1: Optical thickness and the transmission of an absorber.

The gases in the atmosphere absorb radiation with their absorption bands and emit radiation in the same spectral ranges like black bodies, where the emissivity is equal to the absorptivity. These two procedures determine the propagation of infra red radiation if we neglect a very small absorption by particles of dust, aerosols and other additions in the atmosphere.

In general we can determine the optical thickness of a gas with the density $\varrho(s)$ and the mass absorption coefficient $k_\nu(s)$ by the integration along the way s

$$(4.1) \qquad \tau_\nu(s,s') = \int_{s'}^{s} k_\nu(s)\varrho(s)\,ds$$

ν = wave number. $k_\nu(s)$ and $\varrho(s)$ depend on the conditions along the way s. The absorbers between the points s' and s absorb a part of the intensity of a ray. So we can define the transmissivity of a layer in the spectral interval $\Delta\nu$:

$$\tau_\nu(s,s') = \frac{1}{\Delta\nu}\int_{\Delta\nu} e^{-\int_{s'}^{s} k_\nu(s)\varrho(s)\,ds}\,d\nu \qquad (4.2)$$

$$0 \leq \tau_\nu \leq 1.$$

The wave number ν designates the middle of the interval. If we assume homogeneous conditions along the way s the mass absorption coefficient is constant ($k_\nu(s) = k_\nu$) and the absorber quantity can be determined by

$$w = \int_{s'}^{s} \varrho(s)\,ds \qquad (4.3)$$

or only by $w = \varrho \cdot s$ if the density is constant also.

The transmissivity is then determined by

$$\tau_\nu(s,s') = \tau(k_\nu \cdot w) = \frac{1}{\Delta\nu}\int_{\Delta\nu} e^{-k_\nu w}\,d\nu \quad . \qquad (4.4)$$

Instead of τ_ν we can also use the absorptivity A_ν to characterize the "optical property" of gas. It is

$$A_\nu = 1 - \tau_\nu \quad .$$

The absorption of an entire band is determined by

$$A = \int_{\nu_1}^{\nu_2} A_\nu d\nu = (\nu_2 - \nu_1) - \int_{\nu_1}^{\nu_2} \tau_\nu d\nu \quad (cm^{-1}),$$

where ν_1 and ν_2 designate the interval in which the band is located. The quotient $\frac{A}{\Delta\nu} = \frac{A}{\nu_2-\nu_1}$ is the percentage absorption of an entire band.

4.2: Investigation of pressure and temperature dependence of the absorption.

4.21: Line absorption.

The infrared bands of the atmospheric gases consist of a wast number of lines. Their shape is determined at atmospheric conditions by collisions of the molecules of the absorbing gas among one another (selfbroadening) and with molecules of other gases (foreign gas broadening). For these conditions the line shape can be described by the Lorentz pressure broadened line shape

$$k_\nu = \frac{S}{\pi} \frac{\alpha}{\alpha^2 + (\nu - \nu_o^2)} \tag{4.5}$$

ν_o = wave number of the line center.

The Doppler line shape is to be taken into account for heights greater than 50 km (PLASS and FIVEL, 1953). The half width α is proportional to an effective pressure p_e and inversely to the square root of the absolute temperature T, so that

$$\alpha = \alpha_o \frac{p_e}{p_o} \sqrt{\frac{T_o}{T}} \tag{4.6}$$

where the index o refers to the conditions under which α_o was determined. The line intensity is normalized:

$$S = \int_{-\infty}^{+\infty} k_\nu \, d\nu \quad .$$

It is also a function of the temperature (e.g.: see BOLLE, 1963). The effective pressure p_e is defined to give particular weight to the greater effect of the selfbroadening compared to foreign gas broadening, so that:

$$p_e = p_{tot.} + N p_{part.}$$

Under atmospheric conditions the partical pressure $p_{part.}$ of the absorbing gas compared to the total pressure $p_{tot.}$ is small and can be neglected. But in laboratory measurements the partial pressure often must be great to get an absorption effect.

4.22: Pressure and temperature dependence of the absorption.

LADENBURG and REICHE (1911) investigated the absorption of a single line. ELSASSER (1942) and GOODY (1952) computed the transmissivity of small spectral intervals containing some lines (ELSASSER model, statistical model). Not only for the line model but also for the band models it can be distinguished between 2 limiting cases (or approximations) of the absorption:

a. Weak line absorption.
This approximation is valid for a single line if the absorption is small even in the line center. It is also valid if the total absorption due to all lines within a small interval is small at every frequency also if the lines overlap each other.

In both cases the absorption coefficient is only a function of the product of the absorber quantity w with the line intensity S

$$A_\nu \sim A_\nu(w \cdot S). \tag{4.7}$$

A_ν does not depend on the half-width or the pressure.

b. Strong line approximation.
This approximation is valid when incident radiation is completely absorbed in the line centers of strong lines and when the lines therefore have only a transmission in their wings. In this case the absorption is proportional to a function of the product of the line intensity S, the absorber quantity w and the half-width α:

$$A_\nu \sim A_\nu(S \cdot w \cdot \alpha) \; . \tag{4.8}$$

According to (4.6) it depends on the pressure.

Since this case in a first approximation is decisive for the absorption of infrared radiation in the atmosphere many authors introduced a linear pressure correction of the absorber quantity

$$w^* = w \cdot \left(\frac{p_e}{p_o}\right) \quad , \tag{4.9}$$

This includes that absorption coefficients without a pressure dependence and absorber quantity dependence are used. These so-called "generalized absorption coefficients" l_ν depend only on the wave number and the temperature. So the absorption of a spectral interval designated by the wave number ν is a function of the product $l_\nu \cdot w^*$, and

$$A_\nu = A_\nu(l_\nu \cdot w^*) \quad . \tag{4.10}$$

The "linear pressure correction" of the absorber quantity was introduced by ELSASSER and KING (1953) for the derivation of transmission functions for ozone and carbon dioxide from given measurements (SUMMERFIELD, CLOUD). It is also used by YAMAMOTO (1952) and other authors. MATOSSI and RAUSCHER (1949) found for the 6.3μ band of water vapor a correction according to $(p_e/p_o)^n$, where n = 0.5. The same exponent was derived by SCHNAIDT (1939) from measurements of FALCKENBERG (1939) and v. BAHR (1909). HOWARD et al. (1955) inferred from their laboratory measurements for the 6.3μ band of water vapor exponents n = 0.72 for strong absorption and n = 0.6 for weak absorption. On the other hand, MÖLLER(1944) investigated a model atmosphere and derived a more complicated factor for the correction of the quantity of water vapor

$$\chi_\mu = \left[a\left(\frac{p}{p_o}\right)^r + b\left(\frac{p_o}{p}\right)\right]$$

$$a = 0.985, \; b = 0.015, \; r = 0.8 \, .$$

Obviously the pressure dependence of the absorption will be different in different band ranges, because there are strong lines in the band center and weaker lines in the band wings. Furthermore an additional dependence should be expected from the absorber quantity, because at very slight absorber quantities also strong lines have a transmittance in the line center. These various influences on the absorption are shown in the Fig. 4.1 and 4.2, where a derived exponent n is drawn versus the absorber quantity w. n was found from computed absorptivities (WYATT, STULL, and PLASS, 1962, 1963) in the following way:

These authors published tables containing absorption coefficients for water vapor and carbon dioxide for small intervals in a large spectral range and large regions of pressure and absorber quantity. From these tables absorption values (averaged over a spectral interval of 50 cm^{-1}) at fixed wave number and at constant pressure were drawn versus the absorber quantity. This gives a family of curves with the pressure as curve parameter. A correction of the absorber quantity relative to normal conditions (p_o) means now the projection of all curves with constant pressure on the absorption curve $p = p_o$. If this process is carried out by multiplying the absorber quantity w by $(p/p_o)^n$, so that

$$w^* = w \left(\frac{p}{p_o}\right)^n \quad ,$$

then the exponent n is not constant. The dependence of n on the pressure and also on the absorber quantity is shown in both Fig. 4.1 and 4.2 for the 6.3μ-band of water vapor and the 15μ-band of carbon dioxide respectively.

In all cases the exponent n decreases with decreasing absorber quantity. For an explanation one can say that the lines in the spectral interval chosen here are approaching with decreasing absorber quantity also in their center a certain transmission and so the approximation a. (weak lines) without pressure dependence will be more probable.

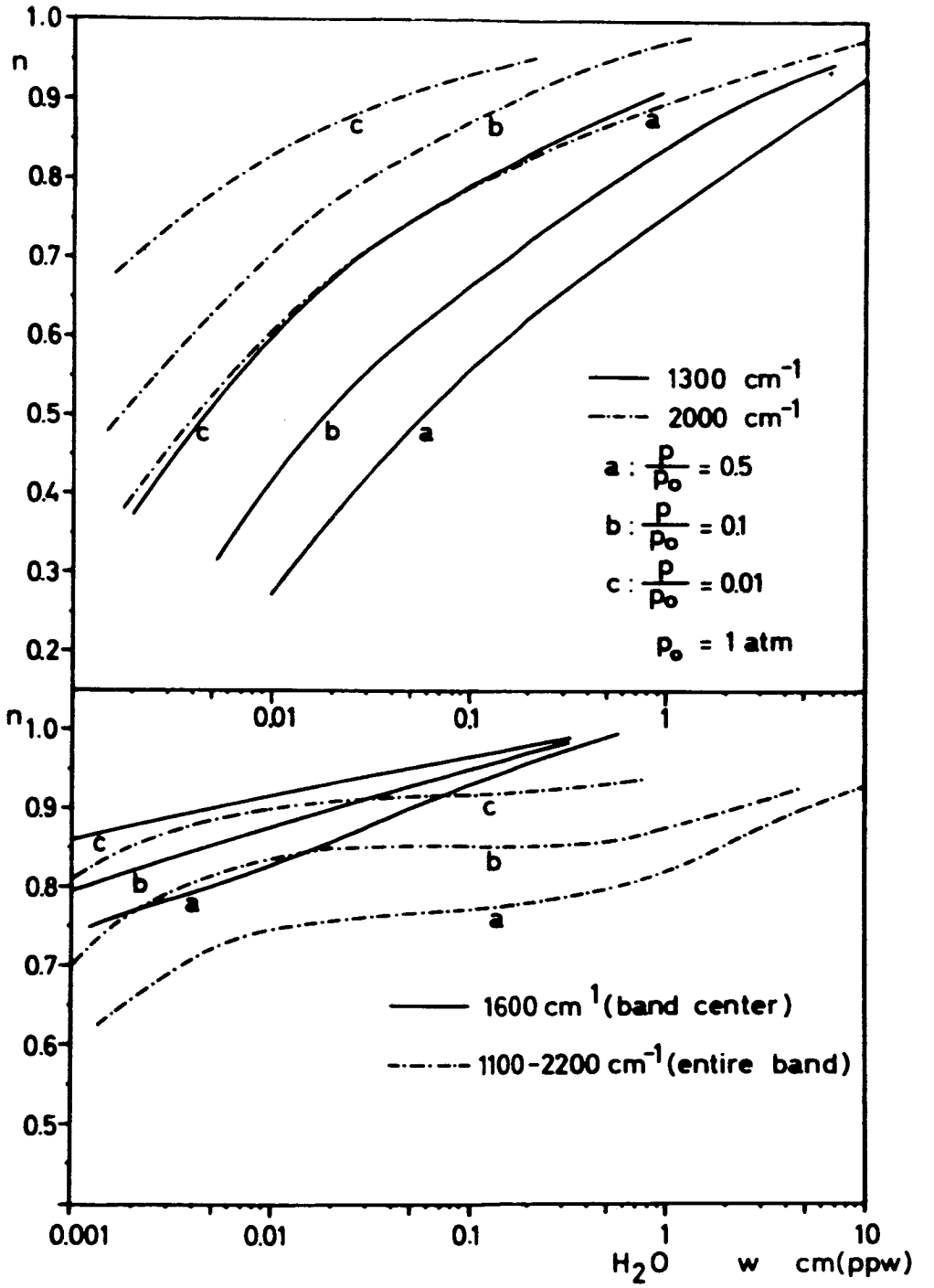

Fig. 4.1 : Pressure correction exponent n versus the absorber quantity (6.3μ - band)

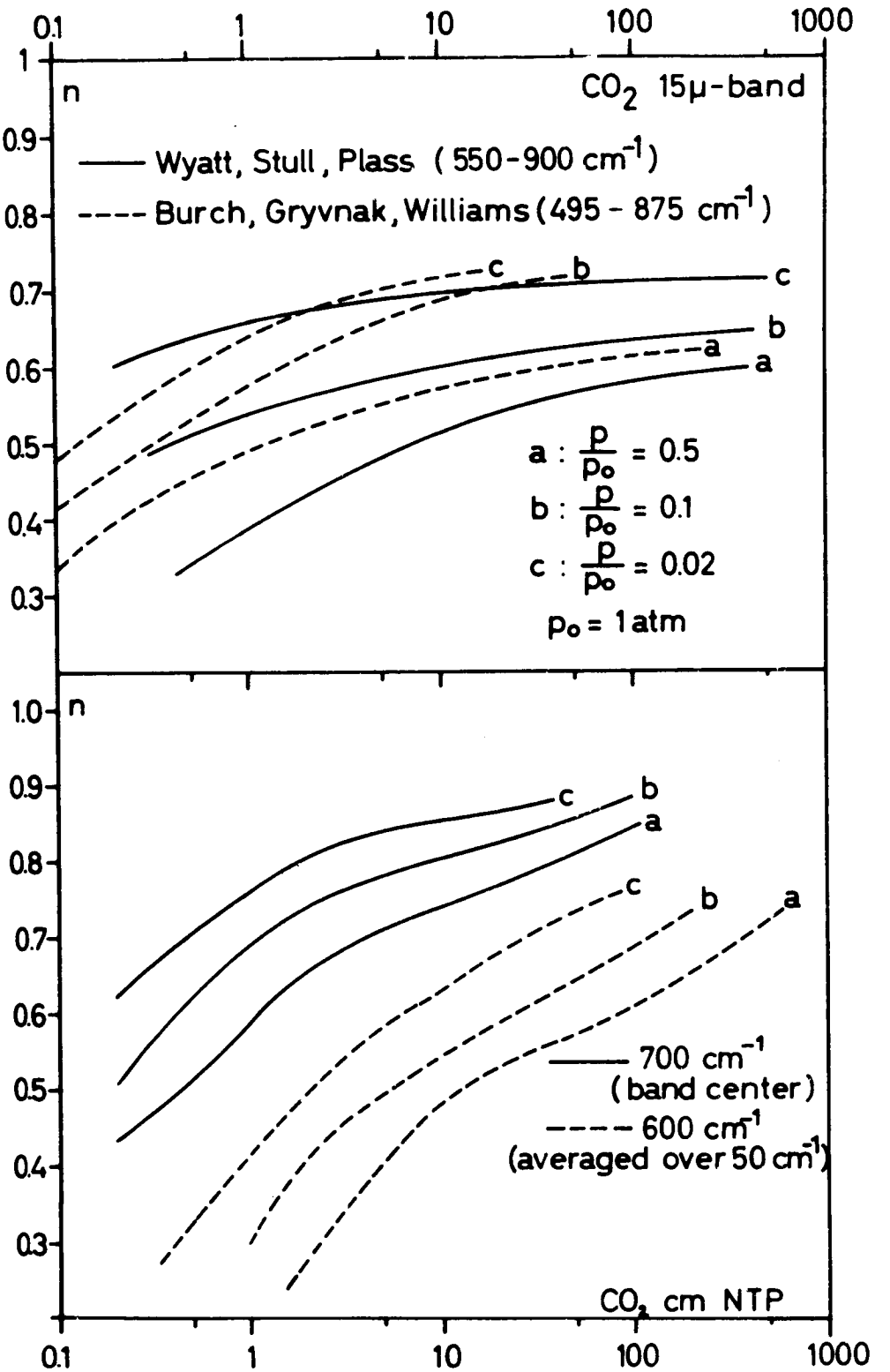

Fig. 4.2 : Pressure correction exponent n versus the absorber quantity

However, the exponent n increases at constant absorber quantity with decreasing pressure. As the absorption coefficient of a single line in the line center is inversely proportional to the half-widths,

$$k(\nu_0) = \frac{S}{\pi} \cdot \frac{1}{\alpha} ,$$

and the line intensity S has no pressure dependence, so $k(\nu_0)$ must increase with decreasing pressure (Eq. (4.6)). Therefore the lines are getting narrower, but the absorption in their center more intensive. So the absorption coefficient has a strong frequency dependence within the band interval. The approach to very small pressures leads to the approximation b. (strong lines), the linear pressure dependence. In both figures two different spectral intervals are chosen to show the behaviour of lines in the band center and of lines in the wing ranges (weaker lines) of a band.

The exponent for the entire band decreases very slowly. Its behaviour is composed by the behaviour of the strong lines and by the weak lines.

The temperature dependence of the absorption of a line is determined by the temperature influence on the line intensity S and the half-width α. Both are more complicated as it is shown in the equation (4.6) (see e.g. BOLLE, 1963). BENEDICT and KAPLAN found that in the temperature range of meteorological interest (220° - 300°K) the temperature dependence of the half-width can be respresented by

$$\left(\frac{\alpha}{\alpha_0}\right)_{p_0=\text{const}} \sim \left(\frac{T_0}{T}\right)^m$$

with T_0 = 3000°K and $\alpha_0 = \alpha(300°K)$. The exponent m varies from line to line between - 0.045 and + 0.756.

As it is shown above the pressure and temperature influence on the absorption is very complicated for practical purposes. For computations of radiation fluxes with radiation diagrams simpli-

fications have to be used. Using high speed computers with a large memory more detailed considerations of the pressure and temeprature dependence may be possible.

4.3: Derivation of transmission functions.

Transmission functions were derived from laboratory measurements accoring to the proposal of ELSASSER and KING (1953). These new transmission function are given as functions of the product of a generalized absorption coefficient l_ν and the pressure-corrected absorber quantity w^*, so that:

$$\tau_\nu = \tau_\nu(l_\nu w^*) \tag{4.11}$$

where

$$l_\nu = l_\nu\,(T) \tag{4.12}$$

and

$$w^* = w\left(\frac{p}{p_o}\right)^n \quad .$$

τ_ν is the spectral transmittance of a band.

All laboratory measurements published by several authors were carried out at constant pressure and constant density of the absorbing gas along the path. In order to get a measurable absorption effect on the short way through the absorption tube relative large absorber quantities at a relative high partial pressure had to be used. So HOWARD et al. (1955) required as the smallest amount of water vapor 0.02 g cm^{-2}. But in the upper atmosphere there are much smaller amounts of water vapor and at lower pressures than used in measurements, so that in the practical computations we have to extrapolate the values to such small amounts. In order to derive transmission functions from measured spectra the effect of selfbroadening is to be consedered and for this reason many authors defined an effective pressure (see chapter 3.22)

$$p_e = p_{total}\ ^{Np}{}_{partial} \tag{4.13}$$

For N they used different values:

authors	absorbing gas	N
HOWARD et al.	water vapor (bands from 1.1μ - 6.3μ)	1
BURCH et al.	carbon dioxide 15μ-band	0.3
PALMER	water vapor rotation band (20μ - 50μ)	6

Table IV.1: Selfbroadening factor N.

According to equation 4.12. the absorber quantities used in the measurements must be corrected to normal pressure p_{o*} in order to determine the spectral transmittance $\tau'_\nu = (l_\nu\ w^*)$.

ELSASSER and KING introduced the linear pressure correction (n=1), in the derivation of their transmission functions for the 15μ-band of CO_2 from measurements of CLOUD (1952) and for the 9.6μ- and 14.1μ-bands of ozone from measurements of SUMMERFIELD (1941), also ELSASSER (1960) for the 6.3μ-band of water vapor (DAW, 1956). But this linear pressure correction is only valid for the spectral ranges with strong absorption lines as it is shown in fig. 4.1 and 4.2.

So we will use other exponents which are found partly by other authors and partly by our own calculations.

For the derivation of transmission functions calculated and measured values of the following publications were used:

absorber gas	band	authors
H_2O	6.3μ	laboratory measurements (HOWARD et al. (1955), tables of WYATT, STULL, PLASS (1963)
	water vapor window (800-1200 cm^{-1}) 8.3μ-12.5μ	Roach - GOODY (1958) BOLLE et a. (1963)
	rotation band 20μ-50μ	laboratory measurements (PALMER 1960)
CO_2	15μ	laboratory measurements (BURCH et al. 1960) calculated spectra (YAMAMOTO and SASAMORI), tables of WYATT, STULL, PLASS (1963)
O_3		laboratory measurements of the absorptions of the entire band (WALSHAW 1957)

An application of calculated absorption coefficients (e.g. WYATT, STULL, PLASS 1963) is to be preferred in the derivation of transmission functions and of generalized absorption coefficients, in experiments the area of a band will be strongly influenced by the slit-width of the spectrometer. HOWARD et al. (1955) demonstrated this, but they could show that the absorption of an entire band will not be influenced by different slit-widths provided that there is no other absorption on both sides of the band.

The division of a band into several small intervals is necessary for the determination of generalized absorption coefficients l_ν, but it brings automatically new errors into the computation. The solution into single strong lines, the behaviour of which determines probably the absorption of atmospheric gases in the upper stratosphere, is lost in this method of calculations of the radiation flux.

4.31: Water vapor.

In the sensitivity ranges of the three infrared channels of TIROS III the water vapor absorbs and emits with the rotation-vibration band (6.3μ-band) and the pure rotation band ($\lambda > 18\mu$). The window region between both bands contains single weak lines and a continuum absorption caused by the wings of the strong lines in the adjacent bands.

Because the sensitivity ranges of the channels 2 and 4 include the three above mentioned absorption ranges an uniform pressure correction has to be used if radiation flux calculations are carried out with radiation diagrams. May be, a large error will be introduced by this procedure in the window region; there are, however, no detailed results of absorption measurements.

For computations in this report we used an uniform water vapor correction:

$$u^* = u \left(\frac{p}{p_o}\right)^{0.72}$$

in all spectral regions. HOWARD et al. found this exponent by their own measurements in the 6.3μ-band.

a.) 6.3μ-band:

HOWARD et al. (1955) derived from spectral measurements in the 6.3μ, 2.7μ, 3.2μ, 1.82μ, 1.38μ, and 1.1μ bands at an effective pressure p_e = 740 mm Hg, a spectral transmittance τ_ν.

All points scattered only a little around a curve, which can be described by a GOODY-formula [Fig. 4.3]

$$(4.13) \qquad \tau(l_\nu u^*) = \exp\left\{\frac{-1.97 \cdot l_\nu \cdot u^*}{[1+6.57 \cdot l_\nu \cdot u^*]}\right\}^{1/2}$$

The same authors determined also generalized absorption coefficients l_ν for all spectral intervals. They are shown in Fig. 4.4 (6.3μ-band).

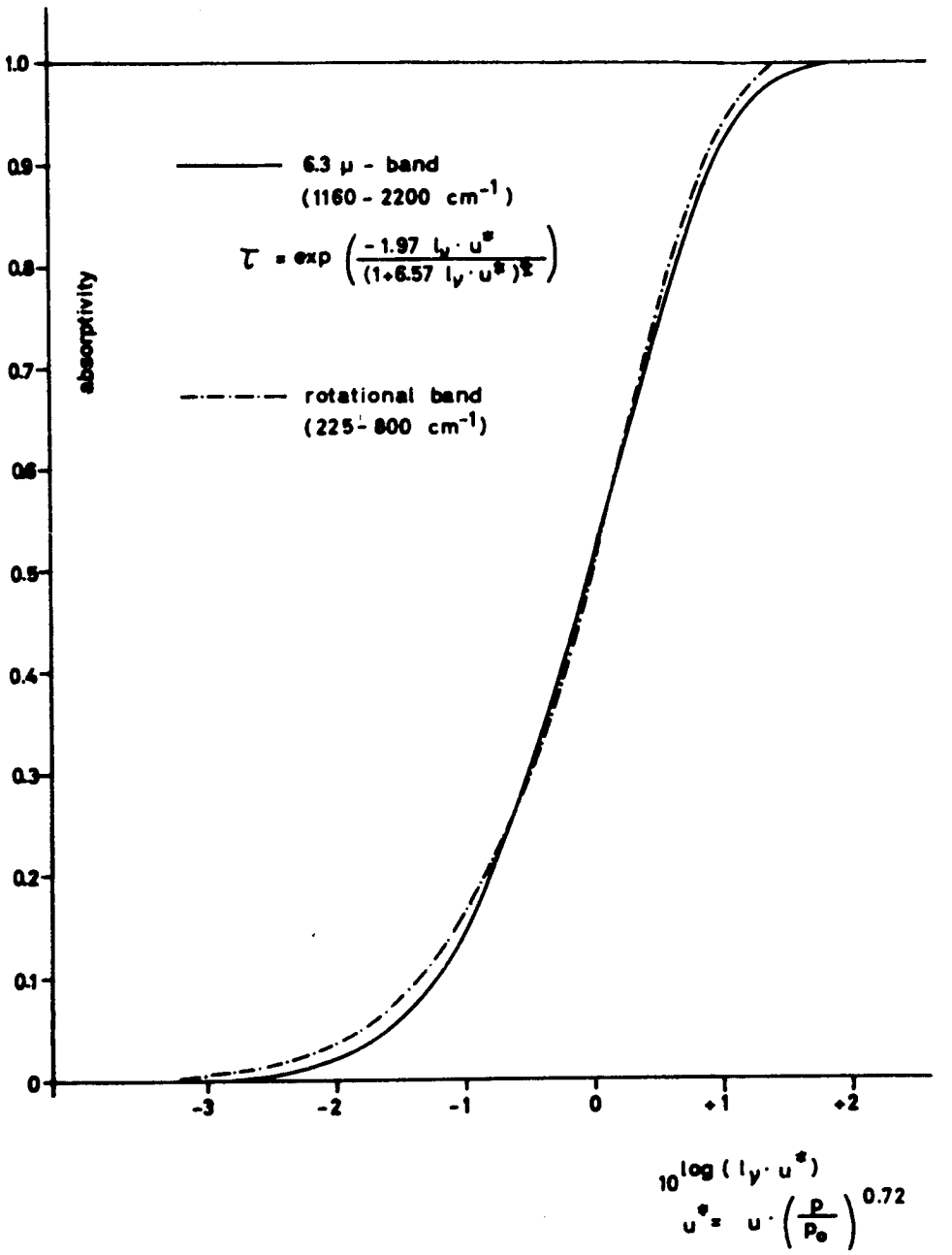

Fig. 4.3 : Spectral absorptance of the 6.3μ - band and rotation band of water vapor

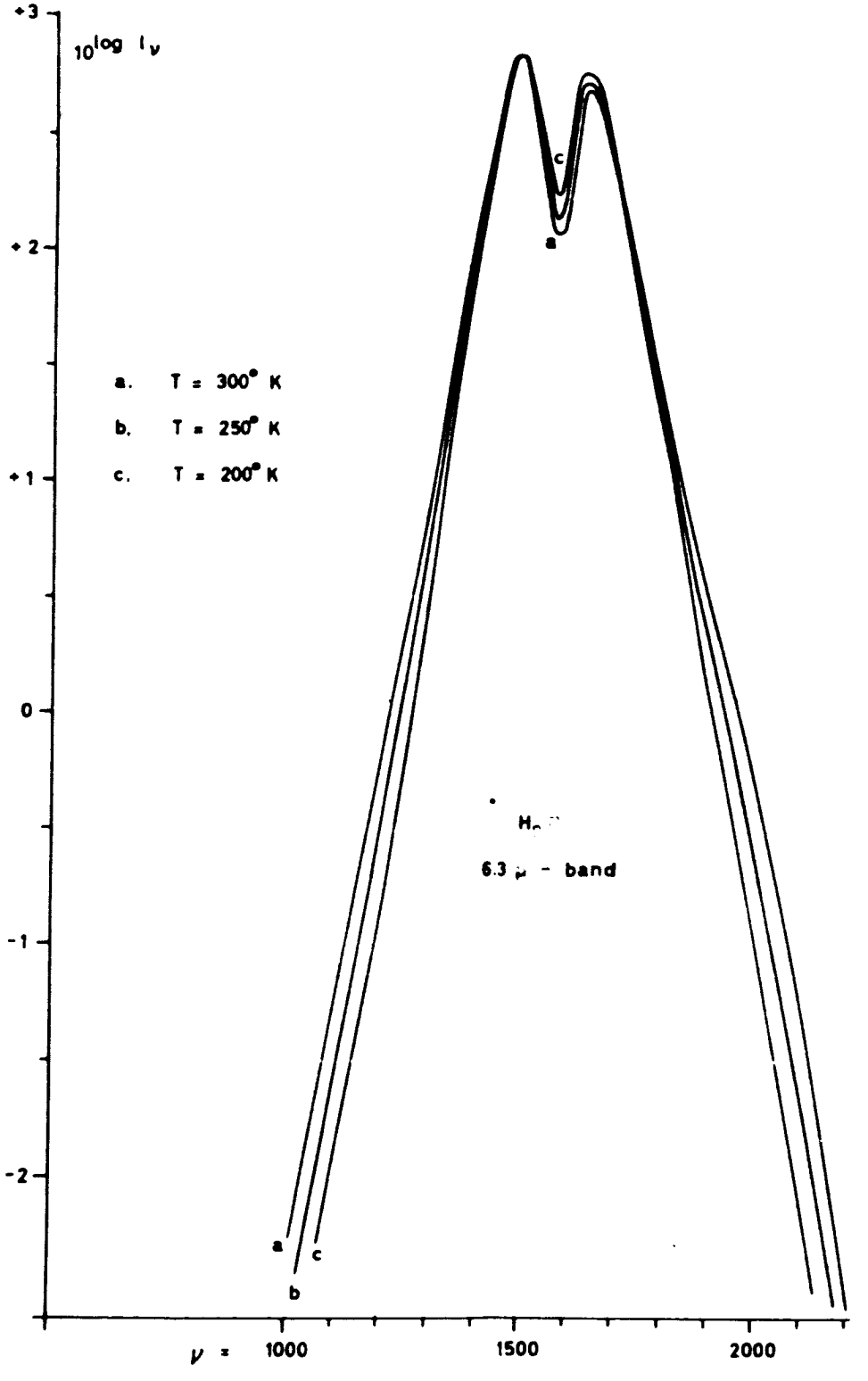

Fig. 4.4 : Generalized absorption coefficient

The transmissivity of a small interval of the band at the wave number ν and the water vapor quantity u^* can be determined using both curves or the tables of the decadic logarithms of the generalized absorption coefficient and of

$$\tau\,(_{10}\log l_\nu + {}_{10}\log u^*), \quad \text{given in Appendix I.}$$

In order to take the temperature effect on the absorption into consideration, the generalized absorption coefficients were determined for temperatures different from the temperature of measurements using a proposal of WEXLER and KAPLAN (1952).

In a first approximation the transmittance of a small spectral interval with lines, which overlap only a little, can be described by the equation:

$$\tau = e^{-K\sqrt{u \cdot \bar{p}}}$$

(see also the strong line approximation).

K is proportional $\sum (S_i \alpha_i)^{1/2}$, where S_i and α_i are the intensity and half-width of the i-th line within the line interval. The product $S_i \cdot \alpha_i$ is a complicated function of the temperature. To consider the temperature variations along the radiation path in the atmosphere KAPLAN and WEXLER used a modified CURTIS-GODSON-approximation:

$$u \cdot \bar{p} = \int_0^{P_1(u)} y p \, du \; ; \qquad p = p(u)$$

where

$$y = \frac{\sum (S_i \, \alpha_i)^{1/2}}{\sum (S_{oi} \alpha_{oi})^{1/2}} \; .$$

The index o refers to the temperature at which the absorption coefficients are determined. KAPLAN and WEXLER calculated y in dependence on the temperature and the distance from the band center (1600 cm^{-1}).

In the construction of the radiation diagrams the transmittance for several absorber quantities is introduced for homogeneous conditions (pressure and temperature are constant). Then the correction factor can be applied to the generalized absorption coefficient, because l_ν in a first approximation is proportional to K^2.

$$\tau = e^{-K\sqrt{u \cdot \bar{p}}} = \tau(K^2 \cdot u \cdot \bar{p}) = \tau(l_\nu \cdot u) \ .$$

With this correction curves of l_ν for various temperatures were obtained (Fig. 4.4).

Because HOWARD et al. measured at room temperatures, the temperature of their generalized absorption coefficients was equalized to 300°K.

The curves of the generalized absorption coefficients (Fig. 4.4) at other temperatures show the different behaviour of the lines in the band center and in the band wings.

b.) "Window-range".

ROACH and GOODY (1958) investigated the absorption of infrared absorption by water vapor in the window range. They were able to explain this absorption by two different causes: a selective absorption by weak lines and continuous absorption. The selective absorption is caused by single lines with a distance which is large in comparison to the half-width, so that

$$\tau_{\nu s} = e^{-\frac{1}{d}\sqrt{\pi \alpha_\nu S u^*}} = e^{-\eta_\nu \sqrt{u^*}} \ . \tag{4.14}$$

The continuum absorption can be described by the law of BOUGUER and LAMBERT:

$$\tau_{\nu c} = e^{-\beta_\nu u^*} \ . \tag{4.16}$$

The cause of this continuum, either absorption by haze, aerosols or by the far wings of strong lines in the adjacent bands, has not yet been elucidated and therefore also the kind of temperature and pressure dependence is not yet clear.

ROACH and GOODY interpreted this continuum as an absorption by the wings of strong lines. They found a good agreement of their measurements with calculated absorption values using values for ß which are derived for the far line wings in different spectral intervals (KAPLAN). These values of ß and also of $\eta_\nu = \frac{1}{d}\sqrt{\pi\alpha_o S}$ are given in the following table. The graphical interpolation gives the curves shown in Fig. 4.5.

spectral intervals cm^{-1}	$\eta_\nu = \frac{1}{d}\sqrt{uS\alpha_o}$ $[cm\ g^{-\frac{1}{2}}]$	$\beta_\nu [cm^2\ g^{-1}]$
1198 - 449	0.088	0.10
1149 - 1100	0.065	0.085
1100 - 948	ozone	
948 - 908	0.043	0.08
908 - 871	0.055	0.095
853 - 814	0.070	0.9
814 - 778	0.187	0.14

The transmissivity in a narrow interval around ν is then determined by

$$\tau_\nu = \tau_{\nu s} \cdot \tau_{\nu c} = e^{-(\eta_\nu \sqrt{u^*} + \beta_\nu u^*)} \qquad (4.17)$$

Because computations of generalized absorption coefficients by YAMAMOTO (1952) did not show a temperature effect, no temperature correction was made here. Using the tables of WYATT, STULL and PLASS, however, a temperature effect could be found for the spectral region of 1080 _ 1200 cm^{-1}, but has not been used here.

c.) Rotation band (12.5μ - 50μ; 800 cm^{-1} - 200 cm^{-1}).
Absorption measurements with a high resolution and over a large scale of pressure and water vapor quantity were carried out by PALMER (1960) in the spectral region between 20μ and 50μ. From his own results, averaged over 50 cm^{-1}, PALMER derived generalized absorption coefficients introducing the linear pressure correction.

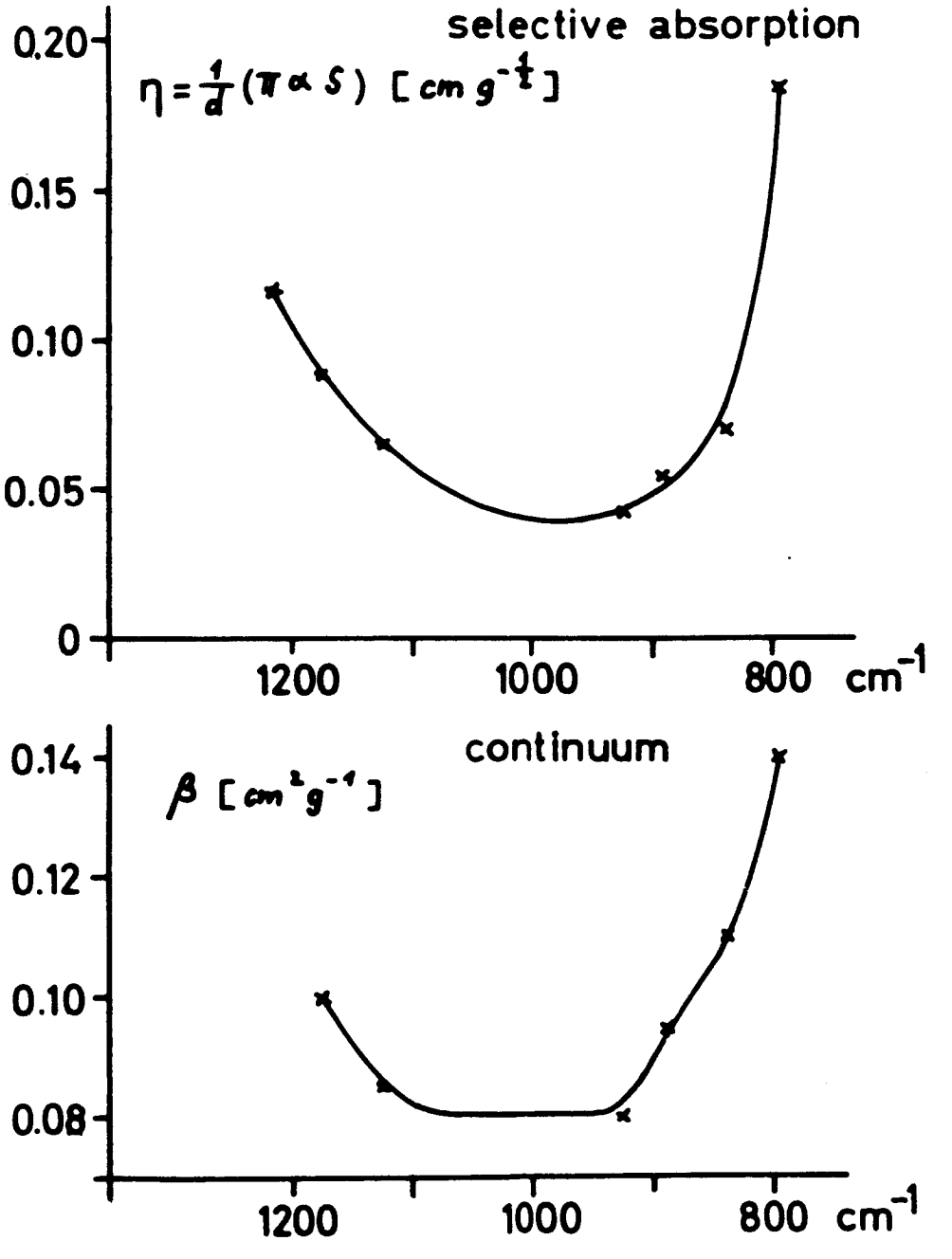
selective absorption
$\eta = \frac{1}{d}(\pi \alpha S)$ [cm g$^{-\frac{1}{2}}$]
0.20
0.15
0.10
0.05
0
1200
1000
800
cm^{-1}
continuum
β [cm^{2}g^{-1}]
0.14
0.12
0.10
0.08
1200
1000
800
cm^{-1}

Fig. 4.5

We used the same values but corrected the water vapor quantity by the formula

$$u^* = u \left(\frac{p}{p_o}\right)^{0.72} .$$

For each spectral interval (50 cm^{-1}) an absorption curve could be derived as a mean curve through all measured values with some scattering around that curve. The reciprocal generalized absorption coefficient was then defined to be equal to the water vapor quantity which is necessary for an absorptivity of 0.5 in each spectral interval.

The superposition of all curves in the common point of intersection in A = 0.5 at the water vapor quantity $u^* = 1$ g cm^{-2} yielded then an averaged curve of spectral transmittance (Fig.4.3) which was used together with the generalized absorption coefficients (Fig. 4.6) for the calculation of the radiation diagrams.

For the spectral region between 800 cm^{-1} and 500 cm^{-1} the generalized absorption coefficients l_ν were determined by measurements of the atmospheric downward radiation with a grating spectrometer (BOLLE et al. 1963). These values of l_ν differ only by a small amount from YAMAMOTO's (1952) calculated values.

Because there were no other computations of the temperature effect on the absorption in this considered spectral region, the temperature correction of the generalized absorption coefficients calculated by YAMAMOTO (1952) was taken over. A linear interpolation was used for intermediate values of the temperature.

4.32: Carbon dioxide.

Extensive measurements of the absorption of the 15μ-band of carbon dioxide were performed by BURCH, GRYVNAK and WILLIAMS (1960). These authors published numerous spectra, measured with high resolution and tables of the mean absorptivities for 4 intervals of the band (495-617, 617-667, 667-720, and 720-825 cm^{-1}) and for the entire band. These values can be used to show the influence of pressure and absorber quantity on the absorption. But the

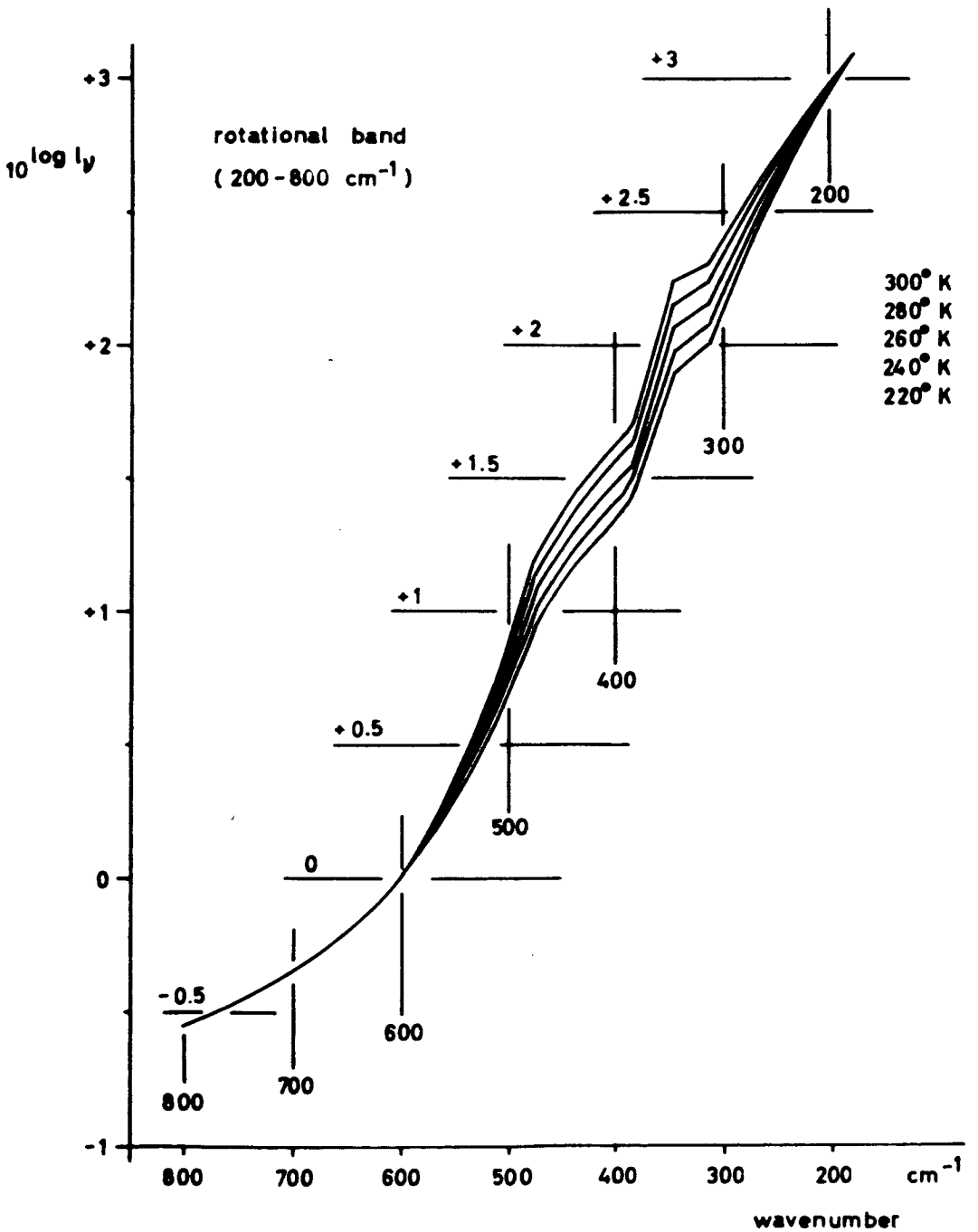
rotational band
(200 - 800 cm^{-1})
$10^{\log I_\nu}$
+3
+2
+1
0
-1
+3
+2.5
+2
+1.5
+1
+0.5
0
-0.5
200
300
400
500
600
700
800
300° K
280° K
260° K
240° K
220° K
800
700
600
500
400
300
200
cm^{-1}
wavenumber

Fig. 4.6

scatter of the given data around mean absorption curves is sometimes large. It influences the accuracy of the determination of the exponent n. In the average the exponent n was determined to be n = 0.65 for both band wing intervals and nearly 0.75 for the center intervals.

An averaged transmittance curve $\tau(1_\nu\ c^*)$ was determined by superposition of the transmittance curves of all 4 intervals. In all spectral regions the carbon dioxide was finally pressure corrected using the formula

$$c^* = c\left(\frac{p}{p_o}\right)^{0.65} ,$$

where p_o = 760 mm Hg.

Using this averaged transmittance curve (Fig. 4.7) generalized absorption coefficients were determined for spectral intervals of 10 cm^{-1} of 15 measured spectra. A graphical interpolation of all averaged values for each interval yielded then the curve for T = 300°K (Fig. 4.8).

In order to determine generalized absorption coefficients for temperatures lower than 300°K, calculated spectra of the 15μ-band (YAMAMOTO, SASAMORI 1961) were used. These authors compared transmittance for the temperatures 265°K, 240°K and 220°K. From these, generalized absorption coefficients were determined using the same curve of spectral transmittance (Fig. 4.7).

4.33: Ozone.

Two absorption bands of ozone lie within the sensitivity of the channels 2 and 4. The influence of the 14.1μ-band on the infrared radiation transfer in the atmosphere can be neglected because this band lies close to the center of the strong 15μ-band of carbon dioxide. But the influence of the 9.6μ-band is to be taken into consideration in determinations of the radiation flux in the atmosphere. There exist only a few measurements of the spectral absorption of O_3. ELSASSER and KING (1953) derived generalized absorption coefficients and a curve for the spectral transmittance from spectra measured by SOMMERFIELD (1941)]. They introduced the linear pressure correction.

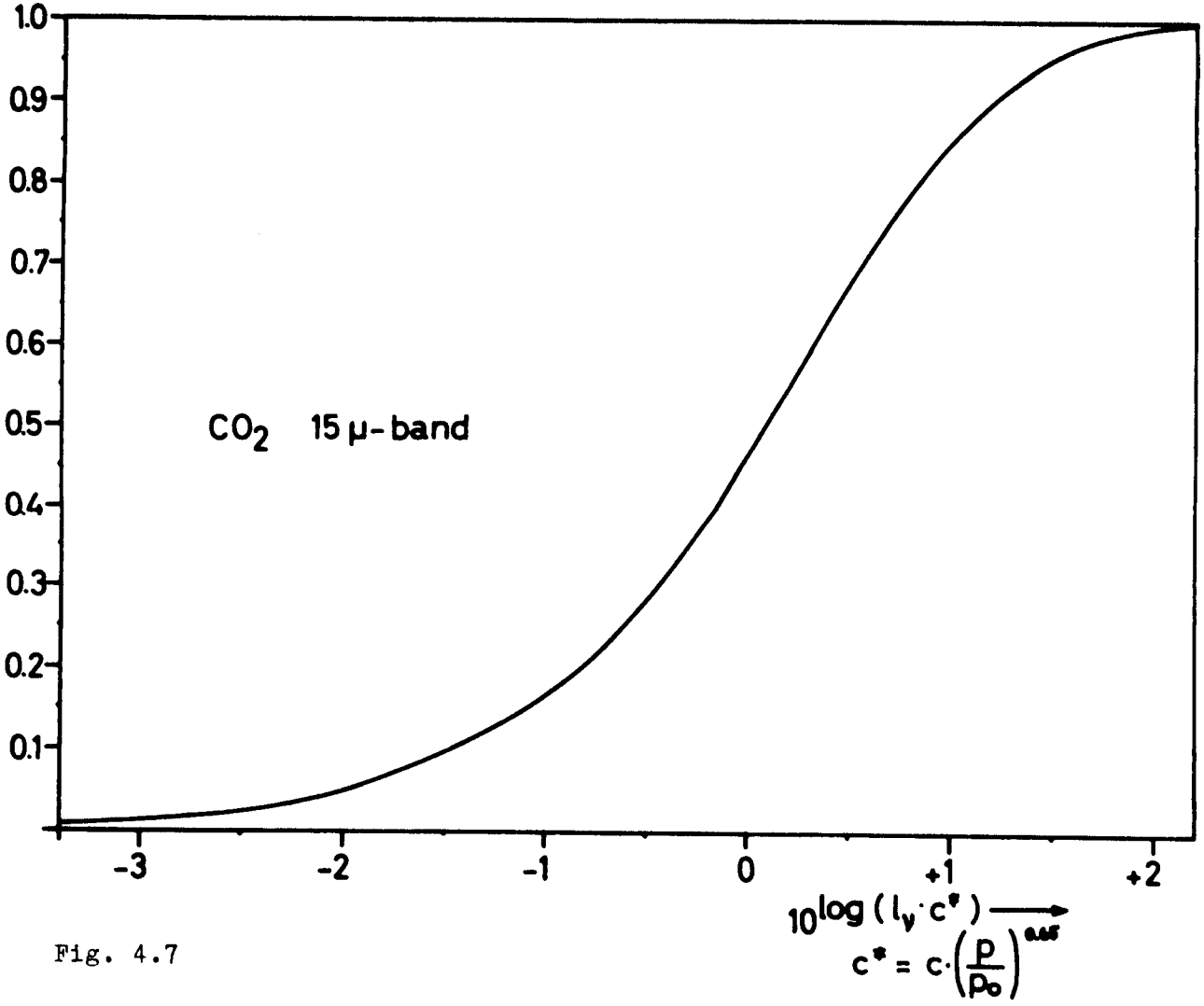
1.0
0.9
0.8
0.7
0.6
0.5
0.4
0.3
0.2
0.1
CO_2 15 μ-band
-3
-2
-1
0
+1
+2
$10^{\log(I_\nu \cdot c^*)}$
$c^* = c \cdot \left(\frac{p}{p_0}\right)^{0.65}$

Fig. 4.7

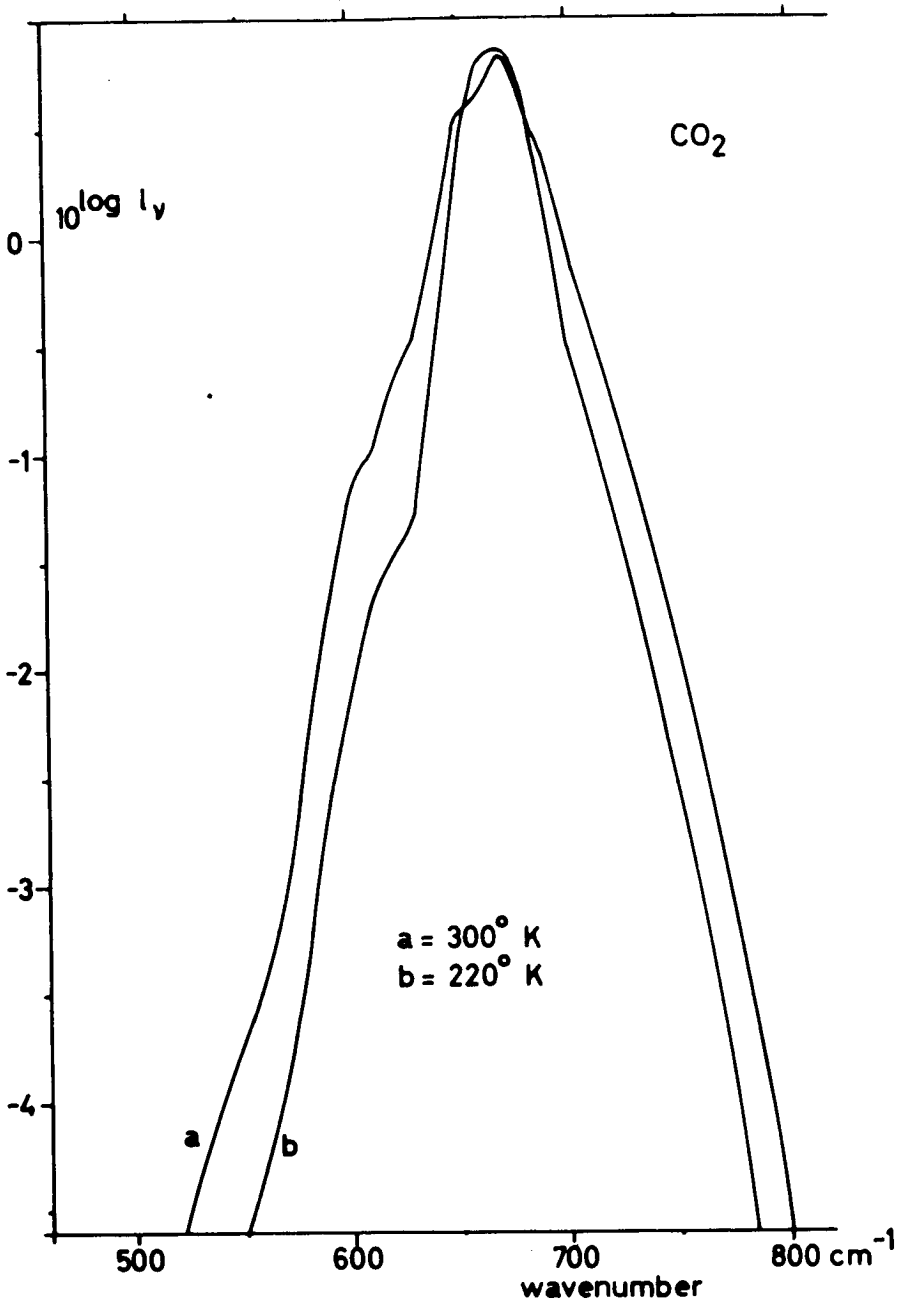
$10^{\log I_\nu}$
0
-1
-2
-3
-4
CO_2
a = 300° K
b = 220° K
a
b
500
600
700
800 cm^{-1}
wavenumber

Fig. 4.8

MÖLLER and MANABE (1961) determined a pressure correction coefficient of n = 0.3 from absorption data of the entire band given by WALSHAW (1957) using the method of least squares, where they assumed the absorption to be proportional to the square root of the ozone quantity.

Using WALSHAW's data, it can be shown that for small ozone quantities ($0.002 < m < 0.02$ cm NTP) and at relative high pressures ($150 \text{ mb} < p < 1000$ mb) the absorption is without any pressure dependence and only a linear function of the ozone quantity (weak line approximation). The dependence of absorption on the ozone quantity m can be described in a first good approximation by the equation (p = constant)

$$ {}_{10}\log \frac{A}{\Delta\nu} = 0.65 \cdot {}_{10}\log m - 0.11 \quad . $$

This formula was found by a graphical process. Using this formula the pressure correction exponent was determined to be 0.41 by the method of least squares. Here, only absorption data for pressures smaller than 150 mb were considered. All measured data scatter only a little around the absorptivity curve (Fig. 4.9), except data for $p > 150$ mb. This curve can be approximated in the lower part also by the GOODY-formula

$$ \tau = \exp\left[-\frac{16.86\, m^*}{\sqrt{1+251\, m^*}}\right] . $$

For the calculation of an auxiliary diagram only the absorption values of the entire band (Fig. 4.9 or table E in Appendix I) were introduced into the equation 3.12.

Because WALSHAW gave his data for a spectral interval of 138 cm^{-1} width and the auxiliary diagram was calculated for an interval of 200 cm^{-1} (940 cm^{-1} - 1140 cm^{-1}; 10.6μ - 8.8μ) all original values of the percentage absorption $\frac{A}{\Delta\nu}$ were multiplied with the factor 138/200 before plotting the data in Fig. 4.9.

At computations of actual ozone profile the ozone quantities in layers of the atmosphere above the 150 mb-layer were pressure corrected according to the formula:

$$ m^* = m \left(\frac{p}{p_o}\right)^{0.41} \quad . $$

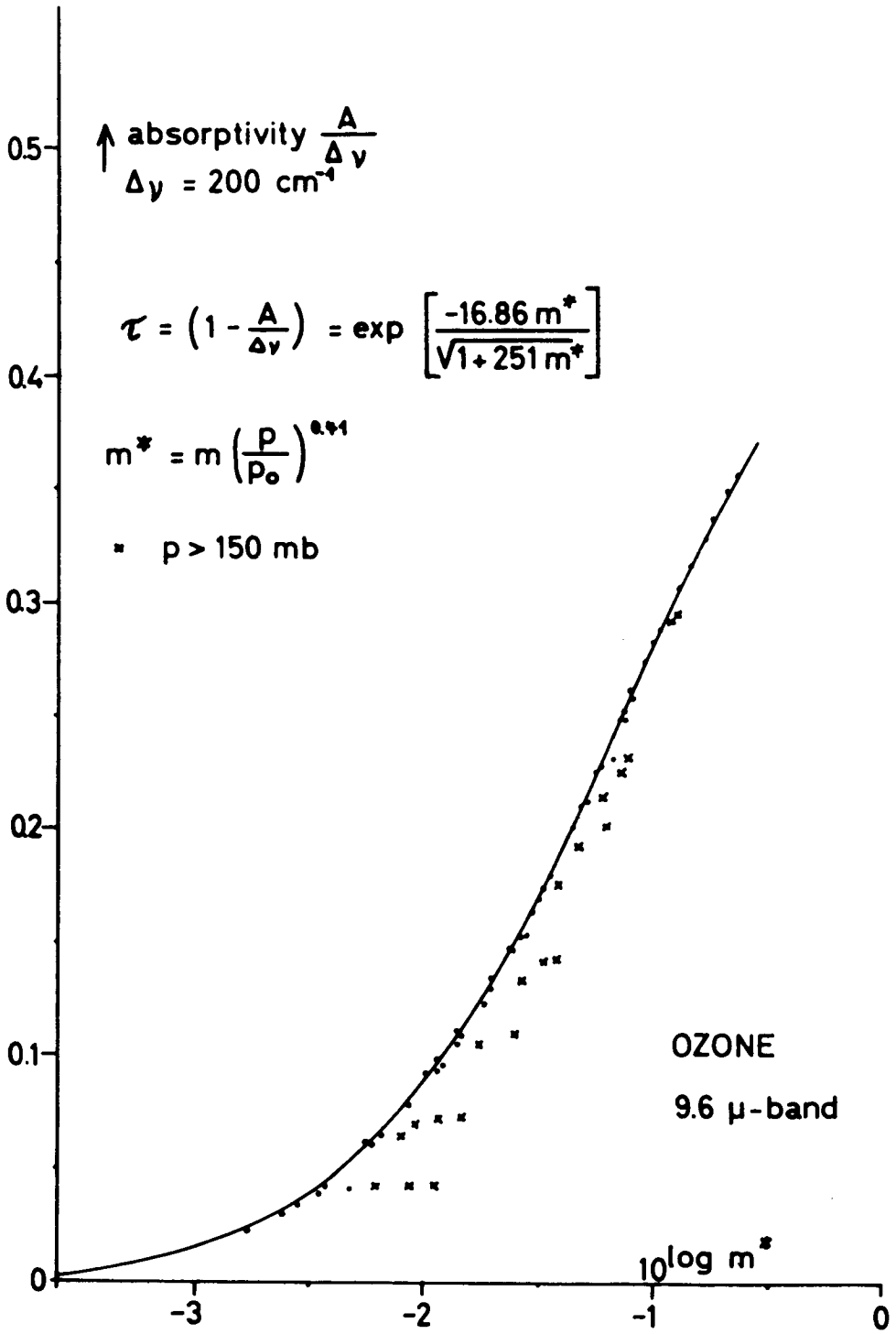
absorptivity $\frac{A}{\Delta\nu}$
$\Delta\nu$ = 200 cm^{-1}
$\tau = \left(1 - \frac{A}{\Delta\nu}\right) = \exp\left[\frac{-16.86\, m^*}{\sqrt{1 + 251\, m^*}}\right]$
$m^* = m\left(\frac{p}{p_o}\right)^{0.91}$
p > 150 mb
0.5
0.4
0.3
0.2
0.1
0
-3
-2
-1
0
$10^{\log m^*}$
OZONE
9.6 μ-band

Fig. 4.9

The low concentration of the ozone in the atmosphere below the 150 mb-layer allows to neglect the pressure correction because of the pressure independence of the absorption at high pressures and the small absorber quantities as it is shown above.

4.34: Comparisons between recalculated and measured spectra.

In order to find an estimation of the reliability of the new derived transmission functions, recalculated and measured spectra, both at the same conditions, were compared. The figures of the 15μ-band of CO_2 (Fig. 4.10) and of the 6.3μ-band of H_2O (Fig. 4.11) show different deviations between measured and recalculated spectra. With decreasing pressure and decreasing absorber quantity in both cases, the absorption of recalculated spectra is larger in the band center, but in the wing regions it is smaller than the measured absorption. This phenomenon can be explained by the application of a constant pressure exponent for all spectral regions of the bands, so that in the band center an effective absorber quantity is introduced into the formula which is too large whereas it is too small in the wing regions. This is a good verification of the dependence of the pressure correction on the spectral interval of a band, what has been shown in chapter 4.22.

In the following table measured absorption data of PALMER (averaged over an interval of 50 cm^{-1}) are compared with recalculated data. The agreement appears very good.

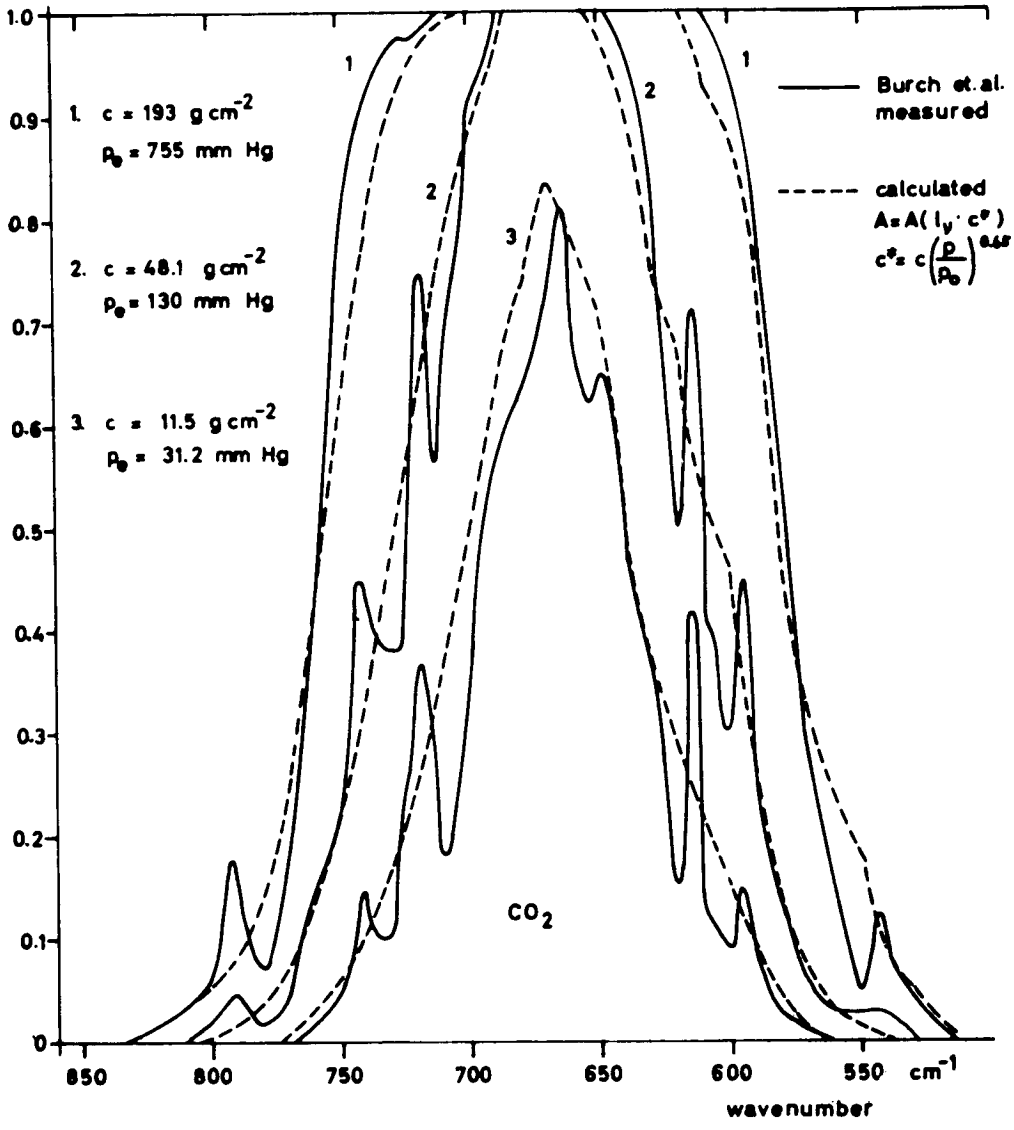
1. c = 193 g cm^{-2}
p_e = 755 mm Hg
2. c = 48.1 g cm^{-2}
p_e = 130 mm Hg
3. c = 11.5 g cm^{-2}
p_e = 31.2 mm Hg
Burch et.al. measured
calculated
$A = A(l_y \cdot c^*)$
$c^* = c\left(\frac{p}{p_0}\right)^{0.65}$
CO_2
wavenumber
cm^{-1}
1.0
0.9
0.8
0.7
0.6
0.5
0.4
0.3
0.2
0.1
0
850
800
750
700
650
600
550

Fi. 4.10

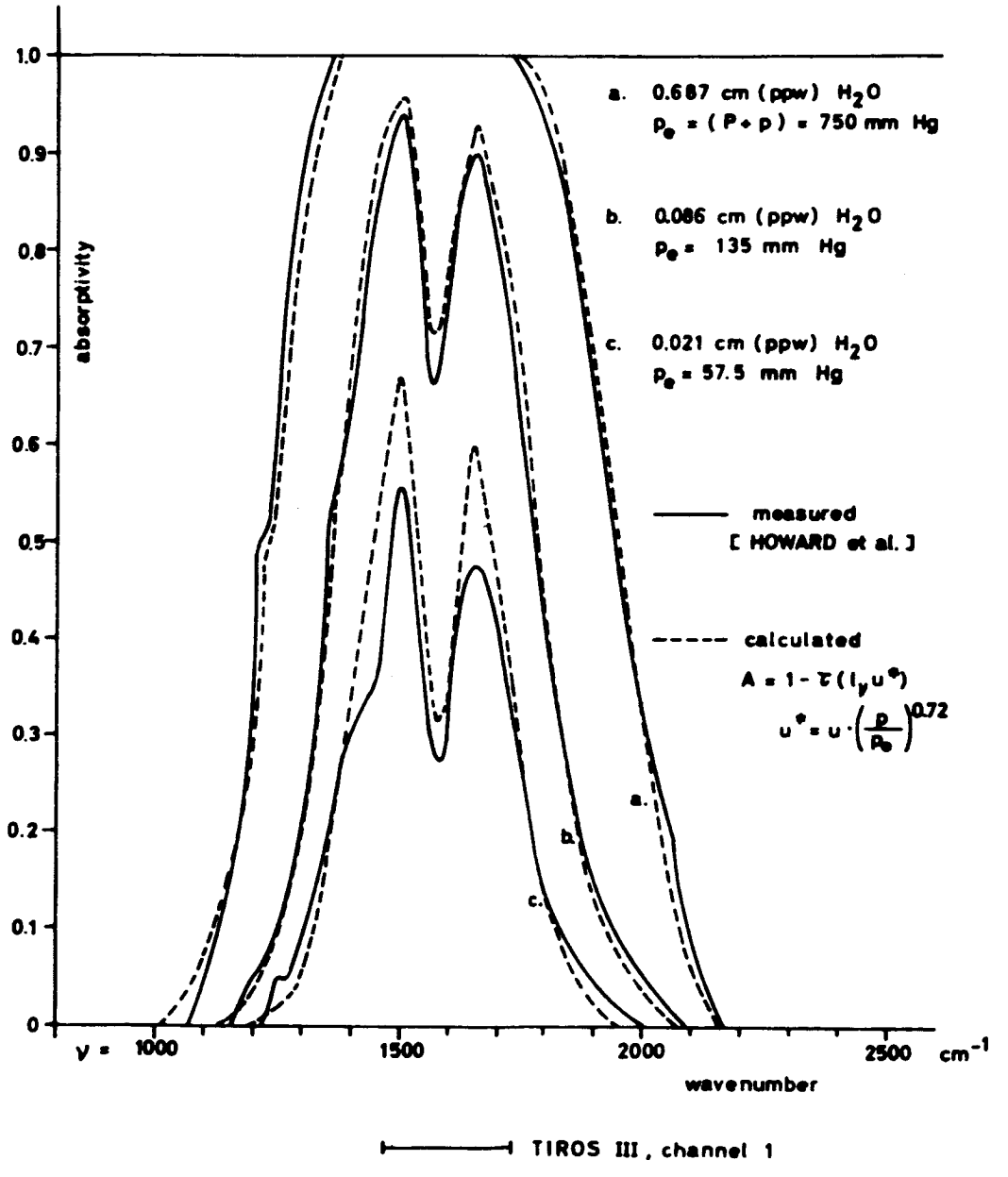
1.0
0.9
0.8
0.7
0.6
0.5
0.4
0.3
0.2
0.1
0
absorptivity
a. 0.687 cm (ppw) H_2O
$p_e = (P + p) = 750$ mm Hg
b. 0.086 cm (ppw) H_2O
$p_e = 135$ mm Hg
c. 0.021 cm (ppw) H_2O
$p_e = 57.5$ mm Hg
measured
[HOWARD et al.]
calculated
$A = 1 - \tau(l, u^*)$
$u^* = u \cdot \left(\frac{p}{p_e}\right)^{0.72}$
a.
b.
c.
ν = 1000
1500
2000
2500 cm^{-1}
wavenumber
TIROS III, channel 1

Fig. 4.11

spectral intervalls		500 - 450	460 - 410	410 - 360	370 - 320		340 - 290	300 - 250		250 - 200
A	$u = 0.0041$	0.968	0.939	0.928	0.872	$u = 0.0025$	0.914	0.869	$u = 0.003$	0.781
B	$p_e = 0.030$	0.978	0.960	0.945	0.880	$p_e = 0.028$	0.910	0.865	$p_e = 0.0273$	0.790
A	$u = 0.0077$	0.903	0.830	0.769	0.590	$u = 0.0071$	0.608	0.477	$u = 0.014$	0.213
B	$p_e = 0.267$	0.895	0.850	0.790	0.620	$p_e = 0.253$	0.620	0.500	$p_e = 0.269$	0.200
A	$u = 0.033$	0.765	0.666	0.576	0.323	$u = 0.027$	0.339	0.217	$u = 0.035$	0.075
B	$p_e = 0.275$	0.760	0.685	0.590	0.320	$p_e = 0.269$	0.345	0.210	$p_e = 0.276$	0.070
A	$u = 0.134$	0.489	0.361	0.255	0.075	$u = 0.132$	0.024	0.003		
B	$p_e = 0.317$	0.510	0.375	0.265	0.070	$p_e = 0.327$	0.040	0.010		

Comparison of transmittance values for spectral intervalls $\Delta\nu$ $[cm^{-1}]$ of the water vapor rotation band : A - measured by **PALMER**

B - $\tau_\nu = \tau_\nu (l_\nu \cdot u^*)$ where $u^* = u \left(\frac{p_e}{p_o}\right)^{0.72}$

p_e = effective pressure [atm] ; u = water vapor quantity $[g\ cm^{-2}]$

4.4: Application of the pressure correction for the computation of radiation fluxes in the atmosphere.

The results derived in the preceding chapter are strictly speaking valid for homogeneous layers with constant pressure and temperature. But in the actual atmosphere these conditions vary along the radiation path.

In order to apply the same absorption coefficients on an actual stratified atmosphere, the CURTIS-GODSON-approximation (CURTIS 1953; GODSON 1955; see also WALSHAW-RODGERS 1963) substitutes the transmissivity of a given layer by the transmissivity of a layer with the mean pressure $\bar{p}$ which is determined according to

$$\bar{p} = \frac{1}{w} \int_0^w p\,dw \quad . \tag{4.18}$$

w is the whole absorber quantity in the layer and p(w) the pressure along the path.

With this $\bar{p}$ and the given absorber distribution the transmissivity for any layer can be determined by using one of the known formulas (ELSASSER, GOODY, etc.). We have, however, to use a somewhat different method in order to calculate the radiation flux in the atmosphere by means of radiation diagrams.

In these, the integration over all emitting layers has been performed already, taking into consideration at the same time also the absorption within the intermediate layers. Absorbing as well as emitting gas layers have to be reduced with regard to pressure broadening of spectral lines. This can simply be done by a procedure analoguous to the above mentioned ones, i.e. by

$$w^* = \int_0^w \left(\frac{p(w)}{p_o}\right)^n dw$$

where n is that exponent which has been found above for the three absorbers respectively. The temperature T as a function of that effective mass w^* has then to be plotted in the radiation diagram.

5. THE RADIATION FLUX IN THE SPECTRAL REGIONS OF THE 3 INFRARED CHANNELS 1, 2, AND 4 OF THE SATELLITE TIROS III.

5.1: Radiation diagrams for the channels 1, 2, and 4.

Using the transmission function derived in chapter 4 and the formulas derived in chapter 3 radiation diagrams for water vapor absorption for the three channels and auxiliary diagrams (O_3, CO_2) for the channels 2 and 4 were calculated. All diagrams are shown in the appendix II. In order to get a summary about the influence of the absorption of infrared radiation by water vapor, carbon dioxide, and ozone within the sensitivity ranges of the channels 1, 2, and 4, small pictures of the 3 diagrams are shown here (Fig. 5.1). In these diagrams are plotted the curves for an atmosphere with two water vapor distributions of constant relative humidity (100 % and 10%) in the troposphere and the corrections for CO_2- and O_3-absorption. The temperature profile was determined according to the ARDC-standard atmosphere. The water vapor content in the stratosphere was calculated according to the mean distribution derived by GUTNICK (1962) from several measurements. The ozone profile needed for the ozone correction was determined according to a mean profile given by PAETZOLD (Fig. 5.2) and the carbon dioxide distribution was calculated for a constant mixing ratio of 0.03% by volume. If the atmosphere is divided into these layers, then the effective pressure corrected absorber quantities are determined by a simple summation along the radiation path beginning at the satellite.

(5.1) Water vapor: $$u^* = 0.438 \cdot 10^{-2} \sum_{i=1}^{n} \frac{\overline{\varepsilon_i}}{\overline{p_i}\, 0.28} \Delta p_i$$

$\overline{\varepsilon_i}$ = vapor pressure corresponding to the assumed relative humidity over ice (for $T < -20°C$) or over water ($T > -20°C$) in the i-th layer.

$\overline{p_i}$ = mean total pressure of the i-th layer of the "thickness" Δp_i.

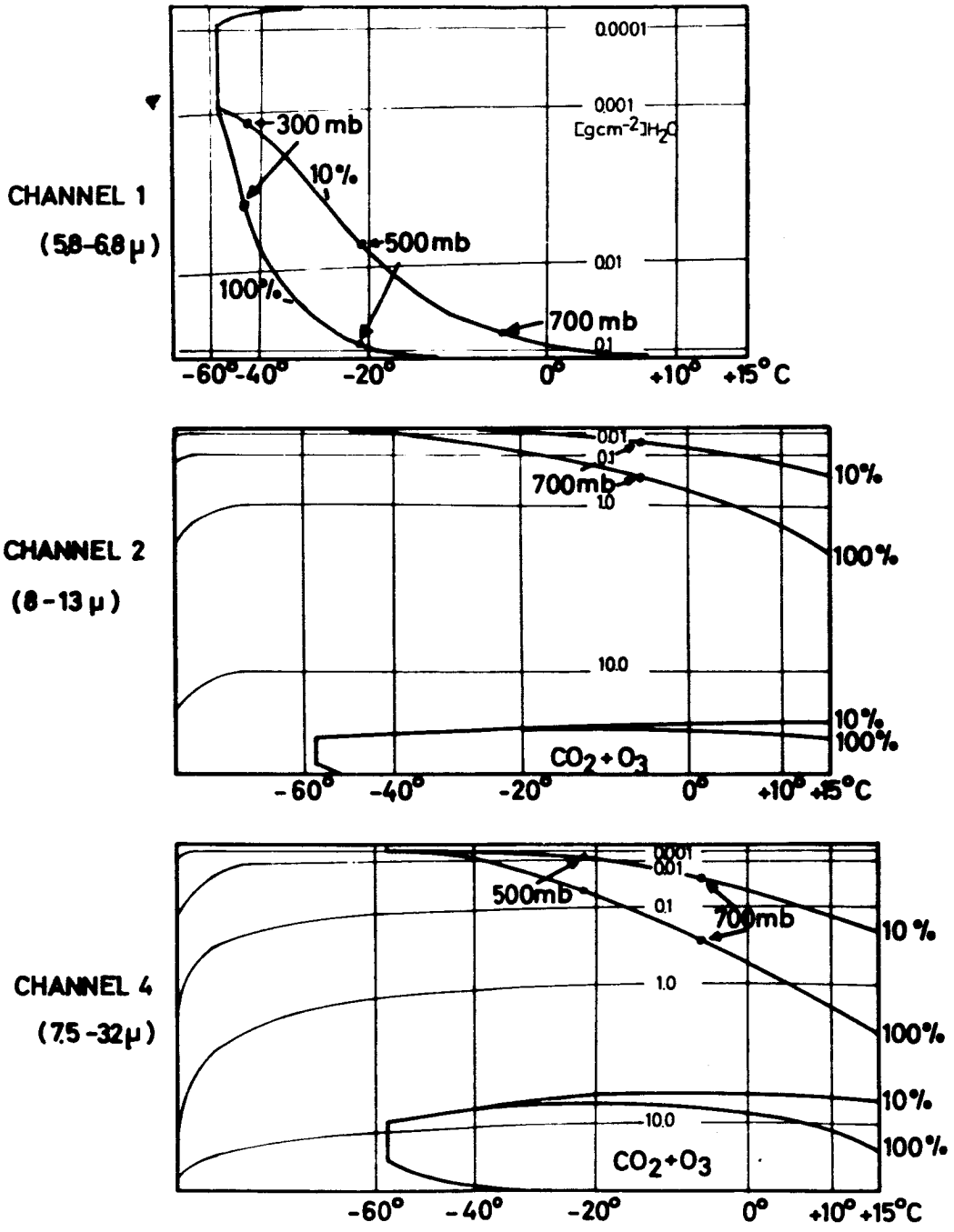
CHANNEL 1
(5.8-6.8 μ)
0.0001
0.001
[gcm⁻²]H₂O
300 mb
10%
500mb
0.01
100%
700 mb
0.1
-60° -40° -20° 0° +10° +15°C
CHANNEL 2
(8-13 μ)
0.01
0.1
700mb
1.0
10%
100%
10.0
10%
100%
CO₂+O₃
-60° -40° -20° 0° +10° +15°C
CHANNEL 4
(7.5-32 μ)
0.001
0.01
500mb
0.1
700mb
10 %
1.0
100%
10%
10.0
100%
CO₂+O₃
-60° -40° -20° 0° +10° +15°C

Fig. 5.1

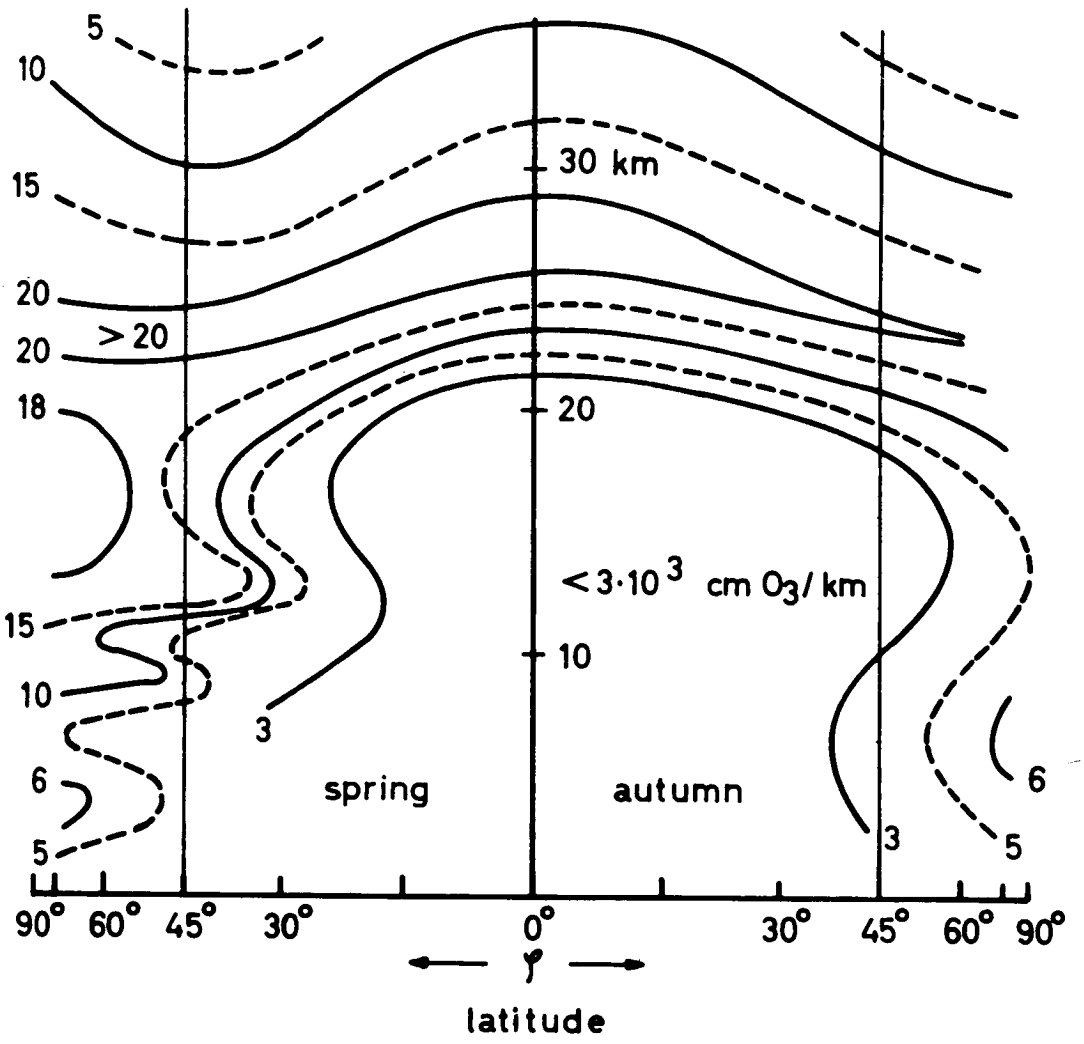

Fig. 5.2 : Ozone stratification after PAETZOLD

(5.2) Carbon dioxide: $c^* = 0.1595 \cdot 10^{-2} \sum_{i}^{n} \left(p_i^{1.65} - p_{i-1}^{1.65} \right)$

p_i and p_{i-1}: mean pressure at the boundaries of the i-th layer.

The ozone quantity was determined by summation over all ozone quantities in the different layers or without pressure correction ($p < 150$ mb or $p > 150$ mb respectively).

5.11: Channel 1 (5.8μ - 6.8μ).

Theupper picture in Fig. 5.1 shows the radiation diagram for channel 1, the sensitivity region of which is located in the center of the 6.3 μ-band of water vapor. By a water vapor quantity of only 0.1 g cm^{-2} approximately 98% of the infrared radiation flux is absorbed. Accordingly only the natural radiation of the water vapor contained in the layers of the upper troposphere and the lower stratosphere will attain the detector of channel 1. The contribution of radiation from the water vapor contained in layers which are below the 700 mb-level or close to the ground is very small, even if the troposphere is extremely dry. Radiation from cloud surfaces can attain the detector only if very high clouds (above hurricanes; or very high reaching cumulo-nimbus or nimbo-stratus clouds or dense cirrus clouds) are present.

The equivalent temperatures of the measured radiation will have values between 230°K and 250°K. As at the wavelength of 6.3μ, the spectral intensity of the radiation of a black body of the temperature T = 240°K amounts only to 28% of the maximum intensity and as the spectral region $\Delta\lambda$ within which channel 1 measures is very narrow, the measured intensities will be small. But a transmission of small measured values without errors requires a very low noise level in the equipment. This condition is not always satisfied, because frequently radiation data measured over high clouds were found to be "noisy" or without any systematical distribution.

5.12: Channels 2 (8μ - 13μ) and 4 (7.5μ - 32.5μ).

Both channels have a high sensitivity in the region of the water vapor window (8μ - 12μ), where the infrared radiation flux is extinguished only a little by water vapor and ozone. Correspondingly the measured data, respectively the areas in the diagram, show a strong dependence on the cloud or ground temperature. The influence of the water vapor absorption and emission on the total measured radiation in channel 2 is smaller than in channel 4, because the latter is also sensitive to radiation in the rotation band of water vapor. This property might allow to deduce from the radiation data some information about the humidity in the lower troposphere at a cloudless sky or at very low clouds. Several tests, however, have demonstrated that the influence of the radiation in the window region is dominant.

The different magnitude of the correction areas for the absorption by CO_2 and O_3 in both radiation diagrams is due to the different sensitivity of both channels in the region of the center of the 15μ-channel of CO_2. These corrections generally effect a smaller radiation flux from an atmosphere containing CO_2 than would emerge from a pure water vapor atmosphere without CO_2. Channel 4 has its maximal sensitivity at 15μ so that the radiation of the CO_2 in the warm layers of the upper stratosphere (20 - 40 km) contributes a small positive amount to the measured radiation. In the diagram this amount is indicated by the small triangular area between tropopause temperature abscissa and a slant curve. The whole correction area includes also the ozone correction. The analogous area in the channel 2-diagram determining the radiation of O_3 and CO_2 in the upper stratosphere is somewhat smaller. As will be shown later, the CO_2 absorption must not be neglected in calculations of the radiation flux in the sensitivity region of channel 2.

5.13: A difference channel "(4 - 2)".

As mentioned above, the measured radiation data of channel 4 are influenced by emission of water vapor within the short wave side of the rotation band. This influence, however, is small compared

with the strong radiation received within the window region (8 - 12μ) by the channel 4 detector.

In order to diminish the influence of the radiation within the window region, the radiation flux which is measured at the same time by channel 2 can be subtracted from the measurement in channel 4. In order to show clearly the influence of the water vapor a radiation diagram has been developed with the sensitivity of channel 4 but for the portion of the rotation spectrum only, i.e. for $\lambda > 18\mu$ (Fig. 5.3a). Here the emission by water vapor in the lower troposphere strongly influences the measured flux.

We subtract the measured flux of channel 2 from that of channel 4 according to

$$\overline{W}^{(4-2)} = \overline{W}^{(4)} - \overline{W}^{(2)} \tag{5.3}$$

We can define the new flux values $\overline{W}^{(4-2)}$ as a measured value of a new channel. This channel will be called the "difference channel (4 - 2)" (shortly: (4-2)) with the sensitivity region defined by the difference of the sensitivities of both channels, so that

$$\Phi_\nu^{(4-2)} = \Phi_\nu^{(4)} - \Phi_\nu^{(2)} \quad . \tag{5.4}$$

$\Phi^{(4-2)}$ has a small "negative area" (Fig. 5.4a), which has been neglected in the calculation of a radiation diagram (4-2) (Appendix II and Fig. 5.4b). As it can be seen by a comparison of the sensitivity curve of the new channel with that of channel 4, the sensitivity region is now narrow and the difference-channel has a very small sensitivity within the window region. So the influence of the water vapor on this new difference value is greater than that one on channel 4, as it can be taken also from the radiation diagram (Fig. 5.4b).

Like channel 4, the difference channel has its maximal sensitivity within the center of the CO_2-15μ-band. Therefore, the CO_2-emission very strongly influences the measured flux. It can be shown by a radiation diagram for the carbon dioxide 15μ-band center (14 - 16μ) only that winthin this range the measured radiation is essentially emitted from the CO_2 in the lower (here isotherm) atmosphere (Fig. 5.3b; temperature profile: ARDC-

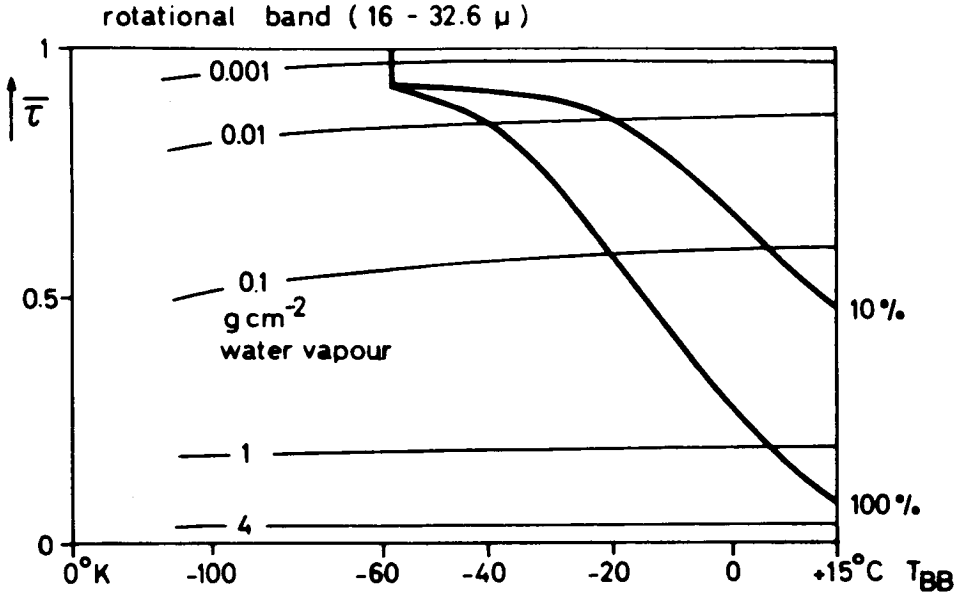
rotational band (16 - 32.6 μ)
1
$\overline{\tau}$
0.5
0
0.001
0.01
0.1
g cm^{-2}
water vapour
1
4
10 %
100 %
0°K
-100
-60
-40
-20
0
+15°C
T_{BB}

a.

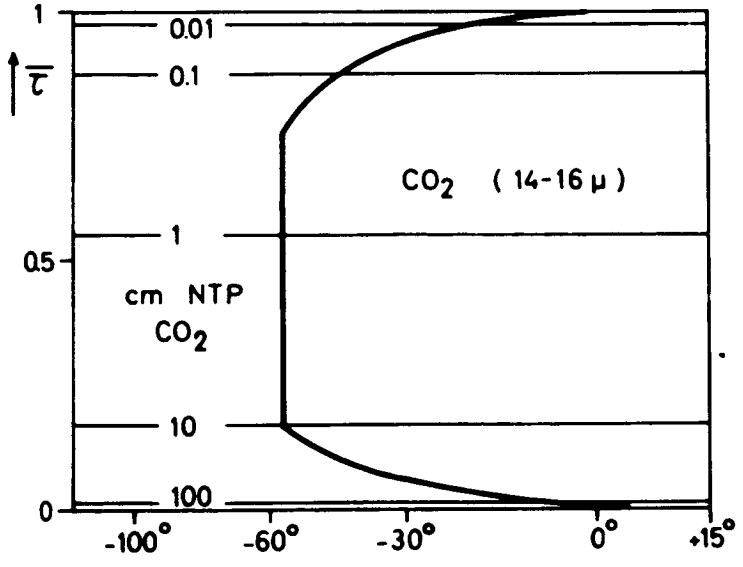
1
$\overline{\tau}$
0.5
0
0.01
0.1
CO_2 (14-16 μ)
1
cm NTP
CO_2
10
100
-100°
-60°
-30°
0°
+15°

b.

Fig. 5.3

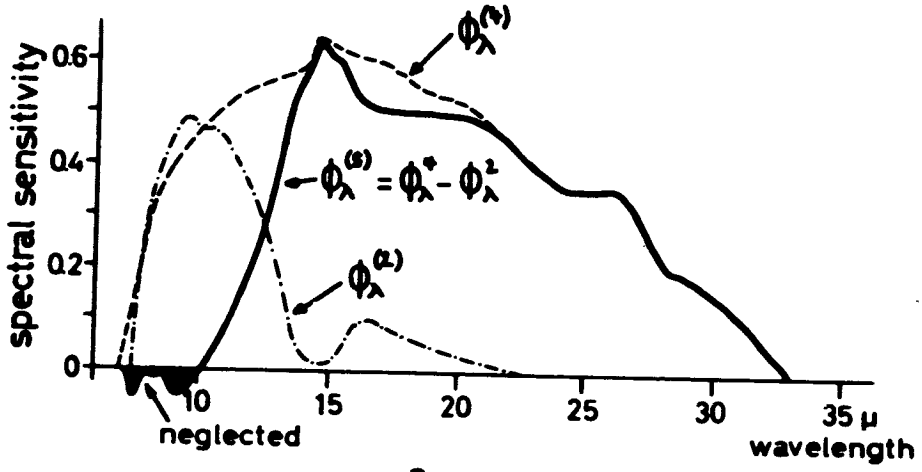
spectral sensitivity
0.6
0.4
0.2
0
$\phi_\lambda^{(v)}$
$\phi_\lambda^{(s)} = \phi_\lambda^* - \phi_\lambda^2$
$\phi_\lambda^{(a)}$
10
15
20
25
30
35 μ
wavelength
neglected

a.

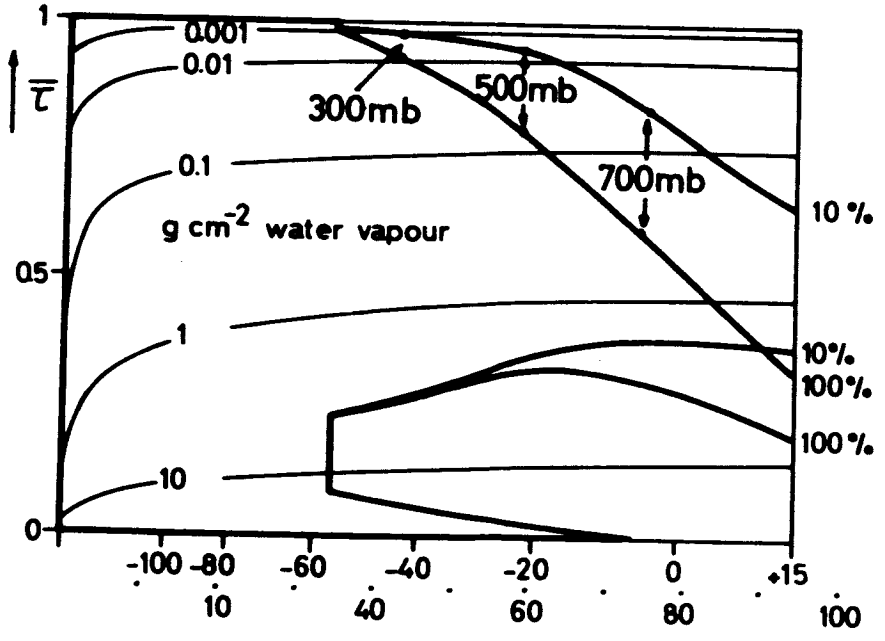
1
0.5
0
$\bar{\tau}$
0.001
0.01
0.1
1
10
300mb
500mb
700mb
g cm^{-2} water vapour
10 %
10%
100%
100 %
-100
-80
-60
-40
-20
0
+15
10
40
60
80
100

b.

Fig. 5.4

atmosphere) and upper troposphere, Therefore, the influence of variations of the tropopause temperature (= temperature of the lower stratosphere) on the radiation flux within all sensitivity regions $\Phi^{(n)}$ (n = 1, 2, 4, 4-2) shall be studied by means of model atmospheres.

5.2: Computations of the radiation flux for several model atmospheres.

The results of the radiation flux computations for the sensitivity regions of the channels 1, 2, 4, and (4-2) were obtained by the radiation diagrams above mentioned.

5.21: Model atmospheres.

The vertical temperature profile in the atmosphere as well as the water vapor distribution are daily measured by radiosonde ascents at numerous stations. Because both quantities of stratification vary strongly with the time of the day and the season, we will consider standardized conditions, which, in the average, represent models of different latitude zones. In table V.1 the surface and tropopause temperatures of three models are given. In all cases the temperature gradient in the troposphere is constant in all heights and amounts to -6.5°/km (Fig. 5.5).

Table V.1: Model atmospheres.

atmosphere	temperature of surface	temperature of tropopause	geographical area
I	+15°C	a -56.5°C b -65°C c -75.0°C	mid - latitude
II	+25°C	a b c	subtropics
III	+35°C	a b c	tropics

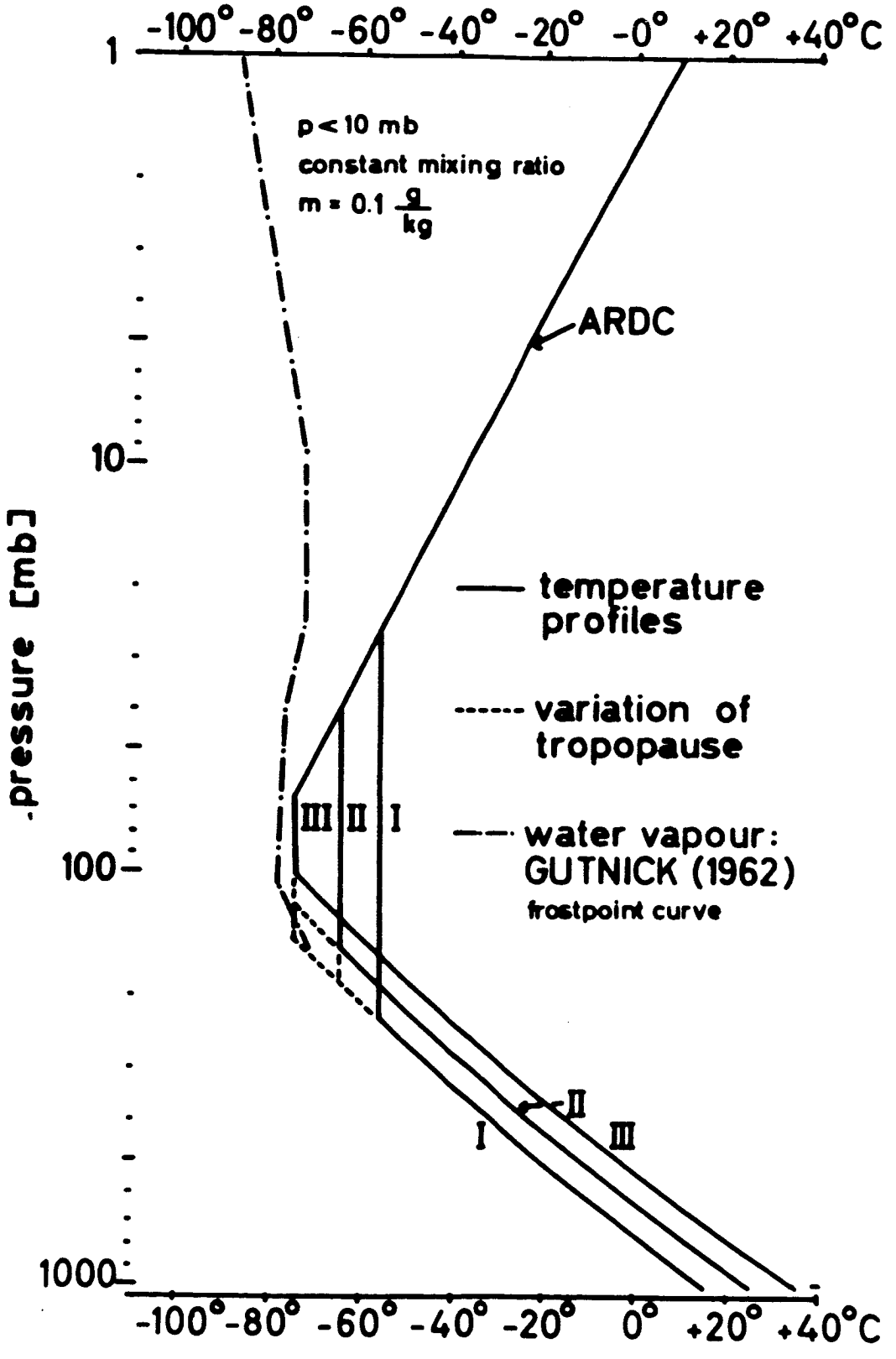
-100° -80° -60° -40° -20° -0° +20° +40°C
1
p < 10 mb
constant mixing ratio
m = 0.1 g/kg
ARDC
10
pressure [mb]
temperature profiles
variation of tropopause
water vapour: GUTNICK (1962)
frostpoint curve
III II I
100
II
I
III
1000
-100° -80° -60° -40° -20° 0° +20° +40°C

Fig. 5.5

The three models have also the same temperature profile in the upper stratosphere, which is given by the ARDC-atmosphere. In each model (I, II or III) the tropopause temperature and also the height was varied according to the scheme in Fig. 5.5.

For the calculation of the water vapor path length the relative humidity was assumed to be constant (100%, 50%, 10%, 5%) and the water vapor content within the stratosphere was varied according to the following scheme:

A: saturation from tropopause up to the 100 mb-level, above that constant mixing ratio.
B: no water vapor above the tropopause.
C: constant frost point at -80°C from tropopause to the 80 mb-level, from there up to the 1 mb-level constant mixing ratio of 0.04 g/kg.

These variations of the water vapor content are supposed to include the possible limits.

GUTNICK (1962) has shown large scatter of single water vapor distribution in the stratosphere (MURCRAY et al., MASTENBROOK and DINGER), but so far not more reliable data, e.g. correlations of the water vapor content with the stratification in the troposphere, are available.

The distribution and content of ozone within the atmosphere varies with daytime and season. Thus, for the correction with regard to ozone absorption, the ozone profiles will be determined from average meridional distributions (Fig. 5.2.) given by PAETZOLD (1963).

5.22: Results.

Results calculated by the radiation diagram are given in the following tables, in units of the equivalent temperature for each channel.

5.22.1: Different water vapor quantities in the stratosphere.

It was found that the equivalent temperatures for the determined radiation in the channels 2 and 4 are not at all affected by variations of the water vapor content or distribution within the stratosphere. Only the calculated equivalent temperatures for the difference-channel (4-2) show a difference of 2° between the extreme assumptions of water-vaporless and saturated (to 100 mb) stratosphere, but only the relative humidity in the troposphere is assumed to be 5 %. With a moister atmosphere this difference is smaller. Therefore, the influence of a variation of humidity in the stratosphere was only investigated for channel 1, not for the other channels.

Results for the radiation flux in channel 1 are given in table V.2. These values show a dependence on the water vapor content and distribution in the stratosphere, but this dependence is the clearer the smaller the relative humidity in the troposphere is and the lower the cloud surface is. An extreme case is given by the difference between the equivalent temperature for the dryest case (5%) of the atmosphere I A and I B, which is 8.5°. The case (I A) of a saturated stratosphere above a very dry stratosphere will certainly be unreliable, but all these values show that a determination of a mean relative humidity of the troposphere from measured radiation data of channel 1 will be also influenced by the water vapor content in the stratosphere.

On the other side, the equivalent temperatures in table V.2 verify the statements of MÖLLER (1961) about the outgoing flux in the spectral region of 6μ - 7μ, measured by a satellite. This flux is only dependent on the water vapor content in the troposphere and stratosphere. Even if there are strong differences of the surface temperature there are almost no differences in the equivalent temperature of the outgoing flux; compare e.g. the columns 263° and 273° in table V.2. Only if there are high clouds, a dependence of their surface temperature on the equivalent temperature is evident. So the radiation received by channel 1 is for the greatest part the natural radiation of the atmospheric water vapor and is a good characteristic of the relative humidity.

Table V.2: Radiation flux in channel 1 at different model atmospheres.
case A: saturated stratosphere (p > 100 mb)
case B: stratosphere without water vapor
case C: frost point = -80°C

model atm.	relat. humid.	case	tropop.	cloud surface temperatures [°K] 223	243	263	273	288
		A	217.7	219.7	227	228.8		
	100%	B	216.5	221	229.5	231.5		
		C	217.3	220.5	229	231.2		
		A		220	230	235.5	235.8	
I	25%	B		222	235.7	241	241.5	
		C		221	234.7	240	240.2	
		A		220	236.6	242.5	245.3	246.5
	5%	B		222.5	240	251	253.5	255
		C		222	238.5	250	253	254.7
		A	209.8	219.4	227	230.7	230.9	
	100%	B	208	220	229.4	231.5	231.8	
		C	208	220	229.5	231.5	231.8	
		A		220	233.3	240	240	
II	25%	B		221	235.5	241.4	242	
		C		221	235.5	241	242	
		A		220.2	236.5	246	251.7	253
	5%	B		222	240.4	251.4	254.2	256
		C		221.7	239	251	253.5	256
	100%	B	198	220	231	232.3	232.7	
		C	198	220	230.5	231.5	232	
III	25%	B		221.3	236	242	242.7	
		C		221	235.7	242	242.5	
	5%	B		222	240	252.5	255.5	257
		C		221.8	239.3	251.5	254.7	256.5

5.22.2: Different tropopause temperatures.

For this investigation the particular water vapor distribution in the stratosphere according to GUTNICK was assumed.

It was found out by our calculations that the influence of different tropopause and stratosphere temperatures on the radiation flux is small for all 4 sensitivity regions, if low clouds or a cloudless sky is assumed. But in the case of high clouds small variations could be found in the results for channel 1.

Channel 1: For an assumed cloud surface in the level of the 243°K-isother, the equivalent temperatures are 2° (f = 100%) respectively 1° (f = 25%) higher for the warm tropopause (-56.5°C) than those for the coldest tropopause (-75°C) (f = relative humidity in the troposphere). With decreasing cloud height these differences decrease because of the dominant influence of the radiation of water vapor in the troposphere on the whole outgoing flux.

Channel 2: No influence was found at all.

Channel 4 and (4-2): Results of computations for two different cloud surface temperatures (243°K and 273°K) and all 3 temperature profiles (I, II, III) are given in the table V.3. The differences within one column do not exceed the amount of 1° anywhere. An influence of the temperature variation of the tropopause on the outgoing flux intensity in these two sensitivity regions (channel 4 and (4-2) can only be effected by the natural radiation of the carbon dioxide within the upper troposphere and isothermal stratospheric layer. The concentration of ozone within these layers is too small to show any influence. But in both cases the influence of variations of the tropopause temperature or tropopause height decreases with decreasing cloud heights, and also slightly with increasing relative humidity in the troposphere because the total radiation flux is larger in these cases. As it is seen from the values in table V.3, this effect will be too small as to give usable correlatiens of the radiation data with tropopause temperatures or heights.

model atmosphere :		I		II		III	
temperature of the tropopause	relative humidity	243	273	243	273	243	273
1. -56.5°	100 %	237.9	256.2	238.0	258.2	238.9	258.4
2. -65°	100 %	237.5	255.7	237.5	257.5	238.5	258.0
3. -75°	100 %	237.3	255.5	237.0	256.8	238.0	257.7
1	25 %	238.5	259.0	238.4	261.0	239.8	260.6
2	25 %	237.8	258.3	238.0	259.7	239.4	260.4
3	25 %	237.5	258.0	237.5	259.5	238.8	260.0
1	5 %	238.8	260.0	238.8	262.2	240.0	262.2
2	5 %	238.0	259.7	238.0	261.2	239.6	262.0
3	5 %	237.8	259.5	237.8	261.0	239.0	261.7
channel 4 (7.5 - 32.5μ)							
1	100 %	237.3	251.4	237.3	252.0	238.1	252.5
2	100 %	236.0	250.0	237.0	251.0	237.5	251.5
3	100 %	235.0	248.8	234.3	250.0	237.0	251.0
1	25 %	237.9	235.7	237.7	255.0	238.7	255.5
2	25 %	237.0	252.2	237.3	254.5	237.8	255.5
3	25 %	236.3	252.0	237.0	253.6	237.5	255.0
1	5 %	238.0	256.0	238.1	256.5	238.1	258.3
2	5 %	237.5	255.3	237.9	256.5	238.0	258.0
3	5 %	237.0	255.0	237.4	256.0	237.6	257.6
difference channel (12 - 32μ)							

Table V.3 : Radiation flux in channels 4 and (4-2) at different model atmospheres with various temperatures of the tropopause

5.22.3: The influence of absorption and emission of CO_2 and O_3.

These investigations were carried out for the temperature profile of the ARDC-Standard-atmosphere (our model I) with a water vapor distribution in the stratosphere according to GUTNICK. The ozone content and profile was taken from Fig. 5.2 for the latitude of 45°. In spring the ozone content is 0.374 cm NTP and in autumn 0.251 cm NTP. The carbon dioxide quantity is determined by assuming a constant mixing ratio of 0.03% by volume in the whole atmosphere.

In table V.4 results are given only for a cloudless sky with 3 different relative humidities in the troposphere (100%, 25%, 5%). These results were found for the following distributions (table V.4) of absorbing and emitting components in the atmosphere.

1. H_2O, CO_2 and O_3(spring)
2. H_2O, CO_2 and O_3(autumn)
3. H_2O, CO_2 without O_3
4. H_2O without CO_2 and O_3
5. H_2O, O_3(spring) without CO_2

The differences between large and small amounts of ozone (case 1 and 2) are small. Total lack of ozone or carbon dioxide are extreme assumptions which never will be realized in the atmosphere. Table V.4 demonstrates, however, that the influence of these two gases must not be neglected in calculations of radiation fluxes.

The differences between the results of all cases in table 5.4 decrease with increasing cloud height, but this is not shown in the table.

relative humidity	case	T = 288°K	288°K	288°K
100	1	275.0 276.0	263.5 263.3	(253.5) (253.5)
	3	284.0	266.5	253.5
	4	284.5	276.5	270.0
	5	276.5	273.5	
25	1	278.0	268.0	(258.8)
	2	279.2	267.7	(258.8)
	3	284.0	271.2	258.8
	4	287.2	282.0	277.3
	5	279.8	279.0	
5	1	279.5	270.7	(263.0)
	2	280.5	270.5	(263.0)
	3	285.5	274.0	263.0
	4	287.5	286.0	283.5
	5	284.2	283.0	

Table V.4: Radiation fluxes as they would be measured by the channels 2, 4, and (4-2) at different cases of ozone, carbon dioxide, and water vapor variations (see text).

case	$\bar{W}^{(4)}-\bar{W}^{(2)}$ [W m^{-2}]	$T_{equ.}(\bar{W}^{(4)}-\bar{W}^{(2)})$ [°K]	$\bar{W}^{(4-2)}$ [W m^{-2}]	$T_{equ.}(\bar{W}^{(4-2)})$ [°K]
1 (100%)	61.3	253.5	61.3	253.5
3 (100)	61.7	253.3	61.3	253.5
1 (5%)	69.2	262.7	69.4	263
3 (5%)	70.0	263.5	69.4	263
1 (25%)	66.0	259	65.8	258.6
3 (25%)	66.2	259.2	65.8	258.6

Table V.5: Control of channel (4-2) data with examples given in table V.4.

According to the definition of their sensitivity region, the directly computed radiation fluxes must be nearly equal to the difference between those of channel 4 and 2 computed for the same conditions.

Table V.5 shows the difference of radiation fluxes $W^{(4)}$ and $W^{(2)}$ and those fluxes which were directly determined for the differance channel $W^{(4-2)}$. The equivalent temperatures derived from both kinds of fluxes are added. It is evident that there are almost no differences in these temperatures. A very small influence of existing or non-existing ozone content remains, which origins from the neglected "negative sensitivity" according to Fig. 5.4a.

5.22.4: Nadir angle dependence.

All considerations of the outgoing radiation flux, which is m measured by the satellite, were carried out only for the vertical direction (nadir angle N = 0°). The influence of variations of the nadir angle has yet to be investigated. Calculations were carried out again for the ARDC-Standard-Atmosphere with constant relative humidity in the troposphere, a water vapor distribution according to GUTNICK in the stratosphere and an ozone profile according to PAETZOLD for autumn and 45° latitude.

Assuming shperical symmetry of all layers within the atmosphere, a factor K_i can be given for each layer i with an averaged height $\overline{h_i}$ above the ground and for each nadir angle N, with which the absorber quantity in the height $\overline{h}$ has to be multiplied:

$$K_i = \frac{1}{\sqrt{1 - \frac{(R+H)^2 \cdot \sin^2 N}{(R + \overline{h_i})^2}}} \qquad (5.5)$$

where R = 6370 km: radius of the earth
H = 780 km: averaged height of the satellite above the ground

Values of K_i are given for several heights and nadir angles in table V.6.

In order to show the variation of the radiation in each channel with the variation of the nadir angle, in Fig. 5.6 the differences of the equivalent temperatures (T(N=0°) - T(N)) are plotted for constant relative humidity (in the troposphere). The results are shown for cloudless sky (Fig. 5.6a) for a cloud surface temperature of -10°C (Fig. 5.6b), and for a cloud surface in the tropopause level (Fig. 5.6c). The computations were carried out only until the nadir angle N=60°, because at N~63° the beam of the radiometer is tangent to the earth's surface.

$\overline{h_i}$ (km)	nadir angle N					
	20°	30°	40°	50°	55°	60°
50	1.081	1.203	1.432	1.913	2.435	3.785
40			1.434	1.924	2.462	3.866
30			1.436	1.933	2.481	3.953
20			1.438	1.941	2.501	4.047
15			1.439	1.945	2.512	4.096
10			1.441	1.949	2.522	4.148
8				1.951	2.526	4.170
6			1.442	1.953	2.531	4.191
4				1.954	2.535	4.214
2				1.956	2.540	4.236
0	1.083	1.208	1.444	1.958	2.544	4.259

Table V.6: Factor K_i (Eq. 5.5) for different nadir angles N and heights h above the earth's surface.

Computations of the phenomena occuring at still greater nadir angles (N > 63°) (see e.g. HANEL et. al., 1962; KONDRATIEV et al. 1962) are without significance for our purposes, because it is our aim to investigate the variation of radiation data, which were measured, when the radiometer is facing directly the earth's surface.

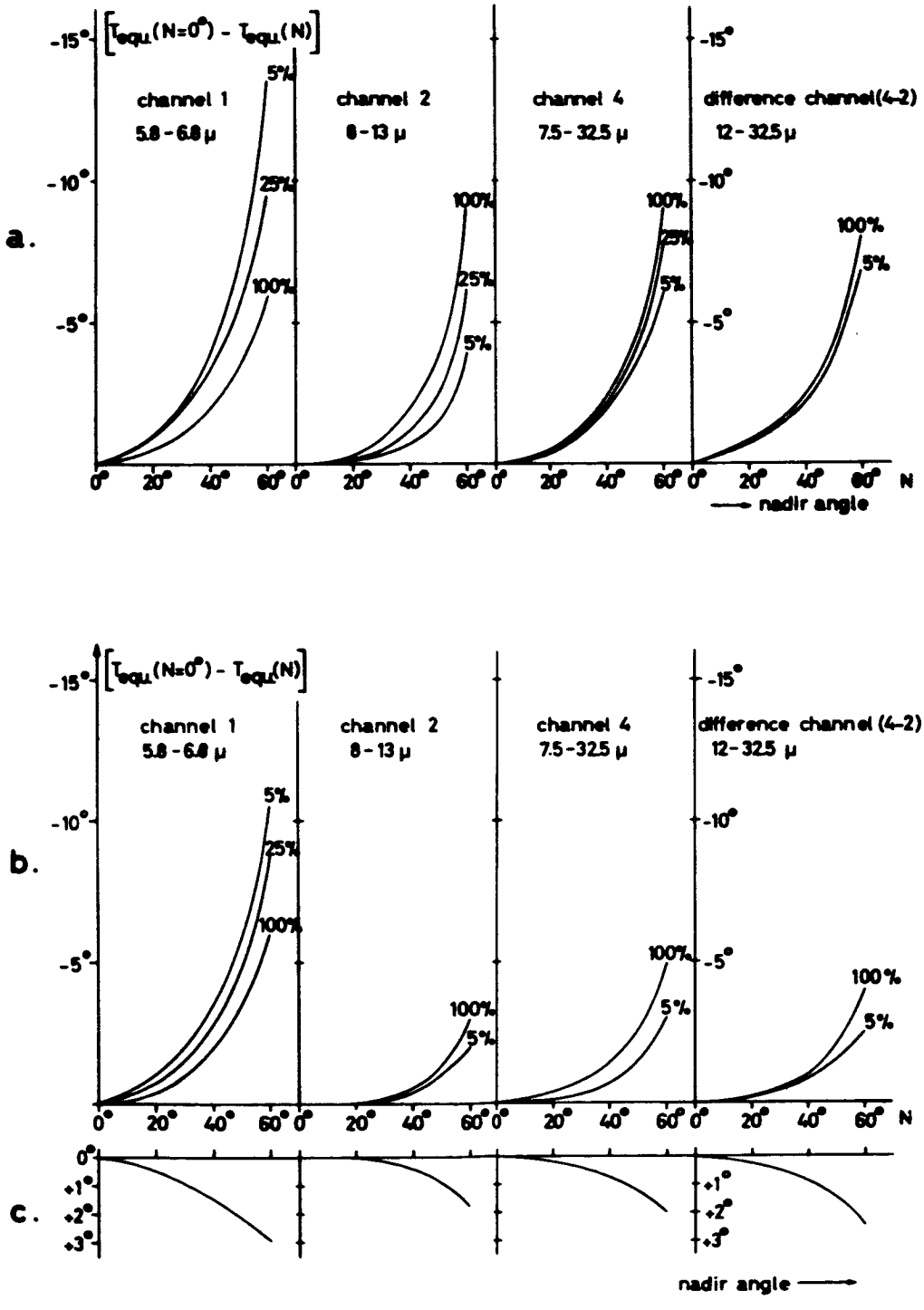
a.
b.
c.
$[T_{equ.}(N=0°) - T_{equ.}(N)]$
channel 1
5.8 - 6.8 μ
channel 2
8 - 13 μ
channel 4
7.5 - 32.5 μ
difference channel (4-2)
12 - 32.5 μ
-15°
-10°
-5°
5%
25%
100%
0° 20° 40° 60°
N
nadir angle
0°
+1°
+2°
+3°

Fig. 5.6

The following results may be taken from Fig. 5.6:

A: The variation of the radiation flux with varying nadir angle depends on the relative humidity of the troposphere. In the sensitivity region of channel 1 this variation is larger for a dry atmosphere than for a moist atmosphere. The other sensitivity channels show the opposite behaviour.

B: At a cloudless sky and (or) low clouds the intensity of the radiation decreases with increasing nadir angle in all sensitivity regions. This is effected by the increasing influence of higher and colder layers on the emitted radiation. If there are very high clouds close to the tropopause (Fig. 5.6c), the intensity of measured radiation increases with increasing nadir angle, because now only absorbers in the nearly isothermal stratosphere and in higher layers, where the temperature increases with the height, modify the emitted radiation.

Variation of the ozone quantity and also of the water vapor distribution in the stratosphere can be added as new parameters into these consideration. But the result will then be ambiguous, and almost useless for a practical analysis of measured radiation data. According to these preliminary results the nadir angle dependence on the radiation data can be neglected for nadir angles smaller than 30° at the analysis of radiation data, because the accuracy of the measurements with all 3 channels amounts approximately (TIROS III, Users Manual) to $\pm 4°$, which is smaller than the correction values for N = 30°. In the practical analysis of radiation data it will be advantageous to use average values for nadir angle correction (see also WARK, YAMAMOTO, and LIENESCH, 1962), since the relative humidity and the cloud height is unknown and shall be inferred from the data only.

6. PRELIMINARY RESULTS OF THE EVALUATION OF RADIATION DATA.

6.1: Determination of mean relative humidity and of a surface temperature (clouds or ground).

6.11: Evaluation diagrams.

To determine a mean relative humidity of the troposphere and a surface temperature (cloud or ground), evaluation diagrams for model atmospheres were designed according to a method proposed by MÖLLER (1962). For that purpose computed radiation fluxes for the spectral ranges of channels 1, 2, and (4-2) for the model atmospheres I, II, and III were plotted into diagrams (Fig. 6.1a, b, c) in which the relative humidity and the surface temperature T_{BB} are used as coordinates. Then one obtains for the 3 channels 3 families of curves of constant equivalent temperature.

For these calculations the 3 temperature profiles of Fig. 5.5were used. The water vapor quantities were determined by assuming constant relative humidity of the troposphere and a water vapor distribution in the stratosphere according to GUTNICK. The ozone profiles were determined out of Fig. 5.2 for a latitude of 45° (autumn) for the model atmospheres I and II and a latitude of 30° (autumn) for the model III. These evaluation diagrams are only valid for the vertical direction (N=0°).

Entering now with the equivalent temperatures of the measured radiation fluxes of the channels 1 and 2 respectively 2 and (4-2) into these diagrams, the average relative humidity of the (upper respectively lower) troposphere and the surface temperature can be read off as values of the coordinates. Practically for each latitude zone a special diagram should be used, which ought to be calculated for the characteristic temperature profile of that ozone. The curvature of all curves of constant equivalent temperature shows the influence of the water vapor content on the propagation of the infrared radiation flux within the single sensitivity ranges. The curves for channel 1 turn into the horizontal with increasing surface temperature (or decreasing cloud height), because radiation of deeper layers has not influence on the radiation amount in channel 1. The curves for the other chan-

a.

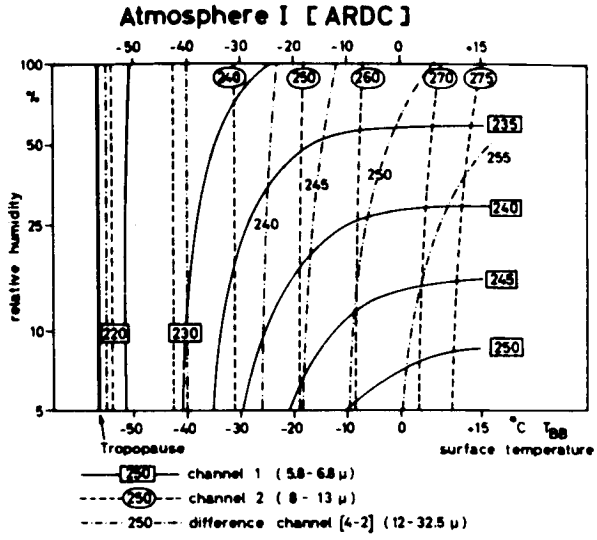

b.

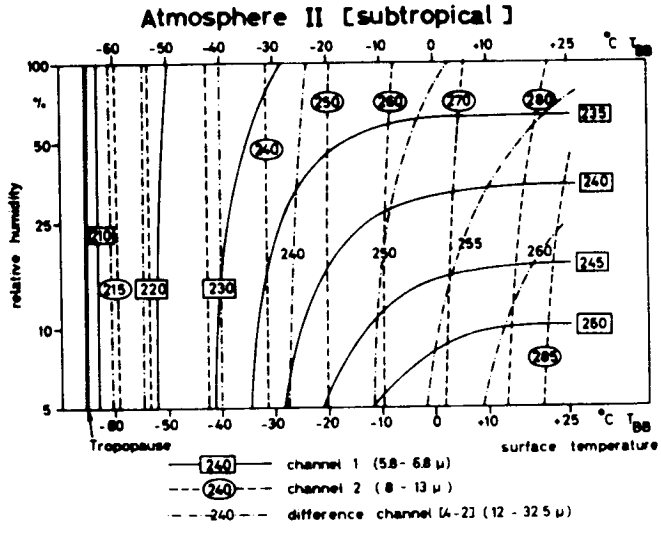

c.

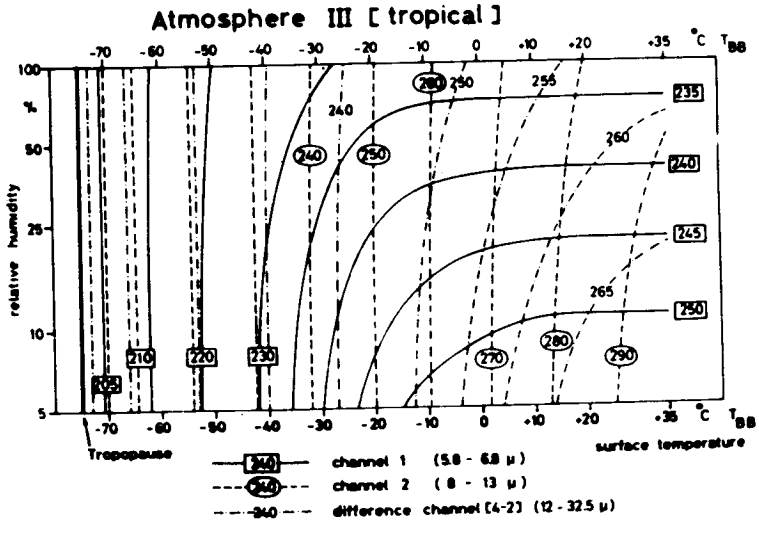

Fig. 6.1: Evaluation diagrams

nels have only a slight curvature but a stronger one for channel (4-2) than for channel 2.

The use of the diagrams and the accuracy of this method can be demonstrated by a particular numerical example. The following temperatures might have been measured:

channel	$T_{equ.}$ [°K]
1	237.5 ± 2.5
2	272.5 ± 2.5
(4-2)	257.5 ± 2.5

Table VI.1: Example of radiation data.

The error of the measurement is assumed to be ± 2.5° in all channels (smaller than the given errors*). In fact, the errors will be larger in the differences (4-2) of the measured radiation fluxes of the channels 4 and 2, because the data of both single channels contain an error which can be additive. If the relative humidity and the surface temperature for these values will be determined in this way the accuracy of the method can be demonstrated by the different areas in Fig. 6.2, which are limited by the equivalent temperatures (in all three model atmospheres) given by the error limits.

In the average the accuracy of the values determined by the combination of the radiation data of the channels 1 and 2 (Fig. (Fig. 6.2a) is ± 3°C for the surface temperature and about ± 15% for the relative humidity. The error limits of the relative humidity determined by the combination of the data of the channels 2 and (4-2) cannot be given at all, because the curve $T_{equ.}$ = 260°K falls outside the diagram (Fig. 6.2b) or at extremely small relative humidities. So it can be seen easily that a determination of the relative humidity of the lower troposphere by channel (4-2) is too incorrect, because the influence of the water vapor on the infrared radiation in the sensitivity range of the channel (4-2) is still too small (or the spectral interval is too wide).

*) see e.g. TIROS III, User's Manual

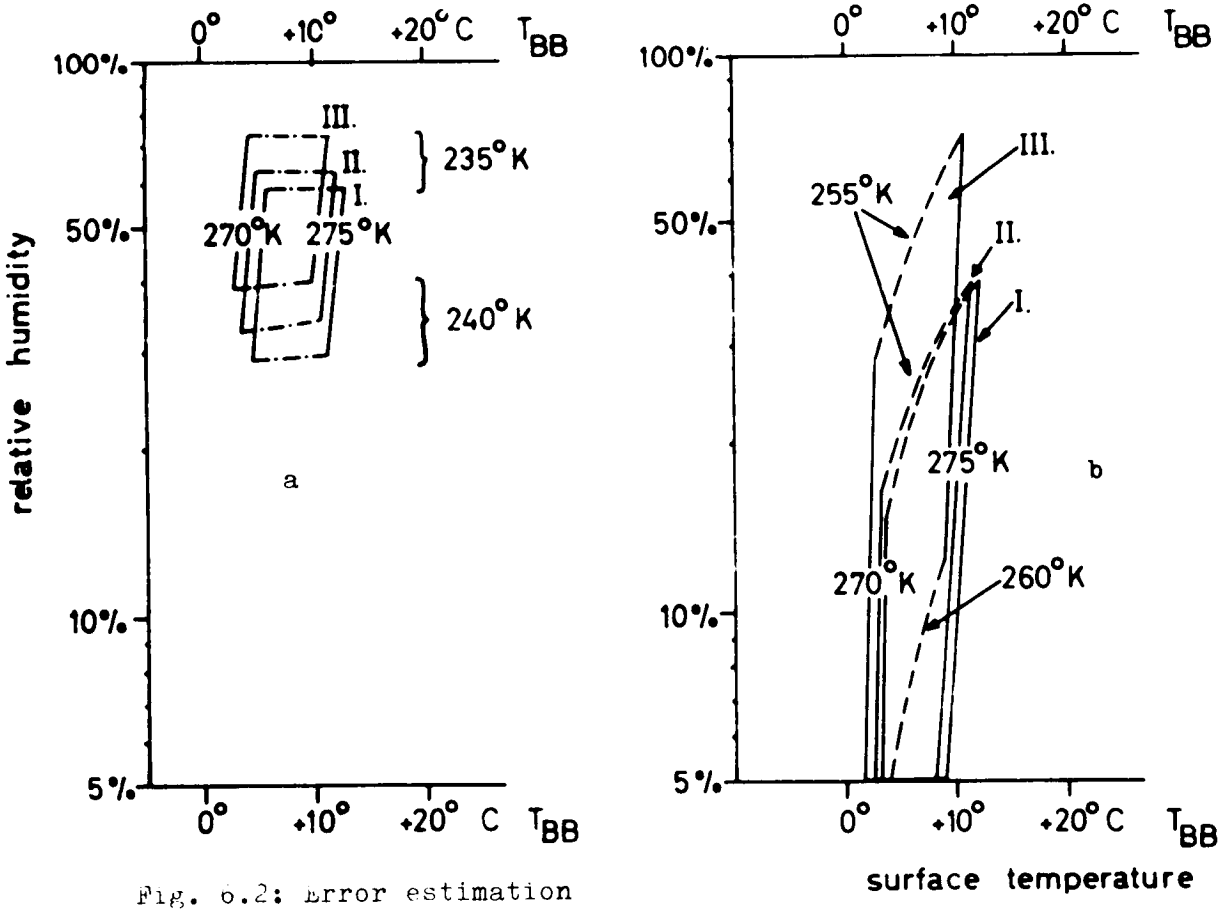

Fig. 6.2: Error estimation

channel 1 235 - 240° K

channel 2 270 - 275° K

difference channel (4-2) 255 - 260° K

channels		I	II	III
1 and 2	surf. t.	+9°C	+8°C	+7°C
	rel. Hum.	40%	45%	55%
2 and (4-2)	surf. t.	+7°	+6.5°C	+6°C
	rel. Hum.			22%

Table VI.2: Evaluation results.

In order to find out the influence of the chosen model atmospheres the results of evaluation of the data given in Table VI.1 are shown in Table VI.2. The assumed errors are now neglected, the equivalent temperatures assumed to be correct. Going from model I to III, the surface temperatures decrease and the relative humidities increase. The decreasing temperature can be explained by the influence of carbon dioxide.

A cloud surface with a temperature of + 10°C is situated in the 3 model atmospheres at the following pressure levels:

atmosphere	pressure
I	930 mb
II	770 mb
III	650 mb

Table VI.3: Pressure levels of the +10°C isotherm.

Since the quantity of CO_2 between the receiver and the cloud surface is greater in the case of the atmosphere I than in the case of the atmosphere III, the equivalent temperature of the measured radiation will be lower in the case I. Or, if the same equivalent temperature is measured in all 3 cases by channel 2, the evaluated surface temperature will be higher for the atmosphere I than for the atmosphere III.

A similar consideration about the influence of different water vapor quantities due to the different pressure levels of the cloud surface (which includes also a different pressure levels of the

cloud surface (which includes also a different influence of the pressure correction) can give an explanation for the different relative humidities determined for the same equivalent temperature.

These error estimations show the limited applicability of the method for the determination of quantitative results.

This method does not work if a cross point of the isothermes cannot be found within the area of the evaluation diagram. Such cases were found mostly in the evaluation of radiation data measured above high clouds. An intersection would then occur only at relative humidities of more than 100%. The errors are mostly caused by the large scatter of the data, or noisy data, or by an insufficient nadir angle correction. In any way the water vapor quantity above high clouds is too small to give sufficient influence on the infrared radiation measured by channel 1. The equivalent temperatures should not differ from one another in the three channels. Therefore cases with cloud surfaces near the tropopause will be investigated by using our evaluation diagrams.

atmosphere	T_{BB} cloud surface	equivalent temperatur of channel 1	2	(4-2)
I	-55°C (218°K)	218.5°K	219°K	220°K
II	-60°C (213°K)	213.5°K	214.5°K	215.5°K
III	-70°C (203°K)	206°K	206°K	207°K

Table VI.4: Equivalent temperature with cloud surfaces near the tropopause.

In all of the three examples given in Table VI.4 the equivalent temperature for the calculated flux of channel (4-2) is larger than that for channel 2, since the former has a higher sensibitlity in the range of the 15μ-band of CO_2 than the latter. In both spectral ranges the higher equivalent temperature (higher than the cloud temperature) is caused by the natural radiation of the ozone and carbon dioxide in the warm layers above the isotherme layer of the lower stratosphere.

The equivalent temperatures for the radiation of channel 1 will be higher than those which are shown in Table VI.4, if the water vapor content within the upper stratosphere is assumed to be greater than in these calculations. Then it may be possible that the equivalent temperatures of channel 1 are higher than those of channel 2 as it is found by an investigation of radiation data measured above the hurricane ANNA (FUJITA, BANDEEN et al.).

6.12: An example of evaluation.

As an example radiation data measured during orbit 42 over Europe were evaluated. Before the evaluation all data located within squares of 2 degrees latitude and 2 degrees longitude were averaged without consideration of the nadir angle for each single data. From the averages plotted in geographic maps isolines could be drawn as it is shown in the Fig. 6.3, 6.4, 6.5, and 6.6. These contourlines allow to distinguish between "warm" and "cold" areas although the spatial resolution was diminished by the averaging. In all figures the area viewed by the satellite is surrounded by a dashed curve. The satellite was flown from west to east. Its subsatellite path is indicated by the circles.

For a comparison with the actual weather situation, in a weather map (Fig. 6.7) all zones with scattered clouds or overcast sky are hatched, cloudless zones are shown without hatching.

A comparison of the weather map with the radiation maps (including also the map for the equivalent temepratures for the differences $\overline{W}^{(4)} - \overline{W}^{(2)}$) shows, that the equivalent temperatures over all cloudy areas are relatively low. The temperature distribution shows structures which might be caused by differently high clouds. Especially a very cold area is remarkable over the Atlantic Ocean near the coast of Spain and Portugal. Going to Central Europe the equivalent temperatures for all 4 channels increase strongly, which might be due to partly lower clouds respectively scattered clouds and partly to cloudless sky (channel 1: decrease of the relative humidity). The ground temperatures given in the weather charts

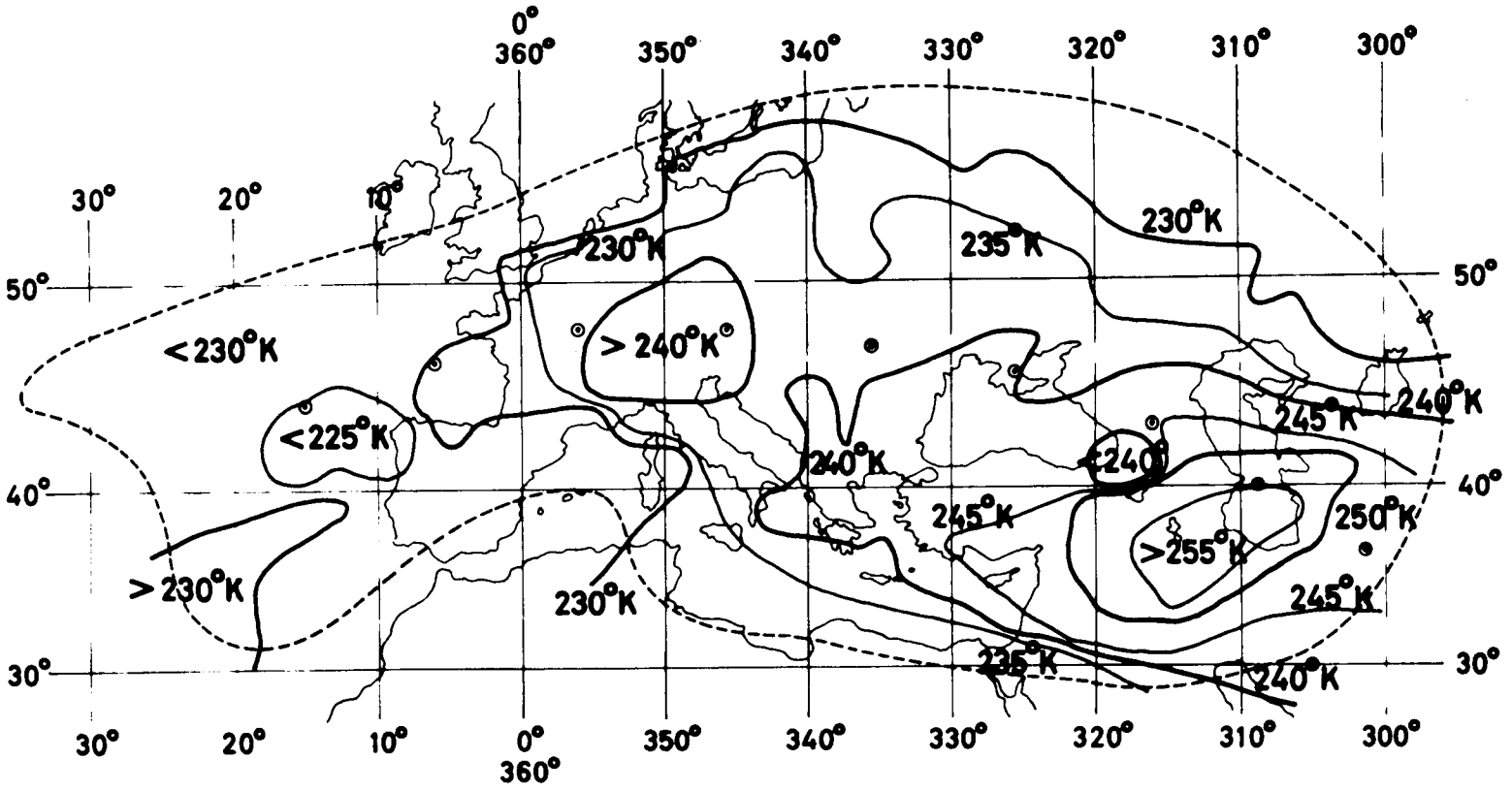

TIROS III: Orbit 42 (15.7.1961, 7.12-7.28 GMT), channel 1(5.8-6.8 μ)

Fig. 6.3

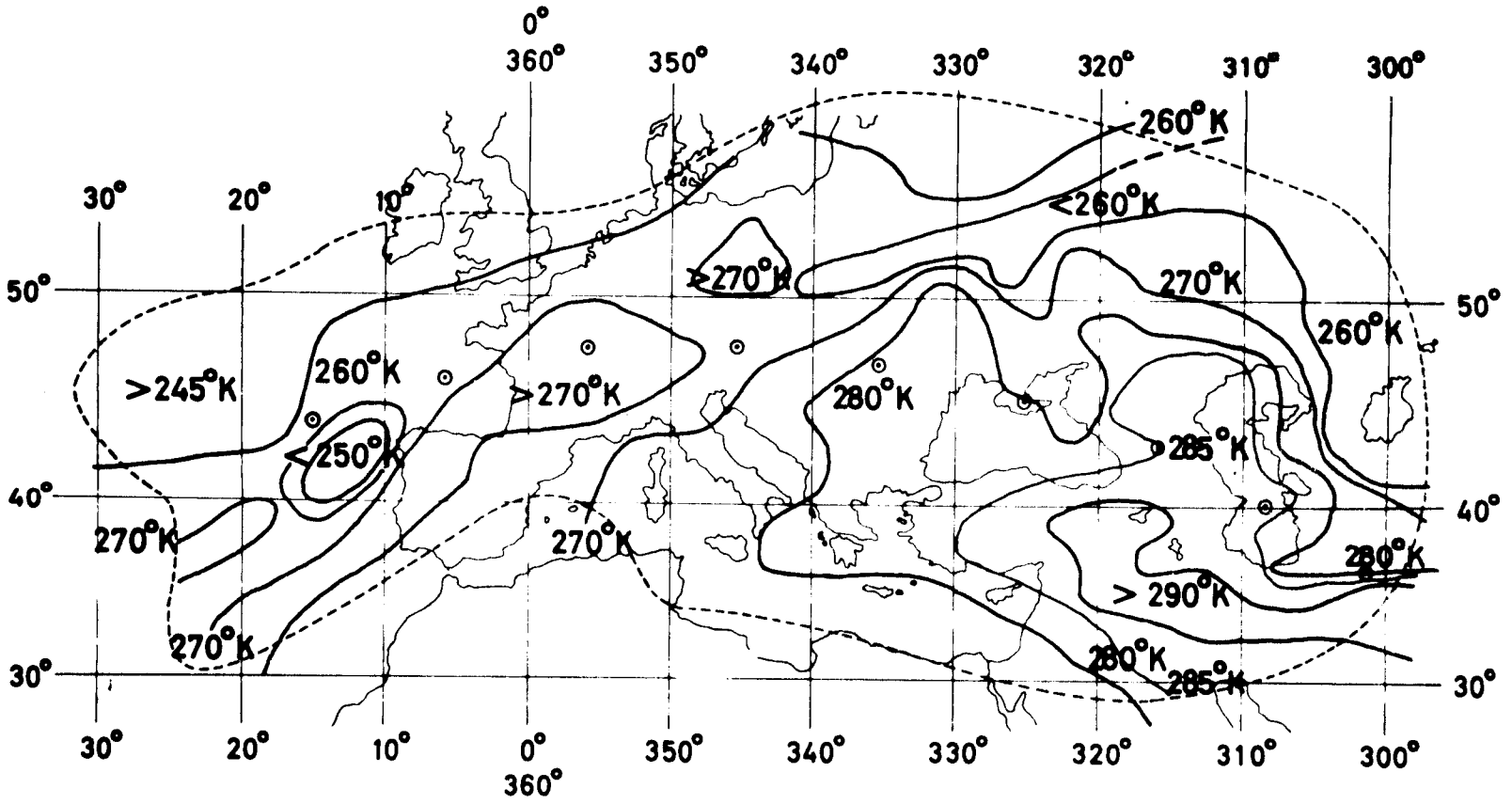

TIROS III: Orbit 42 (15.7.1961, 7.12-7.28 GMT), channel 2 (8-13 μ)

Fig. 6.4

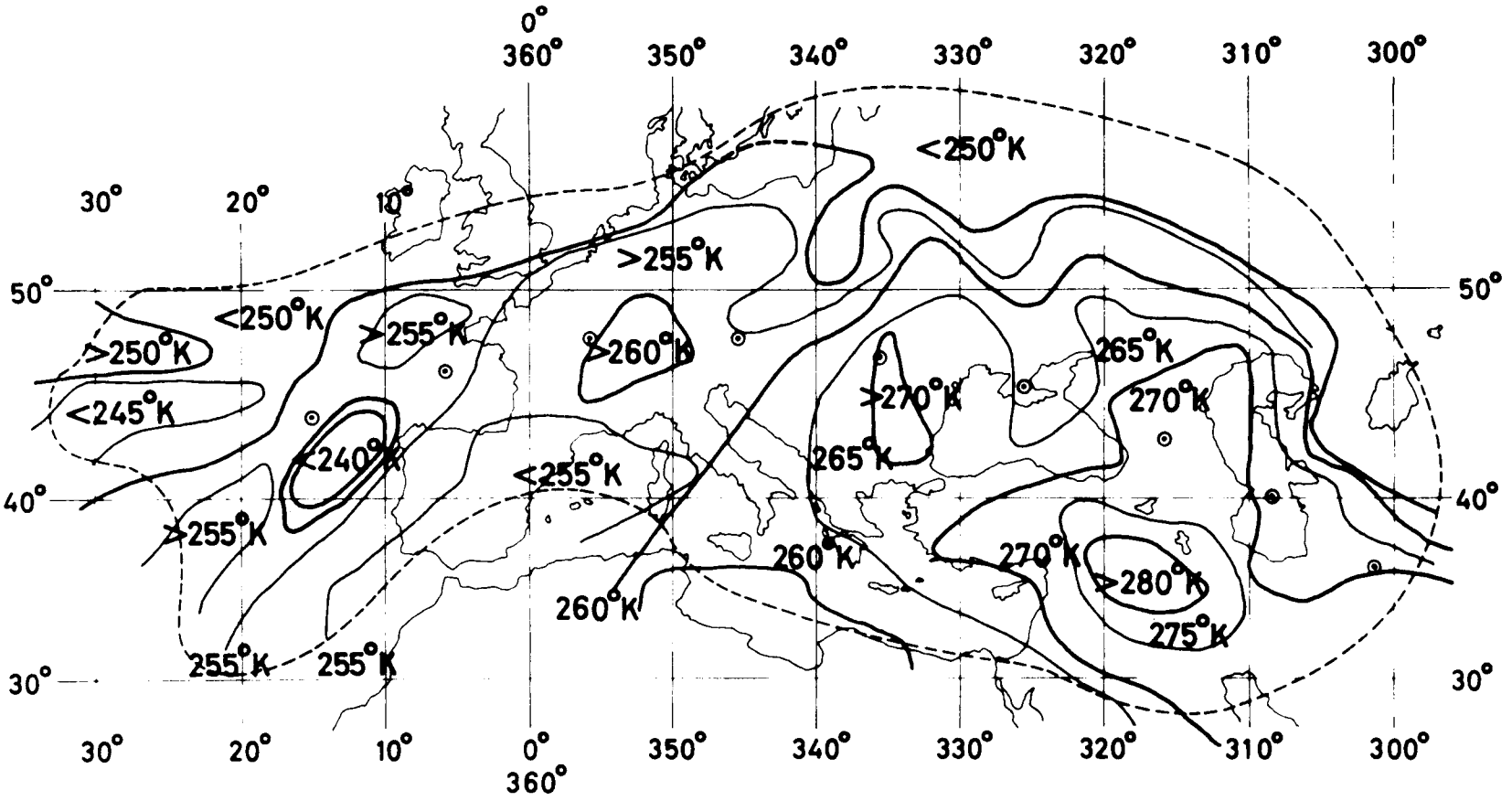

TIROS III : Orbit 42 (15.7.1961, 7.12-7.28 GMT) channel 4 (7.5-32.5 μ)

Fig. 6.5

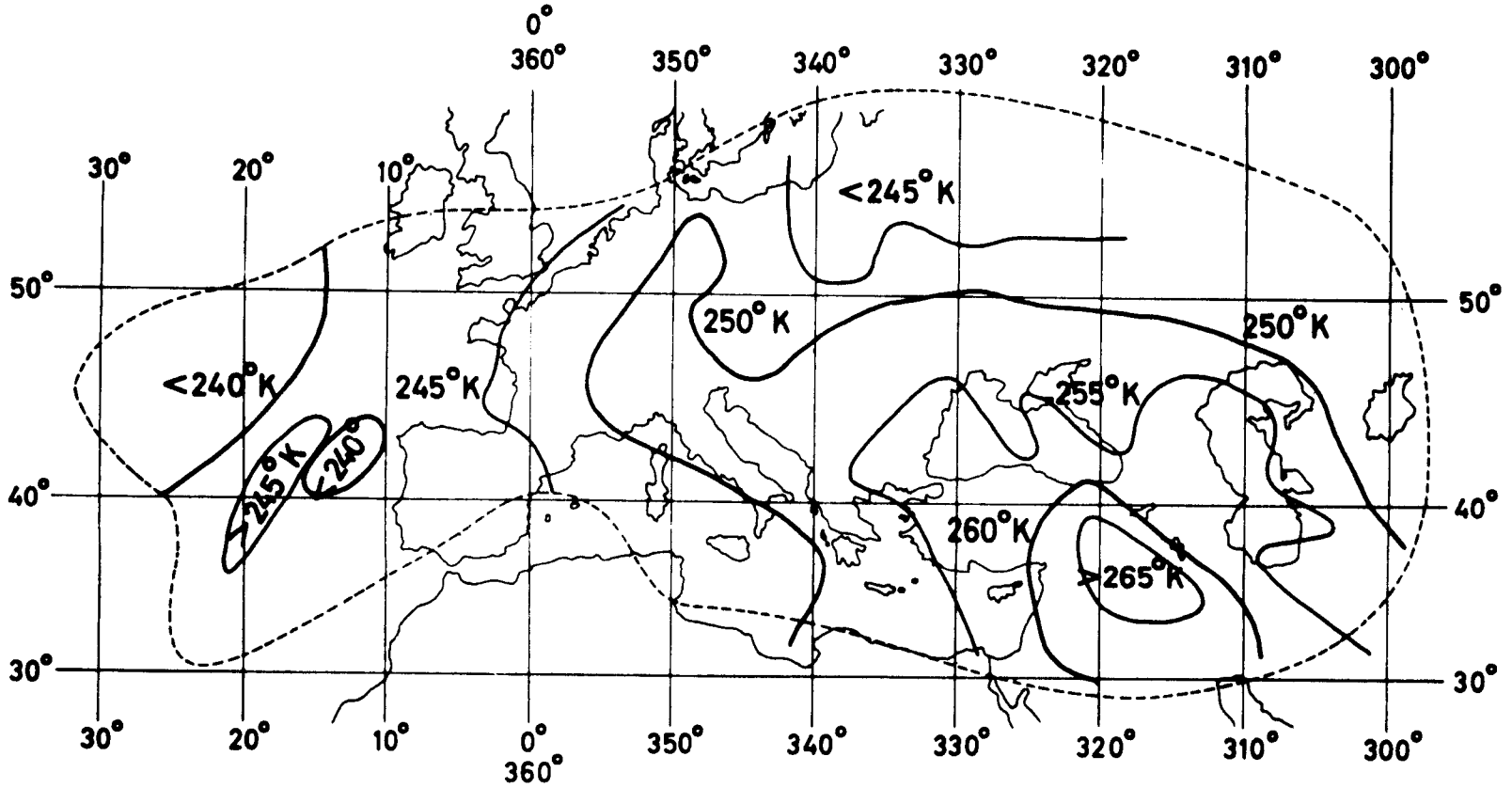

TIROS III, Orbit 42 (15.7.1961, 7.12 - 7.28 GMT), $T_{equ}[\overline{W}^{(2)} - \overline{W}^{(1)}]$

equivalent temperatures of the difference $\overline{W}^{(2)} - \overline{W}^{(1)}$

Fig. 6.6

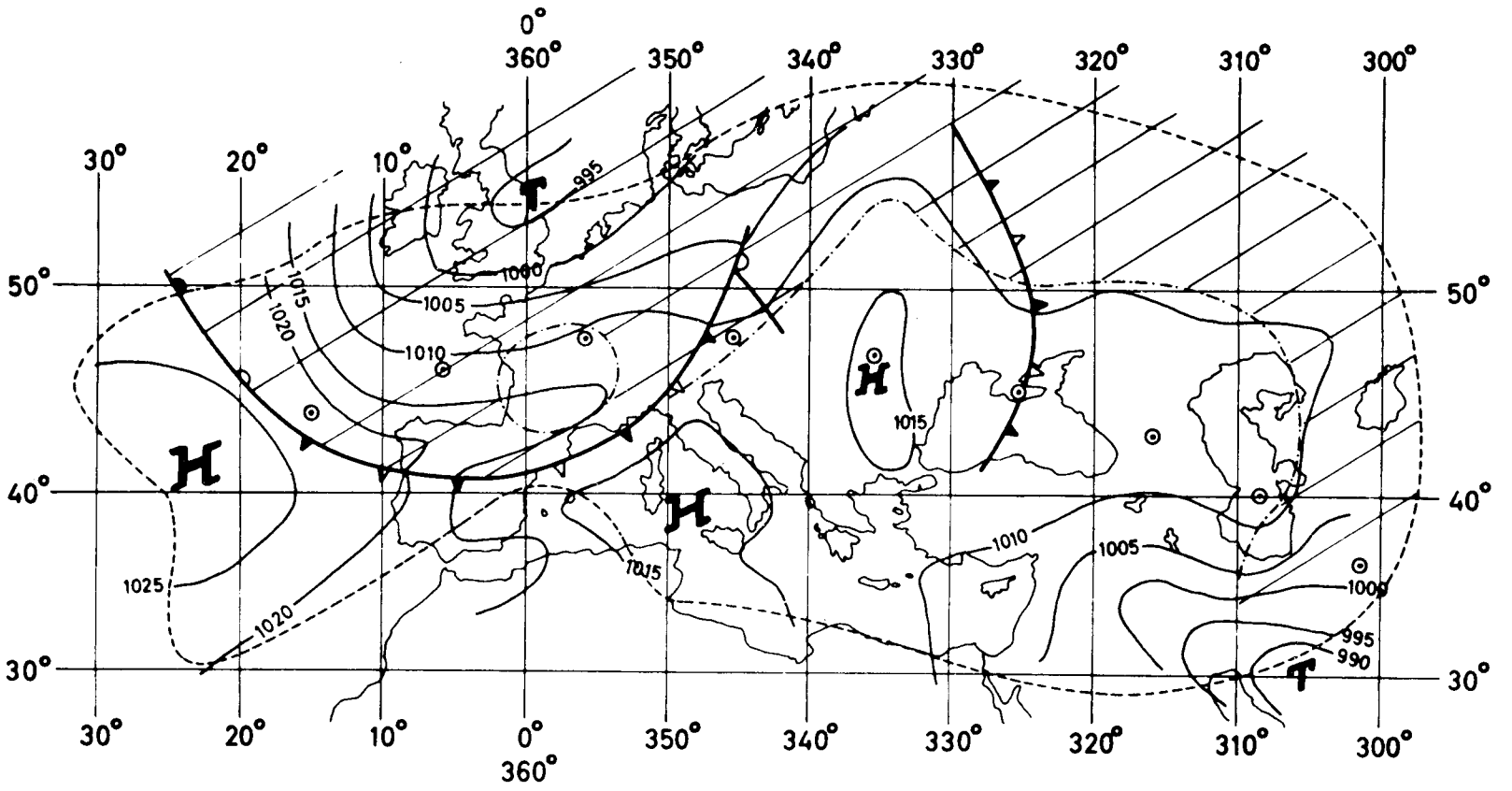

15.7.1961 , 0.00 GMT surface weather chart

cloudy-overcast

Fig. 6.7

were between + 12°C and +15°C. Over South-East-Europe, Turkey and Iraq all maps show very warm regions from which one may conclude on low relative humidities and high ground temperatures.

On the other side the equivalent temperatures decrease in the direction to the northern and southern boundaries of the viewed areas. This is due to the increase of the nadir angle under which these areas were observed. Radiation is measured with small nadir angles over areas near the subsatellite path.

By using the above mentioned evaluation diagrams, from the averages of the radiation data of the channels 1 and 2 mean relative humidites and surface temperatures were determined. The results are plotted into maps and contour-lines could be drawn (Fig. 6.8 and 6.9). In this analysis again the nadir angle effect was neglected, which causes a decrease of the surface temperatures and an increase of the relative humidities in direction to the northern and southern boundaries of the viewed area.

Over the Atlantic Ocean the very low temperatures indicate a high cloud cover, which partly cannot be seen in the weather map. Over this area the relative humidity is determined to 5o -8o %. A sharp increase in eastern direction from temperatures lower than -15°C to temperatures higher than +1o°C can be connected with a boundary of the cloud cover over the ocean. A similar sharp transition is seen over Eastern Europe. It coincides with a cloud cover boundary in the weather map (the same holds for an albedo transition as shown in the chapter 6.13). In the same direction the relative himidity decreases as the temperature increases.

Over France the surface temperatures were found to be higher than +1o°C, which confirms the assumed small amount of cloudiness, because the shelter temperatures given in the weather map are not higher than +14°C.

High temperatures connected with very low relative humidities were found over the areas of Turkey and Iraq.

These preliminary results show the possibility to determine surface temperatures and relative humidities from the radiation data of the channels 1 and 2. But the quantitative values will be influenced

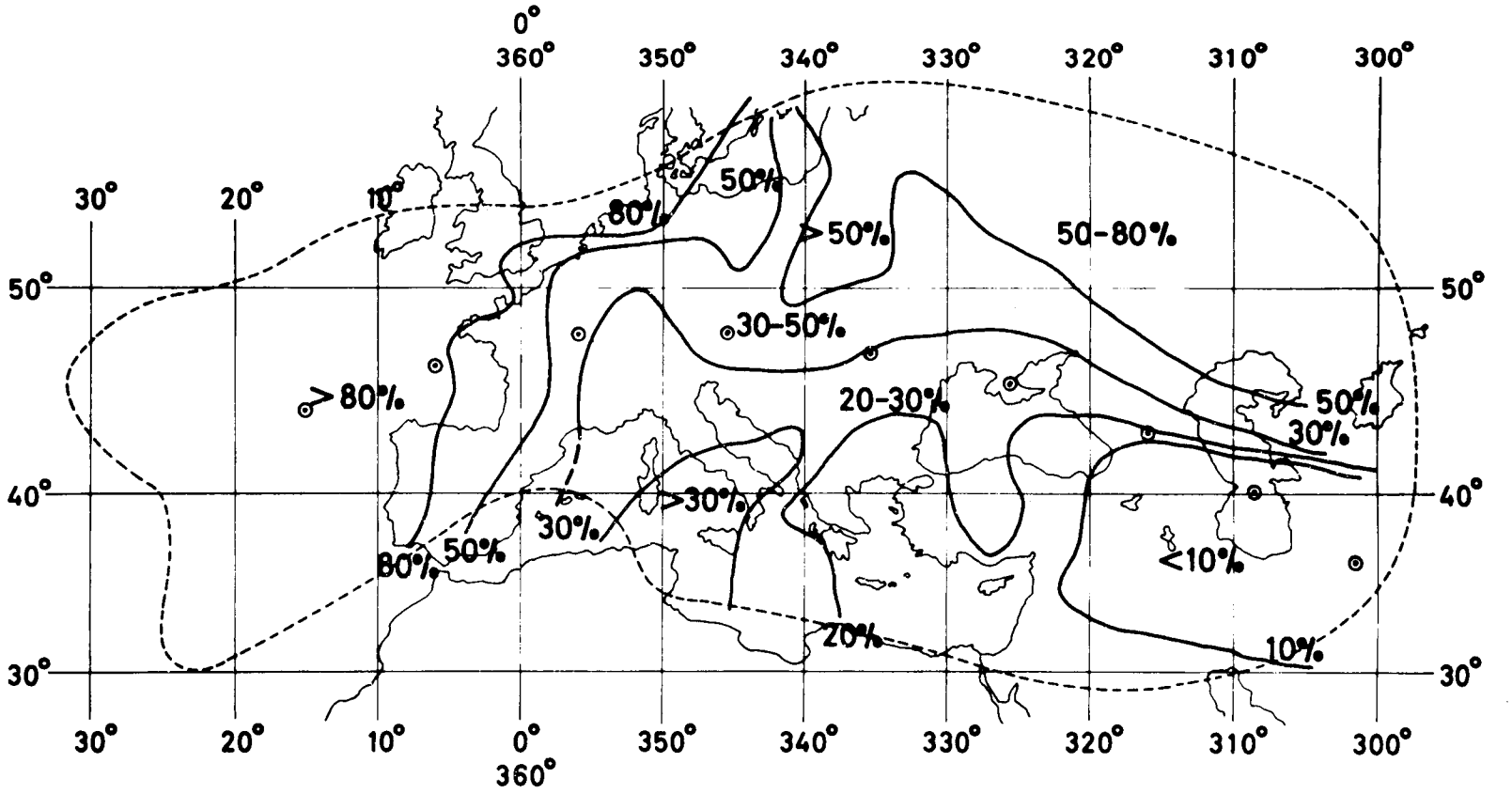

TIROS III : Orbit 42 (15.7.1961, 7.12-7.28 GMT)

mean relative humidity in the upper troposphere

Fig. 6.8

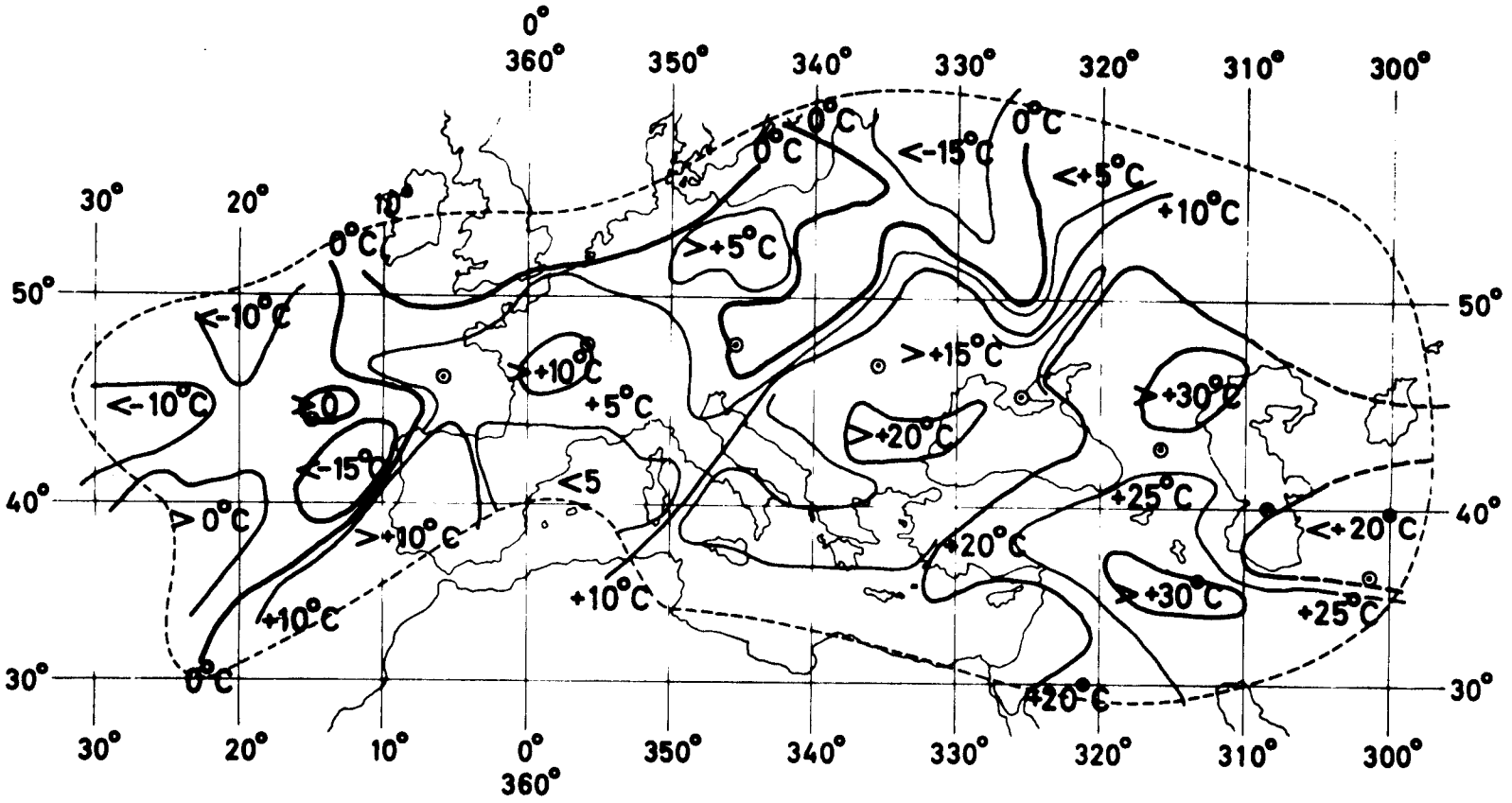

TIROS III : Orbit 42 (15.7.1961, 7.12-7.28 GMT), surface temperature

Fig. 6.9

by large errors which are caused by the scatter of the measured data and by the model assumptions. Since the nadir angle effect was not taken into consideration, a new analysis will give better results.

6.13: Albedo.

In order to give a comparison of the infrared data with the measured reflected solar radiation (channels 3 and 5) albedo values were determined from the radiation data of channel 3 of the same orbit. With the assumption that the spectral intensity of the reflected solar radiation is equal to that of the incident solar radiation, the albedo A can be calculated simply by

$$A = \frac{\bar{W}^{(3 \text{ or } 5)}}{\sin h \cdot H_{\odot}^{(3 \text{ or } 5)}} \quad . \tag{6.1}$$

$\bar{W}^{(3 \text{ or } 5)}$ stands for the radiation measured by the channels 3 or 5, h is the elevation angle of the sun and $H_{\odot}^{(3 \text{ or } 5)}$ is the intensity of the incident solar radiation, which would be measured if the channel 3 or 5 views the sun. $H_{\odot}^{(3 \text{ or } 5)}$ can be determined by

$$H_{\odot}^{(3 \text{ or } 5)} = \int_{0}^{\infty} H_{\lambda} \Phi_{\lambda}^{(3 \text{ or } 5)} \, d\lambda \quad [W \, m^{-2}], \tag{6.2}$$

where $\Phi_{\lambda}^{(3 \text{ or } 5)}$ is the spectral sensitivity of the 2 channels and H_{λ} the extraterrestrial solar irradiance. For our calculations the spectral irradiance of solar radiation determined by JOHNSON (1954) was introduced into equation (6.2) (see also Fig. 2.1).

The albedo values were determined from measurements averaged over squares of 2 deg. latitude and 2 deg. longitude. The results are given in Fig. 6.10 for channel 3.

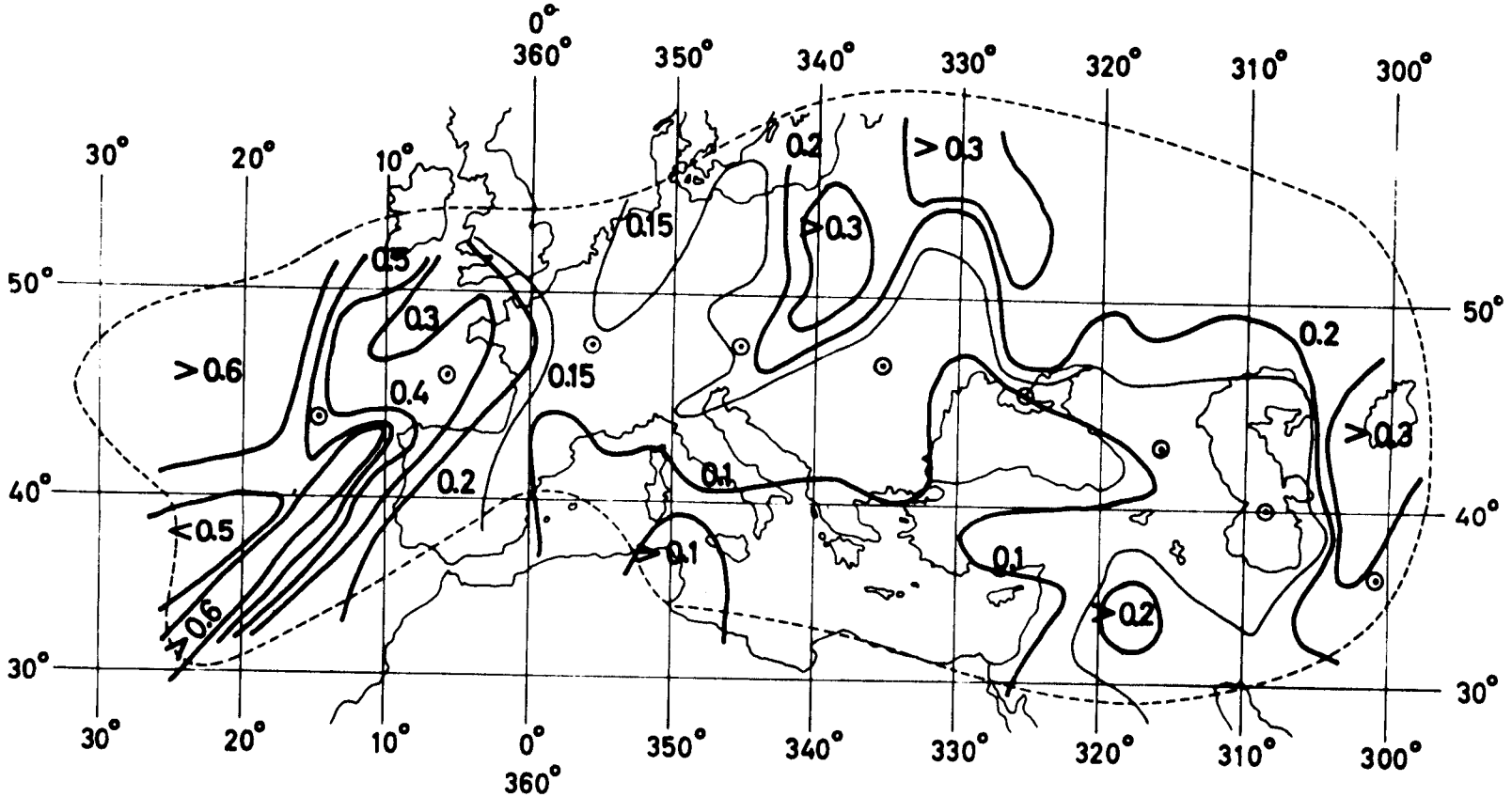

TIROS III : Orbit 42 (15.7.1961, 7.12-7.28 GMT) Albedo channel 3 (0.3 - 6 μ)

Fig. 6.1o

High albedo values over the Atlantic Ocean mean a coverage with clouds. This area coincides with the area of low surface temperatures in Fig. 6.9. The strong transition from high to low albedo values in eastern direction indicates again a boundary of the cloud-cover as did the temperature transition in Fig. 6.9. Similar boundaries over the Ukraina and between the Caspian and the Aral-Sea can be correlated also with a boundary of cloud-cover. The high albedo over Turkey and Iraq must be due to the high reflectivity of the ground (desert). It will be difficult to distinguish between cloud-covered and cloudless areas over these areas by using only albedo measurements.

The albedo isoline A = o.1 runs nearly parallel to the coast line of the Black Sea and the Mediterranian Sea, which allows a good discrimination between sea and land as it is also known from television pictures (o.5μ - o.7μ).

Generally the determined albedo values are too low. FRITZ (1949) computed for clouds a mean albedo of o.55 and for the average albedo of the planet earth o.35. Also the albedo values found over the cloudless sea will be too low (o - o.o6), because direct measurements give o.o8 - o.25 (MÖLLER, 1957). Influence of light scattered in the atmosphere could only increase the values.

6.2: Statistical investigations.

6.21: Correlations between radiation data averaged over large areas.

A comparison between the various measured values averaged over large areas (about squares of 8 deg. altitude and longitude) allows to find correlations between the radiation data and averaged synoptic values for these areas. Moreover, by the average process the scatter of the single date is diminished.

For several areas overflown by the satellite during the orbits 42 and 114 such average values were determined and plotted as ordinates into Fig. 6.11 a and 6.11 b together with averages of the shelter temperature and of the evaluated surface temperatures (T_{BB}).

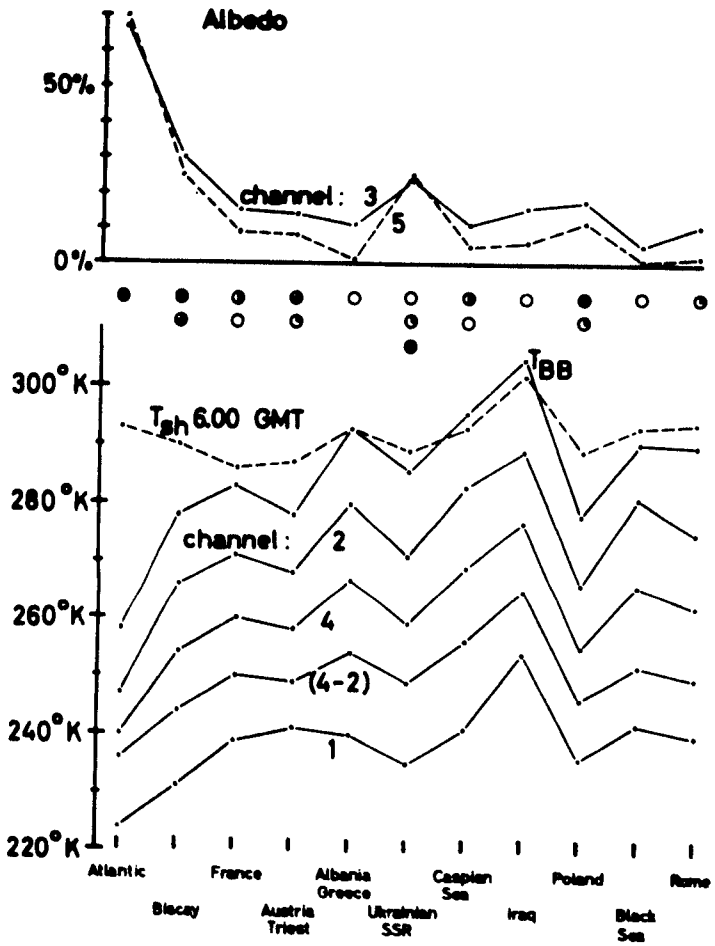

TIROS III: Orbit 42 (15.7.1961, 7.12- 7.28 GMT)

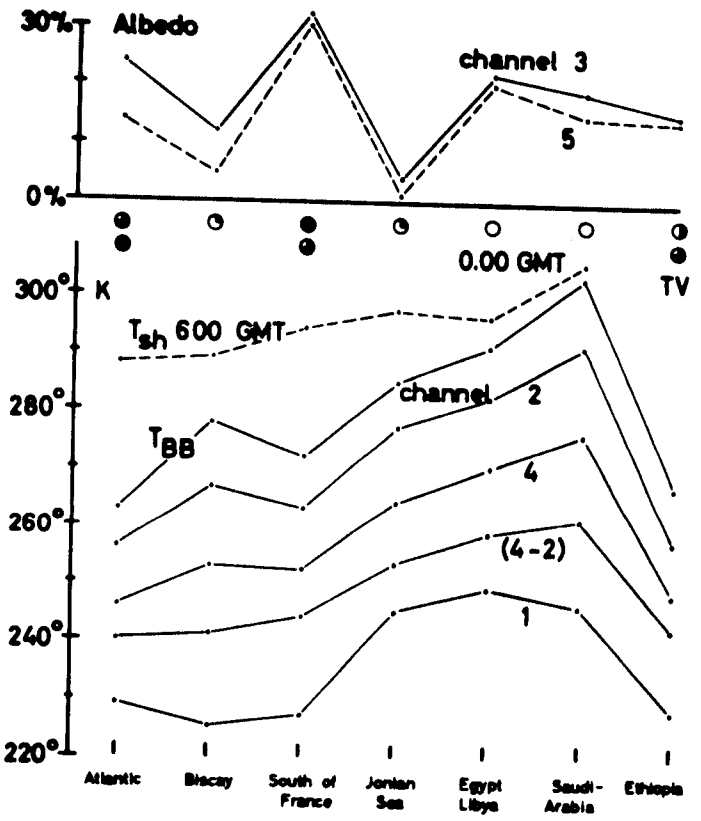

TIROS III: Orbit 114 (20.7.1961, 7.20 - 8.14 GMT)

Fig. 6.11

The straight lines between the single points have no physical significance, because the sequence of the areas given on the abscissa is arbitrary. All these curves show good intercorrelations and are parallel to the surface temperature T_{BB}. The striking correlation between the averages of channel 2 and channel 1 can be explained by the meteorological situation, e.g. over the warm cloudless areas (Iraq) the relative humidity is also low so that the channel 1 measures high equivalent temperatures. But in the same case the albedo values are high due to the high reflectivity of the ground.

On the other hand the infrared radiation data are all low over cloud-covered areas. That means that an increase of the cloud height goes parallel to an increase of the relative humidity.

Only in two cases (Fig. 6.11 a: Triest, Austria; Fig. 6.11 b: Biscay) deviations occur in the slope of the curves for channel 1 and the other channels. In the former case the average of channel 1 increases, while the other data decrease. In the latter case the average of channel 2 decreases while the other data increase. The deviations between the determined surface temperatures T_{BB} and the averaged shelter temperatures are not too large in the cases of a cloudless sky. But the shelter temperatures given in the weather charts are not equal to the temperatures of the surface. At noon they might be several degrees smaller.

6.22: Correlations between single measured data.

In the preceding chapter good correlations between the data of the channels 1, 2 and 4 and the differences $(\overline{W}^{(4)} - \overline{W}^{(2)})$ could be shown with averages for large areas.

Here we will compare single data. The narrowest correlation will be expected between the radiation data of the channels 2 and 4 because the sensitivity ranges of both channels include the water vapor window range with its high spectral radiance. But a frequency counting of of simultaneous data of both channels shows a large scatter (Fig. 6.12). In this counting about 5,000 values measured during orbit 114 over Europe were used. The numbers in

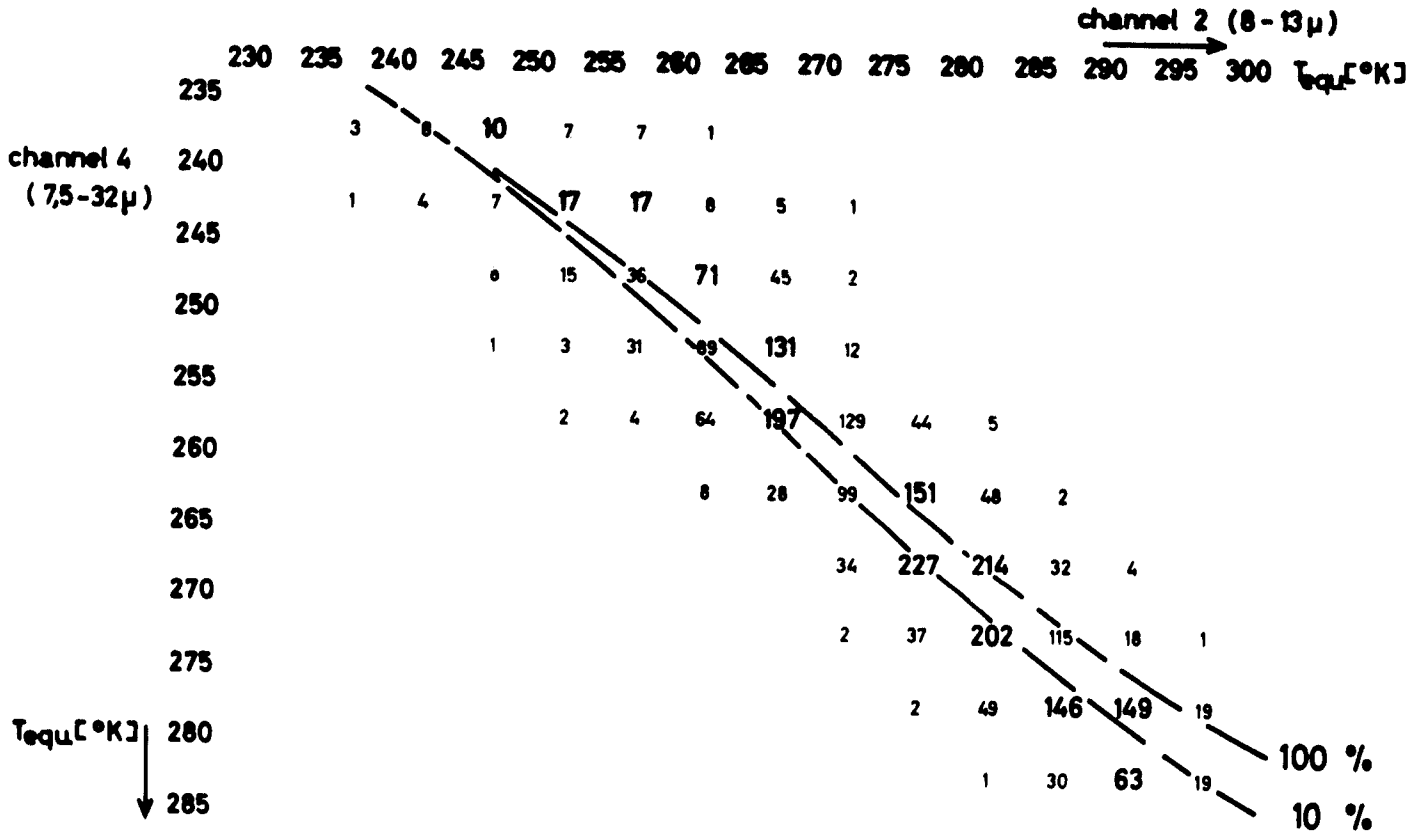

TIROS III : Orbit 114 (20. 7. 1961 , 7.20 - 8.14 GMT)

frequency of measured data of channels 2 and 4 (nadir angle N < 50°)
– – – – model of a tropical atmosphere (nadir angle N = 0°)

Fig. 6.12

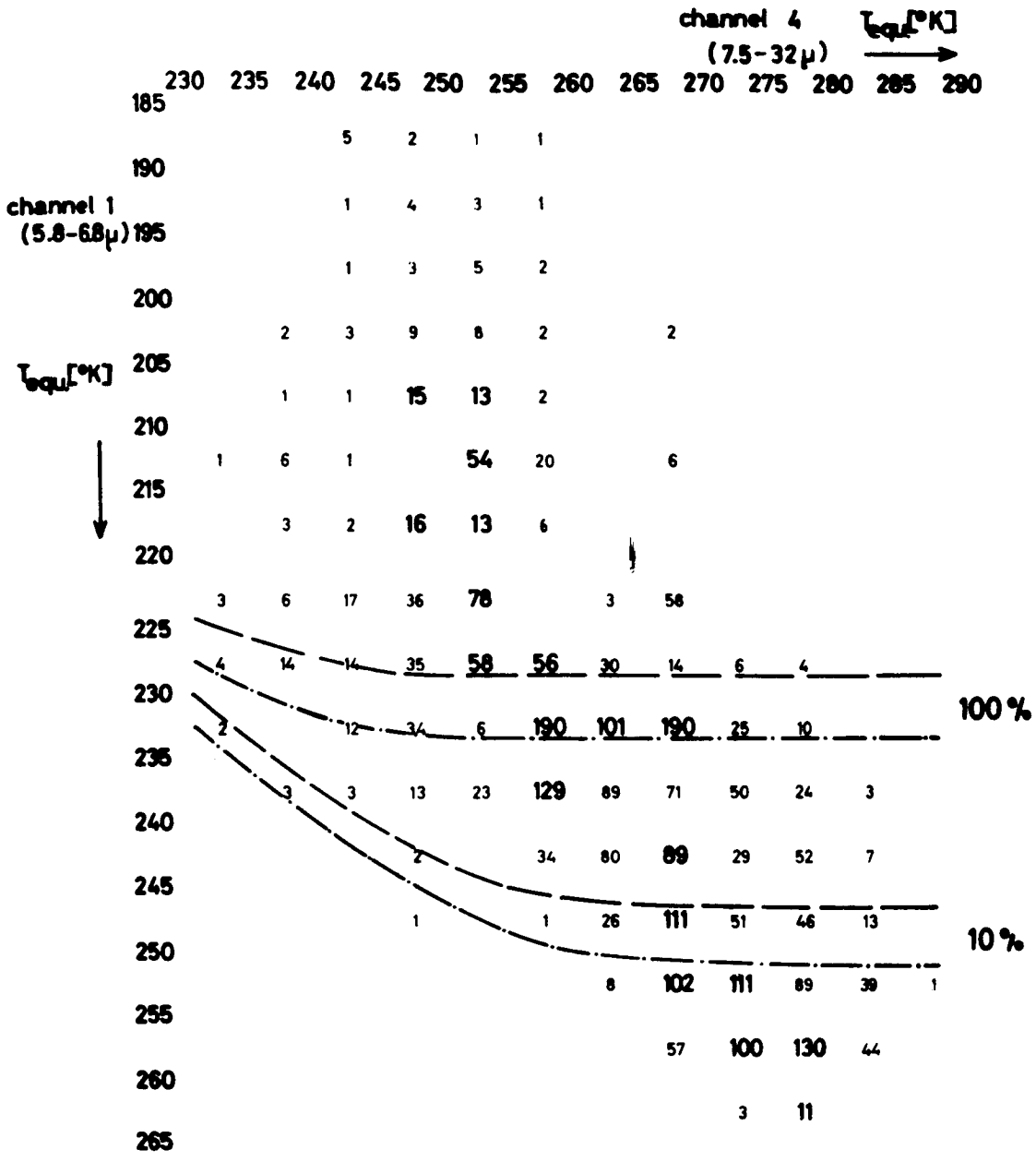

TIROS III : Orbit 114 (20.7.1961, 7.20-8.14 GMT)

frequency of measured data of channels 1 and 4
(nadir angle $N < 50°$)

-·-·-·- model of a tropical / subtropical atmosphere

– – – – – (nadir angle $N = 0°$)

Fig. 6.12 mean the frequency values. They scatter around two curves, which were calculated for the model atmosphere III under the assumption that the satellite views the earth in vertical direction. Both curves (the parameter is the relative humidity of the troposphere) deviate only by a small amount, so that variations of the relative humidity might not have a great influence on the correlation between the radiation data of both of the channels. At this counting all data were used without a selection according to the nadir angle, or the latitude or climatic zone. Perhaps the correlation will be closer if such a selection is observed. But the scatter of the single values will still be large enough to influence the accuracy of the radiation data and to diminish the accuracy of the derived quantities (e.g. the surface temperature). Even a larger scatter has to be expected for the difference data (4-2); so that it would be almost impossible to determined from these any synoptic data as it is mentioned in chapter 6.1.

The results of another combined frequency counting of channels 1 and 4 are shown in Fig. 6.13. The frequency numbers written by larger figures confirm the correlation, which was found in the preceding chapter and demonstrated by Fig. 6.11. But a comparison with the curves calculated for the model atmospheres II and III shows that this correlation is only an apparent one. It is a consequence of the meteorological connexions, namely the occurence of high relative humidity above clouds and of low relative humidity above cloudless area. Investigation with more data will give us better information of the reliability of this connexion.

The large scatter of the data can be partially explained by the influence of the relative humidity as it is shown by the deviations of the two theoretical curves.

With the same radiation data countings of the equivalent temperatures of the channels 1 and 2 were made in dependence on the nadir angle (Fig. 6.14 a and b). In both cases all data were used without any selection according to geographic or synoptic situation. As the theoretical curves for the nadir angle dependence of the radiation flux (chapter 5.22.4) show, the scatter of the single

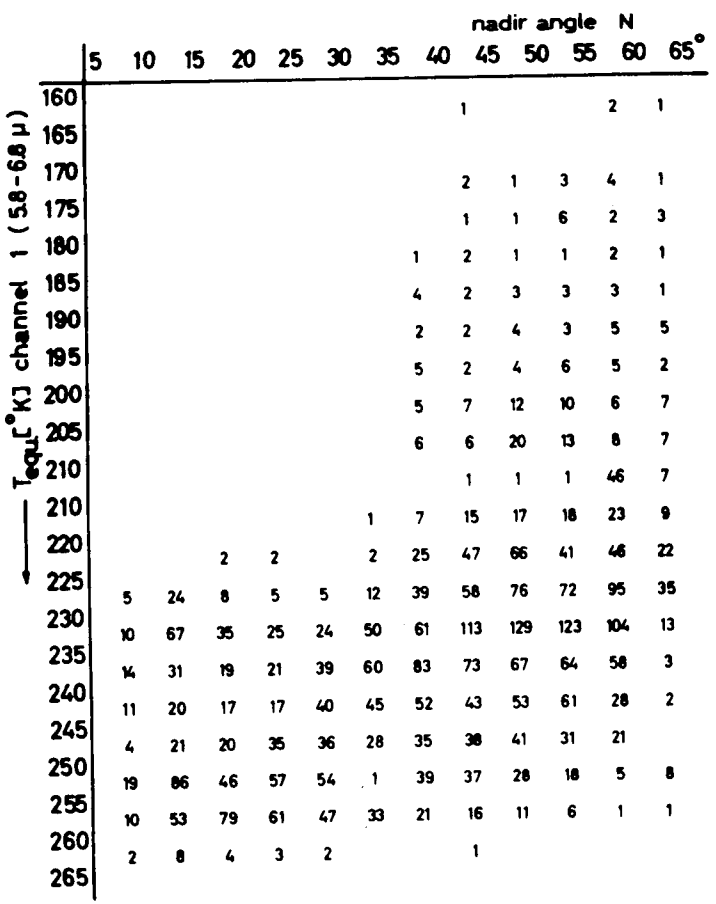

TIROS III: Orbit 114 (20.7.1961, 7.20-8.14 GMT)

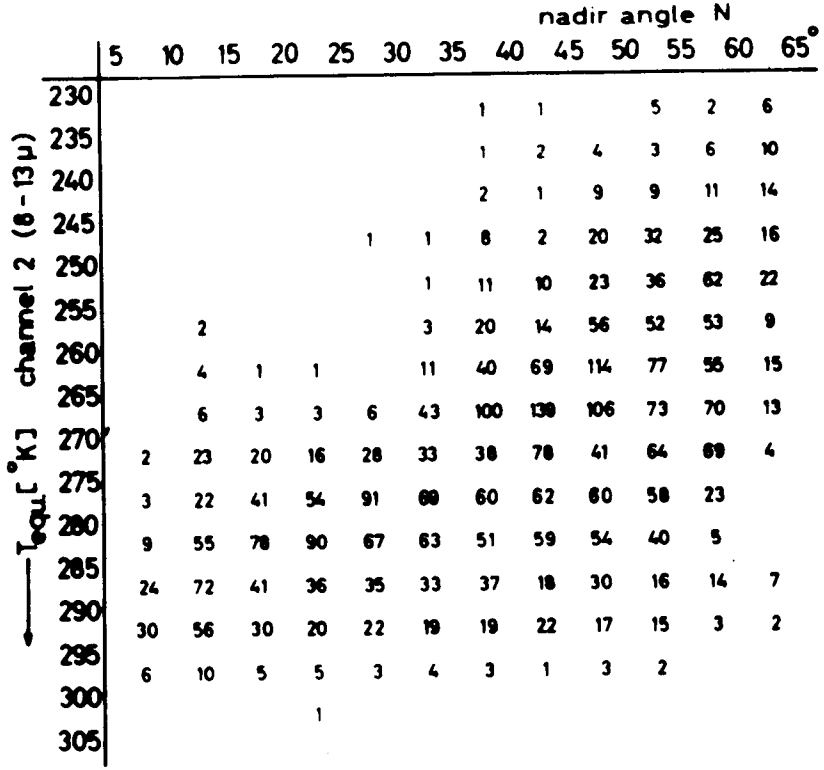

TIROS III: Orbit 114 (20.7.1961, 7.20-8.14 GMT)

Fig. 6.14

values must be large. This is due to the different cloud heights (channels 2, 4) and different relative humidities (channel 1) and also due to the insufficient accuracy of the radiation data. Statistical investigations with a selection according to the cloud height and also different humidities would certainly give clearer results.

All investigations which were discussed in this chapter 6 will be continued in the next future. Since a very extensive material of radiation data is available more extensive statistical investigations can be carried out. Correlation coefficients and also partial correlation coefficients may then give more detailed information about the connexion between all radiation data and also about the influence of meteorological conditions or the nadir angle etc. on these data.

7. CONCLUSIONS.

A detailed analysis of the absorption coefficients calculated by STULL et al. (1963) for water vapor and carbon dioxide had the result that in a pressure correction of the absorbing mass according to the equation

$$w^* = w \left(\frac{p}{p_o}\right)^n$$

the exponent n is not constant. It changes with the absorber quantity and also with the pressure. This variation depends on the spectral range within the band (band center or band wings) and is caused by the different strength of the lines. In order to examine these relations by measurements only the extensive material of BURCH, GRYVNAK and WILLIAMS (1960) for the 15μ-band of CO_2 could be used. Other published spectral measurements (HOWARD et al., etc.) have too little spectral resolution for this purpose. As we need radiation diagrams for calculations in the sensitivity ranges of the 3 infrared channels of satellite TIROS III, pressure correction

exponents independent of wave length must be introduced for each absorbing gas. Probably the greatest error will arise here within the 11μ-water vapor window region, as direct laboratory measurements with respective pressure variations and also calculations of the pressure dependence of the absorption within this spectral interval are not available. These exponents n have been already introduced during the derivation of transmission functions $\tau(l_\nu, w^*)$, which are given in the same form as used by ELSASSER (1960) and ELSASSER and KING (1953).

The exponents used here are:

Gas	exponent
H_2O	0.72
CO_2	0.65
O_3	0.41 ($p < 150$ mb) 0 ($p > 150$ mb)

In radiation flux calculations the absorption and emission of these 3 gases (H_2O, CO_2 and O_3) have to be taken into consideration. Thus, the influence of these three components in the radiation flux in each sensitivity range can be shown.

The determination of an average relative humidity in the upper troposphere as well as of ground or cloud surface temperatures from the radiation data of the channels 1 and 2 has been made possible by a method of MÖLLER (1962) in which the measured data are compared with data calculated for model atmospheres. Frequency countings of simultaneous data show large scatter, so that the result must be influenced by a great error. Nevertheless, from representations of average values in geographical maps "warm" and "cold" respectively "moist" and "dry" areas can be recognized. Narrow correlations between the radiation data of channel 1 and the other channels, averaged over large geographic areas, show that the relative humidity above clouds increases with increasing cloud height. The estimated ground temperatures are only several degrees lower than the shelter temperature given in weather maps for the same regions.

A P P E N D I X I

Tables of the spectral transmittance τ ($_{10}\log$ ($l_\nu w^*$)) and of the decadic logarithms of the generalized absorption coefficients ($_{10}\log l_\nu$) for water vapor and carbon dioxide and a table for the integrated transmittance of the 9.6μ - band of ozone.

The "pressure corrected" absorbing gas quantity is defined by

$$w^* = w \left(\frac{p}{p_o} \right)^n ,$$

where p_o is the standard pressure.

absorbing gas	exponent n	w^*
H_2O	o.72	u^* [g·cm^{-2}]
CO_2	o.65	c^* [cm NTP]
O_3	o.41 for p < 15o mb o for p > 15o mb	m^* [cm NTP]

Table A : Decadic Logarithms of the Generalized Absorption Coefficients ($_{10}\log l_\nu$) for the 6.3μ - Band of Water Vapor

(4.7μ - 8.6μ ; 2120 cm^{-1} - 1160 cm^{-1})

$\nu[cm^{-1}]$	300 °K	280 °K	260 °K	240 °K	220 °K	200 °K
1160	0.38 -1	0.30 -1	0.19 -1	0.04 -1	0.90 -2	0.72 -2
1200	0.80 -1	0.72 -1	0.60 -1	0.45 -1	0.32 -1	0.15 -1
1240	0.25	0.16	0.06	0.96 -1	0.80 -1	0.62 -1
1280	0.66	0.60	0.53	0.46	0.34	0.22
1320	0.10 +1	0.06 +1	0.02 +1	0.95	0.88	0.80
1360	0.58 +1	0.56 +1	0.52 +1	0.48 +1	0.44 +1	0.40 +1
1400	0.08 +2	0.08 +2	0.08 +2	0.08 +2	0.06 +2	0.00 +2
1440	0.50 +2	0.48 +2	0.46 +2	0.44 +2	0.40 +2	0.37 +2
1480	0.86 +2	0.84 +2	0.80 +2	0.80 +2	0.80 +2	0.80 +2
1520	0.76 +2	0.80 +2	0.80 +2	0.80 +2	0.80 +2	0.82 +2
1560	0.20 +2	0.22 +2	0.25 +2	0.30 +2	0.35 +2	0.40 +2
1580	0.08 +2	0.10 +2	0.15 +2	0.18 +2	0.22 +2	0.26 +2
1600	0.16 +2	0.25 +2	0.30 +2	0.36 +2	0.44 +2	0.50 +2
1640	0.70 +2	0.72 +2	0.74 +2	0.76 +2	0.78 +2	0.78 +2
1680	0.56 +2	0.56 +2	0.56 +2	0.56 +2	0.56 +2	0.56 +2
1720	0.20 +2	0.20 +2	0.20 +2	0.20 +2	0.20 +2	0.20 +2
1760	0.80 +1	0.76 +1	0.74 +1	0.72 +1	0.68 +1	0.66 +1
1800	0.45 +1	0.40 +1	0.35 +1	0.33 +1	0.30 +1	0.25 +1
1840	0.00 +1	0.98	0.96	0.94	0.90	0.85
1880	0.66	0.62	0.57	0.52	0.44	0.40
1920	0.36	0.30	0.24	0.15	0.04	0.90 -1
1960	0.06	0.00	0.90 -1	0.76 -1	0.64 -1	0.48 -1
2000	0.75 -1	0.62 -1	0.50 -1	0.37 -1	0.23 -1	0.03 -1
2040	0.31 -1	0.22 -1	0.10 -1	0.97 -2	0.82 -2	0.60 -2
2080	0.90 -2	0.80 -2	0.70 -2	0.55 -2	0.38 -2	0.15 -2
2120	0.46 -2	0.36 -2	0.25 -2	0.10 -2	0.95 -3	0.80 -3

Table B : Decadic Logarithms of the Generalized Absorption Coefficients ($_{10}\log l_\nu$) for the Rotation Band of Water Vapor

(12.5 μ - 50 μ ; 800 cm^{-1} - 200 cm^{-1})

ν [cm^{-1}]	300 °K	280 °K	260 °K	240 °K	220 °K
800	0.45 -1				
760	0.52 -1				
720	0.61 -1				
680	0.72 -1				
640	0.84 -1				
600	0.00				
560	0.28	0.27	0.26	0.25	0.24
520	0.72	0.68	0.65	0.61	0.57
480	0.17 +1	0.10 +1	0.02 +1	0.96	0.90
440	0.44 +1	0.36 +1	0.30 +1	0.22 +1	0.16 +1
400	0.63 +1	0.55 +1	0.50 +1	0.40 +1	0.34 +1
360	0.04 +2	0.96 +1	0.88 +1	0.80 +1	0.70 +1
320	0.30 +2	0.22 +2	0.14 +2	0.06 +2	0.98 +1
280	0.54 +2	0.48 +2	0.42 +2	0.37 +2	0.32 +2
240	0.78 +2	0.75 +2	0.72 +2	0.69 +2	0.66 +2
200	0.00 +3				

Table C : Spectral Transmittance $\tau\,(\,{}_{10}\log\,(\,l_\nu\,u^*)) = \tau(\,{}_{10}\log\,l_\nu + {}_{10}\log\,u^*\,)$ for the 6.3 μ - Band and the Rotation Band of Water Vapor to be Used in Connection with Table A and B

${}_{10}\log(l_\nu\,u^*)$	6.3 μ	rotat.	${}_{10}\log(l_\nu\,u^*)$	6.3 μ	rotat.
0.8 -4	1.000	1.000	0.4 -1	0.737	0.737
0.9	1.000	0.998	0.5	0.700	0.708
0.0 -3	1.000	0.995	0.6	0.662	0.675
0.1	1.000	0.994	0.7	0.620	0.635
0.2	1.000	0.992	0.8	0.575	0.595
0.3	1.000	0.990	0.9	0.531	0.548
0.4	0.998	0.987	0.0 +0	0.485	0.500
0.5	0.995	0.985	0.1	0.438	0.450
0.6	0.993	0.983	0.2	0.393	0.398
0.7	0.990	0.978	0.3	0.350	0.345
0.8	0.987	0.975	0.4	0.307	0.298
0.9	0.984	0.970	0.5	0.262	0.244
0.0 -2	0.980	0.964	0.6	0.223	0.200
0.1	0.975	0.958	0.7	0.185	0.160
0.2	0.969	0.950	0.8	0.147	0.122
0.3	0.962	0.942	0.9	0.115	0.095
0.4	0.953	0.930	0.0 +1	0.087	0.067
0.5	0.944	0.918	0.1	0.065	0.047
0.6	0.932	0.905	0.2	0.047	0.028
0.7	0.917	0.890	0.3	0.033	0.015
0.8	0.900	0.875	0.4	0.022	0.005
0.9	0.880	0.855	0.5	0.014	0
0.0 -1	0.857	0.835	0.6	0.009	0
0.1	0.831	0.815	0.7	0.005	0
0.2	0.802	0.790	0.8	0	0
0.3	0.771	0.763	0.9	0	0

Table D : Absorption Coefficients η_ν and β_ν for the Water Vapor Window (8.3μ - 12.5μ ; 1200 cm^{-1} - 1800 cm^{-1})

$$\tau_\nu (u^*) = \exp - (\eta_\nu \sqrt{u^*} + \beta_\nu u^*)$$

ν	η_ν	β_ν	ν	η_ν	β_ν
$[cm^{-1}]$	$[cm\ g^{-0.5}]$	$[cm^2\ g^{-1}]$	$[cm^{-1}]$	$[cm\ g^{-0.5}]$	$[cm^2\ g^{-1}]$
800	0.160	0.135	1000	0.040	0.080
840	0.080	0.110	1040	0.045	0.080
880	0.050	0.095	1080	0.050	0.080
920	0.045	0.085	1120	0.065	0.085
960	0.040	0.080			

Table E : Integrated Transmittance τ ($_{10}\log m^*$) for the 9.6μ - Band of Ozone
(8.8μ - 11.9μ ; 1140 cm^{-1} - 840 cm^{-1})

$_{10}\log m^*$	τ	$_{10}\log m^*$	τ	$_{10}\log m^*$	τ
0.3 -4	1.000	0.4 -3	0.967	0.5 -2	0.830
0.4	0.998	0.5	0.961	0.6	0.810
0.5	0.996	0.6	0.953	0.7	0.788
0.6	0.995	0.7	0.945	0.8	0.764
0.7	0.993	0.8	0.935	0.9	0.740
0.8	0.990	0.9	0.924	0.0 -1	0.717
0.9	0.988	0.0 -2	0.912	0.1	0.695
0.0 -3	0.985	0.1	0.898	0.2	0.675
0.1	0.981	0.2	0.883	0.3	0.655
0.2	0.977	0.3	0.867	0.4	0.635
0.3	0.973	0.4	0.850	0.5	0.616

Table F : Decadic Logarithms of the Generalized Absorption Coefficients ($_{10}\log l_\nu$) for the 15μ - Band of CO_2 (12.5μ - 19.2μ ; 800 cm^{-1} - 520 cm^{-1})

ν [cm^{-1}]	300 °K	260 °K	240 °K	220 °K
520	0.35 -5	0.25 -5	0.95 -6	0.80 -6
540	0.00 -4	0.65 -5	0.35 -5	0.15 -5
560	0.60 -4	0.30 -4	0.00 -4	0.75 -5
580	0.70 -3	0.30 -3	0.00 -3	0.75 -4
600	0.84 -2	0,45 -2	0.15 -2	0.90 -3
620	0.35 -1	0.10 -1	0.80 -2	0.53 -2
640	0.00	0.88 -1	0.72 -1	0.57 -1
660	0.65	0.70	0.75	0.80
670	0.80	0.82	0.84	0.86
680	0.60	0.62	0.65	0.70
700	0.95 -1	0.88 -1	0.70 -1	0.50 -1
720	0.27 -1	0.20 -1	0.05 -1	0.83 -2
740	0.55 -2	0.40 -2	0.20 -2	0.90 -3
760	0.65 -3	0.50 -3	0.25 -3	0.95 -4
780	0.65 -4	0.50 -4	0.20 -4	0.80 -5
800	0.40 -5	0.20 -5	0.00 -5	0.70 -6

Table G : Spectral Transmittance $\tau\,(\,{}_{10}\log\,(\,l_\nu\, c^*))\;=\;\tau\,(\,{}_{10}\log\, l_\nu\;+\;{}_{10}\log\, c^*\,)$ for the 15μ - Band of Carbon Dioxide to be Used in Connection with the Table F

${}_{10}\log(l_\nu\, c^*)$	τ	${}_{10}\log(l_\nu\, c^*)$	τ	${}_{10}\log(l_\nu\, c^*)$	τ
0.5 -4	1.000	0.5 -2	0.902	0.5 +0	0.325
0.6	0.997	0.6	0.891	0.6	0.287
0.7	0.995	0.7	0.878	0.7	0.250
0.8	0.993	0.8	0.865	0.8	0.213
0.9	0.990	0.9	0.850	0.9	0.180
0.0 -3	0.988	0.0 -1	0.834	0.0 +1	0.150
0.1	0.985	0.1	0.817	0.1	0.125
0.2	0.983	0.2	0.796	0.2	0.100
0.3	0.981	0.3	0.772	0.3	0.080
0.4	0.979	0.4	0.747	0.4	0.063
0.5	0.976	0.5	0.717	0.5	0.048
0.6	0.972	0.6	0.687	0.6	0.035
0.7	0.968	0.7	0.652	0.7	0.025
0.8	0.963	0.8	0.617	0.8	0.018
0.9	0.957	0.9	0.580	0.9	0.010
0.0 -2	0.950	0.0 +0	0.535	0.0 +2	0.008
0.1	0.943	0.1	0.495	0.1	0.005
0.2	0.935	0.2	0.452	0.2	0.003
0.3	0.925	0.3	0.410	0.3	0
0.4	0.913	0.4	0.367	0.4	0

A P P E N D I X I I

Radiation diagrams for the channels 1, 2 and 4 of the satellite TIROS III and for a "difference channel (4-2)" (defined in chapter 5) and auxiliary diagrams for the correction according to the absorption and emission by atmospheric ozone and carbon dioxide (see chapter 3)

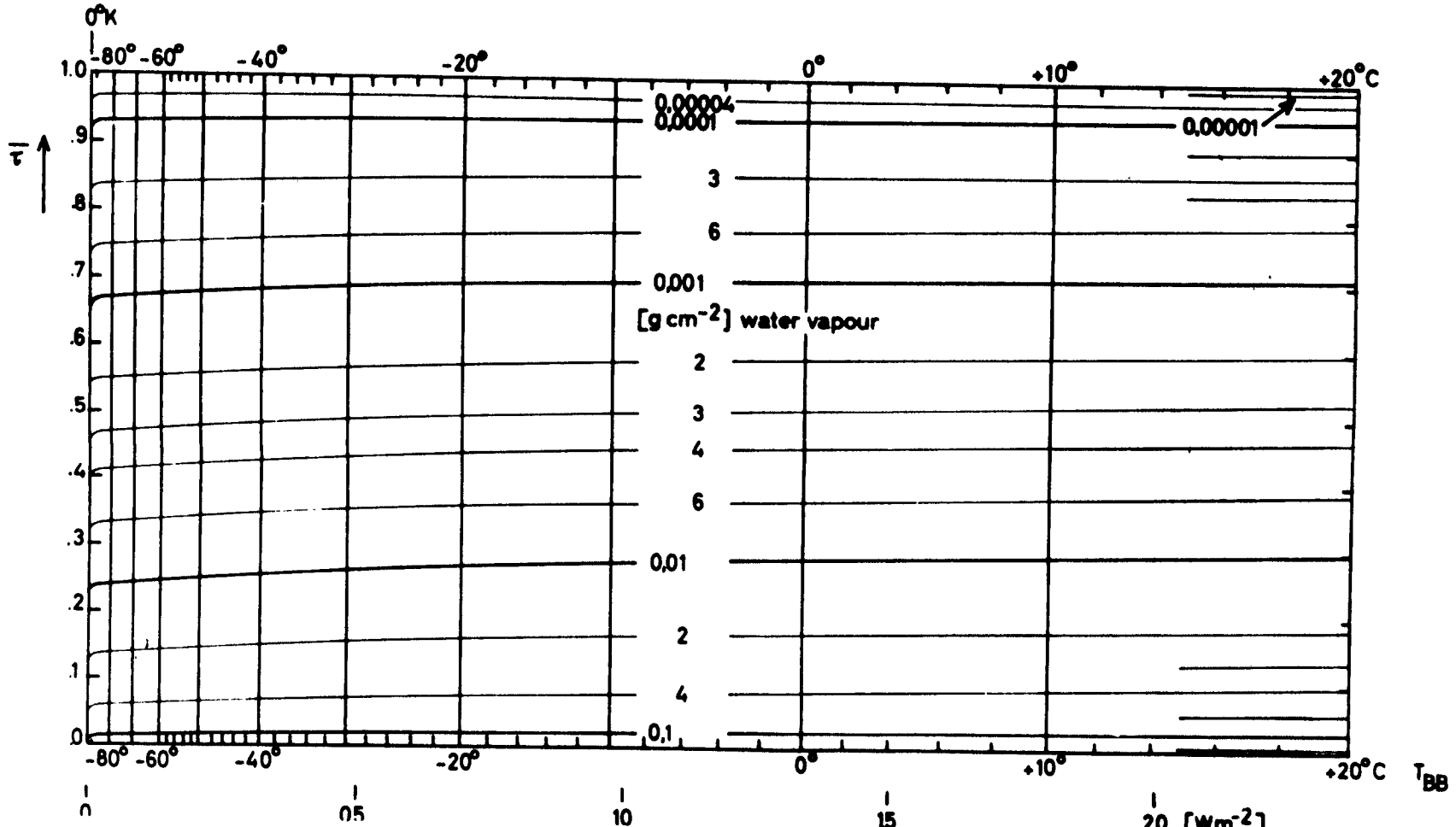

TIROS III : CHANNEL 1 (5.8 - 6.8 μ)

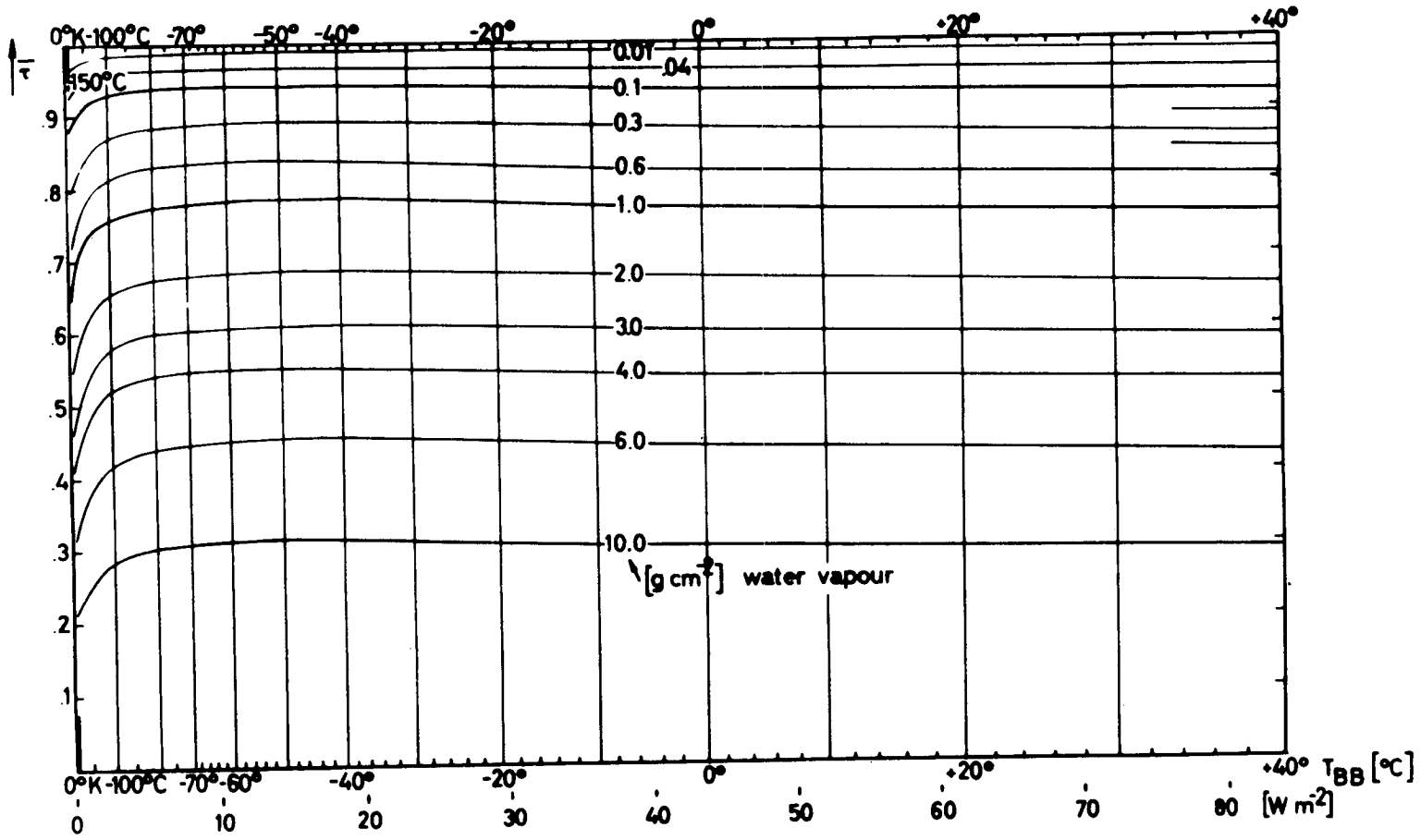

TIROS III : CHANNEL 2 (8 - 13 μ)

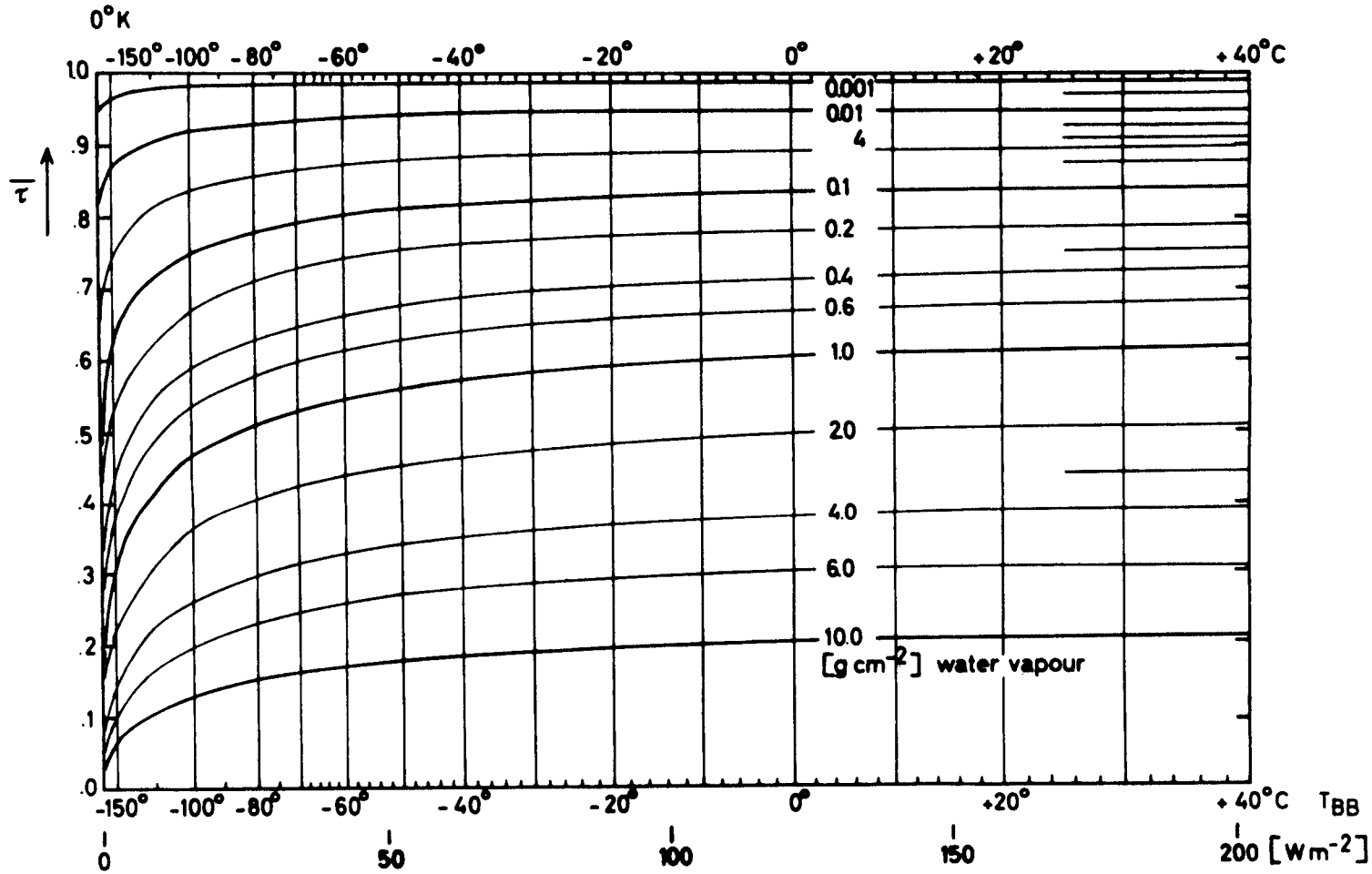

TIROS III : CHANNEL 4 (7.5 - 32.5 μ)

TIROS III : "difference channel (4-2)" (12-32.5 μ)

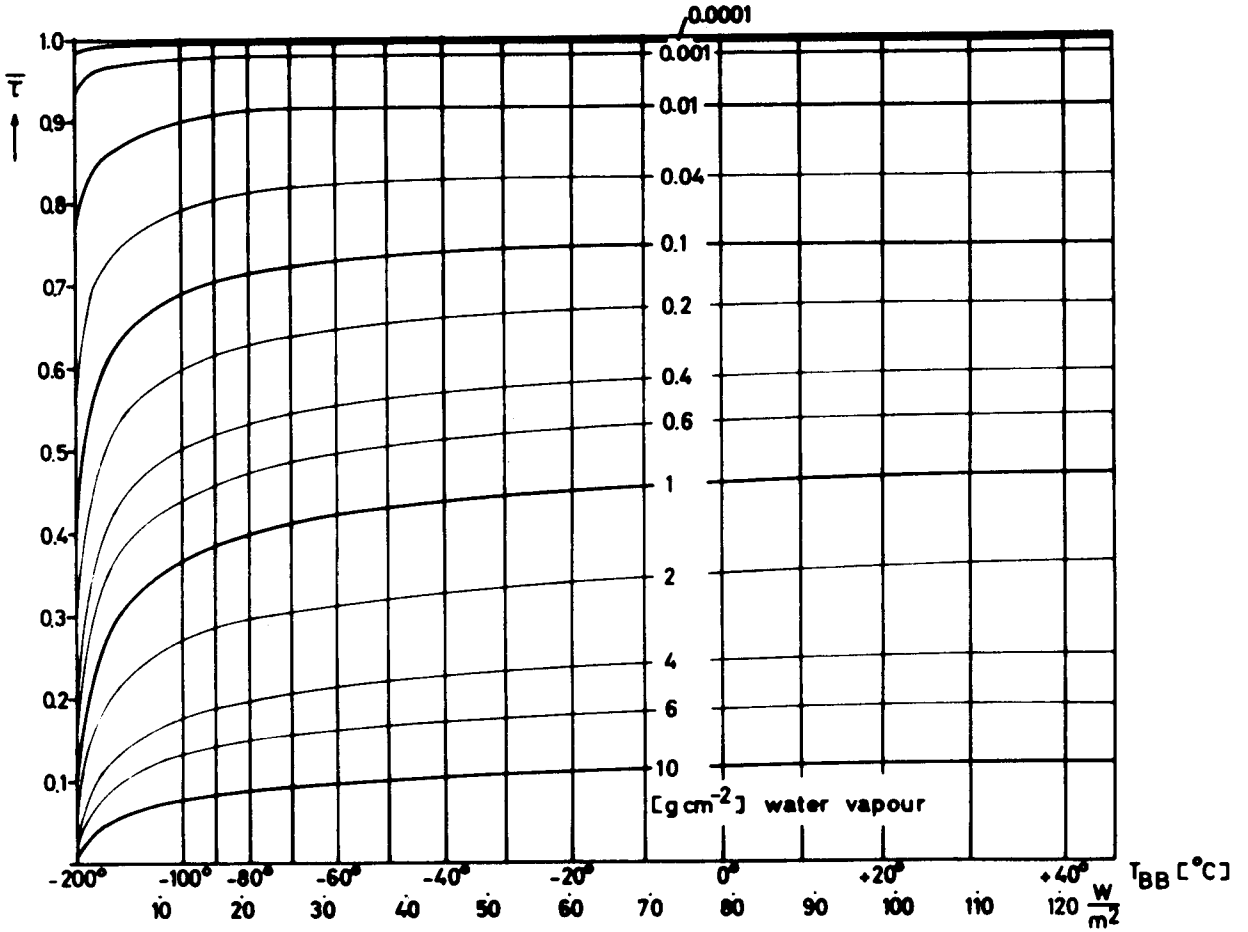

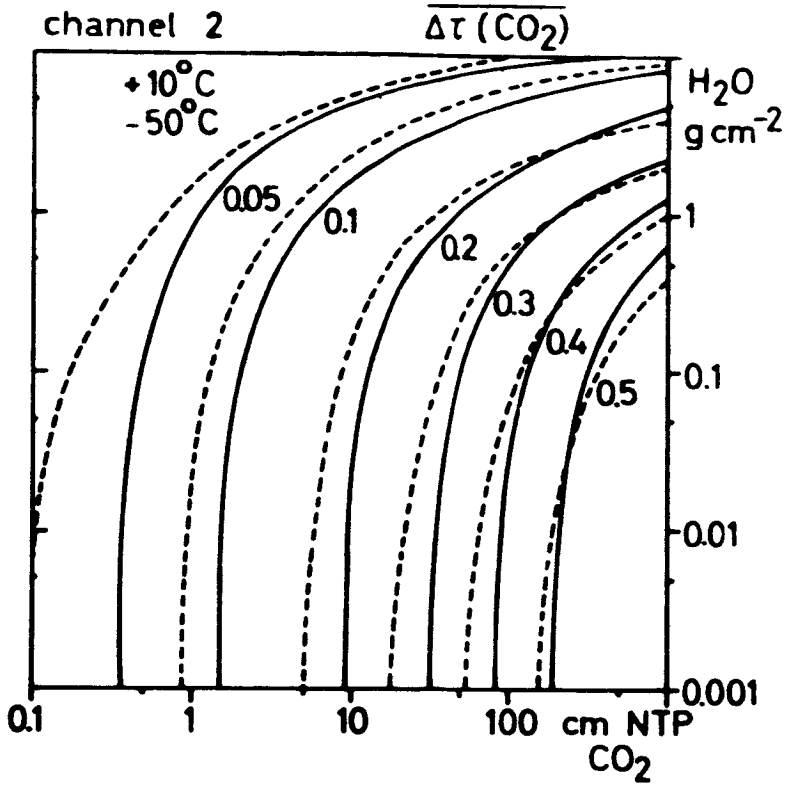
channel 2
$\overline{\Delta\tau\,(CO_2)}$
+10°C
-50°C
0.05
0.1
0.2
0.3
0.4
0.5
H_2O
g cm^{-2}
1
0.1
0.01
0.001
0.1
1
10
100
cm NTP
CO_2

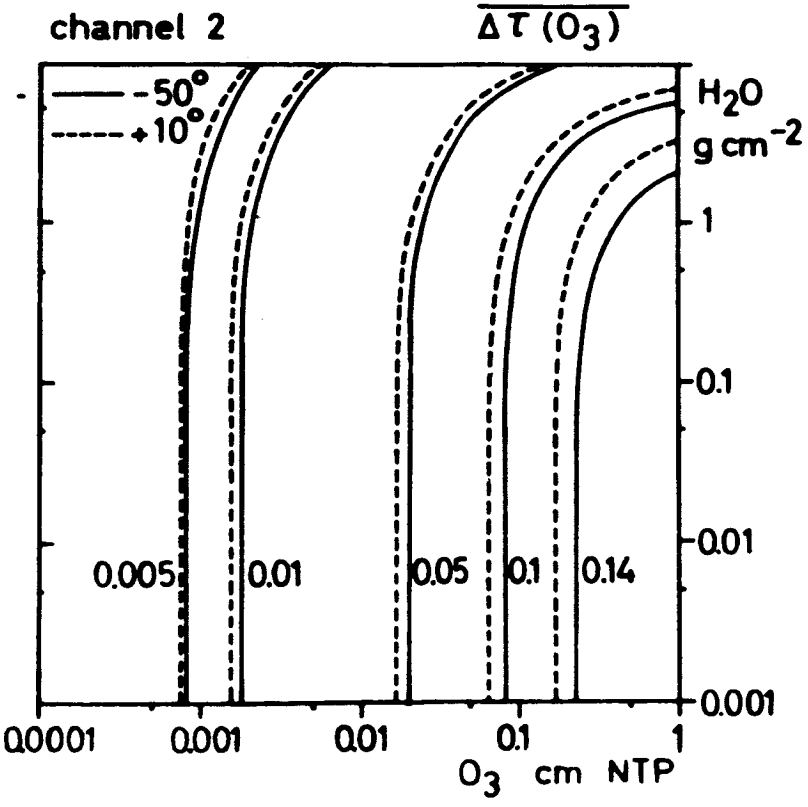
channel 2
$\overline{\Delta\tau\,(O_3)}$
-50°
+10°
H_2O
g cm^{-2}
1
0.1
0.01
0.001
0.005
0.01
0.05
0.1
0.14
0.0001
0.001
0.01
0.1
1
O_3 cm NTP

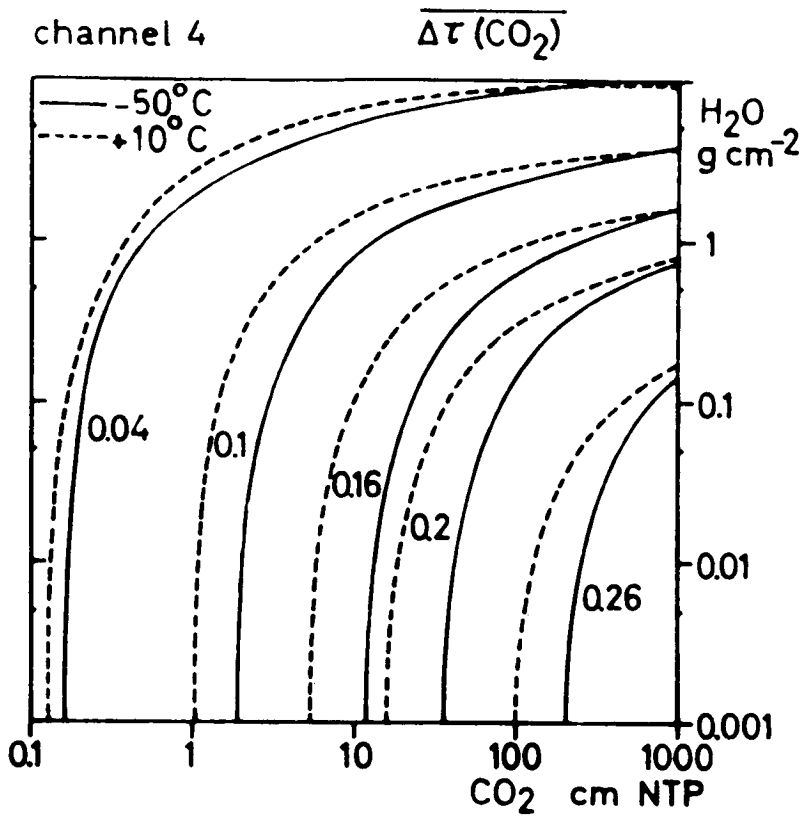
channel 4
$\overline{\Delta\tau(CO_2)}$
-50°C
+10°C
H_2O g cm^{-2}
1
0.1
0.01
0.001
0.04
0.1
0.16
0.2
0.26
0.1
1
10
100
1000
CO_2 cm NTP

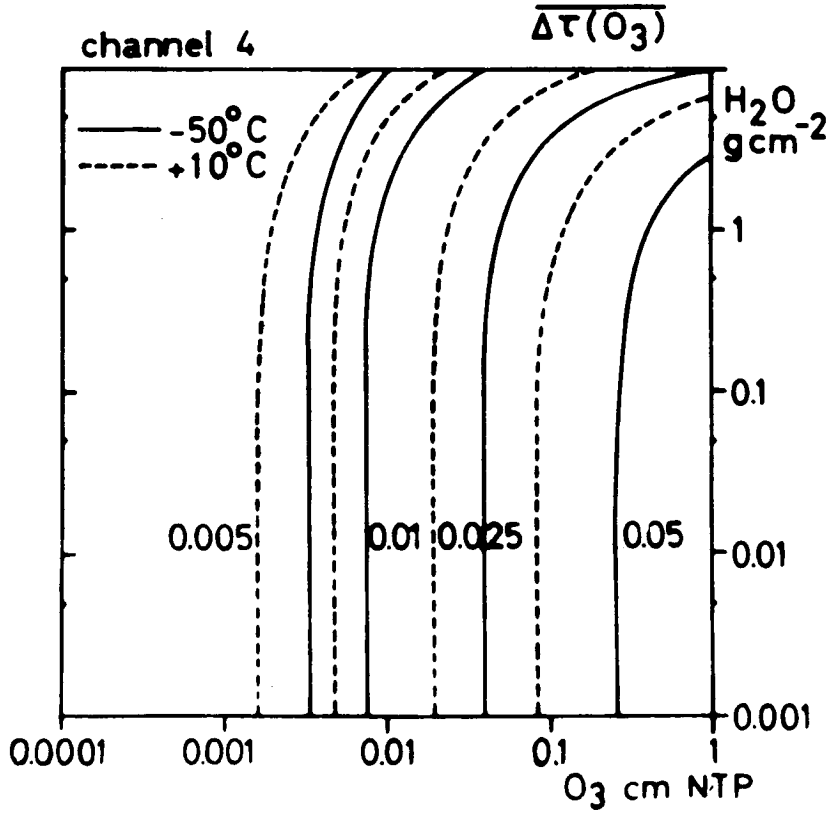
channel 4
$\overline{\Delta\tau(O_3)}$
-50°C
+10°C
H_2O g cm^{-2}
1
0.1
0.01
0.001
0.005
0.01
0.025
0.05
0.0001
0.001
0.01
0.1
1
O_3 cm NTP

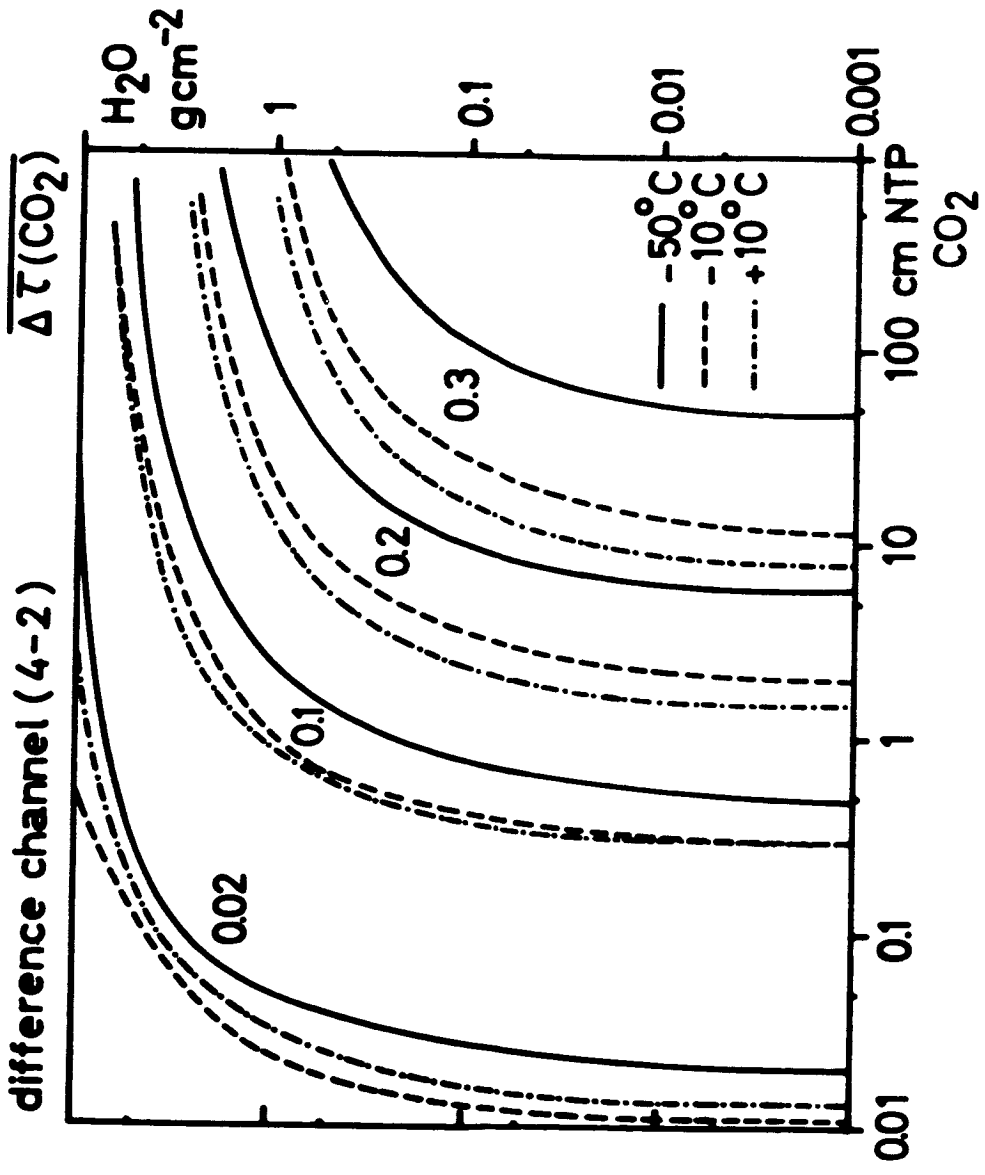
difference channel (4-2)
$\overline{\Delta\tau(CO_2)}$
H_2O gcm^{-2}
1
0.1
0.01
0.001
CO_2
100 cm NTP
10
1
0.1
0.01
0.02
0.1
0.2
0.3
−50°C
−10°C
+10°C

REFERENCES

Bahr, E. v., (1909, 1910): Ann. Phys. 29, 780; 33, 585.

* Bandeen, W.R., (July 1961): Earth Oblateness and Relative Sun Motion Considerations in the Determination of an Ideal Orbit for the NIMBUS Meteorological Satellite. NASA Technical Note D-1045.

(1962): Data Processing from Meteorological Satellites. Proceedings of the NASA-University Conference on the Science and Technology of Space Exploration, Chicago 1962. NASA SP-11; Office of Scientific and Technical Information.

* Bandeen, W.R., R.A. Hanel, John Licht, R.A. Stampfl, and W.G.Strond, (1961): Infrared and Reflected Solar Radiation Measurements from TIROS II Meteorological Satellite. J. of Geoph. Res., 66, 3169-3185, October 1961.

Bolle, H.-J., F. Möller, W. Zdunkowski, (May 1963): Investigation of the Infrared Emission Spectrum of the Atmosphere and Earth. Technical Report Nr. 2, Meteorologisches Institut, München, Germany.

Burch, D.E., D. Gryvnak, and D. Williams, (1960): Infrared Absorption by Carbon Dioxide. The Ohio State University, Research Foundation, Columbus 12, Ohio. Sci. Rep. Nr. 2, Contract Nr. AF 19 (604)-2633.

Chandrasekhar, S., (1960): Radiative Transfer. Dover Publ., Inc., New York.

Cloud, W.H., (1952): The 15 Micron Band of CO_2 Broadened by Nitrogen and Helium. Prof. Rep., Johns Hopkins Univ., Contract Nr. 248-01, 56pp.

Conrath, B.J., (1962): Earth Scan Analogy Signal Relationships in the TIROS Radiation Experiment and their Application to the Problem of Horizon Sensing.
NASA Technical Note D-1341.

Curtis, A.R., (1952): Discussion of Goody's Paper: A Statistical Model for Water Vapor Absorption.
Quart. J. Roy. Soc. 78, 638.

Curtis, A.R., and R.M. Goody, (1952): Thermal Radiation of the Upper Atmosphere.
Proc. Roy. Soc. London A 236, 193.

Daw, H.A., (1956): Transmission of Radiation through Water Vapor Subject to Pressure Broadening in the Region 4.2 to 23.
Techn. Rep. Nr. 10, Univ. Utah,
Contract AF 19(122)-392 with AFRC, 70pp.

Deirmendjan, D., (July 1962): Scattering and Polarization of Polydispersed Suspensions with Partial Absorption.
Memorandum RM-3228-PR. The RAND Corp.,
Santa Monica, Calif.

Elsasser, W.M., (1942): Heat Transfer by Infrared Radiation in The Atmosphere.
Harvard Meteorological Studies Nr. 6,
Harvard University Milton, Mass.

Elsasser, W.M., and J.I. King, (1953): Transmission Data for the Far Infrared Bands of Carbon Dioxide and Ozone.
Techn. Rep. Nr. 9. Utah, Contract AF 19 (122)-392 with AFCRC: 44pp.

Elsasser, W.M., and M.F. Culbertson, (1960): Atmospheric Radiation Tables. Met. Monographs 4.

Falkenberg, G., (1938): Experimentelles zur Druckabhängigkeit der Absorption des Wasserdampfes und der Kohlensäure für die infrarote Schwarzstrahlung.
Met. Z. 55, pp174.

Fritz, S. (1949): The Albedo of the Planet Earth and of Clouds. J. of Met. 6, p.277.

Fujity, F., (Nov. 1961): Outline of a Technique for Precise Rectification of Satellite Cloud Photographs. Research Paper Nr. 3, Dept. of the Geoph. Sci., University of Chicago, (Rechn. Rep. to the USWB, Contract Nr. 10047).

(Jan. 1963): A Technique for Precise Analysis for Satellite Data. Vol. I-Photogrammetry.

(Febr. 1963): Outline of a Theory and Examples for Precise Analysis of Satellite Radiation Data. Research Paper Nr. 15, Dept. of the Geoph. Sci., University of Chicago, (NASA NsG. 333; USWB Cwb WBG-6).

Godson, W.L., (1955): The Computation of Infrared Transmission by Atmospheric Water Vapor. J. of Met. 12, 272-284.

* Goldshlak, Leon, (June 1962): TIROS III Attitude Summary. Allied Research Associates, Inc. 43 Leon Street, Boston 15, Mass.; Contract Nr. NAS 5-1204.

Goody, R.M., (1952): A Statical Model for Water Vapor Absorption. Quart. J. Roy. Meteorol. Soc. 78, 165.

Gutnick, M., (July 1962): Mean Annual Mid Latitude Moisture Profiles to 31 km. AFCRL-62-681, Research Report.

* Hanel, R.A. and D.Q. Wark, (Dec. 1961): Physical Significance of the TIROS II Radiation Experiment. NASA Technical Note D 701.

* Hanel, R.A., W.R. Bandeen, B.J. Conrath, (Aug. 1962): The Infrared Horizon of the Planet Earth. NASA 650-62-164; Goddard Space Flight Center, Greenbelt, Md.

Hinzpeter H., and L. Foitzik, (1958): Sonnenstrahlung und Lufttrübung. Akad. Verlagsges. Geest und Hortig, Leipzig.

Howard, J.N., D.E. Burch, and D. Williams, (1956): Infrared Transmission of synthetic atmospheres. J. Opt. Soc. Am., 46, 186, 237, 242, 334, 452.

Johnson, F.S., (1954): The Solar Constant. J. of Met. 11, 431.

Kaplan, L.D., (1959): A Method for Calculation of Infrared Flux for Use in Numerical Models of Atmospheric Models. The Earth and Sea in Motion. Rossby Memorial Vol. Edited by B. Bolin, Oxford.

Kondratiev, K.Y., (1956): Radiation Heat Exchange in the Atmosphere Hydrometeoizdat, Leningrad.

Kondratiev, K.Y., H.J. Niilisk, (1961/II): The New Radiation Chart. Geofisica Pura e Applicata, Milano, 49, 197-207.

Kondratiev, K.Y., and Jakuschevskaja, K.E.,(1962): Angular Distribution of the Upward Heat Radiation in Different Spectral Ranges. Issk. sputniki semlji (Earth's artificial satellites) No. 14.

Ladenburg, R., and F. Reiche, (1913): Über selektive Absorption. Ann. d. Physik 42, 181.

Mastenbrook, H.J., (Aug. 1962): The Vertical Distribution of Water Vapor over Hyderabad, India, and Comparison with Midlatitude Distribution. U.S. Naval Res. Lab., Washington 25, D.C.

Mastenbrook, H.J., and J.E. Dinger, (1961): Distribution of Water Vapor in the Stratosphere. J. of Geophys. Res., 66, 1437-1444.

Matossi, F., and E. Rauscher, (1949): Zur Druckabhängigkeit der Gesamtatmosphäre in ultraroten Bandenspektren. Z. Phys. 7, 418.

Möller, F., (1944): Grundlagen eines Diagrammes zur Berechnung langwelliger Strahlungsströme. (Fundamentals of a Diagram for Evaluation of Infrared Radiation). Met. Zeitschr. 61, 37.

(1957): Strahlung in der unteren Atmosphäre. Handb. d. Phys., 48, Springer Verl. Berlin.

(1961): Atmospheric Water Vapor Measurements at 6-7 Microns from a Satellite. Planet. Space Sci., 5, 202-206.

Möller, F., (15. Jan. 1962): Some Preliminary Evaluations of TIROS II Radiation Measurements. Univ. München, Meteorologisches Inst. München 13, Amalienstr. 52/III.

(1962): Einige vorläufige Auswertungen der Strahlungsmessungen von TIROS II. Arch. f. Met., Geophys. u. Biokl., Serie B, 12, 78-93.

Möller, F., R. Mügge, (1932): Zur Berechnung von Strahlungsströmen und Temperaturänderungen in Atmosphären mit beliebigem Aufbau. Met. Zeitschr. 50, 95.

Möller, F. and S. Manabe, (1961): On the Radiative Equilibrium and Heat Balance of the Atmosphere. Monthly Weather Rev., 89, Nr. 12, 503-532.

Möller, F., and S. Manabe, (1961): Über das Strahlungsgleichgewicht der Atmosphäre. Zeitschr. f. Met. 15, 3-8.

Murcray, D.G., F.H. Murcray, and W.J. Williams, (1961): Distribution of Water Vapor in the Stratosphere as Determined from Infrared Absorption Measurements. University of Denver Scientific Rep. 1, Contract AF 19(604)-7429.

Nordberg, W., W.A. Bandeen, B.J. Conrath, V. Kunde, and J.Persano, (Jan. 1962): Preliminary Results of Radiation Measurements from TIROS III, Meteorological Satellite. J. Atmos. Sci., 19, 20-30.

Paetzold, H.K., (1963): Communication (unpublished).

Palmer, C.H., Jr., (1957): Long Path Water Vapor Spectra with Pressure Broadening, I. 20μ-31.7μ. J.O.S.A. 47,1024.

(1960): Experimental Transmission Function for the Pure Rotation Band of Water Vapor. J.O.S.A. 50, 1232.

Plass, G.N., (1963): Spectral Band Absorptance for Atmospheric Slant Paths.
Appl. Opt., 2, 515-526.

Plass, G.N., and D.I. Fivel, (1953): Astrophys. J. 117, 225.

Roach, W.T., and R.M. Goody, (1958): Absorption and Emission in the Atmospheric Window from 770 to 1.250 cm^{-1}.
Quart. J. Roy. Met. Soc. 84, 319-333.

Schnaidt, F., (1939): Über die Absorption von Wasserdampf und Kohlensäure mit besond. Berück. der Druck- u. Temperaturabhängigkeit.
Zeitschr. f. Geophys. 54, 203.

Summerfield, M. (1941): Pressure Dependence of the Absorption in the 9.6μ-Band of Ozone.
Thesis, Calif. Inst. Tech., unpublished, 65pp.

* TIROS III, (Aug. 1962), Radiation Data. User's Manual.
NASA-Aeronomy and Meteorology Division, Goddard Space Flight Center, Greenbelt, Md.

Walshaw, C.D., (1957): Integrated Absorption by the 9.6μ-Band of Ozone.
Quart. J. Roy. Met. Soc., 83, 315-321.

Wark, D.Q., G. Yamamoto, and J.H. Lienesch, (1962): Methods of Estimating Infrared Flux and Surface Temperature from Meteorological Satellites.
J. Atmos. Sci., 19, 369-384, Sept. 1962.

Wexler, R., L.D. Kaplan, (1962): Simulated Satellite Observations of Atmospheric Infrared Radiation (unpublished).

Wimmer, M. (1926): Ann. Phys. 81, 1091.

Wyatt, D.J., V.R. Stull, and G.N. Plass, (20. Sept. 1962): Infrared Transmission Studies (Final Report).
Vol. II: The Infrared Absorption of Water Vapor.
SSD-TDR-62-127-Vol. II.

(31. Jan. 1963): The Infrared Absorption of Carbon Dioxide.
SSA-TDR-62-127-Vol. III.
Aeronautic Division, Ford Motor Company, Newport Beach, Calif.
Contract Nr. AF 04(695)-96, Project Nr. 4479-730F.

Yamamoto, G., (1952): On a Radiation Chart.
Sci. Rep. Tohoku Univ. Series 5,
Geophysics, 4, 9-23.

Yamamoto, G., and T. Sasamori, (July 1958): Calculation of the
Absorption of the 15μ-Carbon Dioxide Band.
Sci. Reports of the Tohoku Univ. Series 5,
Geophysics, 10, No. 2.

Yamamoto, G., and T. Sasamori, (1961): Further Studies on the
Absorption by the 15 Micron Carbon Dioxide
Bands.
Sci. Rep. Tohoku Univ., Series 5,
Geophysics, 13, No. 1.

NASA-Langley, 1964